

**Bracing Requirements of  
Cold-Formed Steel Cee-  
Studs Subjected to Axial  
Compression**

**RESEARCH REPORT RP04-1**

**DECEMBER 2004**

**REVISION 2006**

Committee on Specifications  
for the Design of Cold-Formed  
Steel Structural Members

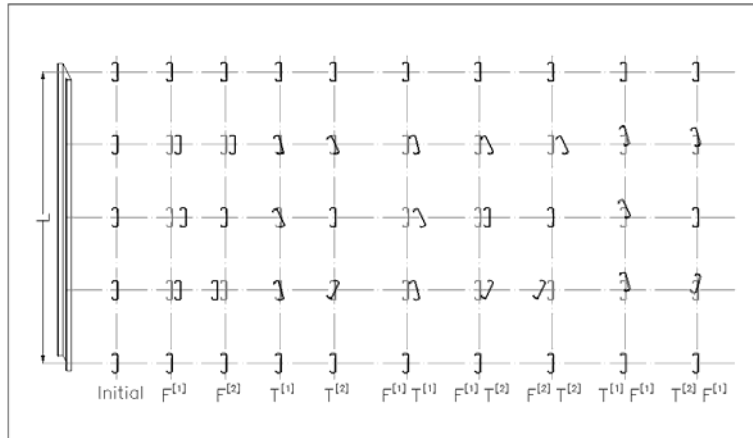


**American Iron and Steel Institute**

The material contained herein has been developed by researchers based on their research findings. The material has also been reviewed by the American Iron and Steel Institute Committee on Specifications for the Design of Cold-Formed Steel Structural Members. The Committee acknowledges and is grateful for the contributions of such researchers.

The material herein is for general information only. The information in it should not be used without first securing competent advice with respect to its suitability for any given application. The publication of the information is not intended as a representation or warranty on the part of the American Iron and Steel Institute, or of any other person named herein, that the information is suitable for any general or particular use or of freedom from infringement of any patent or patents. Anyone making use of the information assumes all liability arising from such use.

# BRACING REQUIREMENTS OF COLD-FORMED STEEL CEE-STUDS SUBJECTED TO AXIAL COMPRESSION



Project # 4910 4504 847 12

Perry S. Green  
Thomas Sputo  
Viswanath Urala



A REPORT PRESENTED TO THE  
AMERICAN IRON AND STEEL INSTITUTE AND THE  
STEEL STUD MANUFACTURERS ASSOCIATION

December 2004

## ACKNOWLEDGMENTS

This research was funded by the American Iron and Steel Institute (AISI) and the Steel Stud Manufacturers Association (SSMA). Test specimens materials were donated by SteelCon and Dietrich Industries. This research was conducted at the Structures Testing Laboratory, University of Florida, Gainesville, FL.

## TABLE OF CONTENTS

	<u>Page</u>
ACKNOWLEDGMENTS .....	ii
LIST OF TABLES .....	vi
LIST OF FIGURES .....	viii
EXECUTIVE SUMMARY .....	xiv
CHAPTER	
1 INTRODUCTION .....	1
1.1 General.....	1
1.2 Objectives of Research .....	1
1.3 Scope of Research.....	3
2 LITERATURE REVIEW .....	6
2.1 General.....	6
2.2 Buckling of Columns .....	7
2.2.1 Elastic Buckling.....	7
2.2.2 Inelastic Buckling .....	8
2.2.3 Local Buckling and Distortional Buckling .....	9
2.3 Bracing Stiffness and Strength.....	11
2.3.1 Column with Concentric Axial Load and an Immovable Point Support at Mid-height.....	12
2.3.2 Column with Concentric Axial Load and an Elastic Lateral Support at Mid-height.....	13
2.4 Long Column Tests.....	19
2.4 AISC-LRFD Specification.....	20
2.5 AISI Specification for Cold-Formed Steel .....	22
3 DESCRIPTION OF EXPERIMENTAL STUDY .....	33
3.1 Introduction.....	33
3.2 Objectives of Experimental Tests .....	34
3.3 Material Properties of Test Specimens .....	34
3.4 As-Built Dimensions of the Test Specimens .....	35
3.5 Measured Geometric Imperfections of the Test Specimens .....	36

3.5.1	Global Imperfections .....	36
3.5.2	Cross-Sectional Imperfections .....	37
3.6	Test Setup and Test Procedure for Single Column Axial Load Tests .....	38
3.6.1	Test Specimens of Single Column Axial Load Tests .....	38
3.6.2	Test Frame for Single Column Axial Load Tests .....	38
3.6.3	Instrumentation for Single Column Axial Load Tests .....	39
3.6.4	Test Procedure of Single Column Axial Load Tests .....	39
3.7	Test Setup and Test Procedure for Bridging Tests .....	40
3.7.1	Test Specimens of Bridging Tests .....	40
3.7.1.1	Screwed-Screwed (SS) Connection: .....	41
3.7.1.2	Welded-Welded (WW) Connection: .....	41
3.7.1.3	Direct-Welded (DW) Connection: .....	41
3.7.2	Test Fixture for Bridging Tests .....	42
3.7.3	Instrumentation .....	43
3.7.4	Out-of-Plane Loading Test Procedure .....	44
3.7.5	In-Plane Loading Test Procedure .....	44
4	EXPERIMENTAL RESULTS AND EVALUATION .....	61
4.1	Single Column Axial Load Test Results .....	61
4.1.1	Bracing Strength and Stiffness .....	62
4.1.2	Evaluation of Experimental Observations .....	64
4.1.2.1	Effect of brace stiffness on axial load capacity .....	68
4.1.2.2	Effect of brace stiffness on buckling type and mode .....	71
4.1.2.3	Effect of cross-sectional dimensions of cee-studs .....	72
4.1.2.4	Effect of experimental load on the brace stiffness and strength ...	73
4.1.2.5	Effect of brace stiffness on lateral displacement .....	74
4.1.2.6	Effect of brace stiffness on effective length of columns .....	74
4.1.2.7	Effect of brace strength on axial capacity .....	75
4.1.2.8	Other effects .....	75
4.2	Bridging Test Results .....	77
4.2.1	Bridging Connection Strength and Stiffness .....	77
4.2.2	Observations of the Out-of-Plane Experimental Tests .....	79
4.2.3	Observations of the In-Plane Experimental Tests .....	80
4.2.4	Observed Bridging Connection Failures .....	82
4.2.4.1	SS type connection .....	82
4.2.4.2	WW type connection .....	82
4.2.4.3	DW type connection .....	83
4.3	Separation of Brace Forces in Flexural and Torsional Components .....	83
4.4	Summary of Experimental Observations .....	85
5	ANALYTICAL EVALUATION .....	147
5.1	Analytical Load Capacity of Unbraced and Fully Braced Studs .....	147
5.2	Analytical Bridging Connection Stiffness of a Flexible Bracing .....	149
5.2.1	Initial Flexural Stiffness of the Bracing Connection .....	149
5.2.1.1	SS type connection .....	151

5.2.1.2	WW type connection .....	152
5.2.1.3	DW type connection .....	152
5.2.2	Initial Torsional Stiffness of the Bracing Connection .....	153
5.3	Total Stiffness of the Bridging Connection .....	154
5.3.1	Initial Flexural Stiffness.....	154
5.3.2	Initial Torsional Stiffness.....	155
<b>6</b>	<b>CONCLUSIONS AND DESIGN RECOMMENDATIONS .....</b>	<b>168</b>
6.1	General Conclusions and Recommendations.....	168
6.2	Design Recommendations .....	171
	<b>LIST OF REFERENCES .....</b>	<b>173</b>

## LIST OF TABLES

<u>Table</u>	<u>page</u>
3.1 As-built Material Properties from the Tension Coupon Tests .....	46
3.2 As-Built Cross-Sectional Dimensions of Test Specimens .....	47
3.3 Initial Geometric Imperfections .....	50
3.4 Average As-Built Geometric Dimensions of Each Stud Series .....	51
3.5 Average As-Built Geometric Dimensions of Each Stud Series .....	51
4.1 Proposed Test Matrix for the Single Column Axial Load Tests .....	88
4.2 Actual Test Matrix of the Single Column Axial Load Tests.....	89
4.3 Nominal Properties of the Test Specimens Using AISIWIN Program .....	90
4.4 Average As-built Properties of the Test Specimens Using AISIWIN Program.....	91
4.5 Calculated Brace Stiffness and Total Brace Stiffness of the Test Specimens.....	92
4.6 Summary of Experimental Test Results for Test Specimens .....	94
4.7 Required Brace Stiffness Based on $P_{max}$ .....	95
4.8 Effective Length Factors Based on $P_{max}$ .....	96
4.9 Measured Values of Brace Force and Mid-height Displacement at $P_{max}$ .....	97
4.10 Calculated Values of Brace Force and Mid-height Displacement at $P_{max}$ .....	100
4.11 Proposed Test Matrix for Bridging Connection Tests .....	102
4.12 Bridging Test Results for Out-of-Plane Loading .....	103
4.13 Initial Torsional Stiffness of the Lower Bound Values of Out-of-Plane Tests.....	104
4.14 Bridging Test Results for In-Plane Loading .....	106
4.15 Initial Flexural Stiffness of the In-Plane Tests.....	107



4.16	Experimental Initial Stiffness of the In-Plane Load Tests .....	109
4.17	Experimental Initial Stiffness of the Out-of-Plane Load Tests .....	109
4.18	Maximum Flexural and Corresponding Torsional Brace Force.....	110
4.19	Maximum Torsional and Corresponding Flexural Brace Force.....	111
5.1	Axial Load Capacities of Test Specimens Using AISI (1999) MathCAD Worksheets .....	157
5.2	Comparison of Initial Flexural Stiffness of the In-Plane Tests.....	158
5.3	Comparison of Initial Torsional Stiffness of the In-Plane Tests.....	159
5.4	Total Flexural Stiffness of the Bridging Connections.....	160
5.5	Calculated Brace Stiffness and Total Brace Stiffness of the Test Specimens.....	162
5.6	Total Torsional Stiffness of the Bridging Connections.....	164

## LIST OF FIGURES

<u>Figure</u>	<u>page</u>
2.1 Reduced Modulus Theory (Figure 1-21, Chajes 1974).....	26
2.2 Imperfect Column with Immovable Mid-height Bracing .....	26
2.3 Imperfect Column with Elastic Mid-height Bracing.....	27
2.4 Critical Loads for Elastically Supported Columns.....	27
2.5 Effect of Bracing Stiffness .....	28
2.6 $P_{cr}/P_e$ versus $\beta L/P_e$ for a Discrete Bracing .....	29
2.7 Effect of Lateral restraint location on Brace behavior .....	29
2.8 Bracing Connection Clips .....	30
2.9 Wall Assembly test setup .....	30
2.10 Types of Bracing (a) Relative Bracing and (b) Nodal Bracing.....	31
2.11 Effect of Initial Out-of-Plumbness .....	31
2.12 Effective Length Factors for Concentrically Loaded Columns .....	32
3.1 Dimensions of a Typical Tension Coupon.....	52
3.2 Offset Method for Determining Yield Stress .....	52
3.3 Autographic Diagram Method for Determining Yield Stress .....	53
3.4 Typical Cross-Section of a Cee-Stud .....	53
3.5 Connection of Cee-Stud and Track (a) at Top, (b) at Bottom.....	54
3.6 Plan View of Single Column Axial Test Setup in the Riehle Universal Testing Machine .....	54
3.7 Schematic Mid-height Bracing and Instrumentation Locations on Test Specimens.....	55

3.8	Close-up View of the Location of Brace-Wires and Instrumentation at Mid-height of the Cee-Stud.....	55
3.9	Types of Bridging Connections.....	56
3.10	Top View of the SS Type Bridging Connection.....	56
3.11	Elevation Views of Bridging Connection Test Setup.....	57
3.12	Schematic Plan View of Bridging Connection Tests.....	58
3.13	Overall View of the Out-of-Plane Bridging Tests.....	59
3.14	Overall View of the In-Plane Bridging Tests.....	59
3.15	Out-of-Plane Loading Test Instrumentation.....	60
3.16	In-plane Loading Test Instrumentatio.....	60
4.1	Typical Bracing for the Single Column Axial Load Tests.....	112
4.2	Axial Load vs. Axial Shortening for the Stud 362S125-33 with Varying Brace Stiffness.....	112
4.3	Axial Load vs. Axial Shortening for the Stud 362S162-43 with Varying Brace Stiffness.....	113
4.4	Axial Load vs. Axial Shortening for the Stud 362S162-68 with Varying Brace Stiffness.....	113
4.5	Axial Load vs. Axial Shortening for the Stud 600S125-33 with Varying Brace Stiffness.....	114
4.6	Axial Load vs. Axial Shortening for the Stud 600S162-43 with Varying Brace Stiffness.....	114
4.7	Axial Load vs. Axial Shortening for the Stud 600S162-97 with Varying Brace Stiffness.....	115
4.8	Axial Load vs. Axial Shortening for the Stud 800S162-43 with Varying Brace Stiffness.....	115
4.9	Axial Load vs. Axial Shortening for the Stud 800S162-97 with Varying Brace Stiffness.....	116
4.10	Schematic Diagram Showing the Various Buckling Shapes and Buckling Modes Observed in the Experimental Testing.....	116
4.11	Comparison of Studs 362S125-33-0 and 600S125-33-0.....	117

4.12	Comparison of Studs 362S125-33-100 (1.7x) and 600S125-33-060 (1.3x) .....	117
4.13	Comparison of Studs 362S125-33-200 (6.2x) and 600S125-33-200 (7.4x) .....	118
4.14	Comparison of Studs 362S162-43-0, 600S162-43-0 and 800S162-43-0.....	118
4.15	Comparison of Studs 362S162-43-200 (1.2x), 600S162-43-250 (1.6x) and 800S162-43-150 (1.3x) .....	119
4.16	Comparison of Studs 362S162-43-400 (2.5x), 600S162-43-500 (3.4x) and 800S162-43-300 (2.3x) .....	119
4.17	Comparison of Studs 600S162-97-0 and 800S162-97-0.....	120
4.18	Comparison of Studs 600S162-97-1000 (1.7x) and 800S162-97-1000 (2.1x) .....	120
4.19	Comparison of Studs 600S162-97-1500 (2.7x) and 800S162-97-2100 (4.3x) .....	121
4.20	Comparison of Studs 362S125-33-0, 362S162-43-0 and 362S162-68-0.....	121
4.21	Comparison of Studs 362S125-33-100 (1.7x), 362S162-43-200 (1.2x) and 362S162-68-500 (1.8x) .....	122
4.22	Comparison of Studs 362S125-33-400 (6.2x), 362S162-43-800 (5.4x) and 362S162-68-1000 (3.3x) .....	122
4.23	Comparison of Studs 600S125-33-0, 600S162-43-0 and 600S162-97-0.....	123
4.24	Comparison of Studs 600S125-33-30 (0.2x), 600S162-43-75 (0.6x) and 600S162-97-160 (0.3x) .....	123
4.25	Comparison of Studs 600S125-33-60 (1.3x), 600S162-43-250 (1.6x) and 600S162-97-1000 (1.7x) .....	124
4.26	Comparison of Studs 600S125-33-200 (7.4x), 600S162-43-500 (3.4x) and 600S162-97-1500 (2.7x) .....	124
4.27	Comparison of Studs 800S162-43-0 and 800S162-97-0.....	125
4.28	Comparison of Studs 800S162-43-150(1.3x) and 800S162-97-500 (1.2x) .....	125
4.29	Comparison of Studs 800S162-43-300 (2.3x) and 800S162-97-2100 (4.3x) .....	126
4.30	Experimental Load vs. Target Brace Stiffness for 362 Series of Lipped Cee Studs .....	126
4.31	Experimental Load vs. Target Brace Stiffness for 600 Series of Lipped Cee Studs .....	127

4.32	Experimental Load vs. Target Brace Stiffness for 800 Series of Lipped Cee Studs .....	127
4.33	Total Brace Stiffness vs. Weak Axis Lateral Displacement for the 362 Series of Lipped Cee-Studs .....	128
4.34	Total Brace Stiffness vs. Weak Axis Lateral Displacement for the 600 Series of Lipped Cee Studs .....	128
4.35	Total Brace Stiffness vs. Target Brace Stiffness for the 800 Series Lipped Cee Studs .....	129
4.36	Effective Length Factor vs. Total Brace Stiffness for 362S-125-33 Series of Lipped Cee Studs .....	129
4.37	Effective Length Factor vs. Total Brace Stiffness for 362S-162-43 Series of Lipped Cee Studs .....	130
4.38	Effective Length Factor vs. Total Brace Stiffness for 362S-162-68 Series of Lipped Cee Studs .....	130
4.39	Effective Length Factor vs. Total Brace Stiffness for 600S-125-33 Series of Lipped Cee Studs .....	131
4.40	Effective Length Factor vs. Total Brace Stiffness for 600S-162-43 Series of Lipped Cee Studs .....	131
4.41	Effective Length Factor vs. Total Brace Stiffness for 600S-162-97 Series of Lipped Cee Studs .....	132
4.42	Effective Length Factor vs. Total Brace Stiffness for 800S-162-43 Series of Lipped Cee Studs .....	132
4.43	Effective Length Factor vs. Total Brace Stiffness for 800S-162-97 Series of Lipped Cee Studs .....	133
4.44	Location of Linear Potentiometers on the Bridging Connection .....	133
4.45	Plot of Applied Load vs. Calculated Rotation at the Center-line of the Web for the 362S Series of Studs.....	134
4.46	Plot of Applied Load vs. Calculated Rotation at the Center-line of the Web for the 600S Series of Studs.....	134
4.47	Plot of Applied Load vs. Calculated Rotation at the Center-line of the Web for the 800S Series of Studs with SS Connection.....	135
4.48	Plot of Applied Load vs. Calculated Rotation at the Center-line of the Web for the 362S Series of Studs with WW Connection .....	135

4.49	Plot of Applied Load vs. Calculated Rotation at the Center-line of the Web for the 600S Series of Studs with WW Connection .....	136
4.50	Plot of Applied Load vs. Calculated Rotation at the Center-line of the Web for the 800S Series of Studs with WW Connection .....	136
4.51	Plot of Applied Load vs. Calculated Rotation at the Center-line of the Web for the 362S Series of Studs with DW Connection .....	137
4.52	Plot of Applied Load vs. Calculated Rotation at the Center-line of the Web for the 600S Series of Studs with DW Connection .....	137
4.54	Plot of Applied Load vs. Calculated Rotation at the Center-line of the Web for the 362S Series of Studs.....	139
4.55	Plot of Applied Load vs. Calculated Rotation at the Center-line of the Web for the 600S Series of Studs.....	139
4.56	Plot of Applied Load vs. Calculated Rotation at the Center-line of the Web for the 800S Series of Studs.....	140
4.57	Plot of Applied Load vs. Calculated Rotation at the Center-line of the Web for the 362S Series of Studs.....	140
4.58	Plot of Applied Load vs. Calculated Rotation at the Center-line of the Web for the 600S Series of Studs.....	141
4.59	Plot of Applied Load vs. Calculated Rotation at the Center-line of the Web for the 800S Series of Studs.....	141
4.60	Plot of Applied Load vs. Calculated Rotation at the Center-line of the Web for the 362S Series of Studs.....	142
4.61	Plot of Applied Load vs. Calculated Rotation at the Center-line of the Web for the 600S Series of Studs.....	142
4.62	Plot of Applied Load vs. Calculated Rotation at the Center-line of the Web for the 800S Series of Studs.....	143
4.63	Plot of Initial Torsional Stiffness vs. Effective Flat-width to Thickness Ratio for the Out-of-Plane loading Tests on SS-type Connection .....	143
4.64	Plot of Initial Torsional Stiffness vs. Effective Flat-width to Thickness Ratio for the Out-of-Plane loading Tests on WW-type Connection .....	144
4.65	Plot of Initial Torsional Stiffness vs. Effective Flat-width to Thickness Ratio for the Out-of-Plane loading Tests on DW-type Connection.....	144

4.66	Plot of Initial Flexural Stiffness vs. Effective Flat-width to Thickness Ratio for the In-Plane loading Tests on SS-type Connection .....	145
4.67	Plot of Initial Flexural Stiffness vs. Effective Flat-width to Thickness Ratio for the In-Plane loading Tests on WW-type Connection .....	145
4.68	Plot of Initial Flexural Stiffness vs. Effective Flat-width to Thickness Ratio for the In-Plane loading Tests on DW-type Connection .....	146
4.69	Brace Forces as a Resultant of Flexural and Torsional Components.....	146
5.1	Flexural Stiffness of the SS Type Connection .....	166
5.2	Flexural Stiffness of the WW Type Connection .....	166
5.3	Flexural Stiffness of the DW Type Connection .....	167
5.4	Torsional Stiffness of the SS Type Connection .....	167

EXECUTIVE SUMMARY  
BRACING REQUIREMENTS OF COLD-FORMED STEEL CEE-STUDS  
SUBJECTED TO AXIAL COMPRESSION

August 2004

An experimental testing program was carried out on single axially loaded cold-formed lipped cee-studs to determine the required flexural and torsional bracing strength and stiffness requirements of the stud. Conventional bridging or nodal bracing has been simulated in the experiments using monofilament steel wires attached to the stud flanges at mid-height. A range of brace stiffness was simulated in the testing frame by using various diameters and lengths of monofilament wire. The brace stiffness that was achieved ranged from less than 30 lbs/in. to greater than 4000 lbs/in. Brace strength was determined from the cross-sectional area of the steel wire and its experimentally determined yield strength. The axial load, individual brace forces, axial shortening, and in-plane (weak-axis) and out-of-plane (strong-axis) lateral displacements were measured in each test. The required bracing stiffness was experimentally determined by varying the brace stiffness for a given stud size and was based on the ability of the stud to develop its nominal axial compressive capacity as predicted by the 1996 AISI Cold-Formed Steel Specification including Supplement No. 1. The experimental results were compared to



existing nodal bracing models, analytical prediction models, and the current column bracing provisions that are part of the 1999 AISC-LRFD Specification for Structural Steel Buildings.

Experimental testing has also been carried out on typical industry bridging configuration to measure bridging assembly strength and stiffness relationships for bridging subjected to in-plane and out-of-plane loadings. Load versus displacement measurements have been compiled for these assemblies for various stud web depths, flange widths, and thicknesses with the goal of categorizing strength and stiffness for these various bridging assemblies.

## CHAPTER 1 INTRODUCTION

The drive to create more cost effective cold-formed steel structural systems, and the current move to designing axially loaded wall stud systems using an “all-steel” approach, has required an alternative to the sheathing braced design. This has resulted in wall stud systems that are more sensitive to global stability limit states than previous designs. Ensuring global stability of axially loaded steel studs requires that the bracing system possess adequate stiffness and strength to develop the predicted axial strength.

### **1.1 General**

Cold-formed steel has been widely used in structural and non-structural wall construction for more than 60 years, and may be found in many residential, commercial and industrial facilities being built today. The lightweight property of cold-formed steel makes it easier and economical to transport and install than other construction materials such as masonry or hot-rolled steel. Other advantages include – resistance to pest attack, rapid construction, long service life and efficiently recyclable. Cold-formed steel sections can be used in most parts of a building, including roofs, trusses, frames etc.

### **1.2 Objectives of Research**

Current North American structural steel design practice using the 3rd Edition of the American Institute of Steel Construction- Load and Resistance Factor Design Specification (AISC 1999) prescribes nodal bracing strength and stiffness requirements, based on a model developed by Winter (1960) and modified by Yura (1995). However, the most recent cold-formed steel design specification, the North American Specification

by the American Iron and Steel Institute (AISI 2001a) does not contain provisions for determining nodal brace strength and stiffness requirements for axially loaded compression members. This research program was conducted to experimentally determine rational requirements for nodal bracing strength and stiffness demand of lipped cee-studs by conducting single column axial compression tests, and bridging strength and stiffness tests. The experimental results were used to formulate a rational methodology to be incorporated into the AISI Specification provisions for design purposes.

The objectives of this research included to determine:

1. the minimum bracing strength and stiffness required for cold-formed steel members subjected to axial loading;
2. the stiffness and strength of typical industry bridging systems;
3. the effective length factors based on unbraced length;
4. the effect of slenderness ratio on the buckling behavior of the cold-formed steel members;
5. the limit state or the governing buckling mode of cold-formed steel members;
6. the effect of support fixity on global buckling of cold-formed steel members.

The strength and stiffness required for bracing hot-rolled steel sections has been investigated by numerous researchers (Winter 1960, Yura 1995) based on experimental testing, analytical studies and feasible design considerations. Research has been conducted on the buckling phenomena of cold-formed steel subjected to axial compression by many researchers including Winter (1959), Miller (1990), Kwon and Hancock (1991), Miller and Pekoz (1994), Young and Rasmussen (1999), Schafer (2000), and Beshara and LaBoube (2001). The current research has been directed towards establishing the strength and stiffness requirements of the bracing and bridging requirements for cold-formed steel lipped cee-studs.

### 1.3 Scope of Research

The scope of this research is limited to determining the strength and stiffness requirements for cold-formed steel lipped cee-studs subjected to axial compression. The lipped cee-studs were tested to determine their axial load capacity in a manner consistent with a typical field installation. With this as a basis, the scope of the single column axial tests was:

1. Standard lipped cee-studs that are widely used in structural and non-structural wall assemblies were tested. The section nominal web depths were 3.625, 6.00, and 8.00 inches, the nominal thickness were 33, 43, 68 and 97 mil. The flange width of the 33 mil studs was 1.25 inches and the flange width of the other studs was 1.625 inches (1 mil = 1/1000 inches).
2. The lipped cee-studs were mounted in industry standard shallow track and attached with #10 self-drilling screws. The lengths of the cee-studs were 8 foot for all the single column tests.
3. The number of nodal brace points was limited to one, at the mid-height of the lipped cee-stud.
4. The support fixity was limited to a shallow track 1.25 inch deep and 12 inches long, attached to the stud with one self-drilling screws on each flange. The track was loosely fixed to the loading plates with two bolts.
5. The simulated bridging used in the single column axial load tests was comprised of high strength steel wires attached to the each flange on both sides of the web. Four wires were used to brace the cee-stud so that for any global buckling at least two brace wires would be effective.

The steel stud industry has employed the use of several typical bridging details for a number of years. The strength of typical bridging has been studied and previously reported (Beshara and LaBoube 2001). However, there is little published information available regarding as-constructed bracing demand. Based on previous testing, and because of the relatively low bracing force required to brace steel studs, bridging strength does not appear to be a significant concern. The most apparent criteria for the bridging

are the strength and stiffness of the connection of the bridging to the stud and the stiffness of the total bridging system. The scope of this experimental program involved:

- The bridging tests were limited to three types of typical industry bridging connections, namely screwed-screwed, welded-welded and direct-welded. In the first two types, a standard clip angle was used to secure the channel bridging to the web of the cee-stud. In the third type, the channel bridging was directly welded to the web punchout.
- The bridging was tested for its in-plane strength and out-of-plane torsional stiffness for all the stud sizes used in the single column axial tests. The load was applied with an actuator attached to the bridging at a distance away from the bridging to stud connection to avoid localized effects of load application.

While the stiffness required to develop the strength of the member will vary depending on whether the member is under axial compression or flexural loading, the actual physical stiffness of the bridging system is independent of the type of loading. Therefore, the stiffness of the bridging system (flexural or torsional stiffness) may be considered independently of the loading.

A general test procedure was developed such that the results of this research may be extended to other types of stud cross-sections, to determine the requirements of any type of bridging. Conventional bridging or nodal bracing was simulated in the single column axial load tests using steel wires attached to the stud flanges at mid-height. A range of brace stiffness, from less than 30 lbs/in. to greater than 4000 lbs/in., was simulated in the testing frame by using various diameters and lengths of high strength steel wire. Brace strength was determined from the cross-sectional area of the steel wire and the experimentally determined yield strength. The axial load, individual brace forces, axial shortening, and in-plane (weak axis) and out-of-plane (strong axis) lateral displacements at mid-height of the cee-stud were measured in each test.

The required bracing stiffness was experimentally determined by varying the brace stiffness for a given stud size and was based on the ability of the stud to develop the nominal axial compressive capacity as predicted by the provisions of AISI Cold-Formed Steel Specification (AISI 1996) including Supplement No. 1 (AISI 1999). The experimental results were compared to existing nodal bracing models, analytical prediction models, and the current column bracing provisions that are part of the 1999 AISC-LRFD Specification for Structural Steel Buildings (AISC 1999).

## CHAPTER 2 LITERATURE REVIEW

### 2.1 General

The use of cold-formed steel in building construction dates back to the 1850s, but cold-formed steel was not widely used until the 1940's (Yu 1991). It is used in constructing walls, slab-decks, beams, columns, storage-racks, and is typically found in small to medium rise structures. This wide application of cold-formed steel in building construction has required a comprehensive understanding of its behavior. The increased use of cold-formed steel as an alternative building material necessitated, in 1946, the first "Specification for the Design of Light Gage Steel Structural Members". Since then, there have been several revisions to the specification as well as design manuals with aids issued by American Iron and Steel Institute (AISI). In 1991, Load and Resistance Factor Design (LRFD) was introduced into the cold-formed steel specification. Today, the current specification edition is the North American Specification for Design of Cold-Formed Steel Structural Members (AISI 2001a).

While considerable research effort has been directed at the problem of bracing hot-rolled structural steel columns, little published information exists specifically addressing the bracing requirements for cold-formed steel columns. This chapter includes a comprehensive review of relevant work done in the field relating cold-formed steel members on – lateral beam bracing, sheathed bracing of wall studs, local and distortional buckling on channel sections, and eccentric loading on wall stud assemblies. Several

analytical models formulated by past researchers to determine the bracing strength and stiffness requirements for axially loaded compression members are also reviewed.

## 2.2 Buckling of Columns

The global buckling of columns has been studied since the 18th century. Even today, in spite of numerous investigations in past decades, research in this specialized field has by no means produced a complete understanding. Based on length and slenderness ratios, columns can be classified as long, intermediate and short. The slenderness ratio is a function of the ratio of effective length of the column and the radius of gyration of the column cross-section.

### 2.2.1 Elastic Buckling

The history of column theory dates back to 1744 when the Swiss mathematician Leonard Euler published the equation for the critical load or the buckling load of an axially loaded prismatic column, assuming that the material is linear and elastic. It is given by

$$P_e = \frac{\pi^2 EI}{L^2} \quad (2.1)$$

where E = Elastic modulus

I = Moment of inertia about the axis orthogonal to buckling plane

L = Unbraced length of the column

This equation is valid for loads acting through the centroidal axis on a perfectly straight column whose ends are perfectly pinned. In practice, it is impossible to realize such conditions, hence the equation serves as an upper bound solution to the buckling problem.



The above equation may be modified to calculate the buckling load for other end conditions by introducing an effective length factor (K). The modified equation is

$$P_e = \frac{\pi^2 EI}{(KL)^2} \quad (2.2)$$

where  $KL$  = effective length of the column

(length between points of zero curvature of the buckled shape)

Eq. 2.2 can be modified to calculate the critical buckling stress by dividing both sides by the cross-sectional area 'A' of the column and replacing the moment of inertia (I) by the second moment of area ( $A r^2$ ), where 'r' is the radius of gyration corresponding to the axis about which the moment of inertia is being computed. The elastic critical buckling stress is thus given by the equation

$$\sigma_e = \frac{\pi^2 E}{\left(\frac{KL}{r}\right)^2} \quad (2.3)$$

where  $\sigma_e$  = critical elastic buckling stress

This equation is applicable when the value of "E" does not change before buckling occurs, meaning the material is completely elastic at the instant of buckling.

### 2.2.2 Inelastic Buckling

In cases of intermediate and short columns, the elastic limit of the material is exceeded before buckling occurs. The modulus of elasticity 'E' hence becomes a function of the critical buckling stress, and to solve this Engesser put forth the Tangent Modulus theory, in 1889. Instead of the elastic modulus 'E', the tangent modulus ' $E_T$ ' was substituted into Eq. 2.3 to calculate the critical buckling stress. This was called the Euler-Engesser Equation and is given by

$$\sigma_e = \frac{\pi^2 E_T}{\left(\frac{K L}{r}\right)^2} \quad (2.4)$$

However, Considère recognized that an axially loaded column stressed beyond the proportional limit starts to bend, and the stresses on the concave side increase according to the compressive stress-strain curve of the material, whereas the stresses on the convex side decrease proportionally to the strain. In 1895, Engesser formulated the Double Modulus theory of buckling, with use of a reduced modulus 'E<sub>R</sub>' in place of the tangent modulus in the Euler-Engesser Equation (see Figure 2.). The reduced modulus is given by

$$E_R = \frac{E I_1 + E_T I_2}{I} \quad (2.5)$$

where  $I_1, I_2$ , represent the moment of inertia of the cross-sectional areas separated by the neutral axis as shown in Figure 2.1.

### 2.2.3 Local Buckling and Distortional Buckling

In calculating the strengths of elastic and inelastic columns, the stability criteria are based on the column as a whole. Other than prismatic sections, columns are made up of plate elements, which are subjected to compressive stresses when the column is loaded. The effect of these compressive stresses on slender plate elements may cause them to buckle locally, which leads to a part of the cross-section to reach its critical buckling stress and become ineffective in carrying the applied load. In local buckling, the instability arises due to a change of cross-sectional shape in a localized region and does not directly alter the overall configuration of the member as a whole (Shanley 1957).

Local buckling of individual compression elements can be calculated by two different approaches to facilitate design – one based on an effective width criterion, the other based on an average or reduced stress criterion. For each approach, the degree of the edge restraint influences the behavior. The cross-section elements are classified as edge-stiffened or unstiffened. An unstiffened compression element is one that is stiffened at only one edge parallel to the direction of applied stress. A stiffened compression element is stiffened at both edges parallel to the direction of applied stress (Galambos 1998). The effective width of locally buckled elements is given by

$$b_e = \frac{b(1 - 0.22/\lambda)}{\lambda} \quad (2.6)$$

where  $b_e$  = Effective width  
 $b$  = Flat width of plate element  
 $\lambda$  =  $(\sigma_e/\sigma_{cr})^{1/2}$   
 $\sigma_e$  = Maximum elastic stress  
 $\sigma_{cr}$  = Plate buckling stress defined by

$$\sigma_{cr} = \frac{\pi^2 Ek}{12(1 - \nu^2)} \left(\frac{t}{b}\right)^2 \quad (2.7)$$

$E$  = Elastic modulus of material  
 $k$  = Plate-buckling coefficient  
 ( $k = 4$  for stiffened elements,  $k = 0.425$  for unstiffened elements)  
 $t$  = Plate thickness  
 $\nu$  = Poisson's ratio

Distortional buckling, also called as “stiffener buckling” by Desmond, Pekoz and Winter in 1981, or “local-torsional buckling” by Sridharan in 1982, is a mode

characterized by rotation of the flanges at the flange/web junction in members with edge stiffened elements. Formulae for computing the elastic distortional buckling stress were provided by Lau and Hancock (1987). Strength tests of cold-formed channel sections, undergoing distortional buckling, were investigated by Kwon and Hancock (1991). The distortional mode of buckling occurs at longer half-wavelengths than local buckling and involves element displacements of the edge or intermediate stiffeners forming the section or of complete flanges (Galambos 1998). A historical review of distortional buckling was compiled by Schafer and Hancock (Schafer 2000). Distortional buckling of cold-formed steel columns was investigated by Schafer (2000) for a project sponsored by AISI. The investigation compares the design methods using the effective width approach and the direct strength approach and states design recommendations for AISI Specification. Teng (2002) extended the axially loaded column investigations by Lau and Hancock (1987) and examined distortional buckling of beam-columns.

### **2.3 Bracing Stiffness and Strength**

Zuk (1956) analytically derived the magnitudes of brace forces by solving the basic second order differential equation of equilibrium assuming elastic behavior of the compression member. It was determined by Zuk that the lateral force is a direct function of the initial crookedness and the critical buckling load. Eight different cases were considered with discrete or continuous lateral bracing on laterally loaded flexural members, axially loaded compression members and eccentrically loaded compression members, all with either fixed or pinned support conditions. Out of these eight cases, the first two are relevant to the present investigation and are summarized below

### 2.3.1 Column with Concentric Axial Load and an Immovable Point Support at Mid-height

In Figure 2.2 (Zuk 1956), the centroidal axis of the column is shown as a straight line passing through the top and bottom pin ends. The initial crookedness is defined by the following

$$y_0 = a \sin \left( \frac{x}{L} \right) \quad (2.8)$$

where  $a$  = Maximum amplitude at the center and is represented by a dashed line in the figure.

Due to the brace at mid-height, the column assumes a buckled shape as shown by the continuous line, and is defined as a function of ' $y_1$ ' and ' $y_2$ ' in the upper and lower halves of the column respectively. The curves ' $y_1$ ' and ' $y_2$ ' represent the additional displacements due to the applied load ' $P$ '. When the applied compressive load on the column, with a fully effective brace, reaches the critical elastic buckling load, given by

$$P_{cr} = \frac{4\pi^2 B_1}{L^2} \quad (2.9a)$$

the maximum brace force, ' $F_{max}$ ', is calculated from the second order differential equation of equilibrium, which reduces to

$$F_{max} = \frac{64\pi^2 B_1 a}{3L^3} \quad (2.9b)$$

where  $B_1$  = Flexural rigidity =  $E I$

$L$  = Length of column from the top pin end to the bottom pin end

$a$  = Amplitude of initial crookedness

It can be seen here that an initial crookedness of  $L/1000$ , shows that  $F_{\max}$  is 0.53% of the critical buckling load ' $P_{cr}$ '. As mentioned earlier, the equation for the brace force is a direct function of the initial crookedness of the column.

### **2.3.2 Column with Concentric Axial Load and an Elastic Lateral Support at Mid-height**

This case is the same as that derived by Winter (1947) and was included by Zuk for purpose of comparison. Winter analytically determined that for a concentrically loaded pin-ended column with mid-height elastic bracing, the brace force is about 2% of the critical load, ' $P_{cr}$ '.

Winter (1960) published the results of a simple analytical model to calculate the required bracing stiffness and strength for both beams and columns. It was found that both bracing strength and stiffness contribute to the critical buckling load of a compression member. Both forms of bracing, discrete and continuous, were considered in Winter's investigation. For an axially loaded column (see Figure 2.3 (Winter 1960)), a nodal brace at mid-height can increase its axial load capacity only if the brace is stiff enough to restrain the column from flexural buckling or flexural-torsional buckling. For a column with mid-height bracing, Winter considered that the unsupported length of the column to be half the overall length of the column. There is a minimum stiffness requirement to effectively brace a member laterally and this is defined as the ideal stiffness, and such bracing is called "full bracing". If an axially loaded column has an initial crookedness ' $d_0$ ', the required strength of the lateral brace increases with the magnitude of the imperfection, but the stiffness demand does not likewise increase. For the column with mid-height bracing shown in Figure 2.3 (Winter 1960), Winter obtained the required bracing stiffness as given by the equation

$$k_{\text{req}} = \frac{2 P_e}{L} \left( \frac{d_o}{d} + 1 \right) \quad (2.10a)$$

where  $L$  = Unbraced length of the column  
 $P_e$  = Euler's critical buckling load for a column of length,  $L$   
 $d_o$  = Amplitude of initial crookedness  
 $d$  = Additional displacement due to buckling

For an ideal column,  $d_o = 0$ , the above equation reduces to

$$k_{\text{ideal}} = \frac{2 P_e}{L} \quad (2.10b)$$

and the strength of the bracing is given by

$$S_{\text{req}} = \frac{2 P_e}{L} (d_o + d) \quad (2.11)$$

Winter also developed the required stiffness and strength for two, three and four symmetric brace points along the length of a column. It was recommended to take the value of  $d_o = 1/500$  or  $1/1000$  and that of  $d = L/250$  or  $L/500$ , depending on the type of cross-section (e.g. wide flange). This is because 'd' is the displacement at incipient failure and under design loads it would be less than half of the above values. Figure 2.4 (Winter 1960) shows the critical loads for elastically supported columns.

Plaut (1993) mathematically derived relations for elastic translational springs at arbitrary points along the length of a column with a pin support at the base and with either a pin support or a brace at the top of the column. Both perfect and imperfect columns were considered and the effect of span length, bracing stiffness and initial imperfection were determined. Plaut stated that for imperfect columns the deflections and the bracing forces tend to increase with the applied load.

If  $P = P_\infty$  then,

$$k = k_{id} \left( 1 + \eta \frac{d_o}{d} \right) \quad (2.12)$$

where for this case  $k_{id} = 16\pi^2 \frac{EI}{L^2}$

For  $P < P_\infty$ , and for a range of  $d_o/d$

$$k = \frac{4P}{L} \left( 1 + \eta \frac{d_o}{d} \right) \quad (2.13)$$

- where
- L = Length of column
  - P = Non-dimensional axial load as a fraction of  $P_\infty$
  - $P_\infty$  = Dimensional axial load for an infinitely stiff brace
  - $d_o$  = Initial deflection at location of the brace
  - d = Additional deflection at location of the brace due to buckling
  - $\eta$  = Dimensionless parameter

When  $\eta = 1.41$ , it gives the upper bound to the required stiffness. Figure 2.5(a), (b), (c) (Plaut 1993) shows the effect of bracing stiffness on the deflection ratio ( $d_o/d$ ), load ratio ( $P/P_\infty$ ), and bracing force to axial load ratio ( $F_1/P$ ), respectively.

Yura (1995) focused on simplicity and easy formulations for the bracing strength and stiffness required for bracing compression members. Relative, discrete, continuous, and lean-on bracing systems were considered in this work. Yura concluded that simply satisfying the strength requirement of 2% of applied compressive load might be detrimental if the bracing is too flexible to restrain displacement. Stiffness of the bridging also affects the behavior of the compression member. It was observed from column tests that the larger the stiffness of the bracing, the smaller was the measured



brace force. Yura proposed the ideal nodal brace stiffness,  $\beta_{ideal}$ , for an axially loaded column to be

$$\beta_{ideal} = \frac{[4 - 2/n]P_n}{L_b} \quad (2.14)$$

and the required brace strength, assuming an initial out-of-straightness of  $L/500$  to be

$$P_{brace} = 0.02 P_n \quad (2.15)$$

where  $L_b$  = Unbraced length  
 $P_{brace}$  = Minimum required brace strength  
 $P_n$  = Nominal axial capacity when the assumed brace stiffness is greater than or equal to  $\beta_{ideal}$   
 $n$  = Number of equally spaced intermediate brace locations  
 $\beta_{ideal}$  = Minimum required brace stiffness

Yura made the following recommendations for design

1. The brace stiffness should be equal to twice the ideal requirement to limit displacement; and
2. The brace strength should be 1% of the nominal capacity of the compression member at the ideal bracing

Figure 2.6 (Yura 1995) shows a plot of  $P_{cr}/P_e$  versus  $\beta L/P_e$  for several discrete bracing systems. The recommendations made by Yura were later incorporated into the American Institute of Steel Construction- Load and Resistance Factor Design Specification (AISC 1999).

Helwig and Yura (1999) conducted a finite element investigation of torsional buckling behavior of columns with lateral bracing located at different points on the cross-section. Their paper describes that many column-bracing details employed in steel construction do not prevent twist, and subsequently torsional buckling may control the

column capacity. Equations were developed for strength and stiffness requirements of bracing to control torsional buckling of doubly-symmetric sections. Connection details for torsional bracing were described and presented. For a doubly-symmetric section, the torsional buckling capacity of a compression member can be computed using Eq. 2.16 (Timoshenko and Gere 1961).

$$P_T = \frac{P_{ey}(d^2/4) + GJ}{r_x^2 + r_y^2} \quad (2.16)$$

When the locations of intermediate lateral restraint are offset from the centroid of the cross-section, the torsional buckling capacity is given by Eq. 2.17 when the offset lies in the plane of the web, and Eq. 2.18 when the offset lies along the strong axis.

$$P_T = \frac{P_{ey}[(d^2/4) + a^2] + GJ}{a^2 + r_x^2 + r_y^2} \quad (2.17)$$

$$P_T = \frac{P_{ey}[(d^2/4) + (I_x/I_y)b^2] + GJ}{b^2 + r_x^2 + r_y^2} \quad (2.18)$$

- where  $G$  = Shear modulus
- $I_x$  = Strong axis moment of inertia
- $I_y$  = Weak axis moment of inertia
- $J$  = Torsional constant
- $P_{ey}$  = Elastic flexural buckling load, based on a column length between points of zero twist (Eq. 2.19)
- $a, b$  = Distances to an axis away from centroidal axis
- $d$  = Distance between flange centroids
- $r_x, r_y$  = Strong-axis and weak-axis radii of gyration

$$P_{ey} = \frac{\pi^2 E I_y}{L_T^2} \quad (2.19)$$

E = elastic modulus

$L_T$  = unbraced length for torsion

Helwig used eight-node shell elements to model a W16x26 wide flange section. Shell elements were also used to model the braces, which consisted of angle sections. Torsional stiffness of the brace was determined by separate analysis (of the brace) by determining the rotation caused by a concentrated moment. Eigenvalue buckling analyses were conducted on straight columns to determine the stiffness requirements of the bracing. Imperfect columns were also considered in the analyses and were analyzed by accounting for the large displacements. Figure 2.7 (Helwig 1999) shows the effect of lateral restraint location on the brace behavior. It was determined that when the lateral bracing is at the centroid of the section and is adequate to control flexural buckling, the torsional bracing behavior is not sensitive to the lateral brace stiffness. Therefore, the recommended lateral brace stiffness is twice the ideal value when the lateral bracing is at the centroid and four times the ideal value when the lateral bracing is at the flange. The equations, formulated to determine the capacity of a compression member, may be found elsewhere (Helwig 1999).

Beshara and LaBoube (2001) conducted an experimental pilot study on lateral bracing of C-sections in flexure. In this investigation, typical industry bridging connections, along with two proprietary systems, were tested for the bracing requirements. It was found that the screw attached typical industry clip and the SPAZZER 5400™ spacer bar provided adequate bracing to achieve the computed moment capacity for all the 3-5/8 and 6 inch deep sections, but failed to provide adequate

bracing for the 8 inch deep sections. The STEEL Network BridgeClip™ provided adequate bracing to achieve the computed moment capacity for all the 3-5/8 and 6 inch 18 gauge sections, but failed to provide adequate bracing for the 6 inch-16 gauge and 8inch sections. Overall, it was found that the typical industry clip provided the highest resistance against rotation followed by the SPAZZER 5400™ and the STEEL Network BridgeClip™. Figure 2.8 (Beshara and LaBoube 2001) shows the three connections tested in the investigation. The observed failure was classified broadly as torsional-flexural buckling and individual tests indicate the actual mechanism of failure.

#### **2.4 Long Column Tests**

Miller (1990) conducted a series of tests on cold-formed steel cee studs at Cornell University. Individual column tests with a length of 8 foot were performed on studs with depths of 3-5/8 and 6 inch. Load was applied to the studs both concentrically and eccentrically with either pin end or fixed end conditions. Several of the studs were tested with one or more perforations in the web. Geometric imperfections were measured and considered when the experimental results were compared to the analytical results. No bridging or bracing was installed as part of the test set-up.

Additionally, Miller conducted wall assembly axial tests on 8 foot members spaced (typically) at 24 inch on-center and having depths of 3-5/8 and 6 inch (see Figure 2.9 (Miller 1990)). Bracing was applied to the wall members in one of three forms: continuous flat straps screwed to both flanges, continuous channel bridging installed through web perforations, and gypsum sheathing screwed to one of the flanges of the members. As in the individual long column tests, end conditions of the studs were either pin-ended or fixed. Miller noted that the use of flat strap bracing and channel bridging resulted in similar ultimate axial loads, while the presence of mid-height bridging

increased the load carrying capacity by at least 25% for 6 inch members and by at least 60% for 3-5/8" members, over those tested without any bridging or bracing.

Miller (1993) presented the results of effectiveness of the bracing for imperforated two stud wall assembly tests. The investigation found that for 6 inch, 20 gage studs, the predicted capacities were about 20% higher than the experimental results, where the predicted capacity was based on the AISI Specification's Cold-Formed Steel Design, (AISI 1986). This was because the AISI Specification considered the load to act through the centroid. When Miller calculated the effect of eccentric load acting through the gross centroids it was found that the predicted loads were conservative in most cases. Individual long column and flat-ended stud tests were also conducted. The flat-ended studs were fitted with short tracks on both the ends, prior to testing.

The effective length factors for the wall studs with and without mid-height bracing were determined for flexure and torsion, and the recommended values by Miller (1993) are

- Unbraced:  $K_x = K_y = K_t = 0.65$
- Braced at mid-height:  $K_x = 0.65$ ,  $K_y = K_t = 0.4$

#### **2.4 AISC-LRFD Specification**

The AISC-LRFD Specification, 3<sup>rd</sup> Edition (AISC 1999) contains provisions for the stability bracing of structural steel members and frames, in Chapter C3. There are two general types of bracing – relative bracing and nodal bracing. The relative brace system shown in Figure 2.10(a) (Figure C-C3.1, AISC 1999) consists of a diagonal and a strut that control the movement at one end of the unbraced length, A, with respect to the other end of the unbraced length, B. A nodal brace controls the movement only at the

particular brace point, as shown in Figure 2.10(b) (Figure C-C3.1, AISC 1999), without interaction with adjacent brace points.

The minimum bracing requirements as given in the AISC-LRFD Specification (AISC 1999), Chapter C3-3, for nodal bracing, are as follows

Required brace strength

$$P_{br} = 0.01P_u \quad (2.20)$$

Brace stiffness:

$$\beta_{br} = \frac{8P_u}{\phi L_b} \quad (2.21)$$

where  $P_u$  = Required compressive strength of the column

$L_b$  = Distance between braces

$\phi$  = 0.75

Recall that Winter (1958) recommended that the brace stiffness for frames, columns, beams be equal to twice the critical stiffness and this same recommendation has been adopted by the AISC-LRFD Specification (1999). The  $\phi = 0.75$  specified for all brace stiffness requirements is consistent with the implied resistance factor for the Euler column buckling. i.e.  $0.877 \times \phi_c = 0.75$ . The initial displacement also known as initial out-of-plumbness,  $\Delta_o$ , for the relative or nodal bracing is defined with respect to the distance between adjacent braces, as shown in Figure 2.11 (Figure C-C3.3, AISC 1999). The brace strength recommendations for frames, columns, and beam lateral bracing are based on an assumed  $\Delta_o = 0.002L$ , where  $L$  is the distance between adjacent brace points. The flexibility or ability of a brace connection to slip should be considered in the evaluation of the actual bracing system stiffness,  $\beta_{act}$ , as follows

$$\frac{1}{\beta_{act}} = \frac{1}{\beta_{conn}} + \frac{1}{\beta_{brace}} \quad (2.22)$$

where  $\beta_{conn}$  = Stiffness of the Connection

$\beta_{brace}$  = Stiffness of the brace

## 2.5 AISI Specification for Cold-Formed Steel

In case of concentrically loaded compression members, there are three limit states namely, (1) yielding, (2) overall column buckling (flexural, torsional, flexural-torsional buckling), and (3) local buckling of individual elements.

Flexural buckling occurs in a slender, axially loaded column about the either of the principal axes. The critical elastic buckling stress for a column is given by Eq. 2.3, which is discussed earlier. The Commentary on North American Specification for Design of Cold-Formed Steel (AISI 2001b) gives the equation for critical inelastic buckling stress as

$$F_{cr} = F_y \left( 1 - \frac{F_y}{4(F_{cr})_e} \right) \quad (2.23)$$

where  $E$  = Elastic modulus of steel

$F_y$  = Yield stress of the material

$(F_{cr})_e$  = Critical elastic buckling stress, given by Eq. 2.24

$$(F_{cr})_e = \left( \frac{\pi^2 E}{(KL/r)^2} \right) \quad (2.24)$$

$KL$  = Effective length of column

$r$  = Minimum radius of gyration

In the above equation, the critical buckling stress is directly proportional to the yield strength of the steel. For cold-formed steel compression members with large width-

to-thickness ratios, local buckling of individual component plates may occur before the applied load reaches the nominal axial strength determined by Eq. 4.4 (Section C4, AISI 2001) for locally stable columns, which is given as

$$P_n = A_g F_{cr} \quad (2.25)$$

where  $A_g$  = Full cross-sectional area of the compression member

$F_{cr}$  = Critical buckling stress, either elastic or inelastic

The interaction effect of the local and overall column buckling may result in a reduction of the overall column strength. In order to reflect the effect of local buckling on the reduction of column strength, the nominal axial strength is determined by the critical buckling stress and the effective area,  $A_e$ , instead of the full sectional area. The nominal axial strength of cold-formed steel compression members can be determined by the following equation

$$P_n = A_e F_{cr} \quad (2.26)$$

where  $A_e$  = Effective area at  $F_{cr}$

$F_{cr}$  = Critical buckling stress, either elastic or inelastic

However, Eq. 2.26 is limited to its applicability in case of singly symmetric or point symmetric sections. The design equations for calculating the inelastic and elastic flexural buckling stresses have been changed to those used in AISC-LRFD Specification (AISC 1999). The AISI Specification (2001a) gives the equations for critical buckling stress as

$$\text{For } \lambda_c \leq 1.5 \quad F_n = \left( 0.658^{\lambda_c^2} \right) F_y \quad (2.27)$$



$$\text{For } \lambda_c > 1.5 \quad F_n = \left[ \frac{0.877}{\lambda_c^2} \right] F_y \quad (2.28)$$

where  $F_n$  = Nominal flexural buckling stress

$$\lambda_c = \sqrt{F_y / F_e}$$

$F_e$  = Elastic flexural buckling stress calculated using Eq. 2.24

Consequently, the nominal axial compressive strength is given by

$$P_n = A_e F_n \quad (2.29)$$

The effective length factor,  $K$ , accounts for influence of restraint against rotation and translation at the ends of a column on its load carrying capacity. For concentrically loaded compression members, the recommended values of effective length factors are given in Figure 2.12 (AISI 1996).

For inelastic buckling, the critical torsional buckling stress is calculated according to Eqs. 2.27 and 2.28 by using  $\sigma_t$  instead of  $F_e$  in calculation of  $\lambda_c$ . In certain cold-formed steel cross-sections, the design strength is limited by the torsional buckling of columns. For relatively short members the elastic torsional buckling stress is given by,  $\sigma_t$ , calculated as follows

$$\sigma_t = \frac{1}{A r_o} \left[ G J + \frac{\pi^2 E C_w}{(K_t L_t)^2} \right] \quad (2.30)$$

where  $A$  = Full cross-sectional area

$C_w$  = Torsional warping constant

$G$  = Shear modulus

$J$  = Saint Venant's torsion constant of the cross-section

$K_t L_t$  = Effective length of twisting

$r_o$  = Polar radius of gyration of the cross-section about the shear center

In case of flexural-torsional buckling of a column, the column undergoes flexural buckling about one of the principal axes, with simultaneous torsional buckling about the shear center. This limit state is to be checked only when there is a chance of flexural-torsional buckling to occur. The governing elastic flexural-torsional buckling stress of a column is given by

$$F_e = \frac{1}{2\beta} \left[ (\sigma_{ex} + \sigma_t) - \sqrt{(\sigma_{ex} + \sigma_t)^2 - 4\beta \sigma_{ex} \sigma_t} \right] \quad (2.31)$$

where  $\sigma_{ex}$  =  $\pi^2 E / (K_x L_x / r_x)^2$  is the flexural buckling stress about the x-axis

$\sigma_t$  = torsional buckling stress

$\beta$  =  $1 - (x_o/r_o)^2$

The flexural-torsional buckling stress is always lower than the Euler stress  $\sigma_{ex}$  for flexural buckling about the axis of axis of symmetry. For inelastic buckling, the torsional buckling stress is given by Eq. 2.27.

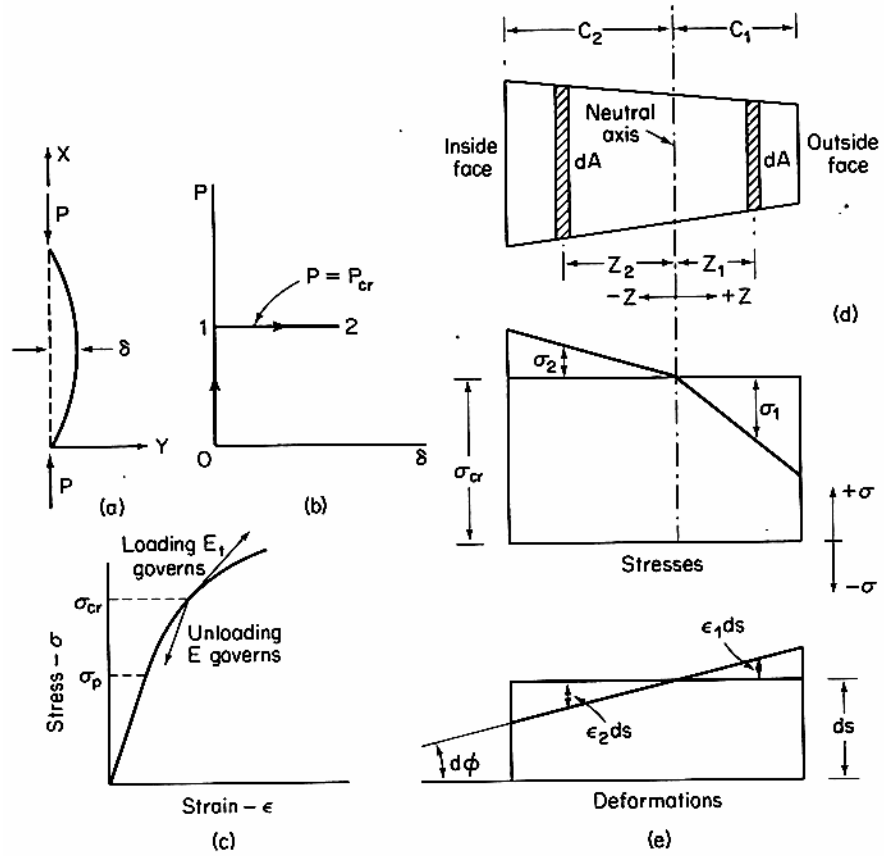


Figure 2.1 Reduced Modulus Theory (Figure 1-21, Chajes 1974)

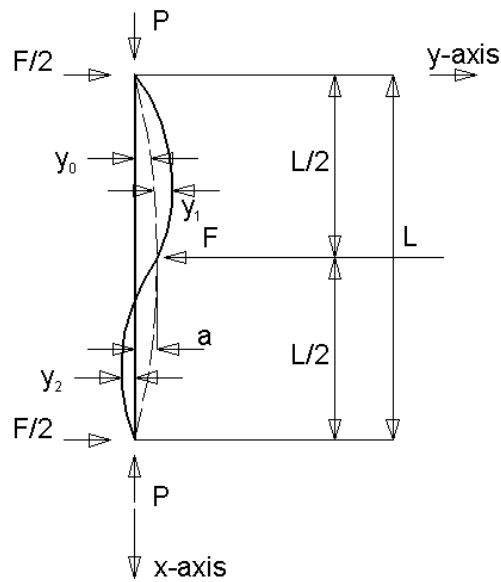


Figure 2.2 Imperfect Column with Immovable Mid-height Bracing

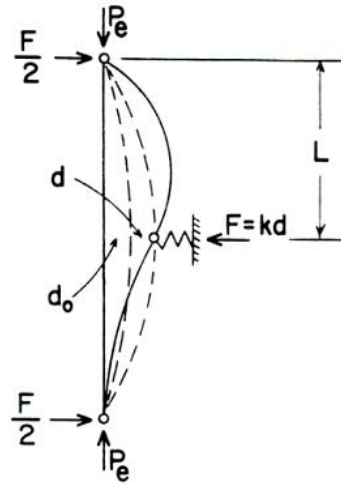


Figure 2.3 Imperfect Column with Elastic Mid-height Bracing

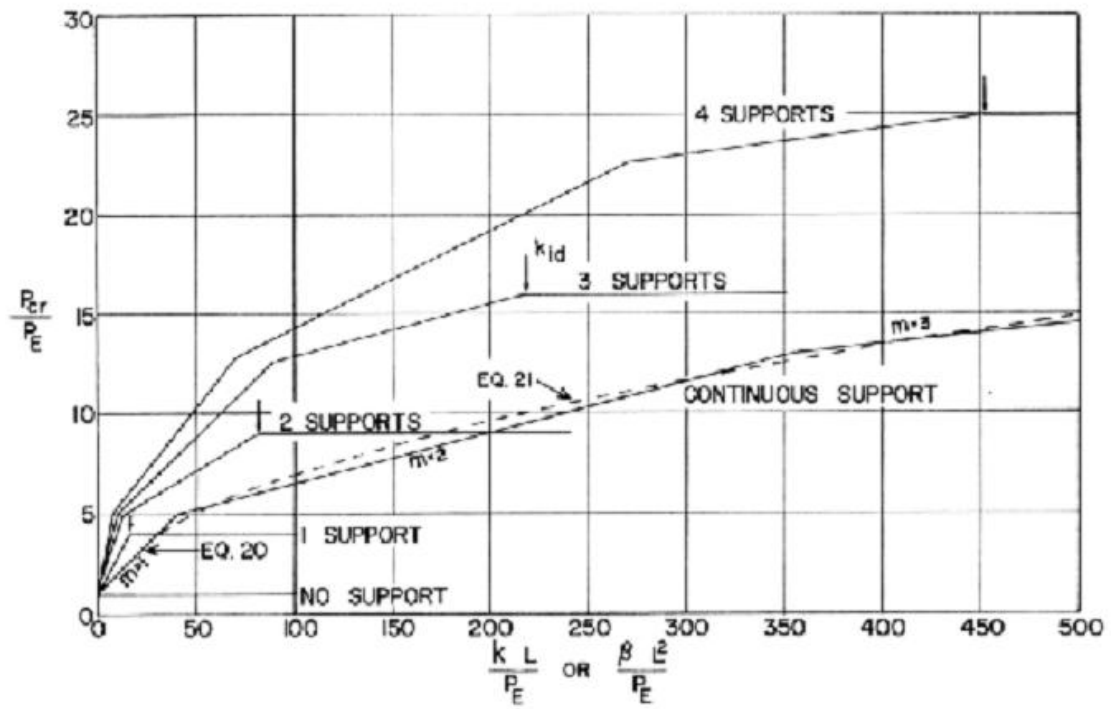
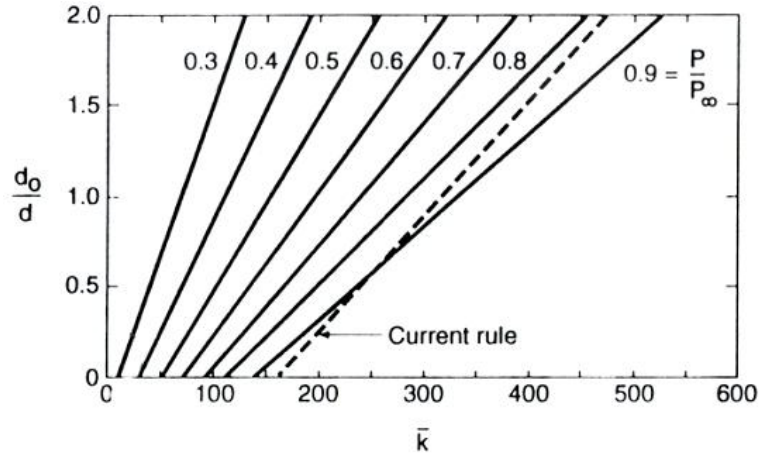
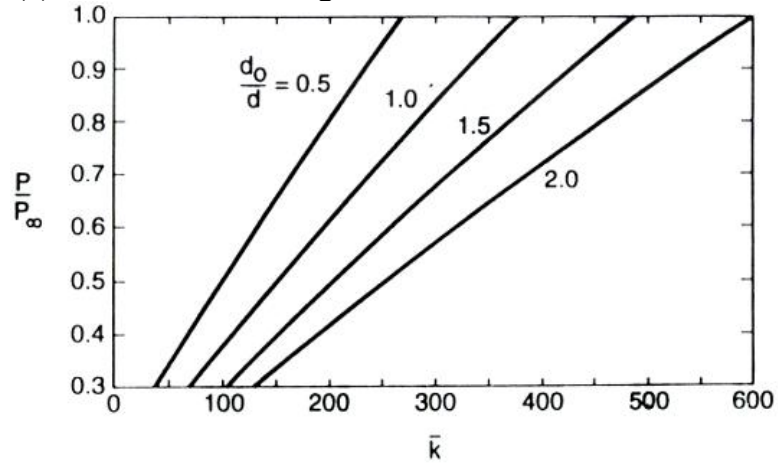


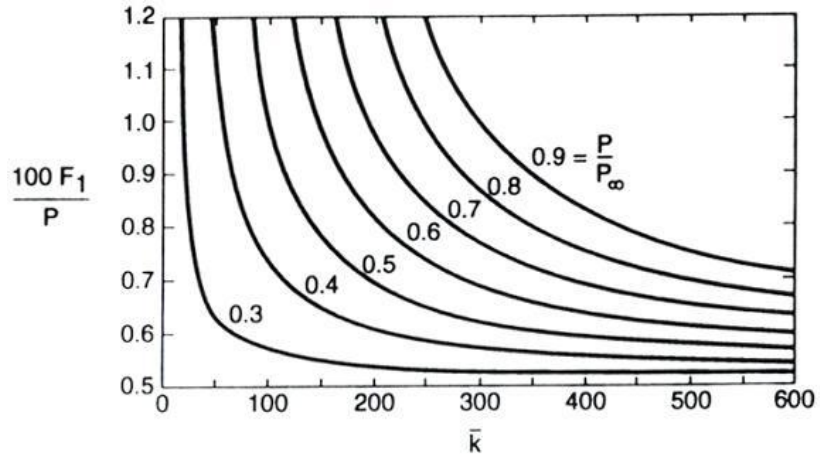
Figure 2.4 Critical Loads for Elastically Supported Columns



(a) Effect of Bracing Stiffness on Deflection Ratio  $d_0/d$



(b) Effect of Bracing Stiffness on Load Ratio  $P/P_\infty$



(c) Effect of Bracing Stiffness on Bracing Force as Percentage of Axial Load for given Load Ratio  $P/P_\infty$

Figure 2.5 Effect of Bracing Stiffness

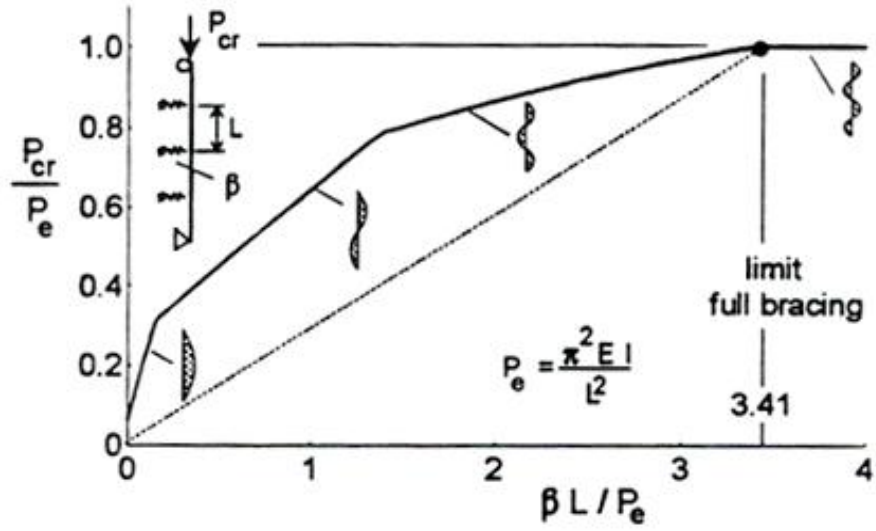


Figure 2.6  $P_{cr}/P_e$  versus  $\beta L/P_e$  for a Discrete Bracing

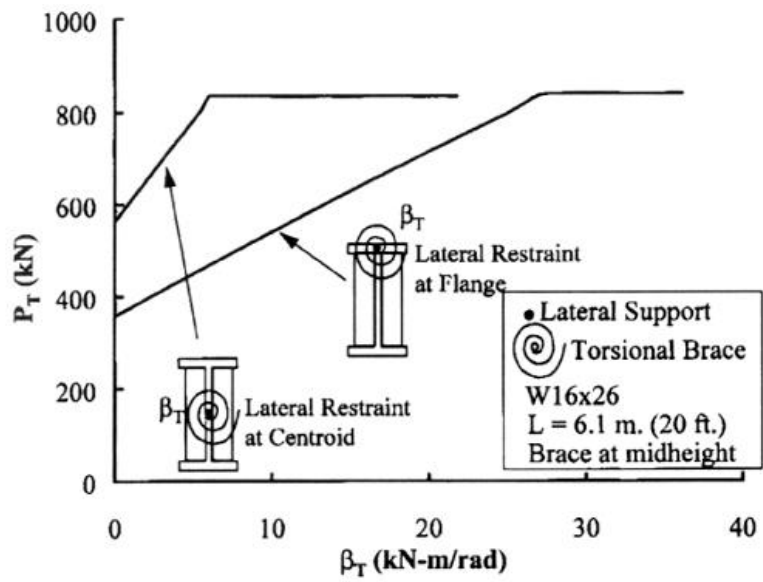


Figure 2.7 Effect of Lateral restraint location on Brace behavior

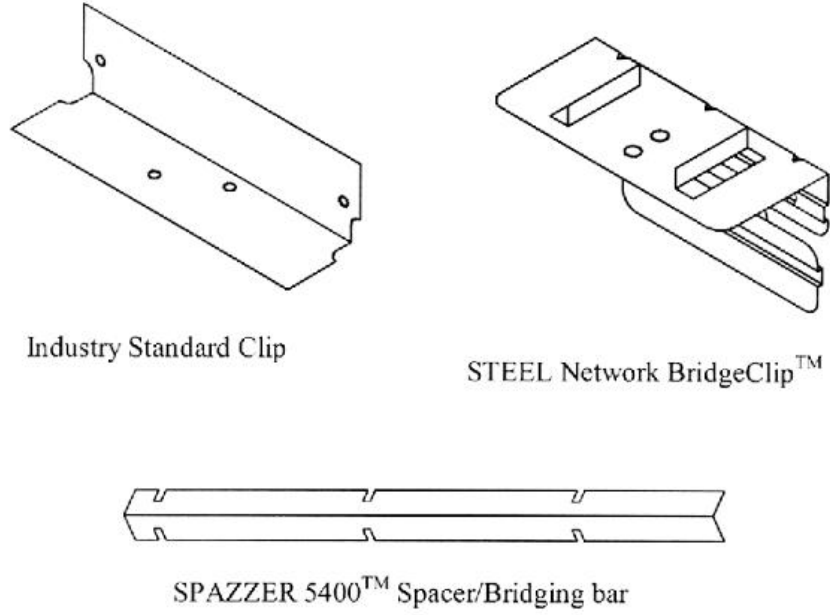


Figure 2.8 Bracing Connection Clips

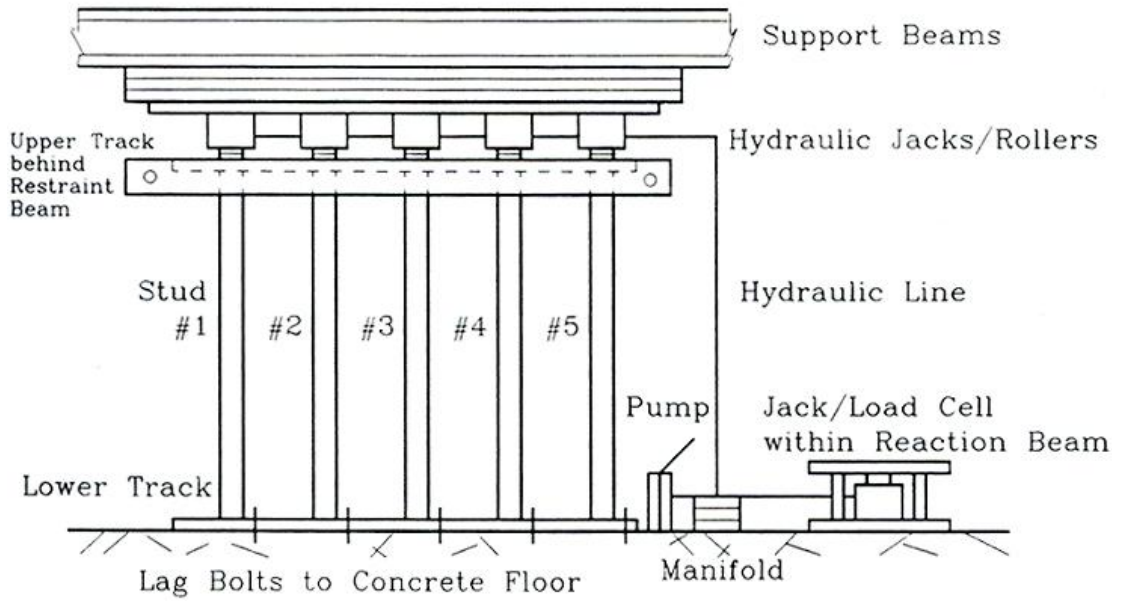


Figure 2.9 Wall Assembly test setup

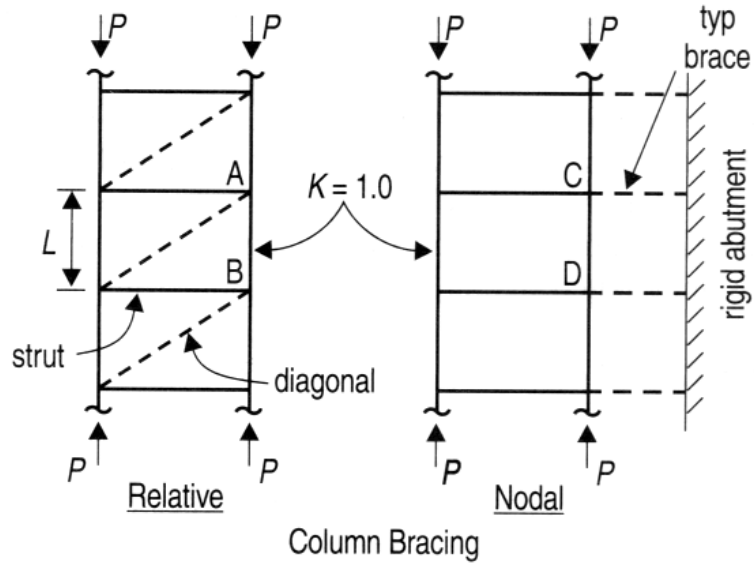


Figure 2.10 Types of Bracing (a) Relative Bracing and (b) Nodal Bracing

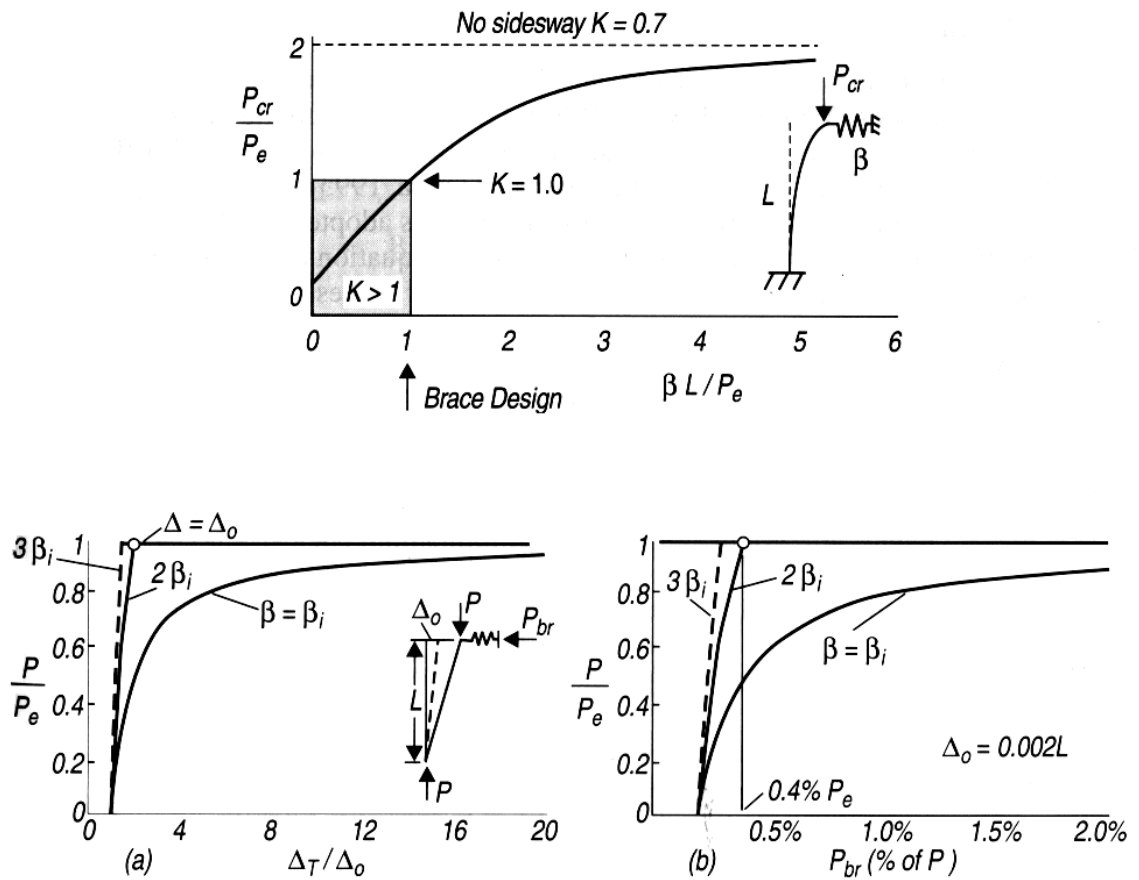


Figure 2.11 Effect of Initial Out-of-Plumbness



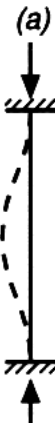
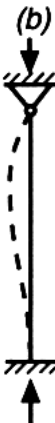
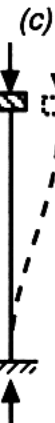

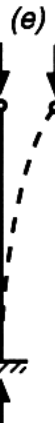
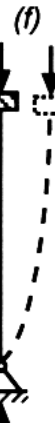




Buckled shape of column is shown by dashed line						
Theoretical K value	0.5	0.7	1.0	1.0	2.0	2.0
Recommended K value when ideal conditions are approximated	0.65	0.80	1.2	1.0	2.10	2.0
End condition code	   	Rotation fixed, Translation fixed Rotation free, Translation fixed Rotation fixed, Translation free Rotation free, Translation free				

Figure 2.12 Effective Length Factors for Concentrically Loaded Columns

## CHAPTER 3 DESCRIPTION OF EXPERIMENTAL STUDY

The purpose of this chapter is to give a brief description of the objectives of the experimental program, the material properties and measured as-built geometry of the test specimens, the test setups, and the test procedures employed in the project. The experimental program consisted of two phases of testing:

- Phase-I: Axial Compression Tests
- Phase-II: Bridging Tests

### **3.1 Introduction**

Phase-I of the experimental program consisted of examining the behavior of single axially loaded cee-studs, with and without mid-height bracing (or bridging). In Phase-II, typical industry bridging was examined for its strength and stiffness by in-plane and out-of-plane loading. Description of the test setups and the test procedures are given in Sections 3.6 and 3.7. Three types of typical industry bridging were tested:

- Type-1: Screwed-Screwed (SS), where the bridging channel and clip angle are screwed to each other and to the web of the cee-stud.
- Type-2: Welded-Welded (WW), where the bridging channel and clip angle is fillet welded to each other and to the web of the cee-stud.
- Type-3: Direct-Welded (DW), where the bridging channel is directly welded to the web of the cee-stud.

The stud specimens tested had nominal web depths of 3.625, 6.00, and 8.00 inches with specified thicknesses ranging from 33 mils to 97 mils. The 33 mil, 43 mil, and 68 mil studs were manufactured by Steel Construction Systems, Orlando, FL and the 97 mil

studs were manufactured at the Wildwood, FL plant of Dietrich Metal Framing Inc., Pittsburgh, PA. The mechanical properties of the stud material used to fabricate the test specimens were determined by tension coupon tests. The as-built dimensions and geometric imperfections of the fabricated test specimens were recorded and this data was utilized in the calculation of the resistance properties of each specimen.

### 3.2 Objectives of Experimental Tests

The main objectives of the experimental study are summarized as follows:

- To investigate the behavior of cold-formed steel cee-studs with and without mid-height lateral bracing by testing a range of studs, subjected to axial compression while providing different bracing stiffnesses and strengths
- To investigate the strength and stiffness of the lateral bridging over the same range of studs subjected to in-plane and out-of-plane loading
- To provide the experimental data for determining the minimum bracing requirements of cold-formed steel cee-studs subjected to axial compression

### 3.3 Material Properties of Test Specimens

A series of standard 2 inch gage length ASTM tension tests were performed on coupons cut from the web material of the cee-studs. The dimensions of a typical tension coupon are shown in Figure 3.1. The nomenclature used to identify the group of cee-stud to which the coupon belonged was represented as:

TC DDDS FFF-TT

where TC = Tension coupon  
 DDD = Overall stud depth  
 (362 = 3.62 inch, 600 = 6.00 inch, and 800 = 8.00 inch)  
 S = Lipped stud section  
 FFF = Flange width (125 = 1.25 inch, 162 = 1.62 inch)  
 TT = Nominal sheet thickness (mils, 1 mil = 0.001 inch)

The tension tests were performed in accordance with ASTM E8-01e2 (ASTM 2001) on a 60 Kip capacity Tinius-Olsen testing machine. The applied load was measured through a load cell and the gage elongation of each coupon was measured using two extensometers, one fixed on the front and the other on the back of the tension coupon. The applied load and the corresponding elongation data was used to plot the stress-strain relationship. From the stress-strain plot, the yield and ultimate stresses were determined as per ASTM E8-01e2 (ASTM 2001). The elastic modulus of the material was not determined by testing and was assumed to be equal to 29500 ksi (AISI 1996). For each cee-stud section, a minimum of three tests were performed. The average values of yield and ultimate stresses were calculated based on either the 0.2% offset method for a continuously yielding material or the autographic diagram method for materials exhibiting discontinuous yielding. Figure 3.2 shows the 0.2% offset method for determination of the yield stress, and Figure 3.3 shows the autographic diagram method for determination of the yield stress. The tension coupon test results are summarized in Table 3.1.

### 3.4 As-Built Dimensions of the Test Specimens

For the single axial load tests, 8 foot long cee-studs were cut from the as-delivered 20.5 foot long members. For the bridging tests, short 3.5 foot stubs were cut from the 20.5 foot long members. For the purposes of this study, each tested stud was identified using a modified Steel Stud Manufacturers Association (SSMA) nomenclature:

DDD S FFF-TT-KKKK

where DDD = Overall stud depth  
 (362 = 3.62 inch; 600 = 6.00 inch; 800 = 8.00 inch)

S = Lipped stud section

FFF	=	Flange width (125 = 1.25 inch; 162 = 1.62 inch)
TT	=	Nominal steel thickness (mils; 1 mil = 0.001 inch)
KKK	=	Axial stiffness of one brace wire in pounds per inch

For each specimen, the cross-section dimensions were measured at three locations along the length of each 8 foot stud with a digital micrometer and tabulated in Table 3.2. The tables provide the stud designation and corresponding brace stiffness used in the testing along with the measured dimensions A through F and thicknesses ‘ $t_a$ ’ through ‘ $t_e$ ’ (see Figure 3.4) for each test specimen. The (+) and (-) symbols denote the direction of camber and sweep of the stud. The camber and sweep were measured as described in Section 3.5.1.

### **3.5 Measured Geometric Imperfections of the Test Specimens**

The geometric imperfections of a stud can be categorized as a global imperfection and/or a local imperfection as described in Sections 3.5.1 and 3.5.2.

#### **3.5.1 Global Imperfections**

The bow/sweep and camber of the studs were measured with a digital micrometer to a least count of 0.005 inch. A nylon monofilament line was stretched from one end to the other end of a stud and then was clamped tight. The out-of-straightness of each flat surface of a stud was measured at mid-height. The distance from the string to the surface of the stud was the initial global imperfection for the stud and tabulated in Table 3.3. The measured out-of-straightness of each stud was found to be within the permissible values as stated, which is 1/32 inches per foot for both bow and camber. The permissible values are found in the Standard Specifications for Load Bearing Steel Studs ASTM C955-01 (ASTM 2001) and for Nonstructural Steel Framing Members ASTM C645-00 (ASTM 2000). The measured cambers were negligible in all the tested specimens except for the

600S162-43 series where it ranged from 0.0 to a maximum of 0.065 inches, or  $L/1500$ . The sweep measurements were more significant as these might directly influence the axial behavior of the cee-studs during testing. The measured sweep ranged from 0.0 to 0.04 inches, or  $L/2400$  for the 362S162-43 and 600S162-43 series; from 0.0 to 0.075 inches, or  $L/1300$  for the 600S162-97 series; and from 0.0 to 0.14 inches, or  $L/700$  for the 362S162-68 series. No geometric imperfection measurements were made of the 800S162-97 series studs. In a few studs there was an initial twist over its length but it would disappear when the bottom end was plumbed with the top end while setting up for a compression test. A note was made of the initial twist, but the degree of twist was not measured.

### **3.5.2 Cross-Sectional Imperfections**

The as-built out-to-out measurements of the cross-section of a stud showed that it was neither symmetric nor of uniform thickness. Also, the intersecting corners of the flange-lip and the web-flange junctions were typically right angular. However, the cross-section was considered to be mono-symmetric and of uniform thickness for calculation purposes. It was observed that in some of the studs the punchout were offset from the web centerline by as much as  $1/8$  inch, and this was documented along with the test data. The average cross-sectional measurements of each of the test specimen series are given in Tables 3.4 and 3.5. In order to calculate the gross cross-section area, the radius of the bend was taken as the maximum of  $3/32$  inches or two times the base-metal thickness, based on the SSMA Manual (SSMA 2001). The studs were fabricated from galvanized coated steel. The base metal thickness was calculated by subtracting a thickness of two mils from the average of the measured values of thickness.

### **3.6 Test Setup and Test Procedure for Single Column Axial Load Tests**

A total of 37 studs were tested in this phase of the experimental study. Each stud was tested in a 400 Kip, screw driven Riehle Universal Testing Machine. The test setup and test procedure for the single column axial load tests is described below.

#### **3.6.1 Test Specimens of Single Column Axial Load Tests**

To simulate actual field installation conditions, each stud was mounted in standard track of type “T DDD 125-43” (where T = track, DDD = depth of stud, 1-1/4 inch flange, 43 mil thickness). Figure 3.5 shows a stud attached to the track with a single #10 self-drilling screw on each flange. The track was then mounted to end bearing plates with two 0.150 inch diameter bolts to simulate attachment to a concrete support or other structural member using 0.144 inch diameter drive pins. Figure 3.5(a) shows the top of the stud attached to the end bearing plate being held in position against the movable crosshead of the Riehle Universal Testing Machine. Figure 3.5(b) shows the bottom of the stud attached to the other end bearing plate that sits just above another plate holding a 150 Kip axial load cell in place and resting on the fixed platen of the testing machine.

#### **3.6.2 Test Frame for Single Column Axial Load Tests**

An adjustable frame attached to the Riehle testing machine was used to hold the flexural-torsional bracing system in place. Figure 3.6 is an overall view of the test frame and its accompanying instrumentation. The mid-height lateral bracing was simulated using steel wires of varying diameters and lengths. As indicated in the figure, the wires were attached to the corners of the flanges of the test specimens using #10 screws. The brace wires terminated at the S-Beam load cells, which were used to measure the tension force in the brace wires during the testing.

### **3.6.3 Instrumentation for Single Column Axial Load Tests**

Five load cells and six linear potentiometers were used to measure the loads and displacements for each single axial compression test for the braced stud specimens. Figure 3.7 shows the locations of the instruments mounted on the test frame. Four S-Beam load cells (Load Cells 1, 2, 3, 4) were used to measure the brace forces in the brace wires. A 150 kip capacity load cell (Load Cell 5) was used to measure the axial load at the base of the stud. The minor axis lateral displacement of a stud was measured by a complementary set of four linear potentiometers (LINEAR POTS 1, 2, 3, 4) positioned directly adjacent to the individual brace wires that made up the lateral bracing system. The major axis lateral displacement was measured at mid-height, by a single linear potentiometer (LINEAR POT 5) located along the minor axis attached to the south flange of a stud. Axial shortening of a stud was measured along the north flange of the test specimen parallel to the longitudinal axis of a stud (LINEAR POT 6). Figure 3.8 shows a close-up view of the stud cross-section at mid-height that shows the attachment points of the bracing wires to their corresponding load cells: A-NE BRACE (BF-1), B-SE BRACE (BF-2), C-NW BRACE (BF-3), and D-SW BRACE (BF-4).

### **3.6.4 Test Procedure of Single Column Axial Load Tests**

Each cee-stud was fixed in the Riehle Universal Testing Machine with the tracks bolted to the top crosshead and bottom base plate and was plumbed along both the strong and weak axis prior to testing. The measuring instruments, described in Section 3.6.2 were connected to an electronic data acquisition system to collect and display the run-time data. The tests were conducted under displacement control since the Riehle is a mechanically screw-driven testing machine, which allowed the studs to be loaded at a rate of approximately 5 to 20 lbs/sec to ensure a static response to the applied load.



Initially, each stud was loaded up to an axial load of 200 lbs to 500 lbs then unloaded. At this time all the instrumentation was checked and balanced. This preliminary loading and unloading cycle also ensured proper seating of the specimen in the Riehle UTM. During the continued loading, the buckling behavior of the stud was observed and photographs were taken at notable points and at certain load levels. Failure was considered to have occurred when the stud could no longer carry additional load or significant axial or cross-sectional deformation of the stud was observed and recorded. The stud was then unloaded and the test was then terminated.

### **3.7 Test Setup and Test Procedure for Bridging Tests**

A total of 54 specimens were tested in this phase of the experimental study to evaluate the strength and stiffness of typical industry bridging. The tests were conducted on 3.5 foot long cee-stud sections. As previously stated, three types of typical industry bridging were tested. The specimens were divided into two groups based on the direction of loading namely, in-plane loading and out-of-plane loading. Twenty-eight specimens were tested in the out-of-plane loading group while twenty-six specimens were tested in the in-plane loading group.

#### **3.7.1 Test Specimens of Bridging Tests**

The 3.5 foot long cee-stud sections were cut from the 20.5 foot long studs such that the elevation to the center of the web punchout was maintained at 23 inches. The test specimens were identified using a modified SSMA nomenclature:

DDD S FFF-TT-N CC

where DDD = Overall stud depth  
(362 = 3.62 inch; 600 = 6.00 inch; 800 = 8.00 inch)

S = Lipped stud section

FFF	=	Flange width (125 = 1.25 inch; 162 = 1.62 inch)
TT	=	Nominal steel thickness (mils; 1 mil = 0.001 inch)
N	=	Number of the test specimen in each series of stud
CC	=	Bridging connection type (SS, WW, DW)

Figure 3.9(a) through (c) show the types of bridging connections tested and they are described below:

**3.7.1.1 Screwed-Screwed (SS) Connection:** The clip angle was first screwed to the bridging channel with two #10 self-drilling screws, as shown in Figure 3.9(a) and Figure 3.10. Position of the screws on the clip angle was marked and then it was centered on the centerline of the web at a height of 23 inches from the bottom. The clip angle was then screwed to the web of the stud. This connection type was called Screwed-Screwed (SS).

**3.7.1.2 Welded-Welded (WW) Connection:** The bridging channel was welded at its flange-web junction to the clip, as shown in Figure 3.9(b). The clip angle was then positioned along the centerline of the web and fillet welded on the edges of the in-line leg. The bridging channel was slid through the punch out and then fillet welded to the outstanding leg of the clip angle. The welding specifications used were – Metal alloy: ER7056, Heat: 1026° F, Gas shielding: Argon-CO<sub>2</sub> (75%-25%). This connection type was called Welded-Welded (WW).

**3.7.1.3 Direct-Welded (DW) Connection:** The bridging channel was slid through the web punchout and then the flanges were welded to the web of the stud, as shown in Figure 3.9(c). The weld specification used was same as in Type-2 connection. This connection type was called Direct Welded (DW).

### 3.7.2 Test Fixture for Bridging Tests

The test fixture used to secure the specimens for the bridging tests is shown in Figure 3.11(a). Figure 3.12(a) and (b) are schematic plan views of the test fixture positioned for the out-of-plane and in-plane bridging tests, respectively, while Figure 3.13 and Figure 3.14 show an overall view of each experimental test setup. The fixture consists of a Specimen Mounting Frame (see Figure 3.11(a)) and an Actuator Armature (see Figure 3.11(b)). The load was applied to the bridging channel by a manually operated screw-driven actuator, fixed to the Actuator Armature (see Figure 3.11 through Figure 3.14). The Specimen Mounting Frame was used to secure the cee-stud in place and to isolate the web portion of the specimen (see Figure 3.11(a)). One end of the actuator was connected to an S-beam load cell, and the other end was connected to the vertical channel of the Actuator Armature by a 3/4 inch diameter SAE Grade 5 bolt. The Actuator Armature was bolted to the web of C8x11.5. The channel section was welded to top flange of a W8x24 whose bottom flange was bolted to the test fixture base plate. A plate-coupler was introduced between the bridging and the S-beam load cell at Point A (see Figure 3.11 and Figure 3.12), that allowed the load to be transmitted to the bridging channel through the plate-coupler by a 3/8 inch diameter SAE Grade 8 bolt. The joint between the actuator and the vertical channel of the Actuator Armature was free to rotate horizontally, while the joint between the plate-coupler and the bridging channel was free to rotate vertically. All members and connections were checked prior to the commencement of any testing to verify that the limit state of the loading system would be at the bridging connection and not at any of the components of the test fixture. A shear test was performed on the 3/8 inch diameter bolt, the design strength of the plate coupler was calculated based on its as-built measurements, and the weld strength used to fabricate

the plate-coupler was checked. For the out-of-plane load tests, a 500 lb load cell was used and for the in-plane load tests, a 10 Kip load cell was used. This change was necessary since the strength predictions for the in-plane tests were found to be beyond the safe working range of the 500 lb load cell.

### **3.7.3 Instrumentation**

The instruments used for the out-of-plane loading tests are shown in Figure 3.15 and for the in-plane loading tests in Figure 3.16. For both the loading conditions, three linear string type potentiometers were used to capture the spatial movement of Point A on the bridging where it is connected to the load actuator, each measuring the X, Y and Z displacements, respectively. Five linear potentiometers located as shown in Figure 4.44 were used to measure the displacement of the bridging connection and the stud web, two on the front side (LP-1, LP-2), two on the back side (LP-3, LP-4), and an additional one on the back side (LP-5) located approximately one foot above the location of the bridging connection to the stud web. For the SS type connection, LP-1 and LP-2 were attached to the screw heads to measure the pullout of the screws, while LP-3 and LP-4 were attached on the back to measure the movement of the web plate just below the screws. The measurements recorded by LP-5 showed that at locations removed from the connection the web is unaffected by the loading. For the WW type connection, LP-1 and LP-2 were attached at relatively the same location as in SS type connection, but to measure the horizontal movement of the vertical leg of the clip angle. For the DW type connection, LP-1 and LP-2 were attached at relatively the same location as in SS type connection, but to measure the horizontal movement of the stud web.

### **3.7.4 Out-of-Plane Loading Test Procedure**

The specimen mounting-frame and the Actuator Armature were aligned and anchored to the floor (see Figure 3.11). In this setup, the Actuator Armature was placed perpendicular to the centerline of the bridging channel, with the armature centerline passing through Point A. The test specimen was placed in the specimen mounting-frame and aligned horizontally and vertically. Figure 3.13 shows an overall view of the specimen in the test fixture, and Figure 3.15(a) shows a view of the connection between the bridging channel and the actuator. The specimen was secured on the front and on the back by four rigid hot-rolled steel members, to isolate the web for testing. To maintain the same spatial position of Point A for all the tests, it was triangulated and the locations of the linear string type potentiometers were adjusted to achieve an orthogonal coordinate system to a reasonable accuracy of 0.10 inch. The actuator arm was rotated at approximately 20 to 25 cycles per minute, manually. As the load-displacement curve started to soften and the connection started to lose its rigidity. The connection eventually failed when it could not carry the applied load, by attaining any of the failure states described in Chapter 4.

### **3.7.5 In-Plane Loading Test Procedure**

The specimen mounting-frame and the Actuator Armature were placed in line with the bridging channel of the stud specimen and anchored to the floor (see Figure 3.12). The test specimen was placed in the specimen mounting-frame and aligned horizontally and vertically. The specimen was then secured on the front and on the back by four rigid hot-rolled steel members, to isolate the web for testing. Figure 3.13 shows the overall view of a specimen in the test fixture, and shows a view of the connection between the

bridging channel and the load actuator. The actuator arm was turned at approximately one-half a revolution per second until the bridging failed.

Table 3.1 As-built Material Properties from the Tension Coupon Tests

Specimen ID						Yield Stress (0.2% offset)	Upper Yield Stress	Lower Yield Stress	Ultimate Stress
TC	D	S	B	t	ID	Ksi	ksi	ksi	ksi
TC	362	S	125	33	1	-	47.26	46.40	54.68
TC	362	S	125	33	2	48.51	49.17	48.59	55.88
TC	362	S	125	33	3	48.55	49.17	49.40	55.89
Average						48.53	48.53	48.13	55.48
TC	362	S	162	43	2	46.65	46.90	46.43	57.62
TC	362	S	162	43	3	46.73	46.84	46.13	57.64
TC	362	S	162	43	4	47.98	48.31	47.22	58.60
TC	362	S	162	43	5	46.80	47.83	47.25	58.94
Average						47.04	47.47	46.76	58.20
TC	362	S	162	68	2	50.12	51.91	51.72	66.62
TC	362	S	162	68	3	51.75	51.78	51.24	67.34
TC	362	S	162	68	4	54.15	54.35	53.96	69.43
Average						52.01	52.68	52.30	67.80
TC	600	S	125	33	1	23.82	-	-	45.22
TC	600	S	125	33	3	26.97	-	-	45.56
TC	600	S	125	33	5	26.73	-	-	44.93
TC	600	S	125	33	7	18.61	-	-	35.70
TC	600	S	125	33	8	-	-	-	36.88
Average						24.03	-	-	45.24
TC	600	S	162	43	2	45.12	45.48	44.06	53.03
TC	600	S	162	43	3	46.65	47.49	48.37	55.65
TC	600	S	162	43	4	46.75	47.28	45.86	55.65
TC	600	S	162	43	5	46.43	47.79	47.16	55.18
Average						46.24	47.01	46.36	54.88
TC	600	S	162	43	3a	50.27	50.81	50.63	59.21
TC	600	S	162	43	4a	50.34	51.58	51.24	59.56
Average						50.30	51.19	50.94	59.38
TC	600	S	162	97	3a	60.40	60.70	59.23	70.38
TC	600	S	162	97	3b	61.10	62.05	59.31	70.28
TC	600	S	162	97	4	59.10	59.87	58.30	69.96
Average						60.20	60.87	58.94	70.21
TC	800	S	162	43	1	-	40.65	40.20	55.03
TC	800	S	162	43	3	-	40.50	40.20	54.47
TC	800	S	162	43	4	-	40.88	40.30	55.20
Average						-	40.68	40.23	54.90
TC	800	S	162	97	1	42.12	45.62	44.39	66.79
TC	800	S	162	97	3	43.32	44.55	44.51	68.00
TC	800	S	162	97	4	42.06	47.01	46.56	67.69
Average						42.50	45.73	45.15	67.49

Table 3.2 As-Built Cross-Sectional Dimensions of Test Specimens

Stud Designation					Target Brace Stiffness	Average As-Built Measurements										
						Lip	Flange	Web	Flange	Lip	Web	Lip	Flange	Web	Flange	Lip
						A	B	C	D	E	F	ta	tb	tc	td	te
D	S	B	t	ID	lbs/in.	in.	in.	in.	in.	in.	in.	in.	in.	in.	in.	in.
362	S	125	33	1	200	0.252	1.317	3.613	1.259	0.209	3.589	0.033	0.039	0.034	0.034	0.032
362	S	125	33	2	400	0.252	1.316	3.613	1.258	0.205	3.584	0.036	0.035	0.033	0.035	0.032
362	S	125	33	3	100	0.251	1.321	3.616	1.258	0.206	3.603	0.036	0.036	0.034	0.036	0.034
362	S	125	33	4	100	0.253	1.318	3.616	1.259	0.208	3.593	0.034	0.035	0.033	0.035	0.032
362	S	125	33	5	0	0.251	1.319	3.612	1.256	0.203	3.589	0.031	0.036	0.034	0.035	0.032
362	S	125	33	6	100	0.250	1.318	3.612	1.256	0.204	3.597	0.032	0.035	0.034	0.035	0.031
362	S	125	33			0.252	1.318	3.613	1.258	0.206	3.590	0.033	0.036	0.034	0.035	0.032
362	S	162	43	1	0	0.541	1.637	3.562	1.603	0.531	3.547	0.044	0.042	0.042	0.042	0.044
362	S	162	43	2	200	0.530	1.606	3.563	1.642	0.538	3.541	0.045	0.043	0.043	0.043	0.043
362	S	162	43	3	800	0.536	1.640	3.563	1.607	0.534	3.540	0.044	0.042	0.042	0.043	0.044
362	S	162	43	4	400	0.528	1.602	3.569	1.639	0.538	3.541	0.042	0.042	0.042	0.042	0.042
362	S	162	43			0.534	1.621	3.564	1.623	0.535	3.542	0.044	0.042	0.042	0.043	0.043
362	S	162	68	2	1000	0.526	1.628	3.642	1.706	0.539	3.631	0.0717	0.070	0.070	0.070	0.072
362	S	162	68	3	500	0.546	1.701	3.638	1.629	0.524	3.633	0.074	0.070	0.070	0.070	0.072
362	S	162	68	4	750	0.542	1.705	3.635	1.630	0.536	3.635	---	0.069	0.069	0.069	0.069
362	S	162	68	5	0	0.543	1.703	3.636	1.629	0.523	3.634	0.076	0.068	0.068	0.068	0.073
362	S	162	68			0.540	1.684	3.638	1.649	0.530	3.633	0.074	0.069	0.069	0.069	0.071



Table 3.2 (Continued) As-Built Cross-Sectional Dimensions of Test Specimens

Stud Designation					Target Brace Stiffness	Average As-Built Measurements										
						Lip	Flange	Web	Flange	Lip	Web	Lip	Flange	Web	Flange	Lip
D	S	B	t	ID	lbs/in.	A	B	C	D	E	F	ta	tb	tc	td	te
						in.	in.	in.	in.	in.	in.	in.	in.	in.	in.	in.
600	S	125	33	1	200	0.206	1.243	6.022	1.307	0.243	5.999	0.032	0.032	0.030	0.032	0.032
600	S	125	33	2	0	0.205	1.247	6.019	1.309	0.245	6.004	0.031	0.030	0.031	0.030	0.031
600	S	125	33	3	60	0.208	1.247	6.019	1.305	0.246	6.008	0.031	0.030	0.030	0.031	0.031
600	S	125	33	4	30	0.210	1.248	6.019	1.308	0.242	6.008	0.032	---	0.031	---	0.033
600	S	125	33			0.207	1.246	6.020	1.307	0.244	6.005	0.032	0.031	0.031	0.031	0.032
600	S	162	43	1	250	0.531	1.603	5.994	1.592	0.536	5.993	0.041	0.044	0.044	0.044	0.042
600	S	162	43	2	75	0.526	1.612	6.017	1.596	0.534	6.041	0.042	0.044	0.044	0.044	0.042
600	S	162	43	4	500	0.533	1.595	6.036	1.616	0.530	6.068	0.044	0.045	0.044	0.044	0.042
600	S	162	43	5	30	0.531	1.596	6.026	1.612	0.529	6.052	0.044	0.044	0.044	0.044	0.042
600	S	162	43	6	0	0.528	1.616	6.034	1.598	0.535	6.066	0.043	0.044	0.044	0.044	0.043
600	S	162	43	6a	0	0.536	1.707	5.984	1.609	0.535	6.092	0.044	0.046	0.046	0.046	0.045
600	S	162	43			0.530	1.604	6.021	1.603	0.533	6.044	0.043	0.044	0.044	0.044	0.042
600	S	162	97	1	1000	0.544	1.652	6.069	1.675	0.610	---	0.100	0.104	0.099	0.110	0.102
600	S	162	97	2	1500	0.533	1.665	6.065	1.671	0.562	---	0.103	0.102	0.100	0.107	0.106
600	S	162	97	3	500	0.557	1.656	6.106	1.658	0.580	---	0.099	0.102	0.101	0.103	0.099
600	S	162	97	4	160	0.527	1.649	6.077	1.673	0.576	6.063	0.100	0.104	0.100	0.105	0.105
600	S	162	97	5	0	0.542	1.648	6.091	1.683	0.584	6.106	0.100	0.101	0.101	0.101	0.102
600	S	162	97			0.541	1.654	6.082	1.672	0.582	6.084	0.100	0.103	0.100	0.105	0.103

Table 3.2 (Continued) As-Built Cross-Sectional Dimensions of Test Specimens

Stud Designation					Target Brace Stiffness	Average As-Built Measurements										
						Lip	Flange	Web	Flange	Lip	Web	Lip	Flange	Web	Flange	Lip
D	S	B	t	ID	lbs/in.	A	B	C	D	E	F	t <sub>a</sub>	t <sub>b</sub>	t <sub>c</sub>	t <sub>d</sub>	t <sub>e</sub>
						in.	in.	in.	in.	in.	in.	in.	in.	in.	in.	in.
800	S	162	43	2	75	0.537	1.597	7.912	1.604	0.530	---	0.042	0.043	0.043	0.043	0.042
800	S	162	43	3	150	0.535	1.598	7.925	1.605	0.533	---	0.042	0.043	0.043	0.043	0.043
800	S	162	43	4	0	0.533	1.597	7.929	1.608	0.532		0.043	0.043	0.043	0.043	0.043
800	S	162	43	5	300	0.528	1.606	7.920	1.597	0.532	---	0.042	0.043	0.044	0.044	0.041
800	S	162	43			0.533	1.599	7.921	1.603	0.532	---	0.042	0.043	0.043	0.043	0.042
800	S	162	97	1	1000	0.562	1.631	8.053	1.670	0.659	---	0.101	0.102	0.102	0.103	0.103
800	S	162	97	2	500	0.651	1.649	8.048	1.647	0.561	---	0.102	0.103	0.103	0.103	0.102
800	S	162	97	3	0	0.553	1.629	8.041	1.650	0.661	---	0.101	0.103	0.104	0.103	0.103
800	S	162	97	4	2100	0.656	1.647	8.033	1.632	0.556	---	0.100	0.105	0.103	0.104	0.101
800	S	162	97			0.605	1.639	8.044	1.650	0.609	---	0.101	0.103	0.103	0.103	0.102

Table 3.3 Initial Geometric Imperfections

Stud Designation					Target Brace Stiffness	Initial Imperfection		
						Camber		Sweep
						B	D	C
D	S	B	t	ID	lbs/in.	in.	in.	in.
362	S	125	33	1	200	0	0	0
362	S	125	33	2	400	0	0	0
362	S	125	33	3	100	0	0	0
362	S	125	33	4	100	0	0	0
362	S	125	33	5	0	0	0	0
362	S	125	33	6	100	0	0	0
362	S	162	43	1	0	0	0	0
362	S	162	43	2	200	0	0	0
362	S	162	43	3	800	0	0	0.01
362	S	162	43	4	400	0.01	0.02	0
362	S	162	68	2	1000	0	0	-0.187
362	S	162	68	3	500	0	0	-0.155
362	S	162	68	4	750	0	0	0.14
362	S	162	68	5	0	0	0	0.1
600	S	125	33	1	200	0	0	0.1
600	S	125	33	2	0	0	0.07	0.13
600	S	125	33	3	60	0	0	0.12
600	S	125	33	4	30	0	0	0.075
600	S	162	43	1	250	0	0	0.04
600	S	162	43	2	75	0	0	0.03
600	S	162	43	4	500	0.055	0.045	0
600	S	162	43	5	30	0.055	0.053	0
600	S	162	43	6	0	0.065	0.065	0
600	S	162	43	6a	0	0	0	-0.036
600	S	162	97	1	1000	---	---	---
600	S	162	97	2	1500	---	---	---
600	S	162	97	3	500	---	---	---
600	S	162	97	4	160	0	0	0.075
600	S	162	97	5	0	0	0	0.015
800	S	162	43	2	75	0	0	0.09
800	S	162	43	3	150	0	0	0.11
800	S	162	43	4	0	0	0	0.11
800	S	162	43	5	300	0	0.12	0
800	S	162	97	1	1000	---	---	---
800	S	162	97	2	500	---	---	---
800	S	162	97	3	0	---	---	---
800	S	162	97	4	2100	0	0	0.12

Table 3.4 Average As-Built Geometric Dimensions of Each Stud Series

Stud Designation				Clear O/O Dimensions						Average Width	
				Lip	Flange	Web	Flange	Lip	Web	Lip	Flange
				A	B	C	D	E	F		
D	S	B	t	in.	in.	in.	in.	in.	in.	in.	in.
362	S	125	33	0.2515	1.3175	3.6131	1.2577	0.2058	3.5904	0.2287	1.2876
362	S	162	43	0.5335	1.6212	3.5643	1.6229	0.5352	3.5423	0.5344	1.6220
362	S	162	68	0.5396	1.6842	3.6377	1.6485	0.5304	3.6329	0.5350	1.6664
600	S	125	33	0.2071	1.2462	6.0197	1.3073	0.2439	6.0045	0.2255	1.2768
600	S	162	43	0.5298	1.6042	6.0213	1.6028	0.5328	6.0439	0.5313	1.6035
600	S	162	43a	0.5363	1.7070	5.9842	1.6092	0.5352	6.0920	0.5358	1.6581
600	S	162	97	0.5405	1.6539	6.0816	1.6717	0.5824	6.0843	0.5615	1.6628
800	S	162	43	0.5330	1.5994	7.9213	1.6033	0.5316	---	0.5323	1.6014
800	S	162	97	0.6053	1.6388	8.0436	1.6498	0.6091	---	0.6072	1.6443

Table 3.5 Average As-Built Geometric Dimensions of Each Stud Series

Stud Designation				Thickness						Radius of Bend	Base Metal Thickness	Internal Radius
				Lip	Flange	Web	Flange	Lip	$t_{avg}$			
				$t_a$	$t_b$	$t_c$	$t_d$	$t_e$		R	$t_{net}$	$R_{int}$
D	S	B	t	in.	in.	in.	in.	in.	in.	in.	in.	
362	S	125	33	0.0333	0.0360	0.0336	0.0348	0.0318	0.0339	0.0938	0.0319	0.07781
362	S	162	43	0.0437	0.0424	0.0425	0.0425	0.0432	0.0429	0.0938	0.0409	0.07332
362	S	162	68	0.0735	0.0691	0.0691	0.0693	0.0714	0.0705	0.1409	0.0685	0.10669
600	S	125	33	0.0316	0.0307	0.0307	0.0308	0.0315	0.0310	0.0938	0.0290	0.07923
600	S	162	43	0.0427	0.0441	0.0442	0.0443	0.0423	0.0435	0.0938	0.0415	0.07299
600	S	162	43a	0.0442	0.0458	0.0460	0.0460	0.0447	0.0453	0.0938	0.0433	0.07209
600	S	162	97	0.1002	0.1027	0.1004	0.1053	0.1028	0.1023	0.2045	0.1003	0.15440
800	S	162	43	0.0421	0.0431	0.0431	0.0430	0.0422	0.0427	0.0938	0.0407	0.07340
800	S	162	97	0.1008	0.1031	0.1029	0.1031	0.1021	0.1024	0.2048	0.1004	0.15458

Note: Radius of Bend = max [(2  $t_{avg}$ ), 3/32"], Clark's tables. Internal Radii = (Radius of Bend -  $t_{net}$  / 2)

Base Metal Thickness = [ $t_{avg}$  - 2 mils for galvanizing]

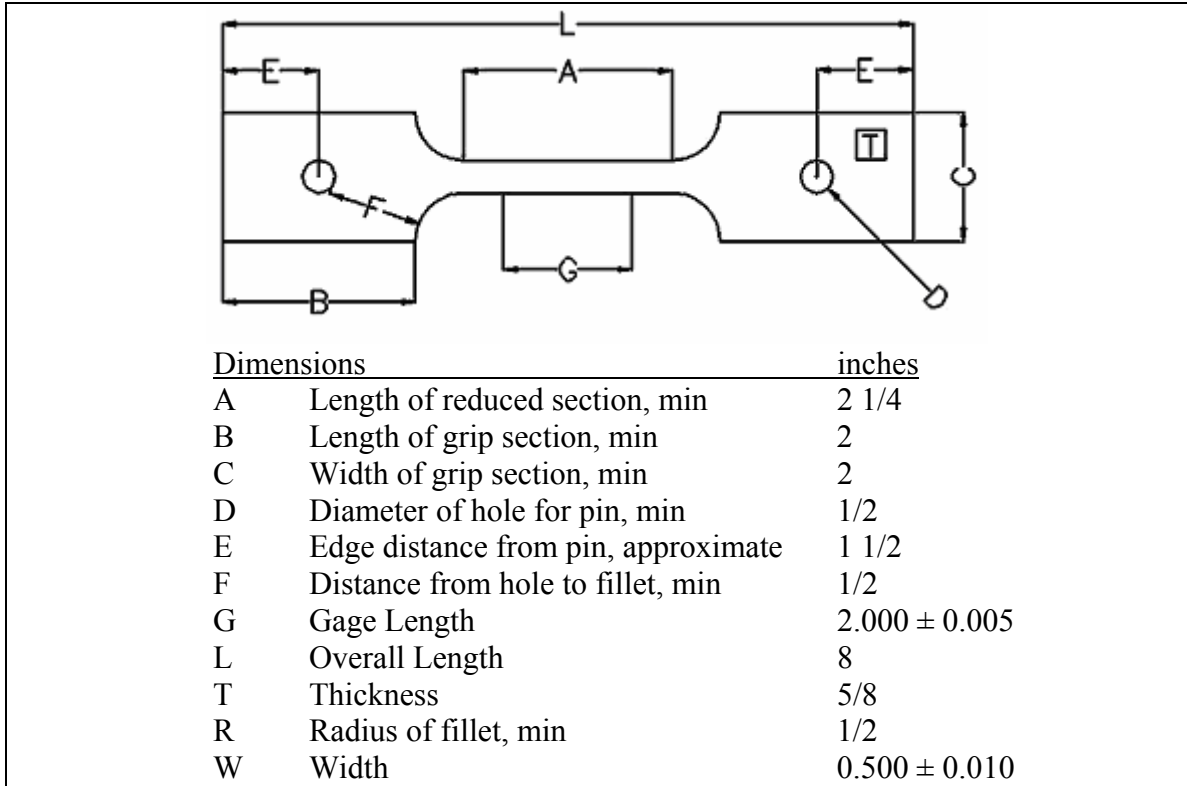


Figure 3.1 Dimensions of a Typical Tension Coupon

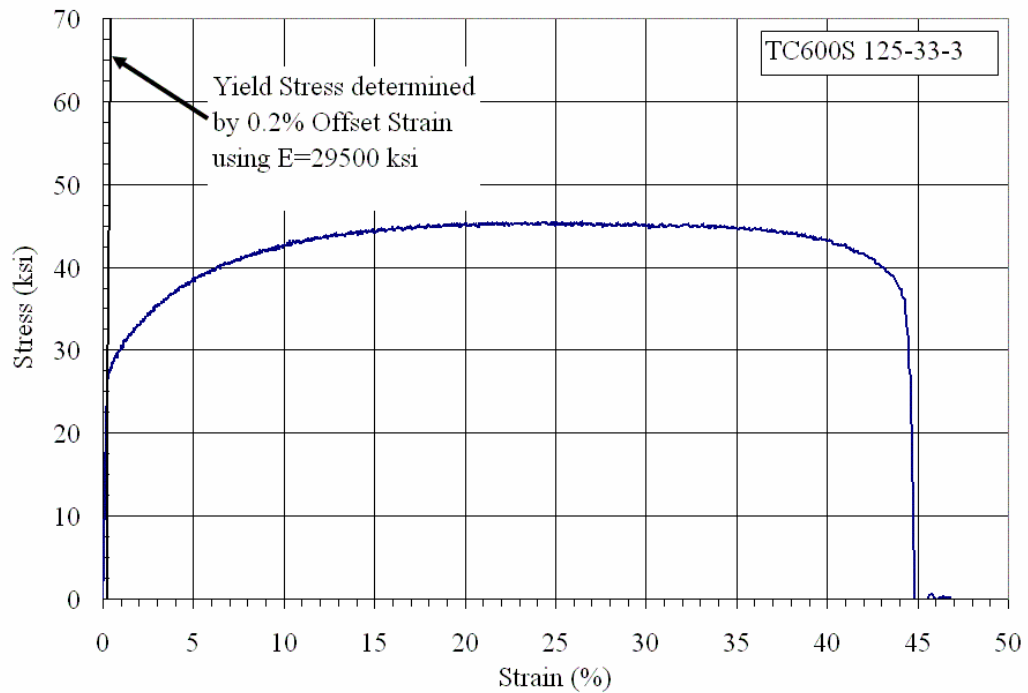


Figure 3.2 Offset Method for Determining Yield Stress

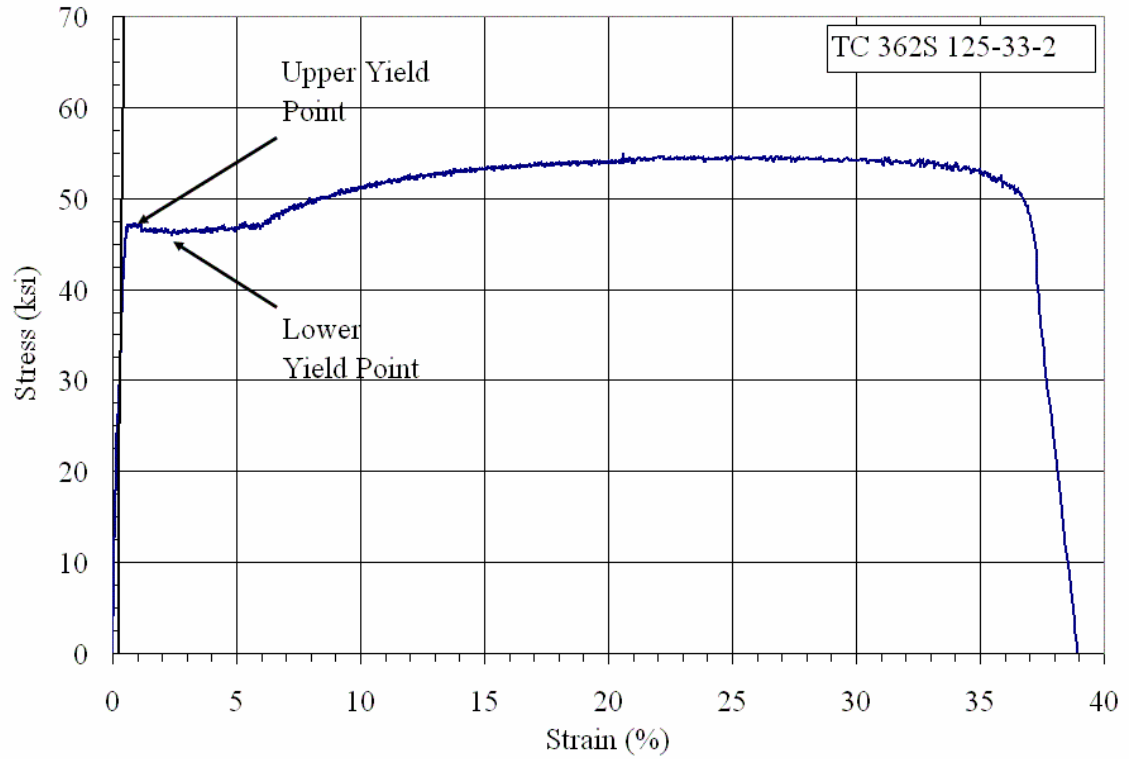


Figure 3.3 Autographic Diagram Method for Determining Yield Stress

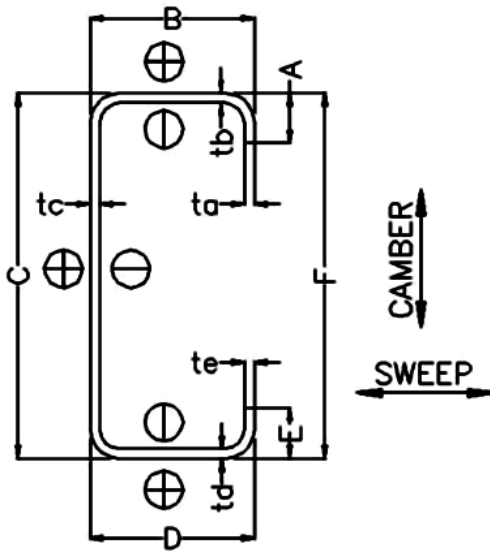


Figure 3.4 Typical Cross-Section of a Cee-Stud



Figure 3.5 Connection of Cee-Stud and Track (a) at Top, (b) at Bottom

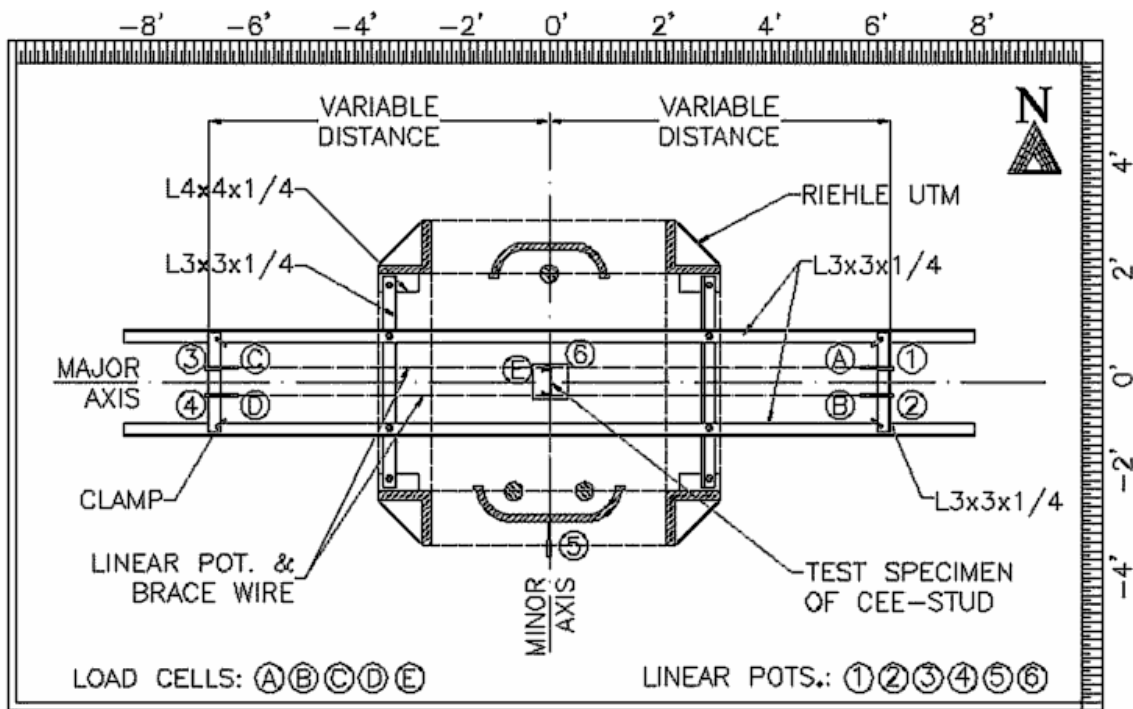


Figure 3.6 Plan View of Single Column Axial Test Setup in the Riehle Universal Testing Machine

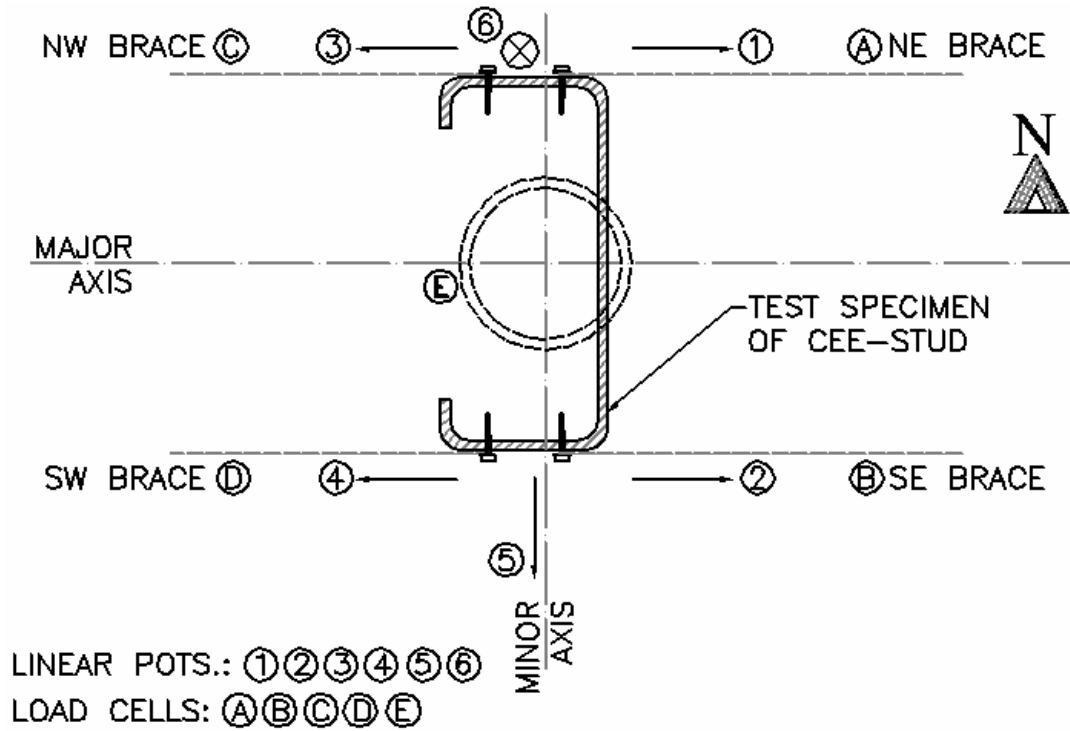


Figure 3.7 Schematic Mid-height Bracing and Instrumentation Locations on Test Specimens

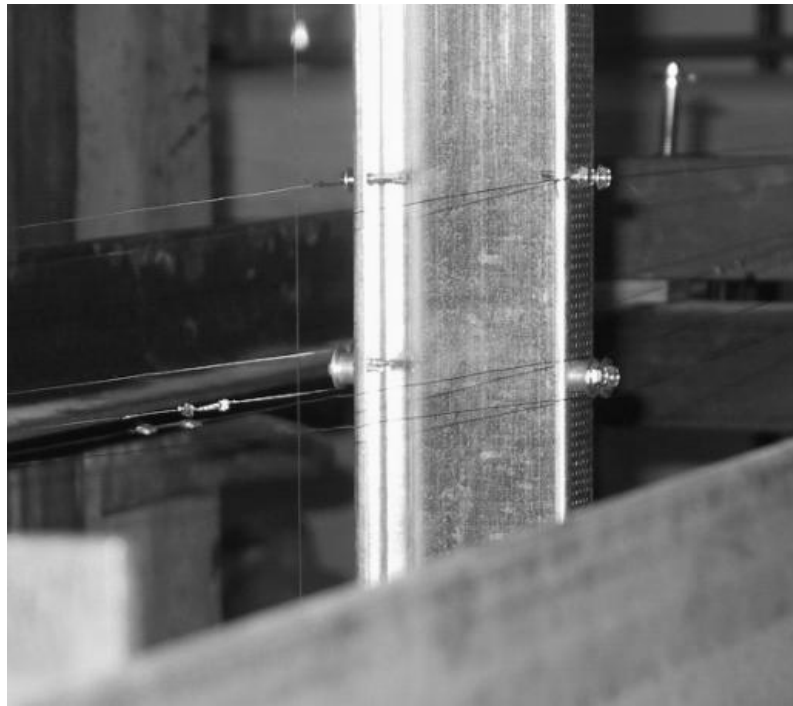


Figure 3.8 Close-up View of the Location of Brace-Wires and Instrumentation at Mid-height of the Cee-Stud. (Screws at the bottom are location of looped brace-wires, and Screws at the top are location of the Linear Potentiometers)



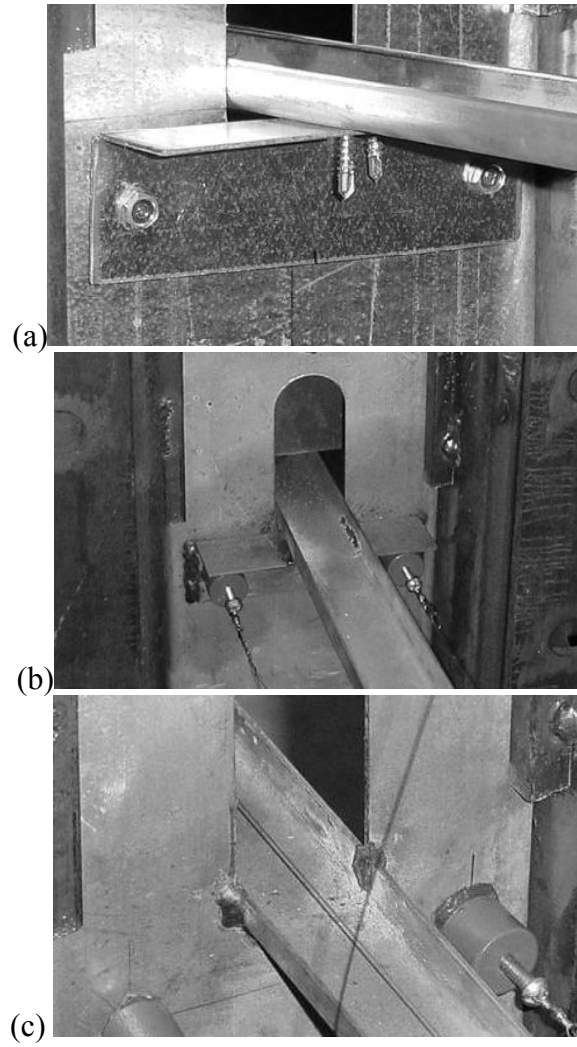


Figure 3.9 Types of Bridging Connections (a) SS (b) WW and (c) DW

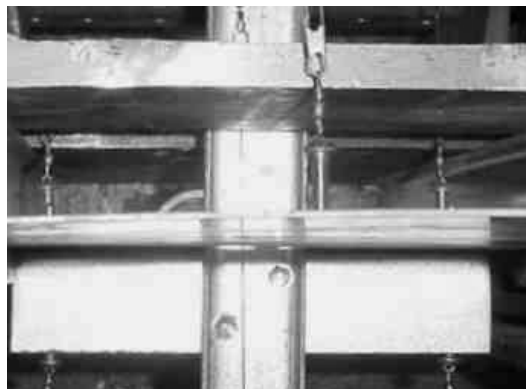
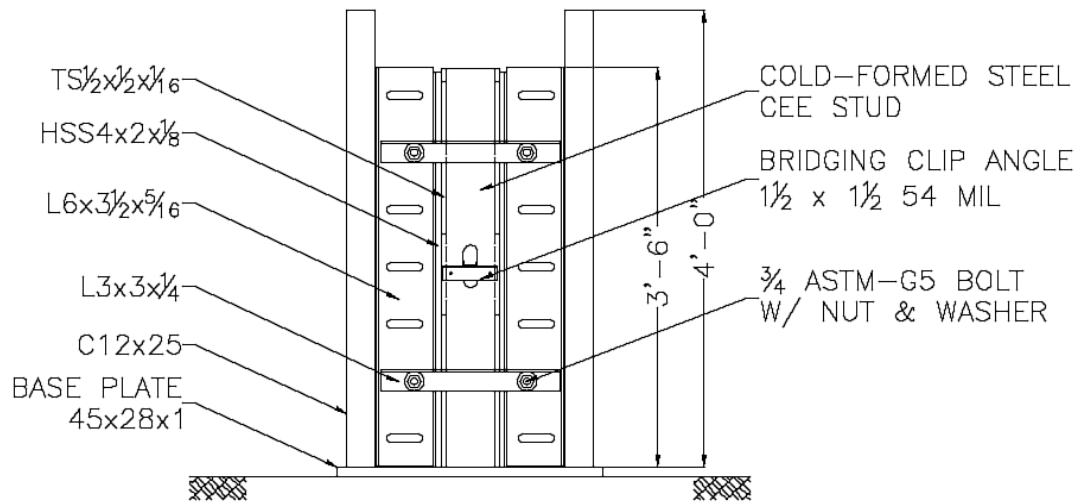
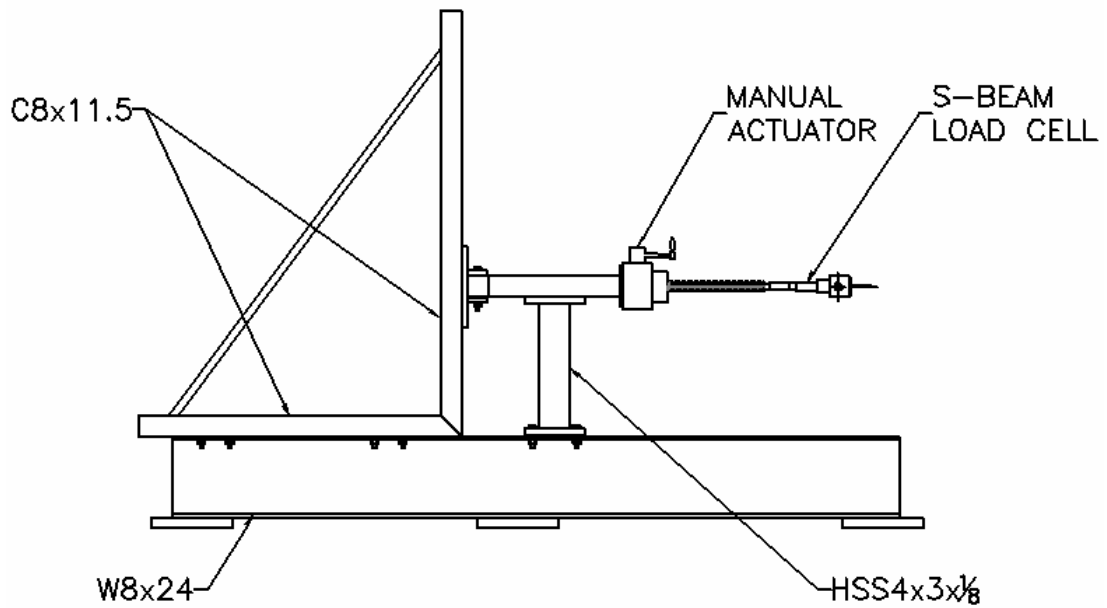


Figure 3.10 Top View of the SS Type Bridging Connection



(a) Elevation View of the Specimen Mounting Frame



(b) Loading Actuator Armature

Figure 3.11 Elevation Views of Bridging Connection Test Setup

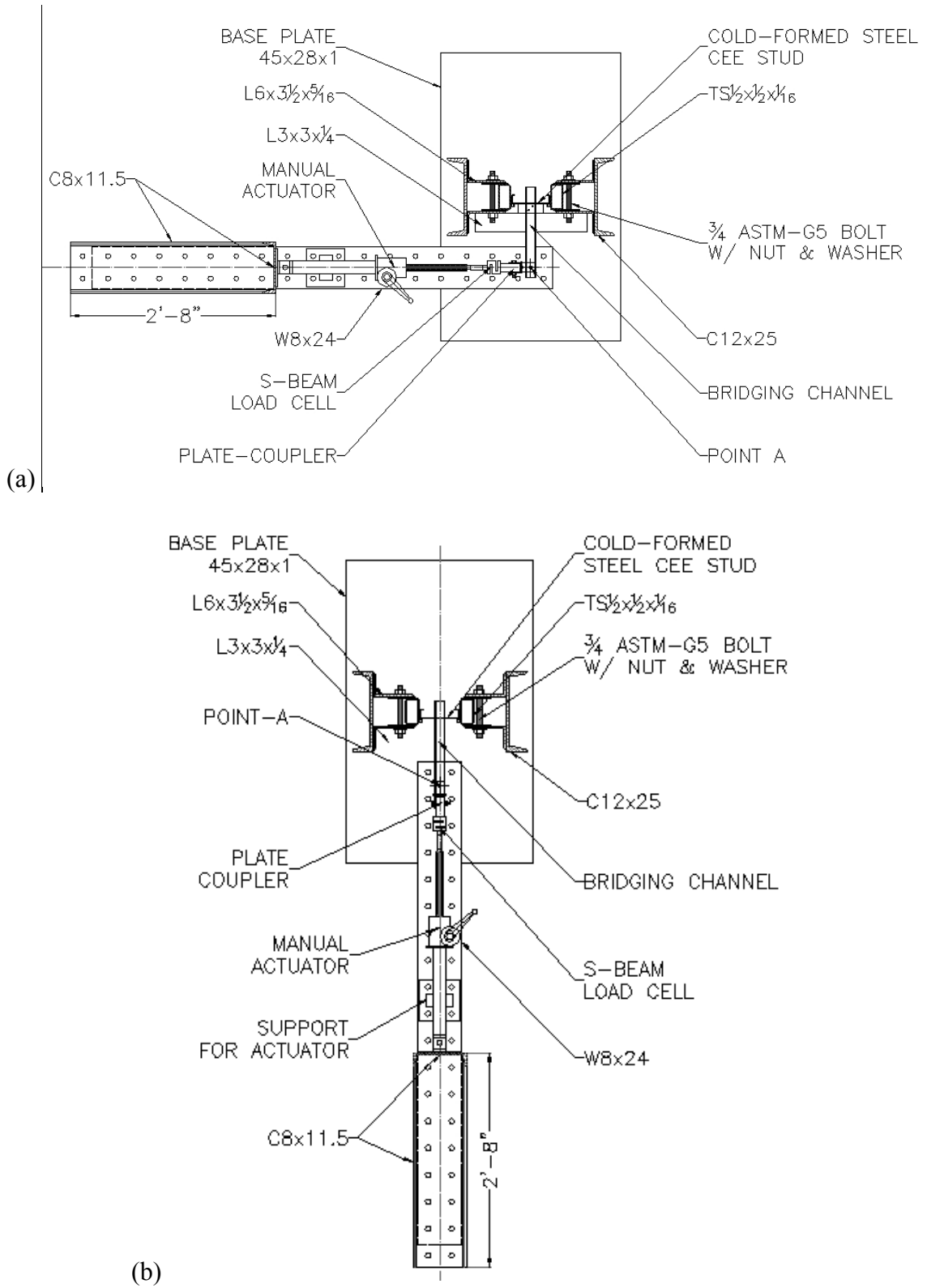


Figure 3.12 Schematic Plan View of the (a) Out-of-Plane Bridging Test (b) In-Plane Bridging Test



Figure 3.13 Overall View of the Out-of-Plane Bridging Tests

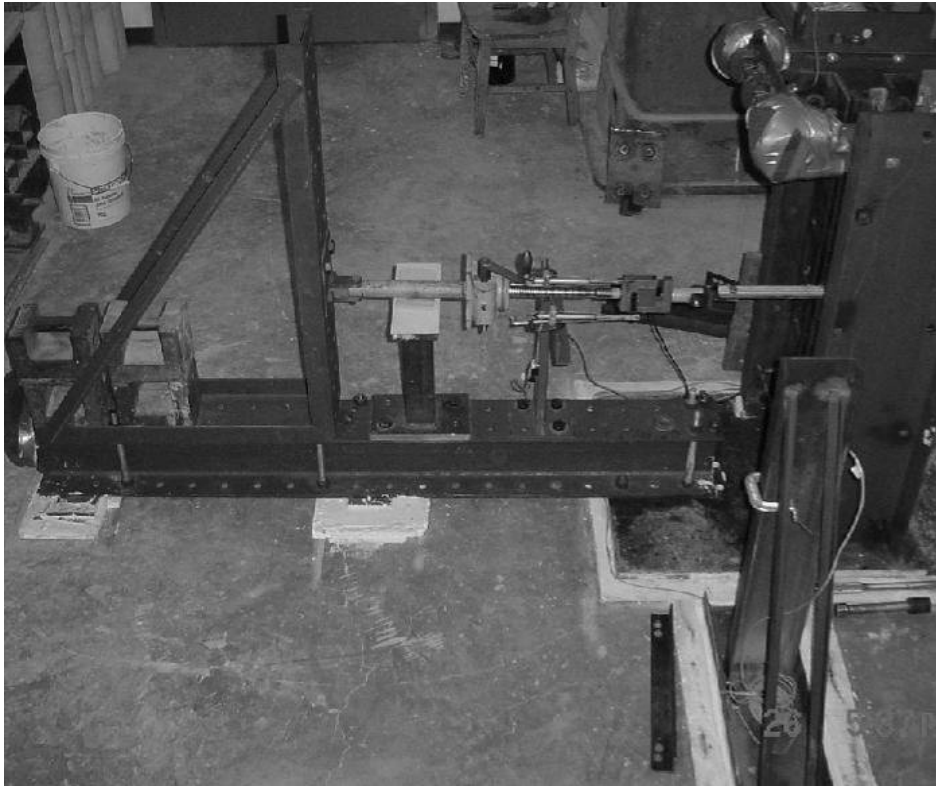


Figure 3.14 Overall View of the In-Plane Bridging Tests



Figure 3.15 Out-of-Plane Loading Test Instrumentation on the (a) Front (b) Back

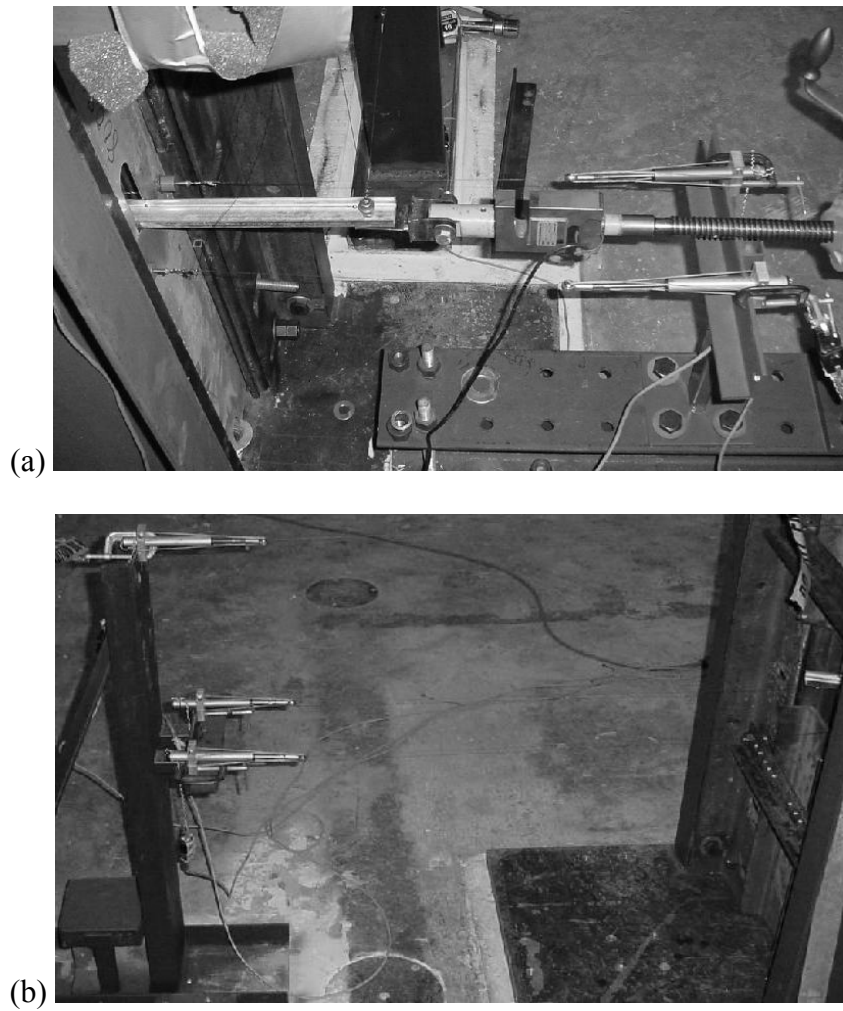


Figure 3.16 In-plane Loading Test Instrumentation on the (a) Front (b) Back

## CHAPTER 4 EXPERIMENTAL RESULTS AND EVALUATION

Experimental tests on single column specimens and bridging specimens were performed as per the test protocols described in Chapter 3. The individual test reports for the single column tests and the bridging test results can be found in Urala (2004). This chapter is divided into four sections, the first section deals with the results of the single column axial tests and discusses the effect of brace stiffness and strength on the load carrying capacity, mid-height lateral displacement and effective length of the braced columns. The second section deals with the axial pullout strength and torsional stiffness of the three bridging connections for eight series of cee-studs. The third section deals with the relationship between the flexible bracing and the bridging strength and stiffness. The fourth section summarizes the experimental evaluation.

### 4.1 Single Column Axial Load Test Results

In the single column axial load tests a total of 37 studs were tested based on the following parameters:

- Cross-sections
  - 362S125-33, 362S162-43, 362S162-68
  - 600S125-33, 600S162-43, 600S162-97
  - 800S162-43, 800S162-97
- Unbraced Test Specimens versus Braced Test Specimens
- Bracing Stiffness
  - Under-Braced – less than ideal bracing
  - Ideally-Braced – equal to ideal bracing
  - Over-Braced – greater than ideal bracing

Table 4.1 provides the proposed test matrix for the 8'-0" long single column axially loaded cee-stud specimens. Due to certain experimental limitations, the actual test matrix is as given in Table 4.2, where the numbers in the table represent the number of tests conducted at that brace stiffness. The specific reasons for the changes from the proposed test matrix compared to the actual test matrix are described in the course of this chapter.

#### 4.1.1 Bracing Strength and Stiffness

Eight groups of cee-studs were tested with a total of 37 test specimens. The AISIWIN software program (AISIWIN 2000) was used to determine the nominal properties of the eight groups of test specimens, with appropriate nominal values of material yield and ultimate stress. Table 4.3 gives the ultimate and unfactored capacities of each of the stud groups. The target brace stiffness, for single nodal bracing ( $n=1$ ), was calculated using Eq. 2.14, as recommended by Yura (1995), where the unbraced length of the column was taken as the distance between the support and the point of bracing ( $L_b = 48.0$  inches). The target bracing stiffness is also tabulated and provided in Table 4.3.

The measured geometric dimensions and the results of the material tension coupon tests for each group of cee-studs were then used to recalculate the ideal brace stiffness using AISIWIN (2002). Table 4.4 gives the values of the required ideal bracing stiffness for each of the studs. The single column axial load tests were conducted on cee-stud specimens with varying brace stiffnesses, which were lesser than, equal to, or greater than the ideal brace stiffness. As discussed earlier, at least one cee-stud per series was tested without any lateral (or torsional) bracing.

The cee-studs were braced with four steel wires attached at mid-height of the member to the flanges, as shown in Figure 4.1. By varying the length and diameter of the brace wires the brace stiffness was varied from one test specimen to the other. The brace strength was

calculated as the product of the cross-sectional area of the wire and its nominal tensile strength. The actual brace stiffness ( $k_{br}$ ) was calculated as the average value of the brace stiffnesses of all four wires. The brace stiffness of each wire was calculated using Eq.4.1a.

$$k_{br} = \frac{AE}{L_{br}} \quad (4.1a)$$

where: A = Cross-sectional area of the wire  
 E = Elastic Modulus of steel wire= 29,000,000 psi.  
 $L_{br}$  = Length of brace wire

At any time during the test only two brace wires, out of the four, were effective in bracing the stud. If the stud buckled in a flexural mode, the two brace wires on the same side of the web were effective, whereas if the stud buckled in a torsional mode, the two diagonally opposite brace wires were effective in bracing the stud. Therefore, the total brace stiffness was taken as twice the average stiffness of the four brace wires, and is given in Table 4.5. The ratio of the total brace stiffness provided to the required ideal brace stiffness, ( $\beta_{provided}/\beta_{required}$ ) is defined as the *brace-factor*. The brace-factor for each of the 37 test specimens is listed in Table 4.5, which was used to categorize the cee-studs as: *under-braced*, *ideally-braced* or *over-braced* (i.e. brace-factor <1.0, =1.0, or >1.0).

The column effective length factors were taken from Table C-C4-1 of the Commentary to the North American Specification for Cold-Formed Steel (AISI 2000). For flexural buckling about the weak axis the effective length factor was taken as  $K_y=1.0$  for the unbraced studs and  $K_y=0.5$  for the braced studs. This effective length factor was assumed to be the same for all three categories of braced studs. For flexural buckling about the strong axis, it was considered that the track offered near full base fixity, and hence the effective length



factor was taken as  $K_x=0.5$ . Since the top and bottom supports prevented the stud from twisting, and the effective length factor was taken as  $K_T=0.5$ .

#### 4.1.2 Evaluation of Experimental Observations

The evaluation of the experiments provided below will be based on a review of the test parameters such as the effect of cee-stud dimensions, the brace stiffness and the brace strength. The experimental results are compared to analytically calculated values of axial load capacity and the expected brace forces based on the measured lateral displacements. The effect of brace stiffness on the axial load capacity has been studied and the graphically illustrated in Figure 4.2 to 4.9 and has been discussed in this section. Figure 4.10 gives the buckling modes and shapes of the experimental observations, which is explained later in this chapter.

While keeping the brace-factor constant between two or more studs, the following parametric studies were performed based on the cross-section dimensions:

- Web depth, keeping the brace-factor relatively the same.
  - Comparing 362S125-33 and 600S125-33 (Figures 4.11 to 4.13)
  - Comparing 362S162-43, 600S162-43 and 800S162-43 (Figures 4.14 to 4.16)
  - Comparing 600S162-97 and 800S162-97 (Figures 4.17 to 4.19)
- Thickness, keeping the brace-factor relatively the same:
  - a. Comparing 362S125-33, 362S162-43 and 362S125-68 (Figures 4.20 to 4.22)
  - b. Comparing 600S125-33, 600S162-43 and 600S162-97 (Figures 4.23 to 4.26)
  - c. Comparing 800S162-43 and 800S162-97 (Figures 4.27 to 4.29)

Figures 4.11 through 4.29 have been normalized with respect to the analytical values of axial load and the corresponding axial shortening using the average as-built properties of each stud group obtained from AISIWIN (2002). The effect of different material properties

has been considered in the above normalization by including it in the AISIWIN program.

With increasing web depth and flange width, the slenderness ratio of the web and flange plate elements increases. This leads to a loss of elastic stiffness in the web and hence the load carrying capacity of the studs decreases and is evident in the comparisons described above. Figures 4.11 to 4.13 indicate that the 600S125-33 studs have undergone nearly twice the axial deformation compared to the 362S125-33 studs, for nearly the same brace factor. Both, the unbraced 362S and 600S studs have attained almost a normalized load of 1.35 times than the analytical prediction, but their normalized axial deformations at the maximum load being 1.6 and 4.6, respectively. In Figure 4.12, the 362S and 600S studs with a brace factor of 1.7x and 1.3x, have attained nearly 1.0 and 1.4 times the analytical prediction for a mid-height braced stud, respectively. Comparing the 362S and 600S studs in Figure 4.13, with brace factors 6.2x and 7.4x, respectively, shows that the normalized axial shortening being 1.25 and 3.3 at normalized axial loads of 1.25 and 1.15, respectively.

Figures 4.14, 4.15 and 4.16 show the comparison of the 362S, 600S and 800S studs for the same plate thickness of 43 mils. The 362S, 600S and the 800S unbraced studs recorded a normalized axial load of 2.6, 1.4 and 2.0 at corresponding normalized axial shortening of 2.6, 3.0 and 3.8, respectively. Comparing the 362S (1.2x), 600S (1.6x) and 800S (1.3x) studs in Figure 4.15 shows that normalized axial loads are 1.4, 1.05 and 0.85 for corresponding normalized axial shortening of 1.75, 2.2 and 2.1 respectively. In the 800S162-43-150 stud the buckling mode was distortional hence the experimental maximum load was less than the analytical value. When the brace factor was greater than 2.0, as in the case of 362S (2.5x), 600S (3.4x) and 800S (2.3x) studs, the normalized axial loads were 1.35, 1.0 and 1.0 with corresponding normalized axial shortening being 1.8, 2.0 and 1.0, respectively. It can be

observed from all the three figures that the 362S studs not only have the highest elastic stiffness but also have the highest load enhancement. In Figure 4.16, due to strong axis buckling of the 800S162-43-300 stud, the axial shortening was neutralized by the elongation in the north flange. However, the slope of latter part of the plot shows that this stud had an elastic stiffness that was less than the stiffness of the other two studs that are in the comparison.

The comparison of the 600S and 800S studs with a plate thickness of 97 mils with varying brace stiffness is shown in Figures 4.17 to 4.19. It can be observed that the 800S (0x, 2.1x, and 4.3x) studs have lesser elastic stiffness and the maximum normalized axial loads attained are 2.5, 1.1, and 1.1 at corresponding normalized axial shortening of 2.5, 2.7, and 2.15, respectively. On the other hand, the 600S (0x, 1.7x, and 2.7x) studs have higher elastic stiffness and the normalized axial loads attained are 2.8, 1.2 and 1.25 at corresponding normalized axial shortenings of 1.4, 1.65, and 1.05. Since the 800S studs have a higher web-depth to thickness ratio for a given thickness than the 600S studs, this results in a lesser elastic stiffness.

Figures 4.20 to 4.22 (362S), Figures 4.23 to 4.26 (600S), and Figures 4.27 to 4.29 (800S) show the comparison of studs with constant web-depth while varying the thicknesses. The brace-factors are maintained approximately the same in these comparisons.

Figure 4.20 compares the 362S unbraced studs with 33, 43 and 68 mil thicknesses. The failure modes were first mode flexural-torsional for all the three studs, where as the maximum normalized axial loads were 1.25, 2.6 and 1.5 at corresponding normalized axial shortenings of 1.3, 2.6 and 6.6, respectively. For the 362S braced studs (see Figure 4.21) of thicknesses 33 mils, 43 mils and 68 mil, with respective brace factors of 1.7x, 1.2x, and 1.8x,

the maximum normalized axial load were 1.0, 1.4 and 1.35 at corresponding normalized axial shortenings of 0.7, 1.75, and 1.7, respectively. In Figure 4.22, the studs had respective brace factors of 6.2x, 5.4x, and 3.3x with maximum normalized axial loads of 1.25, 1.25, and 1.5, at corresponding normalized axial shortenings of 1.2, 1.6, and 2.3, respectively.

Figure 4.23 compares the 600S studs with thicknesses of 33, 43 and 97 mils. For the unbraced studs the maximum normalized axial loads were 1.3, 1.45, and 2.85, at corresponding normalized axial shortenings of 4.1, 3.0, and 1.5, respectively. For the braced studs (see Figure 4.24) with respective brace factors of 0.2x, 0.6x, and 0.3x, the maximum normalized axial loads were 1.05, 0.85, and 1.2, at corresponding normalized axial shortenings of 3.4, 2.0, and 1.05, respectively. In Figure 4.25, the 600S studs with brace factors 1.3x, 1.6x, and 1.7x were compared, and the maximum normalized axial loads were 1.25, 1.05, and 1.25, at corresponding normalized axial shortenings of 3.1, 2.2, and 1.6, respectively. In Figure 4.26, the 600S studs with brace factors 7.4x, 3.4x, and 2.7x were compared, and the maximum normalized axial loads were 1.2, 1.05, and 1.25, at corresponding normalized axial shortenings of 3.3, 2.1, and 1.35, respectively.

For the 800S studs with 43 and 97 mil thicknesses shown in Figure 4.27, with no bracing, the normalized axial load reached maximum values of 2.0 and 2.5 at corresponding normalized axial shortenings of 3.6 and 2.5, respectively. For the braced studs with 1.3x and 1.2x, respective brace factors, the maximum normalized axial load was 0.85 and 1.05 at corresponding normalized axial shortenings of 2.1 and 1.4, respectively. Both, the 800S162-43-150 and 800S162-97-500 studs failed in distortional buckling mode. The distortional buckling prevented the stud to reach the analytically calculated fully braced capacity, in spite of the brace factor being greater than ideal bracing. When the 800S studs with respective

brace factors of 2.3x and 4.3x were compared (see Figure 4.29), the maximum normalized axial loads were 1.0 and 1.1 at corresponding normalized axial shortenings of 0.95 and 2.15, respectively.

#### 4.1.2.1 Effect of brace stiffness on axial load capacity

It can be observed from the combined plots of each series of the studs that there is a considerable enhancement in the load carrying capacity of a braced stud in comparison to an unbraced stud. Figures 4.2 to 4.9 indicate that for brace stiffnesses higher than the ideal bracing requirement, the experimental maximum loads attained remain unchanged. Table 4.6 gives both, the experimental maximum load and the percentage increase in the axial load, which clearly indicates the load enhancement.

Figure 4.2 to 4.9 also show that the initial elastic stiffness ( $k$ ) line, which was calculated using:

$$k = \frac{A_g E}{L} \quad (4.1b)$$

where:  $A_g$  = Gross cross-sectional area of the cee-stud

$E$  = Young's Modulus = 29,500,000 psi

$L$  = Length of an unbraced stud = 8'-0"

The 362S125-33 studs failed by flexural-torsional buckling with flexural buckling occurring about the weak and strong axes and torsional buckling occurring about the shear center. Due to the strong axis flexural buckling, the north flange was elongating and the south flange was shortening, this in combination with the torsional buckling influenced the axial shortening and the studs hence exhibited unanticipated behavior. Beyond the ultimate capacity, these studs seem to lose load gradually. Figure 4.2 shows the plot of axial load versus axial shortening of the 362S125-33 series studs.

It can be observed from Figure 4.3 that the load-deformation behavior of 362S162-43 studs have the same slope as that of the initial elastic stiffness line up to an axial load of approximately 5200 lbs at which the unbraced stud failed. Beyond this load, the plot indicates that the braced studs begin to lose stiffness, and on reaching the ultimate load the failure is instantaneous.

In the case of 362S162-68 series studs, the load-deformation behavior, shown in Figure 4.4, seem to have an initial stiffness that is almost comparable to the initial elastic stiffness up to their ultimate capacities. There is a substantial increase in the ultimate load capacity of the braced studs over the unbraced stud and the studs failed instantaneously on reaching the ultimate load.

The 600S125-33 and 600S162-43 series studs had lower stiffness than the calculated initial elastic stiffness, which can be observed in Figures 4.5 and 4.6. In the 600S125-33 series, the under-braced stud failed by first mode flexural buckling and all the others failed by distortional buckling. In the 600S162-43 series, the unbraced stud failed in first mode flexure, and the remaining studs failed by distortional buckling. In both the series, distortional buckling seems to affect the elastic stiffness in comparison to the 362S series of studs that failed by global buckling. The load-deformation behavior of the 600S162-97 series of studs, shown in Figure 4.7, seems to have the same slope as the initial elastic stiffness line, and braced studs seem to have almost the same ultimate loads.

The 800S162-43 series of studs did not exhibit a very high load enhancement in spite of them being either ideally-braced or over-braced. Due to certain limitations in the experimental setup, two of the studs exhibited strong axis buckling that caused stretching of their north flange, which affected the measured axial shortening. When the axial load

reached a value that was critical to weak axis buckling, the stud exhibited weak axis buckling and the slope of the load-deformation plot changed sharply, which is shown in Figure 4.8. The slope of the remaining plot indicates that the studs had lesser stiffness than the initial elastic stiffness. The ultimate capacities of these studs were comparable to the calculated axial capacities. This indicates that the top and bottom supports do not have any partial restraint and the supports act like a pinned connection. This clearly indicates the requirement of an independent study on the affect of support conditions on the buckling of the cee-studs.

In the case of 800S162-97 stud group, the ultimate capacities of the braced studs are slightly greater than that of the unbraced stud. Figure 4.9 shows that the cee-studs have a lower elastic stiffness than the initial elastic stiffness.

The results of the experimental tests are tabulated in Table 4.6 which gives the maximum experimental load measured, observed failure modes and percentage increase in the axial capacity of the braced stud over the unbraced stud. It was generally observed that the maximum experimental loads are higher than the predicted capacities from AISIWIN (2002). For all the unbraced studs the predicted axial load capacity with nominal cross-section properties and nominal yield strength, in the AISIWIN (2002) program, was less than the measured maximum experimental loads. This is because the AISIWIN (2002) program considers a perfect pin-ended support condition for both flexural and torsional buckling. In the experimental investigation, the cee-studs were seated in standard track at both ends that provided end-conditions of partial fixity for weak axis flexural buckling and near full fixity for both strong axis flexural buckling and torsional buckling. These end restraints led to higher axial load capacities for the studs that failed by global buckling, i.e. flexural, flexural-torsional or torsional buckling. The 600S125-33, 600S162-43 series of studs failed by a

distortional buckling limit state at axial loads lower than those predicted by AISIWIN (2002) for a perfectly pin-ended column. This necessitates the consideration of distortional buckling as a possible controlling and critical limit state for certain stud geometries. AISIWIN does not consider the distortional buckling limit state while predicting the axial capacity of cold-formed lipped cee studs.

The enhancement in the load carrying capacity of a stud is directly related to the type of buckling failure that occurred. The percentage enhancement in the experimental load for the braced studs compared to an unbraced stud, within the same series, is given in Table 4.6. The braced studs of the 362S125-33 series attained nearly 140% more load capacity than the unbraced stud, and the buckling was mainly global second mode flexural-torsional buckling. The braced studs of the 362S162-43, 362S162-68 series showed a load increase of about 35% and 115%, respectively. Though the 600S125-33 and 600S162-43 series studs failed by distortional buckling, they exhibited an average load increase of 87%, and 34%, respectively and the 600S162-97 showed an average load increase of about 38%. The 800S series studs, both 43 and 97 mils, showed only a slight load enhancement as their experimental maximum capacities were in the range of the predicted axial capacities from AISIWIN. As discussed earlier, this indicates that the partial support fixity has reduced with increasing column depth.

#### **4.1.2.2 Effect of brace stiffness on buckling type and mode**

Figure 4.10 is a schematic diagram of the observed buckling shapes and modes of the test specimens. The abbreviations in Table 4.6 and Figure 4.10 represent: F = Flexural Buckling, T = Torsional Buckling and the digit in brackets represents the number of half-sine waves or the order of buckling mode. This figure does not include the distortional buckling mode, which may or may not be associated with the global buckling modes.



It was observed that with an increase in the brace stiffness the test specimens failed after attaining a higher order buckling mode. In some cases, under-braced studs failed at loads higher than the over-braced studs. However, in the former, the failure has been sudden and in the latter, the failure has been gradual. With increasing brace stiffness, the 362S studs exhibited flexural-torsional buckling changing from first mode to second mode. The 600S125-33 and the 600S162-43 studs failed by distortional buckling irrespective of the bracing stiffness. With increasing bracing stiffness, the 600S162-97 studs failed by flexural and/or flexural-torsional buckling. The 43 mil 800S studs failed by first mode flexural which changed to second mode flexural buckling with increasing bracing stiffness, however distortional buckling was also observed in one of the stud. In the 97 mil 800S studs, the nothing definite can be stated in terms of failure since distortional mode controlled two of the studs and only one stud failed by first mode torsional buckling. Among the 33, 43 and 68 mil studs, irrespective of the total depth of the stud, local elastic buckling waves were observed in the web and distortional buckling waves were observed in the flanges. The local elastic buckling is related to the flat-widths to thickness ratio of the web and the flanges. The reader is advised to refer to Urala (2004) for photographs of the buckling modes for various studs.

#### **4.1.2.3 Effect of cross-sectional dimensions of cee-studs**

The 33, 43 and 68 mils studs underwent elastic local and distortional buckling at loads in the range of 10 to 25% of their ultimate capacities. On the other hand, the 97 mil studs did not show the same elastic local buckling. However local buckling was observed near the punchout, at axial deformations beyond those corresponding to the ultimate capacities and was inelastic permanent deformations. The two types of inelastic local buckling generally observed in the 600S162-97 and the 800S162-97 series were local yielding of the lip-flange junction and local distortion around the web-punchouts. The sensitivity of the member to

local buckling depends upon its width-to-thickness ratio (Gotluru 2000). It has been experimentally shown by Young and Rasmussen (1999) that local buckling does not induce overall bending of fixed-fixed singly symmetric columns, as it does for pin-ended singly symmetric columns. In the current research, the cee-studs were supported by the track at the top and bottom, and the degree of fixity offered by the track has to be ascertained. In a later section in this chapter, the effective length factor for each of the cee-studs is determined based on the analytical value of the load capacity that corresponds to the maximum experimental load achieved for each of the test specimens.

#### **4.1.2.4 Effect of experimental load on the brace stiffness and strength**

As discussed earlier, most of the unbraced studs failed at loads higher than the AISIWIN predicted capacities. The higher capacities for the studs necessitated recalculating the ideal brace stiffness as per Eq. 2.14. Table 4.7 gives the required ideal brace stiffness based on these higher load capacities of the unbraced studs. The higher load capacity would require a higher demand on the lateral bracing as given in Table 4.7. This higher demand on the bracing stiffness renders some of the braced cee-studs to fall into the category of under-braced cee-studs since the provided brace stiffness is now less than the new ideal bracing requirement. The bracing strength however remained satisfactory since the brace wires were capable of carrying the increased brace force.

It was observed in the plots of experimental load versus target brace stiffness in Figures 4.3 to 4.9 that by increasing the brace stiffness there is a gradual increase in the axial capacity of the stud. Figures 4.30 to 4.32 show an increase in capacity of the columns with a corresponding increase in target brace stiffness. The axial load carrying capacity for the 362S125-33 studs increased by 162%, for the 362S162-43 studs increased by 25.0% and for the 362S162-68 studs it increased by 129.0% while varying the brace stiffness from an

unbraced stud to an over braced stud. It can also be observed in the figure that there is not much of an increase in the load carrying capacity from an ideally braced stud to an over braced stud. There was a similar increase in the 600S series of studs, for the 33, 43 and 97 mil thicknesses, with respective increases of 32%, 37%, and 40.0%. It must be made note of here that all the 33 and 43 mil studs failed by distortional buckling and that a few of them had lesser experimental maximum loads (see Table 4.6) compared to the analytical prediction of a mid-height braced stud. In the case of the 800S studs with 43 and 97 mils, there is a respective increase of 19.0% and 35% in the axial load carrying capacity.

#### **4.1.2.5 Effect of brace stiffness on lateral displacement**

For any group of cee-studs, the mid-height lateral displacement of the weak axis decreased with increasing brace stiffness, as reported by Yura (1995), which was adopted by the latest edition of the AISC-LRFD Specification (AISC 1999). The plots of axial load versus mid-height strong axis lateral displacement and weak axis lateral displacement for all the cee-studs are given in the individual test reports provided in Urala (2004). Figs 4.33 to 4.35 plot the actual total bracing stiffness versus the mid-height weak axis lateral displacement for the 362S, 600S, and 800S series of studs. These plots show that with increasing brace stiffness, the mid-height lateral displacement of the weak axis decreases. In all the series of studs, there was a decrease in the mid-height lateral displacement by more than 75% from an unbraced stud to an over braced stud.

#### **4.1.2.6 Effect of brace stiffness on effective length of columns**

Table 4.8 gives the effect of total brace stiffness and the effective length factors for the cee-studs. The effective length factors were determined using a MathCAD worksheet developed by Chen (1996) for the AISI Committee on Specifications for the Design of Cold-Formed Steel Structural Members. The effective length factors  $K_x$ ,  $K_y$  and  $K_t$  were varied to

arrive at a predicted load close to the experimental load capacity of each of the eight foot long 37 cee-studs. It can be observed in Figures 4.36 to 4.43 that by increasing the total bracing stiffness, the effective length factor of the columns decrease. The effective length cannot be less than 0.25, hence the plots have been truncated below the limiting value of 0.25. For a column with fully fixed ends, the effective length factor is 0.5, and for such a column with fully effective mid-height bracing, the effective length factor reduces to 0.25. For most of the over-braced studs, the effective length factor was 0.25 in strong axis flexural buckling and torsional buckling. For weak axis buckling, the effective length factor is 0.5, assuming there is no partial rigidity at the supports.

#### **4.1.2.7 Effect of brace strength on axial capacity**

The brace strength, which is dependent upon the cross-sectional area of the wire and its yield stress, does not affect the buckling of the single axial column specimens because the brace forces that were generated during the testing were often less than the capacities of the brace wires. However, the yield strength of the brace wires does affect the behavior of the stud only when the brace forces reach the yield load of the brace wires. In some preliminary tests, outside the scope of the test matrix, it was observed that mild steel brace wires did not provide enough brace strength. When the brace force in the mild steel wire reached its yield capacity, the brace wire stretched at a constant brace force until failure, causing a non-linear lateral displacement. It was then decided to conduct the tests with high-strength steel wires. The steel wire had a tendency to coil and to keep it straight, a threshold brace force of approximately 2 lbs was applied to each of the four braces prior to testing.

#### **4.1.2.8 Other effects**

Among other effects are effects due to geometric imperfections, mechanical properties of the stud material, track resistance and bearing ends of the stud. The measured geometric

imperfections of the test specimens are listed in Table 3.3. As per Winter (1960), the effect of initial imperfection is to increase the brace force, thus necessitating higher brace stiffness. It is stated that the stiffness required to attain “full bracing” in an imperfect column (see Eq. 2.3) exceeds that required for the ideal column (see Eq. 2.4), the more so the larger the imperfection ‘ $d_o$ ’. Hence, the required brace stiffness is given by:

$$\beta_{\text{req}} = \beta_{\text{ideal}} \times (d_o / d + 1) \quad (4.2)$$

where  $\beta_{\text{ideal}}$  = ideal brace stiffness for perfect column

$d_o$  = measured imperfection in the stud

$d$  = deformation of the brace at the maximum brace force

The total measured brace forces at the maximum axial load for all the studs are tabulated in Table 4.9. The measured weak axis lateral displacement at the maximum axial load for all the studs is tabulated in Table 4.10. It is observed that the calculated brace forces based on the measured displacements, given in Table 4.10, are higher than the corresponding values of the measured brace forces, given in Table 4.9. This is because of the initial seating, slipping of brace wires at the loops. However compared to the global effects and at full capacities, these initial limitations are negligible. Yura (1995) had proposed that the required brace strength to be 2.0% of the nominal axial capacity of the column, as discussed earlier in Chapter 2. Table 4.9 gives the measured brace forces as a percentage of the ultimate load. It is observed that the percentage of measured brace forces ranges from as low as 0.08% to as high as 1.34% of the ultimate capacity of the cee-studs.

## 4.2 Bridging Test Results

### 4.2.1 Bridging Connection Strength and Stiffness

In the bridging connection strength and stiffness tests, three types of typical industry bridging connection specimens were fabricated and tested. The connection types and specimen details are described under Section 3.7.1 of this report. A total number of 54 specimens were tested, with 28 specimens subjected to out-of-plane loading and 26 specimens subjected to in-plane loading. In the out-of-plane loading, the load was applied parallel to the web at a distance of 11 inches away on the bridging channel (see Figure 3.13). In the in-plane loading tests, the load was applied perpendicular to the web at a distance of 11 inches away on the bridging channel (see Figure 3.14). Both the test protocols are described in Section 3.7.5 of this report. The proposed test matrix is given in Table 4.11. The results of all the experimental tests are presented in Urala (2004), which is divided into two sections, with the results of the out-of-plane loading tests in one section and the results of the in-plane loading tests in another section. The data collected from the out-of-plane loading tests was used to plot (see Figures 3.11b, 3.12a, 3.15, and 4.44, for visualization):

- the applied load versus the X-direction displacement of Point A;
- the applied load versus the left screw displacement bearing on the adjacent web plate, and
- the applied load versus the right screw pull out displacement from the adjacent web plate.

The data collected from the in-plane load tests were used to generate three plots (see Figures 3.11b, 3.12b, 3.16 and 4.44 for visualization):

- the plot of the applied load versus the Y-direction displacement of Point A,
- the plot of the applied load versus the left screw bearing displacement on the adjacent web plate, and

- the plot of the applied load versus the right screw pull out displacement from the adjacent web plate.

Under both the series of tests, the ultimate load capacity of the connection was taken as the load at which there was a complete failure or at which there was sufficient deformation in the test specimen. Sufficient deformation was considered to have occurred when the measured deformation in the bridging tests, when compared to the single column axially loaded studs tests, would result in influencing the global limit states of the single column axially loaded studs. The torsional stiffness of the connection was calculated as a secant ratio defines as ratio of ultimate load to the rotation of the connection and the flexural stiffness was calculated as the ratio of the ultimate load to the measured in-plane displacement. The rotation angle for the torsional stiffness was the angle between the initial center-line and the final center-line of the bridging channel. The X-direction displacement was used to calculate the change in angle as the inverse tangent of ratio of the measured displacement and the distance to Point A from the web of stud.

For the out-of-plane load tests, the right side displacement measured by LP-2 was used in calculating the torsional stiffness of the bridging. For the in-plane load tests, the average of the displacements measured by LP-1 and LP-2 (see Figure 4.44) was used to calculate the flexural stiffness of the bridging. The observed failure modes of the bridging systems are described later in this chapter.

As described in Chapter 3, the displacements of the clip angle and/or the web were measured using two linear potentiometers, LP-1 and LP-2, attached to the web as shown in Figure 4.44 and the displacements of the back of the web were measured using two linear potentiometers, LP-3 and LP-4. These measurements were common to both out-of-plane and in-plane loading directions and are given in Tables 4.12 and 4.14. Spatial displacement of

Point A was measured, the purpose of which is described in Chapter 3. The experimental observations for each connection type and the failure mode are described in the following two sections.

#### 4.2.2 Observations of the Out-of-Plane Experimental Tests

The observations of the out-of-plane loading tests for the three types of connections are as follows:

- SS type connection (Figure 3.9a): With the application of the out-of-plane load on the bridging channel, the eccentricity of the load created a moment on the connection. The center of rotation of the moment was at the center-line of the stud causing the right screw to pull out and the left-half of the clip-angle to bear against the web plate of the stud. The load capacity of the SS type connection increased with increasing thickness of the web as and is shown in the plots of applied load versus rotation about the center-line of the web in Figures 4.45 to 4.47. The clip-angles failed by forming multiple yield-lines. The increase in plate thickness resulted in proportional increase in the contact area of the screw and the stud causing the increase in pull out capacity.
- WW type connection (Figure 3.9b): On application of the out-of-plane load, the right half of the clip angle started to pull on the stud web, developing tension in the weld, with the left half bearing on the web. In all the tests with WW type connections, failure occurred at the connection of the clip angle to the stud web. The observed failure types are described in a subsequent section in this chapter. The plot of the applied load versus the rotation about the center-line of the web is shown in Figures 4.48 through 4.50.
- DW type connection (Figure 3.9c): In this connection type, the flange of the bridging channel was welded to the stud web at the punchout. This connection failed mainly by tearing of the weld. The plot of the applied load versus the rotation about the center-line of the web is shown in Figures 4.51 through 4.53. It can be seen from these plots, that the initial connection stiffness is not dependent upon the depth of the stud. The effect of the varying web thickness on the connection stiffness cannot be determined, since only one thickness per depth of stud was tested with the DW type connection.

The maximum loads attained and corresponding displacements measured by LP-1 are given in Table 4.12. The values of displacement given in the table were measured on the front and on the back, to the right half of the centerline of the web. The final torsional stiffness of the connection was calculated as a ratio of the maximum load to the corresponding X-direction displacement at Point A. The initial torsional stiffness was



calculated as the initial slope of the load versus rotation plots shown in Figures 4.45 through 4.53. Table 4.13 gives the initial torsional stiffness of the out-of-plane loading tests, at 10% of the maximum load, calculated as the ratio of the load to the corresponding rotation. It was observed that within this load range, the initial slope of the plot was linear. For the three connection types, the plots of torsional stiffness versus the flat-width to thickness ratio are given in Figures 4.63 through 4.65. It can be observed in Figure 4.63 that for all the three groups of studs, the slope of the trend line is nearly equal and with the increase in the flat-width to thickness ratio the stiffness of the connection drops. However, in Figure 4.64 for the WW-type connection, the stiffness increases with increase in the depth of stud, whereas the same trend is not true for the DW connection (see Figure 4.65). The DW connection has the least torsional stiffness, followed by SS type and the maximum torsional stiffness is observed in the WW type connection.

### 4.2.3 Observations of the In-Plane Experimental Tests

The observations of the in-plane loading tests for three types of connections were as follows:

- SS type connection (see Figure 3.9a): With the application of the in-plane load, the screws began to pull out. It was observed that when the clip angle deformed by forming the yield-lines between the two screws attached to the web, there was tilting of the screws. This tilting of the screw caused an increase in the pull out capacity and hence an increase in both the connection strength and stiffness. However, at this load the connection had undergone sufficient deformation and hence failure was considered to have occurred at the load at which this stiffening effect was observed in the plot of the applied load versus the X-axis displacement. The plots of the applied load versus Y-direction displacement for the three groups of stud are shown in Figures 4.54 to 4.56.
- WW type connection (see Figure 3.9b): On application of the in-plane load, the load was transferred from the bridging channel to the clip angle and finally to the stud web through the connecting welds. In all the tests with WW type connection, the failure occurred at the connection of the clip angle to the stud web, either at the weld or the base metal. The plot of applied load versus Y-Direction displacement is given in Figures 4.57 to 4.59.

- DW type connection (see Figure 3.9c): In this connection type, the flanges of the bridging channel were welded to the web at the punchout. In this case too, the load path was from the bridging channel to the stud web across these small lengths of weld between the channel flanges. This type of connection was very strong due to the high stiffness of the stud webs and the capacity of the welds. The plot of applied load versus Y-Direction displacement is given in Figures 4.60 to 4.62.

The maximum load and the corresponding displacement of the connection measured on the front of the web by LP-1 and LP-2 are given in Table 4.14. The displacement values in the table were measured on the left and right sides on the front of the web. The final flexural stiffness of the connection was calculated as a ratio of the maximum load to the corresponding average displacements measured by LP-1 and LP-2. The initial flexural stiffness was calculated as the initial slope of the load versus displacement plots in Figures 4.54 through 4.62. Table 4.15 gives the initial flexural stiffness at 10% of the maximum load, calculated as the ratio of the load to the corresponding Y-displacement. The 10% of the maximum load was taken since it was found that the plot of the load versus displacement was initially linear within this load range.

The plots of flexural stiffness versus the flat-width to thickness ratio are given in Figures 4.66 through 4.68 for each connection type. In Figures 4.67 and 4.68 it can be observed that flexural stiffness decreases with an increase in the depth of the stud for both WW type and DW type connections. It can be observed that the slopes of the linear fit trend lines in Figure 4.66 are not the same for the three groups of studs and with the increasing flat-width to thickness ratio, the flexural stiffness decreases. With increasing web thickness and for a constant web depth, the flexural stiffness of the SS type connection increases for a selected series of cee-stud. For a given thickness the flexural stiffness decreases with the increase in web depth. On comparing the three connection types, the SS type has the least flexural stiffness, followed by the WW type with highest being for the DW type connection.

#### 4.2.4 Observed Bridging Connection Failures

The observed failure types in the out-of-plane loading tests and the in-plane loading tests for each of the three types of bridging connection are described below. The figures showing the failure types are given in Urala (2004), and the failure types for each test specimen are given in Tables 4.12 and 4.14.

##### 4.2.4.1 SS type connection

- Single screw pull out without distortion of the clip angle: This occurred when the clip angle separated from the web plate without any bending deformation or cross-sectional distortion.
- Single screw pull out with either deformation or distortion of the clip angle: The clip angle separated from the web plate by either bending deformation or by distorting. The bending deformation of the clip occurred in the out-of-plane tests, where the clip angle behaved as a cantilever beam subjected to a point load at the right screw, with the fixity at the left screw. For the in-plane tests, the cross-section distortion occurred when the clip angle formed a yield line in the angle leg connected to the stud web, at the level of the screws.
- Tensile failure of the screw connecting the clip angle to the stud web: The axial tension in the screws attached to the web exceeded the axial tension capacity of the screw, resulting in a sudden failure. These screws failed in the neck region.
- Shear failure of screw connecting the bridging channel to the clip angle: The failure of the connection occurred when the screw capacity in single shear of the screws attaching the clip angle to the bridging channel was exceeded.

##### 4.2.4.2 WW type connection

- Weld failure without angle distortion: In this case, tearing of the weld material between the angle and the cee-stud was observed. Connection failure occurred when the weld strength was exceeded. This was the anticipated mode of failure.
- Angle tear along the leg welded to the cee-stud: In this case, the tearing strength of the clip angle was exceeded, whereas the weld remained intact. In a few specimens, the weld thickness was greater than the design weld, and in few other specimens there was a weld return at the root of the clip angle.
- Weld separation between the clip angle and the cee-stud: The weld remained intact and stripped off with the clip angle, which indicates poor weld penetration.

#### 4.2.4.3 DW type connection

- Tearing of weld between the bridging channel and the cee-stud: This occurred when the load on the weld exceeded the weld strength and there was a good weld between the connected elements.
- Tearing of cee-stud web around the weld material: This occurred when there was complete weld penetration and there was block tear out of the web plate.
- Weld separation between the bridging channel and the cee-stud: The weld remained intact and stripped off with the bridging channel, which indicates poor weld penetration.

The summary of results for the out-of-plane load tests and in-plane load tests, giving the initial torsional stiffness and initial flexural stiffness are given in Table 4.16 and 4.17, respectively. The initial stiffnesses have been arranged based on the web depth and on the thickness of the cross-section. This table represents the same data discussed previously and is provided for convenience purposes.

### 4.3 Separation of Brace Forces in Flexural and Torsional Components

The brace forces BF-1, BF-2, BF-3 and BF-4 were measured using load cells A, B, C, D (as shown in Figure 3.6) and are plotted against the axial load for all 36 stud tests, which are presented in Urala (2004). The axially loaded braced cee-studs buckled either in flexural, torsional or flexural-torsional buckling. Due to the aforementioned configuration of the brace wires, the center of torsional buckling shifted from the shear center to the centroid of the brace forces. Flexural buckling of the stud resulted in brace forces in two brace wires on the same side of the minor axis of the stud cross-section. Torsional buckling resulted in brace forces in the brace wires that were on the diagonally opposite corners of the stud cross-section. In the case of flexural-torsional buckling there were both flexural and torsional brace forces.

The total brace force was a resultant of the flexural and the torsional components, which can be resolved as shown in Figure 4.69. The measured brace forces in the brace wires were the resultant brace force due to global buckling. At any axial load level, the measured brace force was separated into two components, namely flexural and torsional brace force components. The flexural brace force component is the brace force in the two brace wires as shown in Figure 4.69(b), which have the same magnitude and direction. The torsional brace force component is the brace force in the two brace wires as shown in Figure 4.69(c), which have the same magnitude but opposite directions. The maximum magnitude of the flexural brace force component, the corresponding torsional brace force component and the corresponding axial load are given in Table 4.18. Similarly, the maximum magnitude of the torsional brace force component, the corresponding flexural component and the corresponding axial load are given in Table 4.19. In most specimens, the above maximum values did not occur at the same axial load, and depended upon the buckling shape and mode at the maximum axial load. The sum of maximum flexural brace force component and the corresponding torsional brace force component was compared to the sum of maximum torsional brace force component and the corresponding flexural brace force component. The greater of the two values was considered as the total maximum brace force.

The brace forces as a percentage of the axial load was computed and is given in Tables 4.18 and 4.19, and the magnitude of the brace factors are given in Table 4.5 for comparison. It is observed that from an under-braced stud to an over-braced stud in the 362S125-33, 362S162-43, 600S162-97 and 800S162-43 series, the total maximum brace force increased with the increase in the brace factor. In the case of 600S125-33 and 600S162-43 series of studs, the observed failure was mainly due to distortional buckling, resulting in brace forces

that did not bear any relation to the brace factor. In the case of the 362S162-68 and 800S162-97 series, the provided brace factors were greater than the ideal requirement and hence the total maximum brace forces are almost the same.

#### 4.4 Summary of Experimental Observations

The axial capacities of the cee-studs were determined by the AISIWIN (2002) program by considering the nominal cross-section dimensions and nominal yield stress of 33 ksi. and of 50 ksi. These values were used to calculate the ideal brace stiffness. The test matrix given in Table 4.1 was proposed for target bracing stiffnesses less than, equal to and more than the ideal bracing stiffness, and the studs being categorized as being – under-braced, ideally-braced or over-braced. The nominal values from AISIWIN and the average as-built values of test specimen geometry and the material yield and ultimate strength are given in Tables 4.3 and 4.2B, respectively. The target brace stiffness, the total brace stiffness and the brace-factor was determined for each stud, which is given in Table 4.5. The single column axial load tests on the unbraced cee-studs showed that the predicted axial capacities were lower than the experimental maximum loads. Since the required bracing stiffness and strength are functions of the axial capacity, they increase with an increase in the axial capacity. This required recalculation of the brace stiffness and modification of the test matrix as given in Table 4.2. The required brace stiffnesses and the brace-factors were determined as given in Table 4.7.

The observed failure types were broadly classified as global or local. Figure 4.10 shows the global buckling types (flexural, torsional and flexural-torsional) and modes (first and second). The local buckling types were elastic plate buckling and distortional buckling. Table 4.6 gives the buckling type and mode for each stud at failure. The bracing was not designed to prevent flexural buckling about the strong axis. The elastic waves in the web

owing to local elastic plate buckling were observed in the 33, 43, 68 mils cee-studs at loads as low as 10% of the ultimate capacity. The elastic waves had a half wavelength equal to width of the web. In addition to the elastic waves, the 600S series (33, 43 mils) and the 800S series (43 mils) exhibited distortional buckling in the flanges with a half wavelength of about 18 inches. The 600S series studs with a plate thickness of 33 and 43 mils, failed by distortional buckling of the flanges. The strength prediction using AISIWIN (2002) does not consider the effect of distortional buckling, and in the case of the stud 600S125-43 with total brace stiffness of 148 lbs/in, the analytical value was greater than the experimental maximum load. The 600S and 800S series of studs with a plate thickness of 97 mils exhibited local inelastic plate buckling at loads beyond the ultimate capacity. These studs failed by global buckling in first mode, which indicates that the brace stiffness was inadequate to force the stud to buckle in a higher mode. This may be attributed to the decrease in the resistance offered by the end track supports. For a given stud thickness, the ratios of strong axis to weak axis moment of inertias of the 800S and the 600S studs is higher than that of the 362S studs, which bears direct relation to the buckling shape. The resistance offered by the end tracks is lesser for studs that buckled in flexural modes than that offered to the studs that buckled in torsional modes.

Enhancement in the load carrying capacity of the cee-studs with increase in the bracing stiffness is observed in Figures 4.2 to 4.9 and in Figures 4.30 to 4.32. The mid-height lateral displacement of the weak axis decreases with increasing brace stiffness, and is shown in Figures 4.33 to 4.35, and the average of the measured value (north & south flange) as a factor of  $L/250$ , is given in Table 4.9. The column effective length factors also decrease with increasing brace stiffness and is shown in Figures 4.36 to 4.43. Table 4.9 gives the total

measured brace force as a percentage of the ultimate load, which ranged from 0.08% to 1.34%.

In the bridging connection tests, for both out-of-plane loading and in-plane loading tests, the maximum load attained, corresponding displacements are given in Table 4.12 and 4.14, respectively. The initial flexural stiffness and the initial torsional stiffness were computed at 10% of the applied load and the corresponding displacement. These are given in Tables 4.13 and 4.15, respectively. Figures 4.63 through 4.68 give the initial torsional stiffness of each of the tested specimen. The summary of calculated initial stiffnesses from the bridging connection tests are given in Tables 4.16 and 4.17 for the in-plane and out-of-plane load tests.



Table 4.1 Proposed Test Matrix for the Single Column Axial Load Tests

Series	Stud Designation				Unbraced Studs	Total Bracing Stiffness of Braced Studs		
	D	S	B	t		$< \beta_{ideal}$	$\approx \beta_{ideal}$	$> \beta_{ideal}$
1	362	S	125	33	X	X	X	X
2	362	S	162	43	X	X	X	X
3	362	S	162	68	X	X	X	X
4	600	S	125	33	X	X	X	X
5	600	S	162	43	X	X	X	X
6	600	S	162	97	X	X	X	X
7	800	S	162	43	X	X	X	X
8	800	S	162	97	X	X	X	X

Table 4.2 Actual Test Matrix of the Single Column Axial Load Tests

Series	Stud Designation				Unbraced Studs	Total Bracing Stiffness of Braced Studs			
	D	S	B	t		$< \beta_{ideal}$	$\approx \beta_{ideal}$	$\approx 2 \beta_{ideal}$	$> 2 \beta_{ideal}$
1	362	S	125	33	1	0	1	2	2
2	362	S	162	43	1	0	1	1	1
3	362	S	162	68	1	0	0	1	2
4	600	S	125	33	1	1	1	0	1
5	600	S	162	43	2	2	0	1	1
6	600	S	162	97	1	2	0	1	1
7	800	S	162	43	1	1	1	1	0
8	800	S	162	97	1	0	1	1	1

Table 4.3 Nominal Properties of the Test Specimens Using AISIWIN Program

Stud Designation				Nominal Values		AISIWIN					Target Ideal Brace Stiffness
				Yield Stress	Ultimate Stress	SSMA Section Area	Ultimate Capacity ( $P_u$ )		Unfactored Capacity ( $P_n$ )		$\beta_{ideal, target}$
				$F_y$	$F_u$		Unbraced	Mid-Point Brace	No Brace	Mid-Point Brace	
D	S	B	t	ksi	ksi	in. <sup>2</sup>	lbs	lbs	lbs	lbs	lbs/in.
362	S	125	33	33	45	0.2275	746	2041	878	2401	100
362	S	162	43	33	45	0.3398	1775	4117	2088	4844	202
362	S	162	68	50	65	0.5237	3352	7974	3944	9381	391
600	S	125	33	33	45	0.3097	691	2052	813	2414	101
600	S	162	43	33	45	0.4469	2251	5079	2648	5975	249
600	S	162	97	50	65	0.9655	5677	16894	6679	19875	828
800	S	162	43	33	45	0.5371	2104	4965	2475	5841	243
800	S	162	97	50	65	1.1689	5903	16594	6945	19522	813

Table 4.4 Average As-built Properties of the Test Specimens Using AISIWIN Program

Stud Designation				Tension Coupon Test Results		AISIWIN					Required Ideal Brace Stiffness
				Yield Stress	Ultimate Stress	As-Built Section Area	As-Built Ultimate Capacity ( $P_u$ )		As-Built Unfactored Capacity ( $P_n$ )		$\beta_{ideal}$
				$F_y$	$F_u$		Unbraced	Mid-Point Brace	No Brace	Mid-Point Brace	
D	S	B	t	ksi	ksi	in. <sup>2</sup>	lbs	lbs	lbs	lbs	lbs/in.
362	S	125	33	48.53	55.48	0.2028	704	1978	828	2327	97
362	S	162	43	47.04	58.20	0.3089	1688	4411	1986	5189	216
362	S	162	68	52.01	67.80	0.5154	3515	8448	4135	9939	414
600	S	125	33	24.03	45.24	0.2537	592	1548	696	1821	76
600	S	162	43	46.24	54.88	0.4135	2156	5832	2536	6861	286
600	S	162	43a	50.30	59.38	0.4346	2465	6721	2900	7907	329
600	S	162	97	60.20	70.21	0.9807	6277	19888	7385	23398	975
800	S	162	43	40.23	54.90	0.4829	1967	5180	2314	6094	254
800	S	162	97	42.50	67.49	1.1843	6686	17989	7866	21164	882

AISIWIN program was used to calculate the As-Built values of the test specimens  
Ideal Brace Stiffness was obtained using Yura's Bracing Equation 2.14 (Yura 1995)  
Design factor used in calculating the Unfactored Capacity is 0.85

Table 4.5 Calculated Brace Stiffness and Total Brace Stiffness of the Test Specimens

Stud Designation					Target Brace Stiffness	Wire				Actual Stiffness per Wire	AISIWIN Unfactored Load $P_n$	Total Brace Stiffness	Ideal Brace Stiffness	Brace Factor
						$\beta_{provided}$	$\beta_{ideal}$	$\frac{\beta_{provided}}{\beta_{ideal}}$						
D	S	B	t	ID	lbs/in.	Dia. in.	Area in. <sup>2</sup>	L in.	Nos.	lbs/in.	lbs	lbs/in.	lbs/in.	$\beta_{ideal}$
362	S	125	33	1	200	0.016	0.000201	56.50	2	206	2327	413	97	4.3
362	S	125	33	2	400	0.016	0.000201	30.50	2	382	2327	765	97	7.9
362	S	125	33	3	100	0.016	0.000201	60.75	1	96	2327	192	97	2.0
362	S	125	33	4	100	0.016	0.000201	60.75	1	96	2327	192	97	2.0
362	S	125	33	5	0	0	0.000000	0	0	0	828	Not Braced		
362	S	125	33	6	100	0.016	0.000201	58.00	1	101	2327	201	99	1.9
362	S	162	43	1	0						1986	Not Braced		
362	S	162	43	2	200	0.024	0.000452	70.75	1	185	5189	371	216	1.7
362	S	162	43	3	800	0.024	0.000452	35.50	2	739	5189	1478	216	6.8
362	S	162	43	4	400	0.024	0.000452	35.75	1	367	5189	734	216	3.4
362	S	162	68	2	1000	0.033	0.000855	24.25	1	1023	9939	2046	414	4.9
362	S	162	68	3	500	0.033	0.000855	48.50	1	511	9939	1023	414	2.5
362	S	162	68	4	750	0.033	0.000855	32.25	1	769	9939	1538	414	3.7
362	S	162	68	5	0					0	4135	Not Braced		

Table 4.5 (Continued) Calculated Brace Stiffness and Total Brace Stiffness of the Test Specimens

Stud Designation					Target Brace Stiffness	Wire				Actual Stiffness per Wire	AISIWIN Unfactored Load $P_n$	Total Brace Stiffness	Ideal Brace Stiffness	Brace Factor
						Dia.	Area	L	Nos.					$\beta_{provided}$
D	S	B	t	ID	lbs/in.	in.	in. <sup>2</sup>	in.		lbs/in.	lbs	lbs/in.	lbs/in.	$\beta_{ideal}$
600	S	125	33	1	200	0.016	0.000201	29.00	1	201	1821	402	76	5.3
600	S	125	33	2	0					0	696	Not Braced		
600	S	125	33	3	60	0.01	0.000079	37.00	1	62	1821	123	76	1.6
600	S	125	33	4	30	0.01	0.000079	75.00	1	30	1821	61	76	0.8
600	S	162	43	1	250	0.024	0.000452	52.75	1	249	6861	497	286	1.7
600	S	162	43	2	75	0.016	0.000201	79.00	1	74	6861	148	286	0.5
600	S	162	43	4	500	0.024	0.000452	26.50	1	495	6861	990	286	3.5
600	S	162	43	5	30	0.01	0.000079	75.25	1	30	6861	61	286	0.2
600	S	162	43	6	0					0	2536	Not Braced		
600	S	162	43	6a	0					0	2900	Not Braced		
600	S	162	97	1	1000	0.0625	0.003068	86.00	1	1035	23398	2069	975	2.1
600	S	162	97	2	1500	0.0625	0.003068	53.00	1	1679	23398	3357	975	3.4
600	S	162	97	3	500	0.0348	0.000951	53.00	1	520	23398	1041	975	1.1
600	S	162	97	4	160	0.024	0.000452	81.00	1	162	23398	324	975	0.3
600	S	162	97	5	0					0	7385	Not Braced		
800	S	162	43	2	75	0.016	0.000201	78.25	1	75	6094	149	254	0.6
800	S	162	43	3	150	0.016	0.000201	39.00	1	150	6094	299	254	1.2
800	S	162	43	4	0					0	2314	Not Braced		
800	S	162	43	5	300	0.016	0.000201	38.75	2	301	6094	602	254	2.4
800	S	162	97	1	1000	0.0625	0.003068	85.00	1	1047	21164	2093	882	2.4
800	S	162	97	2	500	0.0348	0.000951	53.00	1	520	21164	1041	882	1.2
800	S	162	97	3	0					0	7866	Not Braced		
800	S	162	97	4	2100	0.0475	0.001772	24.50	1	2098	21164	4195	882	4.8

Table 4.6 Summary of Experimental Test Results for Test Specimens

Stud Designation					Target Brace Stiffness	Axial Capacity			Observed Failure Mode	Increase in $P_{max}$ of Braced over Unbraced Studs
						Analytical		Experimental Load		
						No Brace	Mid-Pt Brace			
D		B	t	ID	lbs/in.	$P_n$ (lbs)	$P_n$ (lbs)	$P_{max}$ (lbs)		%
362	S	125	33	5	0	828	-	1127	F[1] - T[1]	0.00
362	S	125	33	3	100	-	2327	2749	F[2] - T[2]	143.80
362	S	125	33	4	100	-	2327	2306	F[2] - T[2]	104.51
362	S	125	33	6	100	-	2327	2399	Distortional	112.79
362	S	125	33	1	200	-	2327	3012	F[2]	167.17
362	S	125	33	2	400	-	2327	2959	F[2] - T[2]	162.47
362	S	162	43	1	0	1986	-	5223	T[1] - F[1]	0.00
362	S	162	43	2	200	-	5189	7268	F[1] - T[2]	39.15
362	S	162	43	4	400	-	5189	7029	F[1] - T[2]	34.58
362	S	162	43	3	800	-	5189	6557	T[2]	25.54
362	S	162	68	5	0	4135	-	6451	F[1] - T[1]	0.00
362	S	162	68	3	500	-	9939	13384	T[1] - F[1]	107.47
362	S	162	68	4	750	-	9939	14029	T[2]	117.47
362	S	162	68	2	1000	-	9939	14792	T[2]	129.30
600	S	125	33	2	0	696	-	984	Distortional	0.00
600	S	125	33	4	30	-	1821	1951	F[1]	98.27
600	S	125	33	3	60	-	1821	2271	Distortional	130.79
600	S	125	33	1	200	-	1821	1302	Distortional	32.32
600	S	162	43	6	0	2536	-	5144	Distortional	0.00
600	S	162	43	6a	0	2900	-	4258	F[1]	0.00
600	S	162	43	5	30	-	6861	7163	Distortional	39.25
600	S	162	43	2	75	-	6861	6052	Distortional	17.65
600	S	162	43	1	250	-	6861	7308	Distortional	42.07
600	S	162	43	4	500	-	6861	7075	Distortional	37.54
600	S	162	97	5	0	7385	-	21029	F[1]	0.00
600	S	162	97	4	160	-	23398	28306	F[1] - T[1]	34.60
600	S	162	97	3	500	-	23398	30085	F[1] - T[1]	43.06
600	S	162	97	1	1000	-	23398	28553	T[1]	35.78
600	S	162	97	2	1500	-	23398	29472	T[1]	40.15
800	S	162	43	4	0	2314	-	4591	F[1]	0.00
800	S	162	43	2	75	-	6094	4306	F[1]	-6.21
800	S	162	43	3	150	-	6094	5333	Distortional	16.16
800	S	162	43	5	300	-	6094	6213	F[2]	35.33
800	S	162	97	3	0	7866	-	19703	F[1]	0.00
800	S	162	97	2	500	-	21164	21626	Distortional	9.76
800	S	162	97	1	1000	-	21164	23811	Distortional	20.85
800	S	162	97	4	2100	-	21164	23537	T[1]	19.46

Table 4.7 Required Brace Stiffness Based on  $P_{max}$ 

Stud Designation					Total Brace Stiffness	Brace Factor	AISIWIN Unfactored Load	Experimental Load	Required Total Stiffness	Brace Factor
					$\beta_{provided}$	$\beta_{provided}$	$P_n$	$P_{max}$	$\beta_{required}$	$\beta_{provided}$
D	S	B	t	ID	lbs/in.	$\beta_{ideal}$	lbs	lbs	lbs/in.	$\beta_{required}$
362	S	125	33	5	0	-	828	1127	-	-
362	S	162	43	1	0	-	1986	5223	-	-
362	S	162	68	5	0	-	4135	6451	-	-
600	S	125	33	2	0	-	696	984	-	-
600	S	162	43	6	0	-	2536	5144	-	-
600	S	162	43	6a	0	-	2900	4258	-	-
600	S	162	97	5	0	-	7385	21029	-	-
800	S	162	43	4	0	-	2314	4591	-	-
800	S	162	97	3	0	-	7866	19703	-	-
600	S	125	33	4	61	0.8	1821	1951	81	0.7
600	S	162	43	5	61	0.2	6861	7163	298	0.2
600	S	162	43	2	148	0.5	6861	6052	252	0.6
600	S	162	97	4	324	0.3	23398	28306	1179	0.3
800	S	162	43	2	149	0.6	6094	4306	179	0.8
600	S	125	33	3	123	1.6	1821	2271	95	1.3
600	S	162	97	3	1041	1.1	23398	30085	1254	0.8
800	S	162	43	3	299	1.2	6094	5333	222	1.3
800	S	162	97	2	1041	1.2	21164	21626	901	1.2
362	S	125	33	3	192	2.0	2327	2749	115	1.7
362	S	125	33	4	192	2.0	2327	2306	96	2.0
362	S	125	33	6	201	1.9	2327	2399	100	2.0
362	S	162	43	2	371	1.7	5189	7268	303	1.2
362	S	162	68	3	1023	2.5	9939	13384	558	1.8
600	S	162	43	1	497	1.7	6861	7308	305	1.6
600	S	162	97	1	2069	2.1	23398	28553	1190	1.7
800	S	162	43	5	602	2.4	6094	6213	259	2.3
800	S	162	97	1	2093	2.4	21164	23811	992	2.1
362	S	125	33	1	413	4.3	2327	3012	126	3.3
362	S	125	33	2	765	7.9	2327	2959	123	6.2
362	S	162	43	4	734	3.4	5189	7029	293	2.5
362	S	162	43	3	1478	6.8	5189	6557	273	5.4
362	S	162	68	4	1538	3.7	9939	14029	585	2.6
362	S	162	68	2	2046	4.9	9939	14792	616	3.3
600	S	125	33	1	402	5.3	1821	1302	54	7.4
600	S	162	43	4	990	3.5	6861	7075	295	3.4
600	S	162	97	2	3357	3.4	23398	29472	1228	2.7
800	S	162	97	4	4195	4.8	21164	23537	981	4.3



Table 4.8 Effective Length Factors Based on  $P_{max}$ 

Stud Designation					Total Brace Stiffness	Observed Failure Mode	Effective Length Factors based on $P_{max}$			
							$\beta_{provided}$	$K_x$	$K_y$	$K_t$
D	S	B	t	ID	lbs/in.					lbs
362	S	125	33	5	0	F[1] - T[1]	0.50	0.67	0.64	1127
362	S	125	33	3	192	F[2] - T[2]	0.50	0.25	0.25	2749
362	S	125	33	4	192	F[2] - T[2]	0.50	0.36	0.34	2306
362	S	125	33	6	201	Distortional	0.50	0.33	0.31	2399
362	S	125	33	1	413	F[2]	0.50	0.25	0.25	3012
362	S	125	33	2	765	F[2] - T[2]	0.50	0.25	0.25	2959
362	S	162	43	1	0	T[1] - F[1]	0.50	0.52	0.43	5223
362	S	162	43	2	371	F[1] - T[2]	0.50	0.25	0.25	7268
362	S	162	43	4	734	F[1] - T[2]	0.50	0.25	0.25	7029
362	S	162	43	3	1478	T[2]	0.50	0.25	0.25	6557
362	S	162	68	5	0	F[1] - T[1]	0.50	0.69	0.62	6451
362	S	162	68	3	1023	T[1] - F[1]	0.50	0.25	0.25	13384
362	S	162	68	4	1538	T[2]	0.50	0.25	0.25	14029
362	S	162	68	2	2046	T[2]	0.50	0.25	0.25	14792
600	S	125	33	2	0	Distortional	0.50	0.80	0.96	984
600	S	125	33	4	61	F[1]	0.50	0.45	0.52	1951
600	S	125	33	3	123	Distortional	0.50	0.32	0.37	2271
600	S	125	33	1	402	Distortional	0.50	0.68	0.80	1302
600	S	162	43	6	0	Distortional	0.50	0.65	0.70	5144
600	S	162	43	6a	0	F[1]	0.50	0.80	0.85	4258
600	S	162	43	5	61	Distortional	0.50	0.47	0.49	7163
600	S	162	43	2	148	Distortional	0.50	0.57	0.60	6052
600	S	162	43	1	497	Distortional	0.50	0.46	0.47	7308
600	S	162	43	4	990	Distortional	0.50	0.48	0.50	7075
600	S	162	97	5	0	F[1]	0.50	0.54	0.65	21029
600	S	162	97	4	324	F[1] - T[1]	0.50	0.39	0.45	28306
600	S	162	97	3	1041	F[1] - T[1]	0.50	0.35	0.40	30085
600	S	162	97	1	2069	T[1]	0.50	0.39	0.44	28553
600	S	162	97	2	3357	T[1]	0.50	0.37	0.41	29472
800	S	162	43	4	0	F[1]	0.50	0.66	0.77	4591
800	S	162	43	2	149	F[1]	0.50	0.69	0.80	4306
800	S	162	43	3	299	Distortional	0.50	0.58	0.67	5333
800	S	162	43	5	602	F[2]	0.50	0.48	0.56	6213
800	S	162	97	3	0	F[1]	0.50	0.52	0.66	19703
800	S	162	97	2	1041	Distortional	0.50	0.46	0.58	21626
800	S	162	97	1	2093	Distortional	0.50	0.39	0.48	23811
800	S	162	97	4	4195	T[1]	0.50	0.40	0.49	23537

Table 4.9 Measured Values of Brace Force and Mid-height Displacement at  $P_{max}$

Stud Designation					Target Brace Stiffness	Experimental Load	Measured Initial Bow	Measured Values at $P_{max}$				$P_{br}$ as % of $P_{max}$	Average $\Delta_w$ in terms of L/250
								Brace Force	Weak Axis Displacement, $\Delta_w$				
						$P_{br}$		N-Flange	S- Flange	Average			
D	S	B	t	ID	lbs/in.	lbs	in.	lbs	in.	in.	in.	%	
362	S	125	33	5	0	1127	0.000	-	0.4065	0.8289	0.618	-	1.61
362	S	125	33	3	100	2749	0.000	9.55	0.0835	0.0661	0.075	0.35	0.19
362	S	125	33	4	100	2306	0.000	22.41	0.1577	0.0006	0.079	0.97	0.21
362	S	125	33	6	100	2399	0.000	14.47	0.0099	0.1561	0.083	0.60	0.22
362	S	125	33	1	200	3012	0.000	10.55	0.0173	0.0451	0.031	0.35	0.08
362	S	125	33	2	400	2959	0.000	32.43	0.0906	0.1925	0.142	1.10	0.37
362	S	162	43	1	0	5223	0.000	-	0.8281	0.0845	0.456	-	1.19
362	S	162	43	2	200	7268	0.000	19.37	0.1007	0.0411	0.071	0.27	0.18
362	S	162	43	4	400	7029	0.000	39.07	0.0815	0.0324	0.057	0.56	0.15
362	S	162	43	3	800	6557	0.010	34.67	0.0852	-0.0246	0.055	0.53	0.08
362	S	162	68	5	0	6451	0.100	-	2.8548	-0.2529	1.554	-	3.39
362	S	162	68	3	500	13384	-0.155	159.31	0.4032	-0.0366	0.220	1.19	0.48
362	S	162	68	4	750	14029	0.140	131.92	0.1315	0.0118	0.072	0.94	0.19
362	S	162	68	2	1000	14792	-0.187	144.26	0.0644	0.1814	0.123	0.98	0.32

Table 4.9 (Continued) Measured Values of Brace Force and Mid-height Displacement at  $P_{max}$ 

Stud Designation					Target Brace Stiffness	Experimental Load	Measured Initial Bow	Measured Values at $P_{max}$				$P_{br}$ as % of $P_{max}$	Average $\Delta_w$ in terms of L/250
								$P_{max}$	Brace Force	Weak Axis Displacement, $\Delta_w$			
						$P_{br}$			N-Flange	S- Flange	Average		
D	S	B	t	ID	lbs/in.	lbs	in.	lbs	in.	in.	in.	%	
600	S	125	33	2	0	984	0.130	-	0.7034	0.2548	0.479	-	1.25
600	S	125	33	4	30	1951	0.075	25.05	0.6312	0.2406	0.436	1.28	1.14
600	S	125	33	3	60	2271	0.120	11.86	-0.1936	-0.0529	0.123	0.52	-0.32
600	S	125	33	1	200	1302	0.100	1.10	-0.0146	-0.0208	0.018	0.08	-0.05
600	S	162	43	6	0	5144	0.015	-	0.3305	0.2255	0.278	-	0.72
600	S	162	43	6a	0	4258	0.090	-	-1.0398	-0.9219	0.981	-	-2.55
600	S	162	43	5	30	7163	0.075	15.51	0.0298	-0.4001	0.215	0.22	-0.48
600	S	162	43	2	75	6052	-	57.49	1.0127	0.0393	0.526	0.95	1.37
600	S	162	43	1	250	7308	-	7.43	-0.0378	-0.0064	0.022	0.10	-0.06
600	S	162	43	4	500	7075	-	14.85	0.0238	0.0102	0.017	0.21	0.04
600	S	162	97	5	0	21029	-	-	-0.1614	-0.9538	0.558	-	-1.45
600	S	162	97	4	160	28306	-	45.23	0.0961	-0.1869	0.142	0.16	-0.12
600	S	162	97	3	500	30085	0.000	137.53	-0.3179	0.0125	0.165	0.46	-0.40
600	S	162	97	1	1000	28553	0.110	171.51	-0.3955	-0.0472	0.221	0.60	-0.58
600	S	162	97	2	1500	29472	0.110	154.42	-0.0220	-0.2422	0.132	0.52	-0.34

Table 4.9 (Continued) Measured Values of Brace Force and Mid-height Displacement at  $P_{max}$

Stud Designation					Target Brace Stiffness	Experimental Load	Measured Initial Bow	Measured Values at $P_{max}$				$P_{br}$ as Percentage of $P_{max}$	Average $\Delta_w$ in terms of L/250
								Brace Force	Weak Axis Displacement				
						$P_{br}$		N- Flange	S- Flange	Average			
D	S	B	t	ID	lbs/in.	lbs	in.	lbs	in.	in.	in.	%	
800	S	162	43	4	0	4591	0.000	-	-0.4082	-0.8840	0.646	-	-1.68
800	S	162	43	2	75	4306	-	24.69	-0.0027	0.4608	0.232	0.57	0.60
800	S	162	43	3	150	5333	0.120	71.52	0.3110	-0.2260	0.269	1.34	0.11
800	S	162	43	5	300	6213	0.000	16.81	-0.0482	-0.0811	0.065	0.27	-0.17
800	S	162	97	3	0	19703	0.000	-	0.4080	0.3385	0.373	-	0.97
800	S	162	97	2	500	21626	0.000	85.60	0.1250	0.2550	0.190	0.40	0.49
800	S	162	97	1	1000	23811	0.000	115.45	0.2014	0.1889	0.195	0.48	0.51
800	S	162	97	4	2100	23537	0.000	69.64	0.2314	0.0723	0.152	0.30	0.40

Table 4.10 Calculated Values of Brace Force and Mid-height Displacement at  $P_{max}$

Stud Designation					Target Brace Stiffness	Experimental Load	Measured Initial Bow	Measured Weak Axis Displacement at $P_{max}$		Calculated Brace Force for Measured Weak Axis Displacement			$P_{br}$ as % of $P_{max}$
						$P_{max}$		N-Flange	S-Flange	N-Flange	S-Flange	Total	
D	S	B	t	ID	lbs/in.	lbs	in.	in.	in.	lbs	lbs	lbs	%
362	S	125	33	5	0	1127	0.000	0.4065	0.8289	-	-		
362	S	125	33	3	100	2749	0.000	0.0835	0.0661	9.6	7.6	17.1	0.62
362	S	125	33	4	100	2306	0.000	0.1577	0.0006	15.2	0.1	15.2	0.66
362	S	125	33	6	100	2399	0.000	0.0099	0.1561	1.0	15.6	16.6	0.69
362	S	125	33	1	200	3012	0.000	0.0173	0.0451	2.2	5.7	7.8	0.26
362	S	125	33	2	400	2959	0.000	0.0906	0.1925	11.2	23.7	34.9	1.18
362	S	162	43	1	0	5223	0.000	0.8281	0.0845	-	-		
362	S	162	43	2	200	7268	0.000	0.1007	0.0411	30.5	12.5	43.0	0.59
362	S	162	43	4	400	7029	0.000	0.0815	0.0324	23.9	9.5	33.4	0.47
362	S	162	43	3	800	6557	0.010	0.0852	-0.0246	26.0	4.0	30.0	0.46
362	S	162	68	5	0	6451	0.100	2.8548	-0.2529	-	-		
362	S	162	68	3	500	13384	-0.155	0.4032	-0.0366	138.4	106.9	245.3	1.83
362	S	162	68	4	750	14029	0.140	0.1315	0.0118	158.7	88.8	247.5	1.76
362	S	162	68	2	1000	14792	-0.187	0.0644	0.1814	75.6	3.5	79.0	0.53
600	S	125	33	2	0	984	0.130	0.7034	0.2548	-	-		
600	S	125	33	4	30	1951	0.075	0.6312	0.2406	57.4	25.7	83.1	4.26
600	S	125	33	3	60	2271	0.120	-0.1936	-0.0529	7.0	6.3	13.3	0.59
600	S	125	33	1	200	1302	0.100	-0.0146	-0.0208	4.6	4.3	8.9	0.69

Table 4.10 (Continued) Calculated Values of Brace Force and Mid-height Displacement at  $P_{max}$

Stud Designation					Target Brace Stiffness	Experimental Load	Measured Initial Bow	Measured Weak Axis Displacement at $P_{max}$		Calculated Brace Force for Measured Weak Axis Displacement			$P_{br}$ as % of $P_{max}$
						$P_{max}$		N-Flange	S-Flange	N-Flange	S-Flange	Total	
D	S	B	t	ID	lbs/in.	lbs	in.	in.	in.	lbs	lbs	lbs	%
600	S	162	43	6	0	5144	0.000	0.3305	0.2255	-	-		
600	S	162	43	6a	0	4258	-0.036	-1.0398	-0.9219	-	-		
600	S	162	43	5	30	7163	0.000	0.0298	-0.4001	8.9	119.4	128.3	1.79
600	S	162	43	2	75	6052	0.030	1.0127	0.0393	262.9	17.5	280.4	4.63
600	S	162	43	1	250	7308	0.040	-0.0378	-0.0064	0.7	10.2	10.9	0.15
600	S	162	43	4	500	7075	0.000	0.0238	0.0102	7.0	3.0	10.0	0.14
600	S	162	97	5	0	21029	0.015	-0.1614	-0.9538	-	-		
600	S	162	97	4	160	28306	0.075	0.0961	-0.1869	201.8	220.4	422.2	1.49
600	S	162	97	3	500	30085	-	-0.3179	0.0125	398.6	15.7	414.3	1.38
600	S	162	97	1	1000	28553	-	-0.3955	-0.0472	470.5	56.1	526.6	1.84
600	S	162	97	2	1500	29472	-	-0.0220	-0.2422	27.0	297.4	324.4	1.10
800	S	162	43	4	0	4591	0.110	-0.4082	-0.8840	-	-		
800	S	162	43	2	75	4306	0.090	-0.0027	0.4608	15.7	82.7	98.3	2.28
800	S	162	43	3	150	5333	0.110	0.3110	-0.2260	93.5	25.8	119.3	2.24
800	S	162	43	5	300	6213	0.000	-0.0482	-0.0811	12.5	21.0	33.5	0.54
800	S	162	97	3	0	19703	-	0.4080	0.3385	-	-		
800	S	162	97	2	500	21626	-	0.1250	0.2550	112.6	229.8	342.4	1.58
800	S	162	97	1	1000	23811	-	0.2014	0.1889	199.8	187.4	387.2	1.63
800	S	162	97	4	2100	23537	0.120	0.2314	0.0723	344.6	188.5	533.2	2.27

Table 4.11 Proposed Test Matrix for Bridging Connection Tests

Specimen Type	Stud Designation						Number of Tests	
	D	S	B	t	N	C	Out-of-Plane	In-Plane
1	362	S	125	33	1	SS	2	2
2	362	S	162	43	1	SS	2	2
3	362	S	162	68	1	SS	2	2
4	362	S	162	68	1	WW	2	2
5	362	S	162	68	1	DW	2	2
6	600	S	125	33	1	SS	2	2
7	600	S	162	43	1	SS	2	2
8	600	S	162	97	3	SS	2	2
9	600	S	162	97	1	WW	2	2
10	600	S	162	97	1	DW	2	2
11	800	S	162	43	1	SS	2	2
12	800	S	162	97	1	SS	2	2
13	800	S	162	97	1	WW	2	2
14	800	S	162	97	1	DW	2	2

Table 4.12 Bridging Test Results for Out-of-Plane Loading

Stud Designation						Applied Load	Displacement		Final Torsional Stiffness	Failure Types
							R <sub>FRONT</sub>	R <sub>BACK</sub>		
						T <sub>max</sub>	Δ <sub>RB</sub>	Δ <sub>RF</sub>	K <sub>T</sub>	
D	S	B	t	N	C	lbs.	in.	in.	lbs/in.	
362	S	125	33	1	SS	57.37	0.184	-0.008	311	Screw Pullout
362	S	125	33	2	SS	71.10	0.208	-0.005	342	Screw Pullout
362	S	162	43	1	SS	69.19	0.073	0.014	945	Screw Pullout, Angle Distortion
362	S	162	43	2	SS	63.05	0.098	0.002	640	Screw Pullout, Angle Distortion
362	S	162	68	1	SS	128.91	0.067	0.003	1925	Screw Pullout, Angle Distortion
362	S	162	68	2	SS	102.39	0.059	-0.002	1731	Screw Pullout, Angle Distortion
362	S	162	68	1	WW	138.81	0.028	0.009	4908	Angle Tear
362	S	162	68	2	WW	150.23	0.031	0.008	4917	Angle Tear
362	S	162	68	1	DW	166.15	0.04	0.027	4491	Weld Failure
362	S	162	68	2	DW	149.83	0.036	0.031	4149	Weld Failure
600	S	125	33	1	SS	113.91	0.31	0.024	370	Screw Pullout
600	S	125	33	2	SS	83.59	0.200	0.019	418	Screw Pullout
600	S	162	43	1	SS	66.09	0.109	-0.008	605	Screw Pullout, Angle Distortion
600	S	162	43	2	SS	137.95	0.202	-0.009	682	Screw Pullout
600	S	162	97	3	SS	280.33	0.061	0.001	4564	Screw Pullout
600	S	162	97	4	SS	272.34	0.067	0.002	4094	Screw Pullout
600	S	162	97	1	WW	380.67	0.044	0.014	8747	Angle Tear
600	S	162	97	2	WW	421.57	0.067	0.021	6276	Angle Tear
600	S	162	97	1	DW	199.59	0.047	0.041	4267	Weld Failure
600	S	162	97	2	DW	156.88	0.042	0.019	3753	Weld Failure
800	S	162	43	1	SS	161.23	0.150	0.002	1075	Screw Pullout, Angle Distortion
800	S	162	43	2	SS	145.14	0.129	0.000	1128	Screw Pullout, Angle Distortion
800	S	162	97	1	SS	255.75	0.029	0.004	8735	Screw Shear Failure
800	S	162	97	2	SS	273.51	0.039	0.003	7049	Screw Shear Failure
800	S	162	97	1	WW	291.13	0.015	0.002	20036	Weld Failure, Angle Distortion
800	S	162	97	2	WW	388.28	0.026	0.014	14797	Weld Failure, Angle Distortion
800	S	162	97	1	DW	207.52	0.038	0.030	5503	Weld Separation
800	S	162	97	2	DW	162.02	0.031	0.020	5272	-



Table 4.13 Initial Torsional Stiffness of the Lower Bound Values of Out-of-Plane Tests

Stud Designation						Initial Load at 10% of $T_{max}$ ( $T_{10}$ )	Experimental X-Displacement ( $\Delta$ )	Rotation ( $\Phi=\Delta/l_a$ )	Initial Torsional Stiffness ( $T_{10}*l_a/\Phi$ )	Flat-width at Hole ( $w-d_h$ )	Flat-width to Thickness Ratio	Slenderness Factor ( $\lambda$ )
D	S	B	t	N	C	lbs	in.	rad	kip-in./rad	in.	( $w-d_h$ )/t	( $w-d_h/t$ )/ $\sqrt{(f_v/E)}$
362	S	125	33	2	SS	7.18	0.294	0.027	2.95	1.90	57.71	2.34
362	S	125	33	1	SS	5.45	0.165	0.015	4.00	1.90	57.71	2.34
362	S	162	43	1	SS	7.31	0.166	0.015	5.33	1.89	44.06	1.76
362	S	162	43	2	SS	7.35	0.126	0.011	7.04	1.89	44.06	1.76
362	S	162	68	1	SS	12.79	0.112	0.010	13.88	1.79	26.25	1.10
362	S	162	68	2	SS	10.42	0.080	0.007	15.72	1.79	26.25	1.10
600	S	125	33	2	SS	8.86	0.153	0.014	7.02	4.28	129.83	3.71
600	S	125	33	1	SS	11.01	0.185	0.017	7.20	4.28	129.83	3.71
600	S	162	43	1	SS	6.81	0.039	0.004	21.04	4.27	99.41	3.94
600	S	162	43	2	SS	15.60	0.078	0.007	24.08	4.27	99.41	3.94
600	S	162	97	3	SS	32.91	0.127	0.012	31.38	4.02	41.44	1.87
600	S	162	97	4	SS	31.24	0.087	0.008	43.60	4.02	41.44	1.87

Table 4.13 (Continued) Initial Torsional Stiffness of the Lower Bound Values from the Out-of-Plane Tests

Stud Designation						Initial Load at 10% of $T_{max}$ ( $T_{10}$ )	Experimental X-Displacement ( $\Delta$ )	Rotation ( $\Phi=\Delta/l_a$ )	Initial Torsional Stiffness ( $T_{10}^*l_a/\Phi$ )	Flat-width at Hole ( $w-d_h$ )	Flat-width to Thickness Ratio	Slenderness Factor ( $\lambda$ )
D	S	B	t	N	C	lbs	in.	rad	kip-in./rad	in.	( $w-d_h$ )/t	( $w-d_h/t$ ) $\sqrt{(f_v/E)}$
800	S	162	43	2	SS	13.22	0.031	0.003	51.41	6.27	145.92	5.39
800	S	162	43	1	SS	31.77	0.064	0.006	60.32	6.27	145.92	5.39
800	S	162	97	2	SS	28.30	0.049	0.004	70.32	6.02	62.06	2.36
800	S	162	97	1	SS	29.99	0.046	0.004	78.95	6.02	62.06	2.36
362	S	162	68	1	WW	11.03	0.018	0.002	75.79	1.79	26.25	1.06
362	S	162	68	2	WW	13.51	0.016	0.001	99.27	1.79	26.25	1.06
600	S	162	97	2	WW	49.88	0.031	0.003	197.38	4.02	41.44	1.68
600	S	162	97	1	WW	41.71	0.024	0.002	211.10	4.02	41.44	1.68
800	S	162	97	2	WW	132.07	0.068	0.006	236.61	6.02	62.06	2.52
800	S	162	97	1	WW	144.52	0.056	0.005	314.45	6.02	62.06	2.52
362	S	162	68	2	DW	21.84	0.091	0.008	28.89	2.06	30.25	1.23
362	S	162	68	1	DW	21.40	0.080	0.007	32.40	2.06	30.25	1.23
600	S	162	97	2	DW	21.67	0.100	0.009	26.31	4.41	45.44	1.84
600	S	162	97	1	DW	22.02	0.100	0.009	26.72	4.41	45.44	1.84
800	S	162	97	2	DW	14.12	0.095	0.009	18.04	6.41	66.06	2.68
800	S	162	97	1	DW	21.26	0.093	0.008	27.58	6.41	66.06	2.68

Note: Elastic Modulus = 29500.0 ksi  
 Lever Arm for Moment = 11.0 in.  
 Width of punchout = 1.5 in.

Table 4.14 Bridging Test Results for In-Plane Loading

Stud Designation						Applied Load	Displacement of		Flexural Stiffness	Failure Type
							L <sub>FRONT</sub>	R <sub>FRONT</sub>		
D	S	B	t	N	C	F <sub>max</sub>	Δ <sub>LF</sub>	Δ <sub>RF</sub>	K <sub>F</sub>	
						lbs	in.	in.	lbs/in.	
362	S	125	33	3	SS	391.94	0.219	0.229	1752	Screw Pullout
362	S	125	33	4	SS	431.48	0.321	0.174	1743	Screw Pullout
362	S	162	43	3	SS	545.56	0.130	0.088	5005	Screw Pullout, Angle Distortion
362	S	162	43	4	SS	448.67	0.100	0.089	4755	Screw Pullout, Angle Distortion
362	S	162	68	3	SS	937.28	0.087	0.092	10496	Angle Distortion
362	S	162	68	4	SS	889.78	0.092	0.054	12225	Angle Distortion, Screw Tension
362	S	162	68	3	WW	1503.76	0.118	0.127	12263	Weld Failure
362	S	162	68	4	WW	1462.17	0.121	0.127	11817	Angle Tear
362	S	162	68	3	DW	3064.03	0.31	0.307	9883	Block Shear Rupture of Web
362	S	162	68	4	DW	2642.63	0.349	0.401	7054	Block Shear Rupture of Web
600	S	125	33	3	SS	425.80	0.29	0.223	1658	Screw Pullout
600	S	125	33	4	SS	302.94	0.174	0.186	1684	Screw Pullout
600	S	162	43	4	SS	640.80	0.131	0.125	5001	Screw Pullout
600	S	162	43	5	SS	587.06	0.214	0.381	5001	Screw Pullout
600	S	162	97	1	SS	1514.38	0.131	0.147	10902	Angle Distortion, Screw Tension
600	S	162	97	2	SS	1172.38	0.105	0.130	9996	Angle Distortion, Screw Tension
600	S	162	97	3	WW	1169.53	0.163	0.200	6444	Weld Failure
600	S	162	97	4	WW	1653.71	0.212	0.230	7477	Angle Tear
600	S	162	97	3	DW	-	-	-	-	-
600	S	162	97	4	DW	3159.07	0.469	0.464	6772	-
800	S	162	43	3	SS	275.60	0.073	0.093	3307	Screw Pullout
800	S	162	43	4	SS	522.66	0.137	0.151	3632	Screw Tension
800	S	162	97	3	SS	1402.04	0.064	0.030	29965	Screw Tension
800	S	162	97	4	SS	1719.25	0.221	0.427	5303	Screw Tension
800	S	162	97	3	WW	1238.18	0.143	0.148	8493	Angle Tear
800	S	162	97	4	WW	1101.97	0.151	0.111	8417	Angle Tear
800	S	162	97	3	DW	2908.04	0.526	0.553	5390	Weld Failure
800	S	162	97	4	DW	-	-	-	-	-

Table 4.15 Initial Flexural Stiffness of the In-Plane Tests

Stud Designation						Initial Load at 10% of $F_{max}$ ( $F_{10}$ )	Experimental Y-Displacement ( $D$ )	Initial Flexural Stiffness ( $F_{10}/\Delta$ )	Flat-width to Thickness Ratio	Slenderness Factor ( $\lambda$ )
D	S	B	t	N	C	lbs	in.	kip/in.	$(w-d_h)/t$	$(w-d_h/t) \sqrt{(f_y/E)}$
362	S	125	33	4	SS	45.25	0.027	1.68	57.71	2.34
362	S	125	33	3	SS	46.65	0.023	2.07	57.71	2.34
362	S	162	43	3	SS	52.00	0.015	3.57	44.06	1.76
362	S	162	43	4	SS	44.26	0.011	4.20	44.06	1.76
362	S	162	68	3	SS	104.77	0.017	6.10	26.25	1.10
362	S	162	68	4	SS	104.83	0.013	7.94	26.25	1.10
600	S	125	33	4	SS	30.21	0.030	1.00	129.83	3.71
600	S	125	33	3	SS	44.59	0.039	1.14	129.83	3.71
600	S	162	43	4	SS	69.11	0.018	3.78	99.41	3.94
600	S	162	43	3	SS	58.36	0.015	3.82	99.41	3.94
600	S	162	97	1	SS	149.64	0.027	5.57	41.44	1.87
600	S	162	97	2	SS	370.12	0.054	6.86	41.44	1.87
800	S	162	43	4	SS	99.58	0.048	2.07	145.92	5.39
800	S	162	43	3	SS	156.23	0.063	2.46	145.92	5.39
800	S	162	97	3	SS	124.78	0.018	7.08	62.06	2.36

Table 4.15 (Continued) Initial Flexural Stiffness of the In-Plane Tests

Stud Designation						Initial Load at 10% of $F_{max}$ ( $F_{10}$ )	Experimental Y-Displacement ( $D$ )	Initial Flexural Stiffness ( $F_{10}/\Delta$ )	Flat-width to Thickness Ratio	Slenderness Factor ( $\lambda$ )
D	S	B	t	N	C	lbs	in.	kip/in.	$(w-d_h)/t$	$(w-d_h/t) \sqrt{f_y/E}$
800	S	162	97	4	SS	172.05	0.058	2.95	62.06	2.36
362	S	162	68	4	WW	137.82	0.005	30.42	26.25	1.06
362	S	162	68	3	WW	183.14	0.004	40.79	26.25	1.06
600	S	162	97	3	WW	109.88	0.007	16.52	41.44	1.68
600	S	162	97	4	WW	95.25	0.006	15.24	41.44	1.68
800	S	162	97	4	WW	114.06	0.011	10.51	62.06	2.52
800	S	162	97	3	WW	178.58	0.009	19.67	62.06	2.52
362	S	162	68	3	DW	378.77	0.008	45.36	30.25	1.23
362	S	162	68	4	DW	206.19	0.004	50.41	30.25	1.23
600	S	162	97	3	DW	363.78	0.044	8.26	45.44	1.84
600	S	162	97	4	DW	-	-			
800	S	162	97	3	DW	364.75	0.152	2.40	66.06	2.68
800	S	162	97	4	DW	-	-			

Note: Elastic Modulus = 29500.0 ksi.  
Lever Arm for Moment = 11.0 in.  
Width of punchout = 1.5 in.

Table 4.16 Average Experimental Initial Stiffness of the In-Plane Load Tests

<b>SS Type Connection</b>				
<b>Initial Flexural Stiffness in kip/in.</b>				
<b>D vs. T</b>	<b>33</b>	<b>43</b>	<b>68</b>	<b>97</b>
<b>362</b>	1.88	3.89	7.02	
<b>600</b>	1.07	3.80		6.22
<b>800</b>		2.27		5.02
<b>WW Type Connection</b>				
<b>Initial Flexural Stiffness in kip/in.</b>				
<b>D vs. T</b>	<b>33</b>	<b>43</b>	<b>68</b>	<b>97</b>
<b>362</b>			35.61	
<b>600</b>				15.88
<b>800</b>				15.09
<b>DW Type Connection</b>				
<b>Initial Flexural Stiffness in kip/in.</b>				
<b>D vs. T</b>	<b>33</b>	<b>43</b>	<b>68</b>	<b>97</b>
<b>362</b>			47.89	
<b>600</b>				8.26
<b>800</b>				2.40

Table 4.17 Average Experimental Initial Stiffness of the Out-of-Plane Load Tests

<b>SS Type Connection</b>				
<b>Initial Torsional Stiffness in kip-in./rad</b>				
<b>D vs. T</b>	<b>33</b>	<b>43</b>	<b>68</b>	<b>97</b>
<b>362</b>	3.48	6.19	14.80	
<b>600</b>	7.11	22.56		37.49
<b>800</b>		55.87		74.64
<b>WW Type Connection</b>				
<b>Initial Torsional Stiffness in kip-in./rad</b>				
<b>D vs T</b>	<b>33</b>	<b>43</b>	<b>68</b>	<b>97</b>
<b>362</b>			87.53	
<b>600</b>				204.24
<b>800</b>				275.53
<b>DW Type Connection</b>				
<b>Initial Torsional Stiffness in kip-in./rad</b>				
<b>D vs T</b>	<b>33</b>	<b>43</b>	<b>68</b>	<b>97</b>
<b>362</b>			30.64	
<b>600</b>				26.52
<b>800</b>				22.81

Table 4.18 Maximum Flexural and Corresponding Torsional Brace Force

Stud Designation					Target Brace Stiffness	Brace Force		Corr. Axial Load	Flexural BF as % of P
						Maximum Flexural	Corr. Torsional		
D	S	B	t	ID	lbs/in.	lbs	lbs	lbs	%
362	S	125	33	3	100	5.92	0.44	1866.86	0.32
362	S	125	33	4	100	11.28	2.42	2299.90	0.49
362	S	125	33	6	100	7.23	7.22	2398.96	0.30
362	S	125	33	1	200	5.28	1.78	3012.17	0.18
362	S	125	33	2	400	16.22	2.15	2959.05	0.55
362	S	162	43	2	200	13.31	3.09	6190.00	0.22
362	S	162	43	4	400	25.53	4.59	5197.30	0.49
362	S	162	43	3	800	18.97	7.23	4466.38	0.42
362	S	162	68	3	500	79.65	76.57	13384.46	0.60
362	S	162	68	4	750	67.63	49.63	13787.71	0.49
362	S	162	68	2	1000	73.35	50.17	14596.98	0.50
600	S	125	33	4	30	12.53	6.50	1951.03	0.64
600	S	125	33	3	60	6.86	4.77	2241.37	0.31
600	S	125	33	1	200	1.47	0.65	823.73	0.18
600	S	162	43	5	30	7.75	6.77	7163.83	0.11
600	S	162	43	2	75	28.74	27.45	6052.34	0.47
600	S	162	43	1	250	5.05	0.61	1310.44	0.39
600	S	162	43	4	500	10.78	3.74	4231.99	0.25
600	S	162	97	4	160	22.61	12.37	28306.23	0.08
600	S	162	97	3	500	68.77	62.12	30085.90	0.23
600	S	162	97	1	1000	85.76	45.83	28553.51	0.30
600	S	162	97	2	1500	77.21	48.38	29472.16	0.26
800	S	162	43	2	75	12.35	10.36	4306.04	0.29
800	S	162	43	3	150	35.76	9.92	5333.03	0.67
800	S	162	43	5	300	21.42	12.67	3917.25	0.55
800	S	162	97	2	500	37.05	16.85	21626.00	0.17
800	S	162	97	1	1000	53.18	2.34	23811.17	0.22
800	S	162	97	4	2100	34.82	25.29	23537.15	0.15

Table 4.19 Maximum Torsional and Corresponding Flexural Brace Force

Stud Designation					Target Brace Stiffness	Brace Force		Corr. Axial Load	Torsional BF as % of P
						Corr. Flexural	Maximum Torsional		
D	S	B	t	ID	lbs/in.	lbs	lbs	lbs	%
362	S	125	33	3	100	4.78	2.67	2748.51	0.10
362	S	125	33	4	100	7.48	5.53	2066.30	0.27
362	S	125	33	6	100	7.23	7.22	2398.96	0.30
362	S	125	33	1	200	5.28	1.78	3012.17	0.06
362	S	125	33	2	400	12.86	2.37	2940.58	0.08
362	S	162	43	2	200	9.69	5.77	7268.46	0.08
362	S	162	43	4	400	19.53	16.96	7029.71	0.24
362	S	162	43	3	800	13.50	14.53	6338.90	0.23
362	S	162	68	3	500	79.65	76.57	13384.46	0.57
362	S	162	68	4	750	65.96	59.11	14029.50	0.42
362	S	162	68	2	1000	72.13	54.23	14792.16	0.37
600	S	125	33	4	30	12.53	6.50	1951.03	0.33
600	S	125	33	3	60	6.85	4.77	2249.36	0.21
600	S	125	33	1	200	1.11	1.15	1566.29	0.07
600	S	162	43	5	30	7.75	6.77	7163.83	0.09
600	S	162	43	2	75	28.74	27.45	6052.34	0.45
600	S	162	43	1	250	3.37	3.96	7079.07	0.06
600	S	162	43	4	500	9.86	3.86	3954.20	0.10
600	S	162	97	4	160	22.61	12.37	28306.23	0.04
600	S	162	97	3	500	68.77	62.12	30085.90	0.21
600	S	162	97	1	1000	84.46	45.87	28549.18	0.16
600	S	162	97	2	1500	77.21	48.38	29472.16	0.16
800	S	162	43	2	75	12.35	10.36	4306.04	0.24
800	S	162	43	3	150	35.76	9.92	5333.03	0.19
800	S	162	43	5	300	21.10	12.84	4001.41	0.32
800	S	162	97	2	500	28.81	19.10	20549.82	0.09
800	S	162	97	1	1000	20.66	14.66	19679.07	0.07
800	S	162	97	4	2100	34.82	25.29	23537.15	0.11



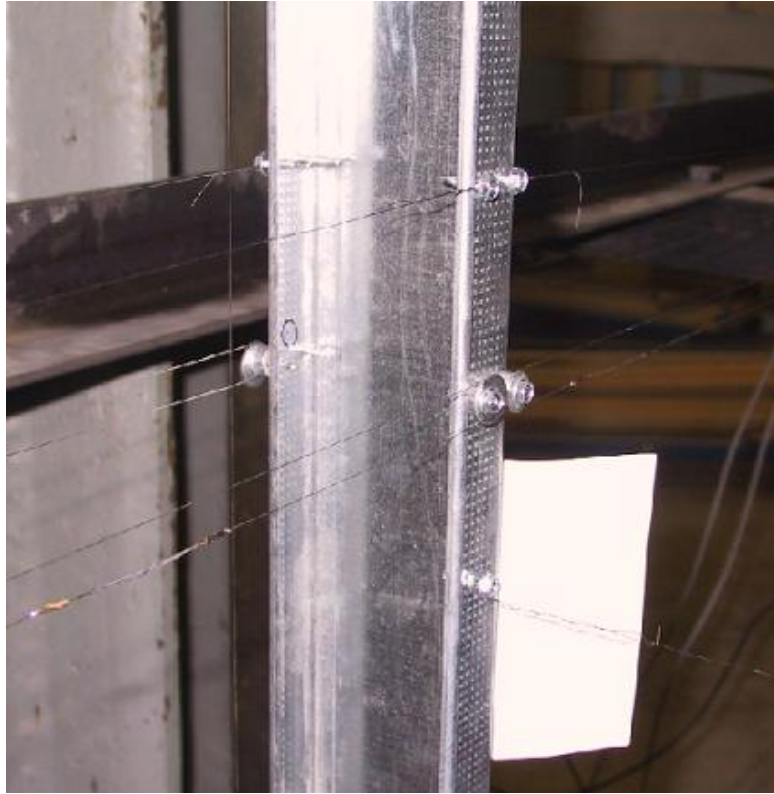


Figure 4.1 Typical Bracing for the Single Column Axial Load Tests

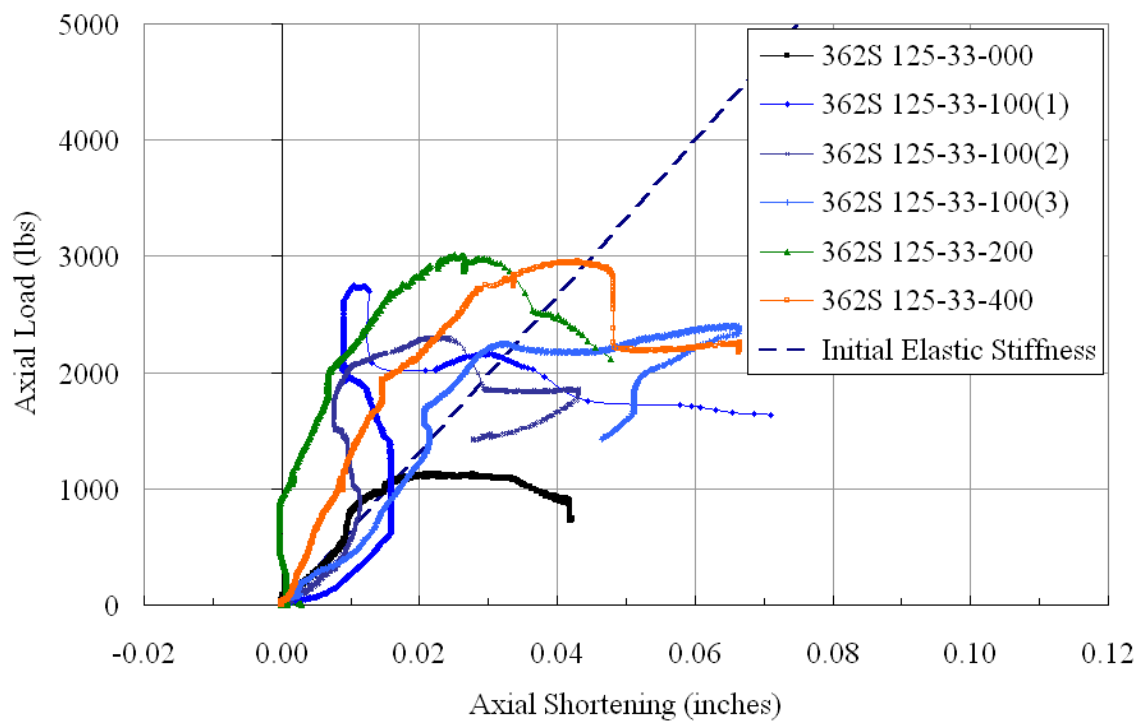


Figure 4.2 Axial Load vs. Axial Shortening for the Stud 362S125-33 with Varying Brace Stiffness

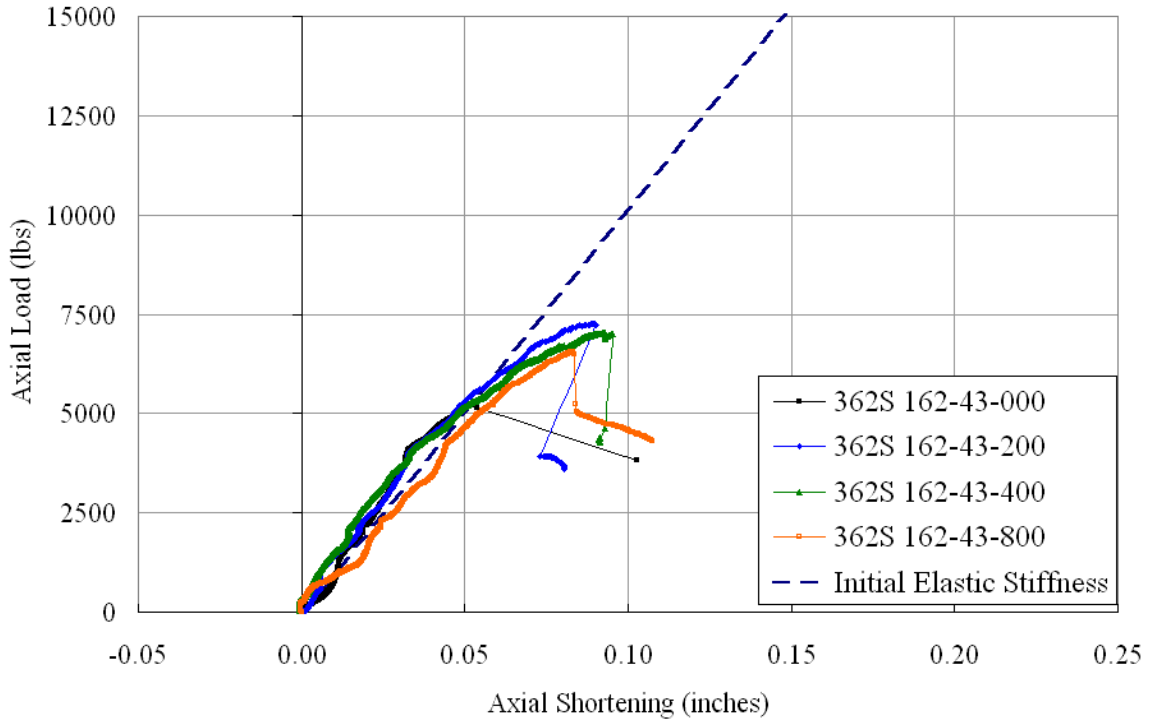


Figure 4.3 Axial Load vs. Axial Shortening for the Stud 362S162-43 with Varying Brace Stiffness

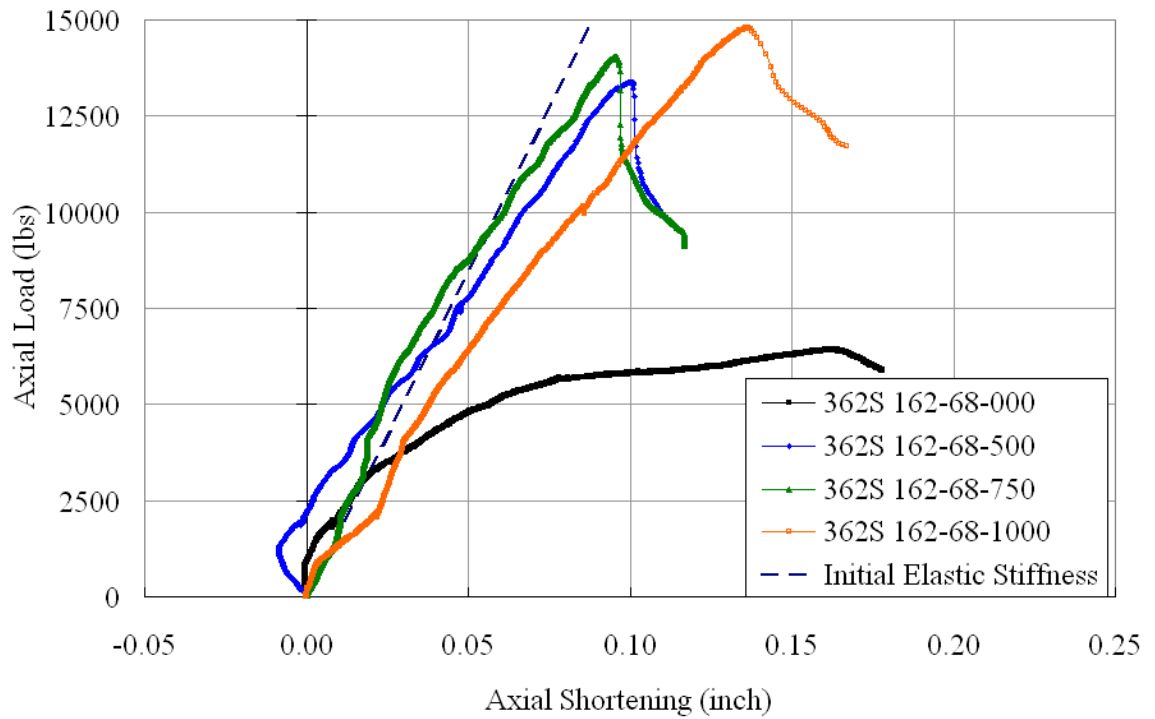


Figure 4.4 Axial Load vs. Axial Shortening for the Stud 362S162-68 with Varying Brace Stiffness

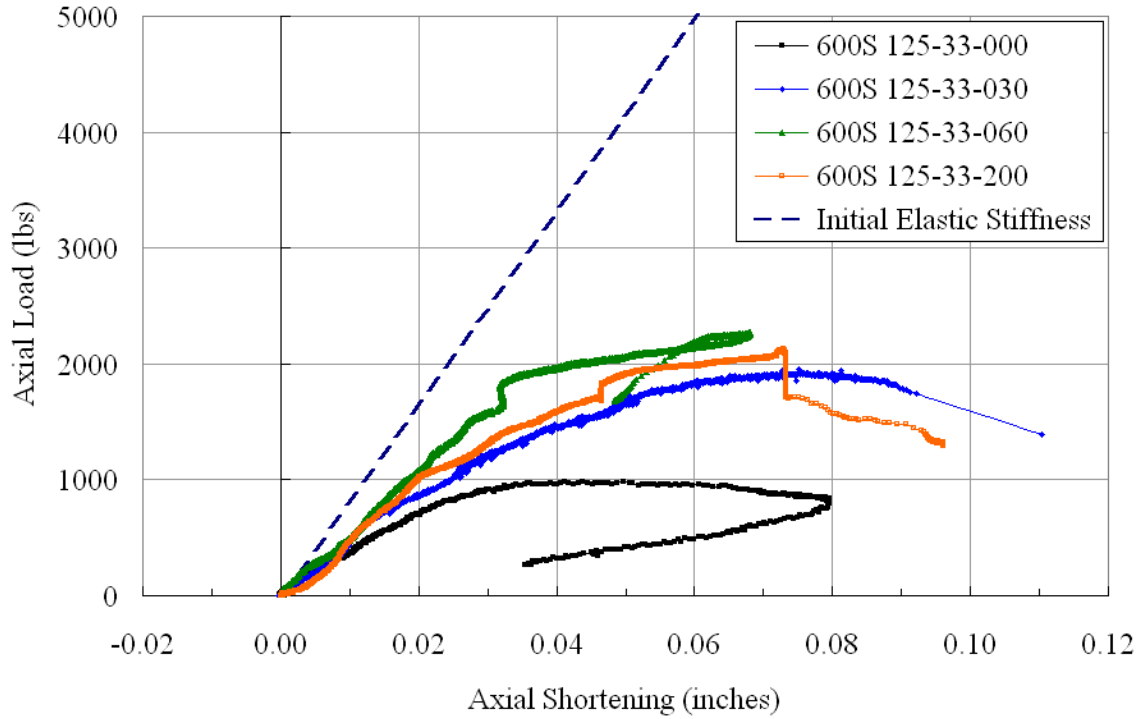


Figure 4.5 Axial Load vs. Axial Shortening for the Stud 600S125-33 with Varying Brace Stiffness

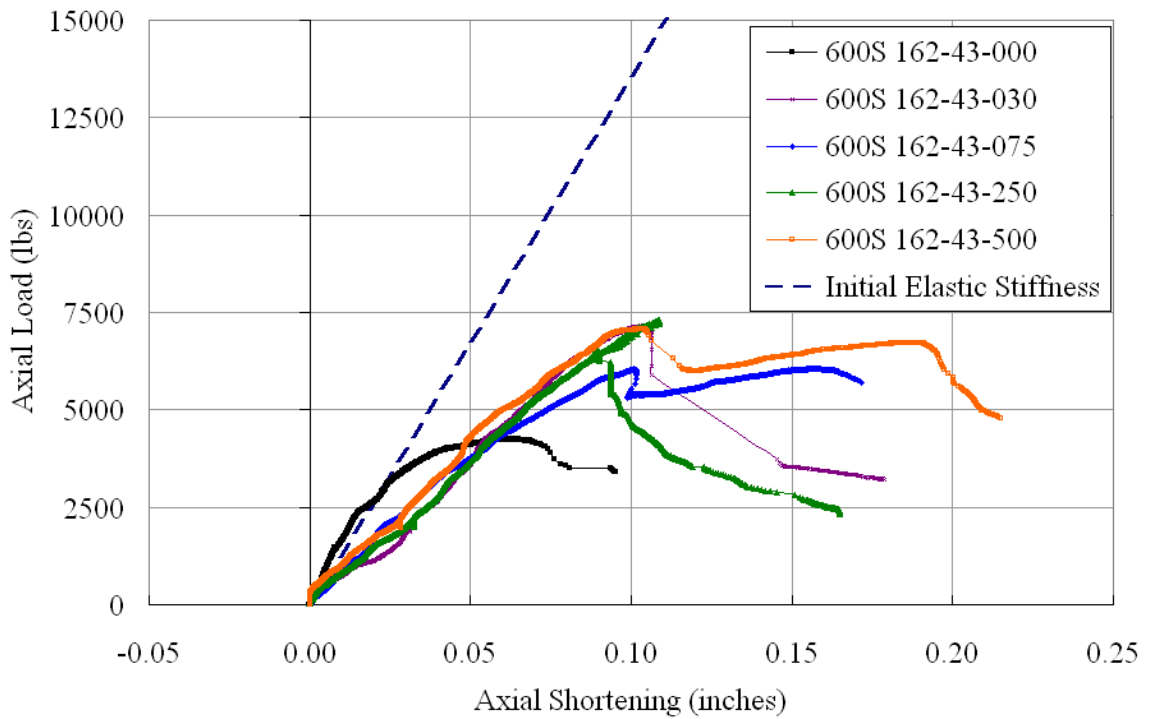


Figure 4.6 Axial Load vs. Axial Shortening for the Stud 600S162-43 with Varying Brace Stiffness

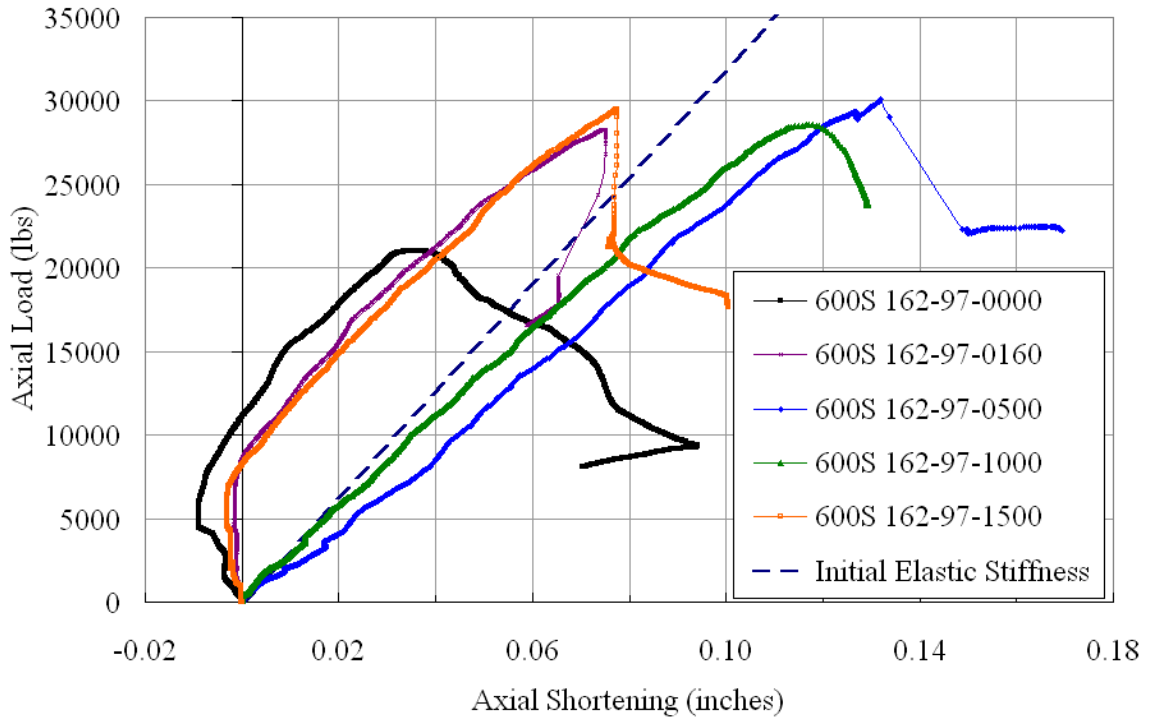


Figure 4.7 Axial Load vs. Axial Shortening for the Stud 600S162-97 with Varying Brace Stiffness

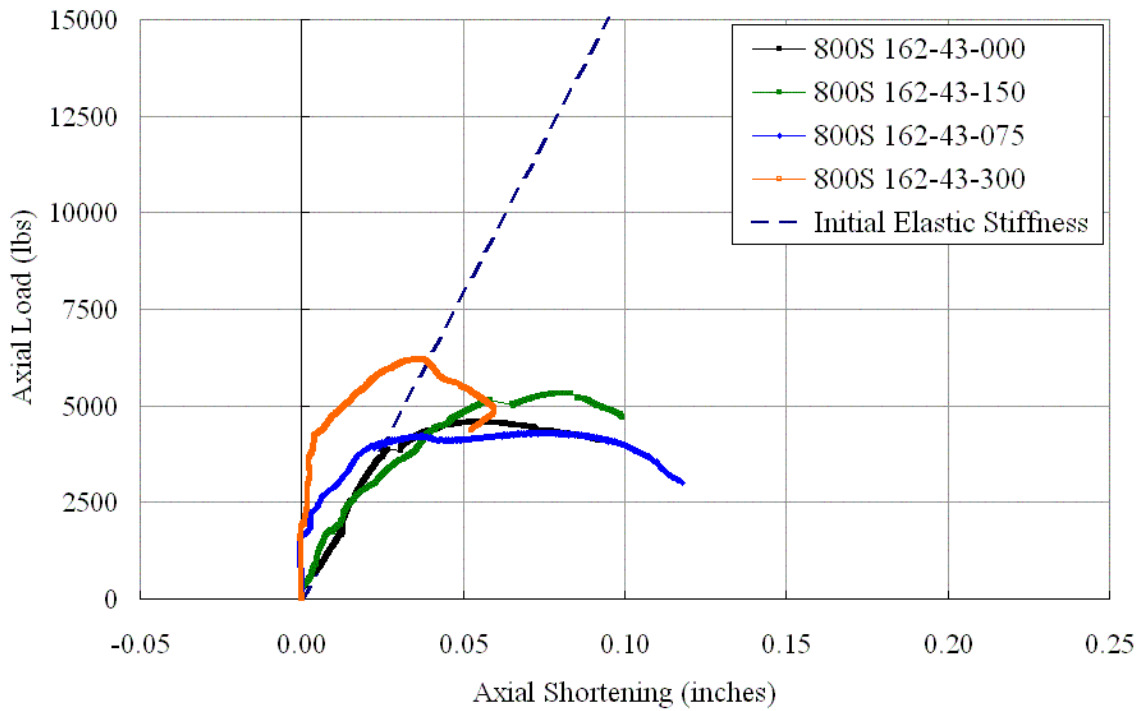


Figure 4.8 Axial Load vs. Axial Shortening for the Stud 800S162-43 with Varying Brace Stiffness

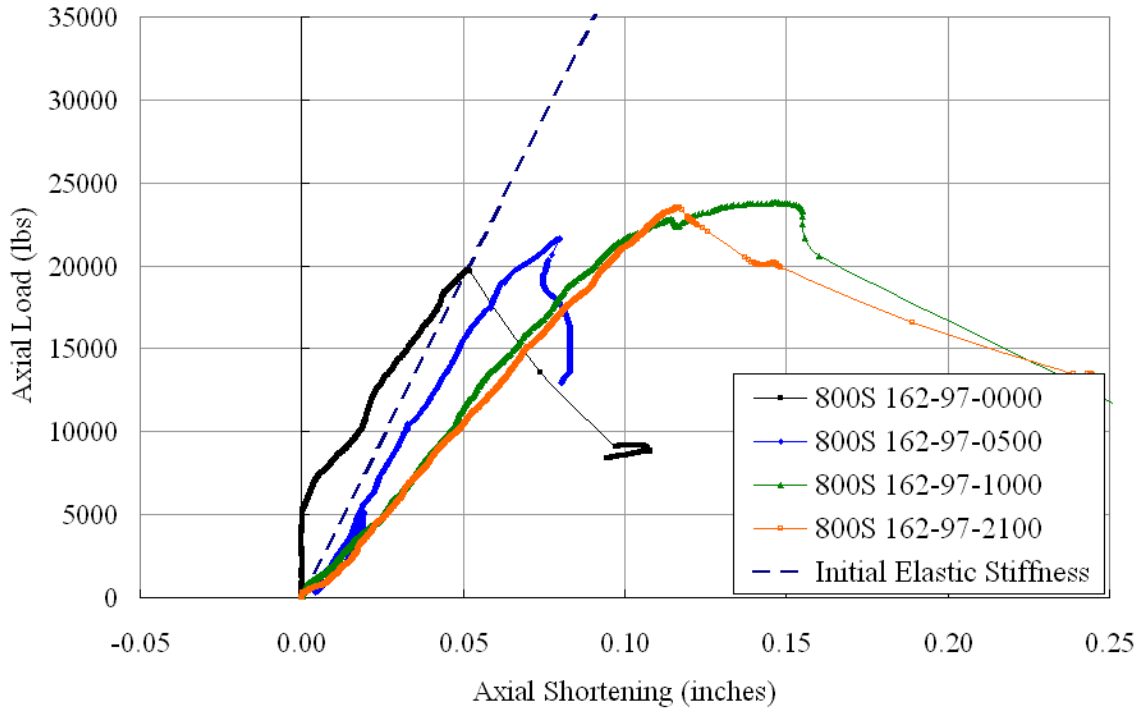


Figure 4.9 Axial Load vs. Axial Shortening for the Stud 800S162-97 with Varying Brace Stiffness

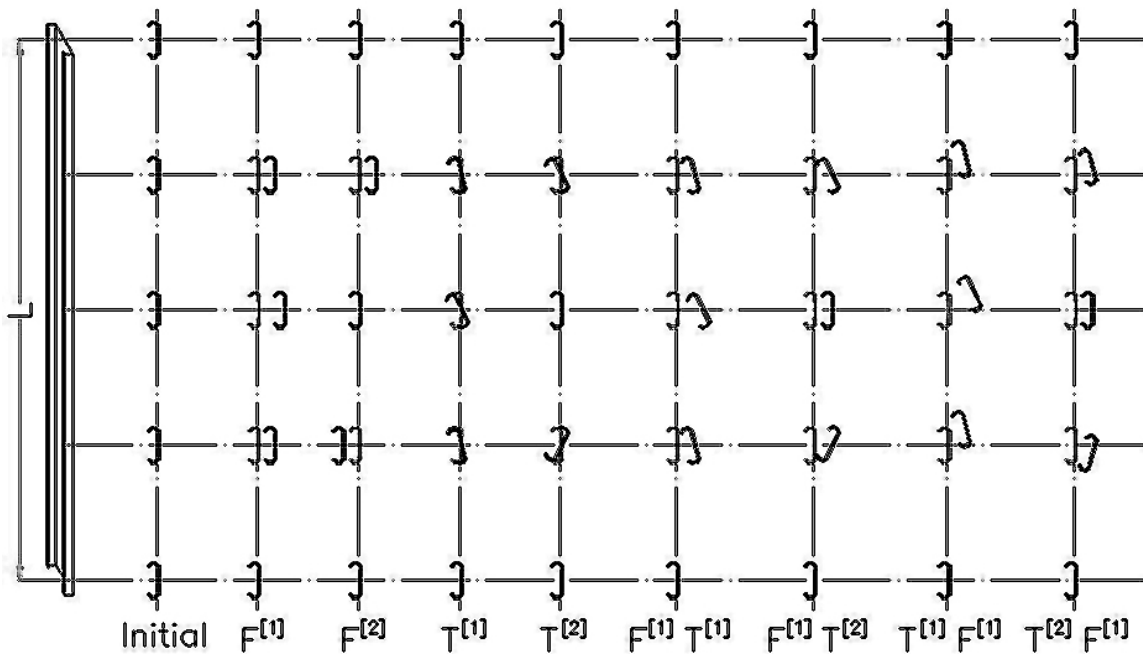


Figure 4.10 Schematic Diagram Showing the Various Buckling Shapes and Buckling Modes Observed in the Experimental Testing

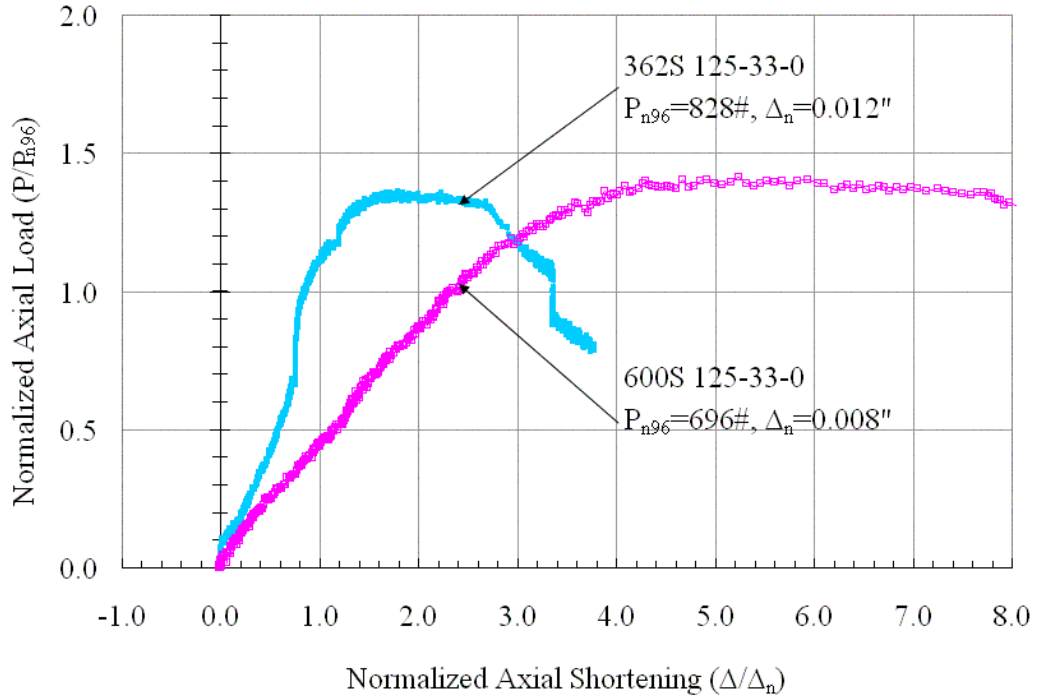


Figure 4.11 Comparison of Studs 362S125-33-0 and 600S125-33-0

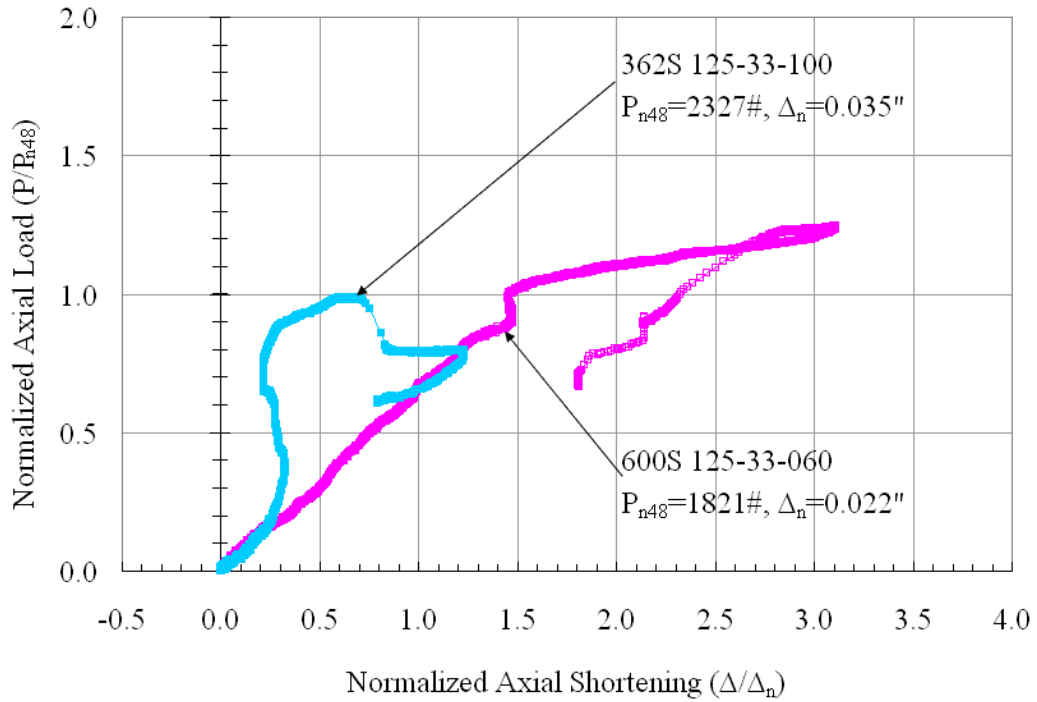


Figure 4.12 Comparison of Studs 362S125-33-100 (1.7x) and 600S125-33-060 (1.3x)

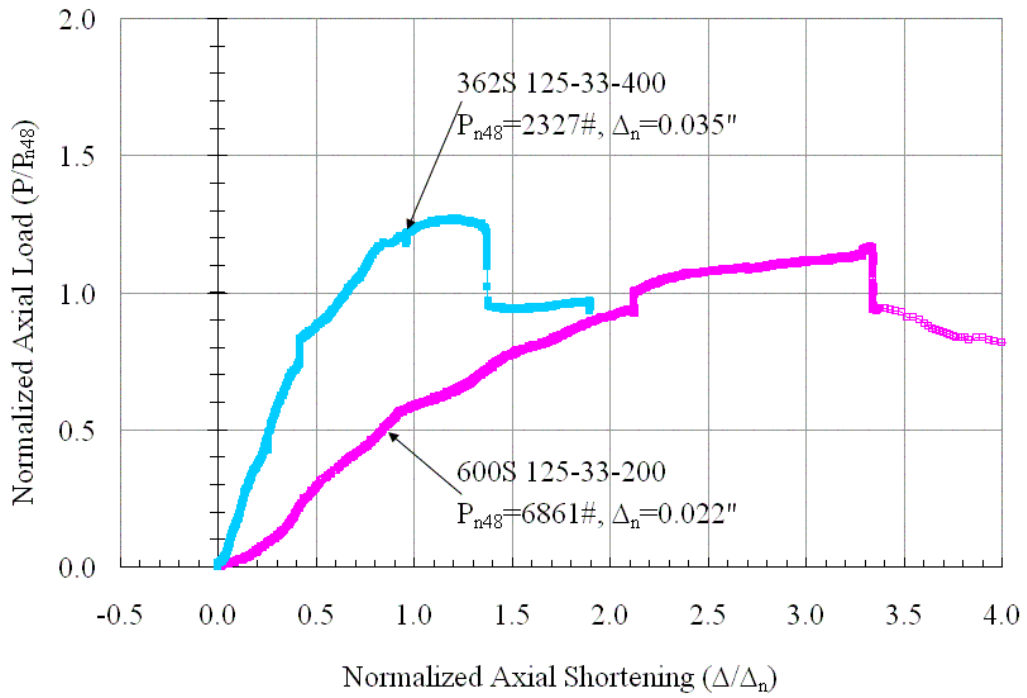


Figure 4.13 Comparison of Studs 362S125-33-200 (6.2x) and 600S125-33-200 (7.4x)

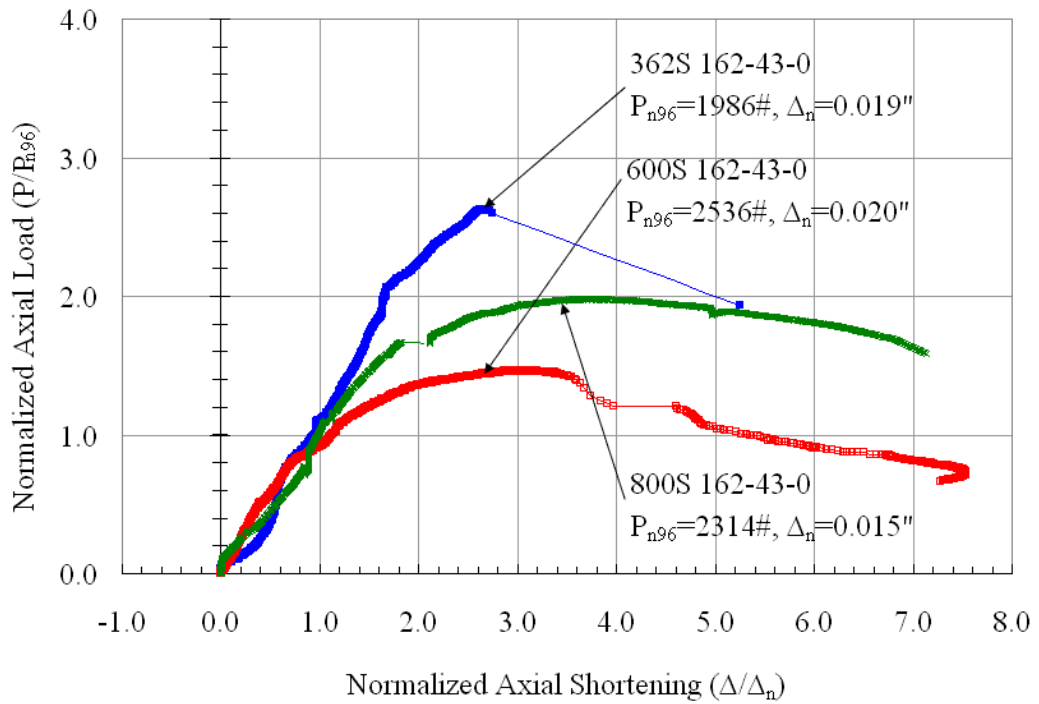


Figure 4.14 Comparison of Studs 362S162-43-0, 600S162-43-0 and 800S162-43-0

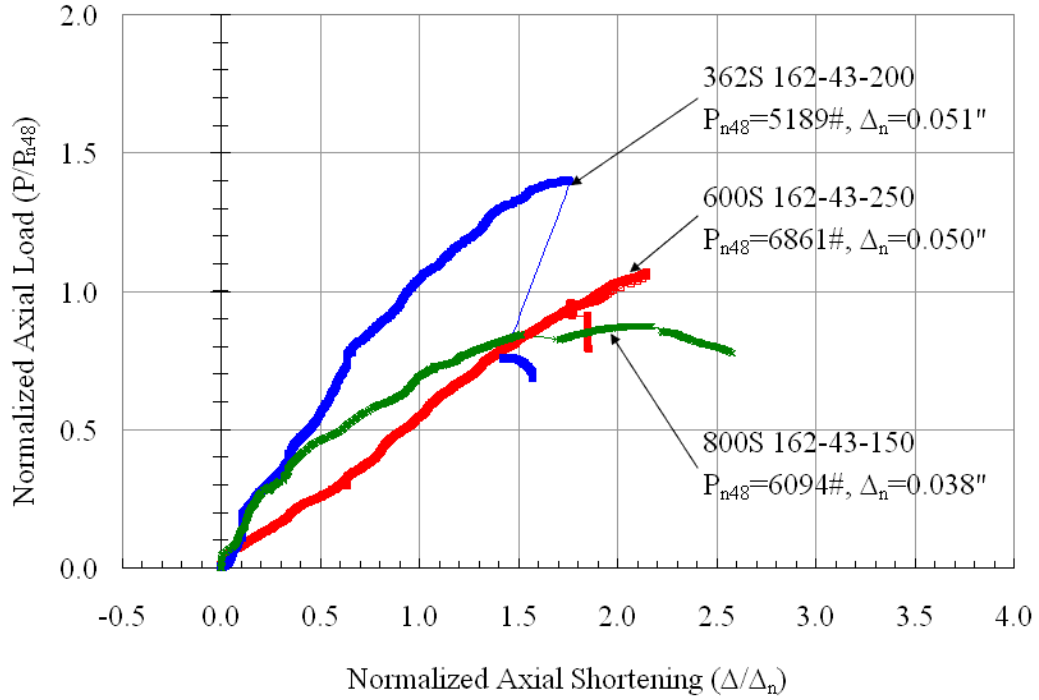


Figure 4.15 Comparison of Studs 362S162-43-200 (1.2x), 600S162-43-250 (1.6x) and 800S162-43-150 (1.3x)

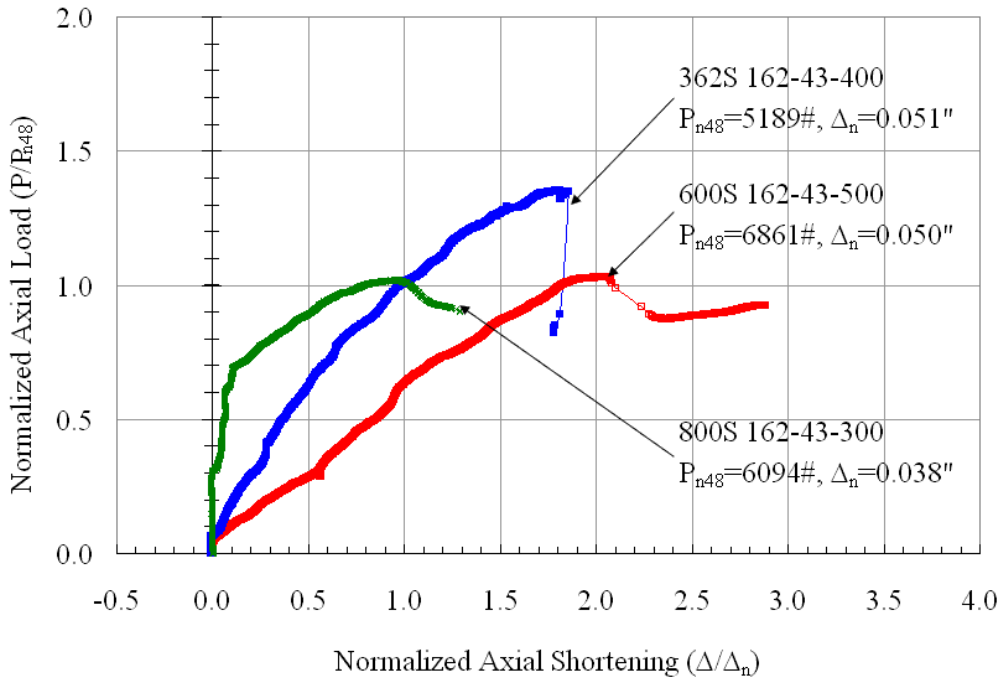


Figure 4.16 Comparison of Studs 362S162-43-400 (2.5x), 600S162-43-500 (3.4x) and 800S162-43-300 (2.3x)



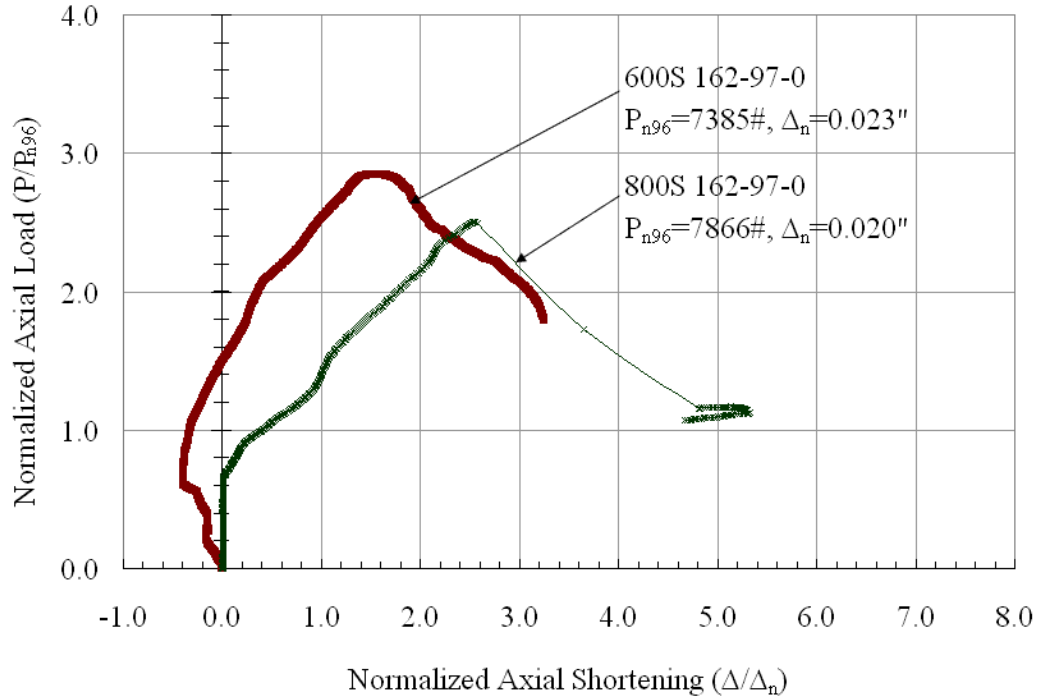


Figure 4.17 Comparison of Studs 600S162-97-0 and 800S162-97-0

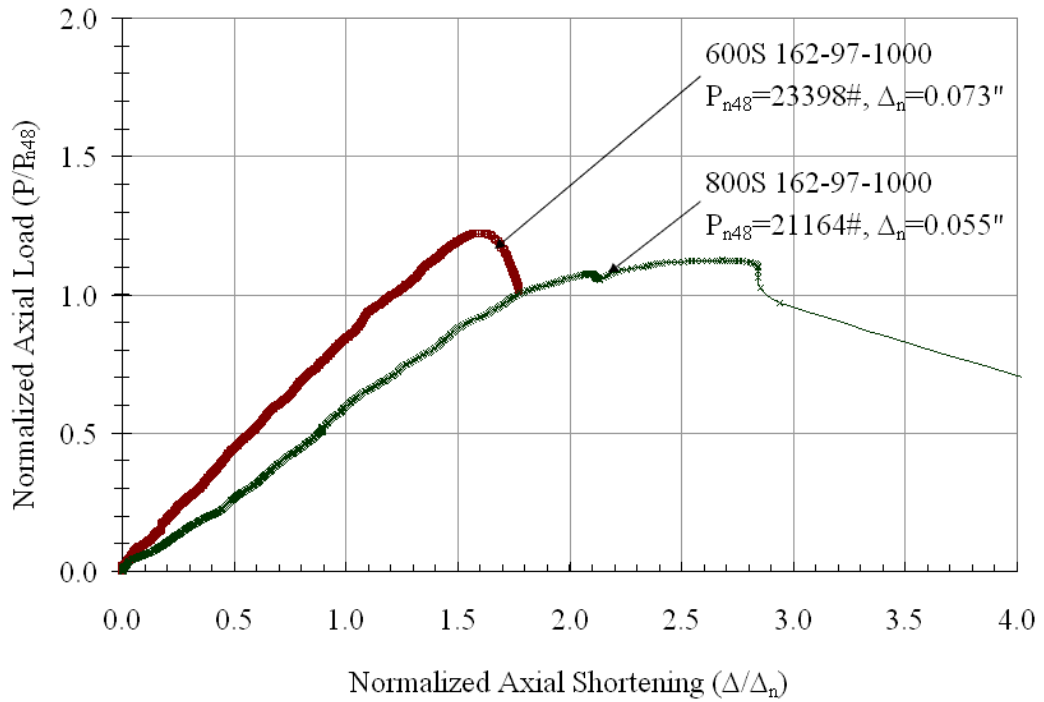


Figure 4.18 Comparison of Studs 600S162-97-1000 (1.7x) and 800S162-97-1000 (2.1x)

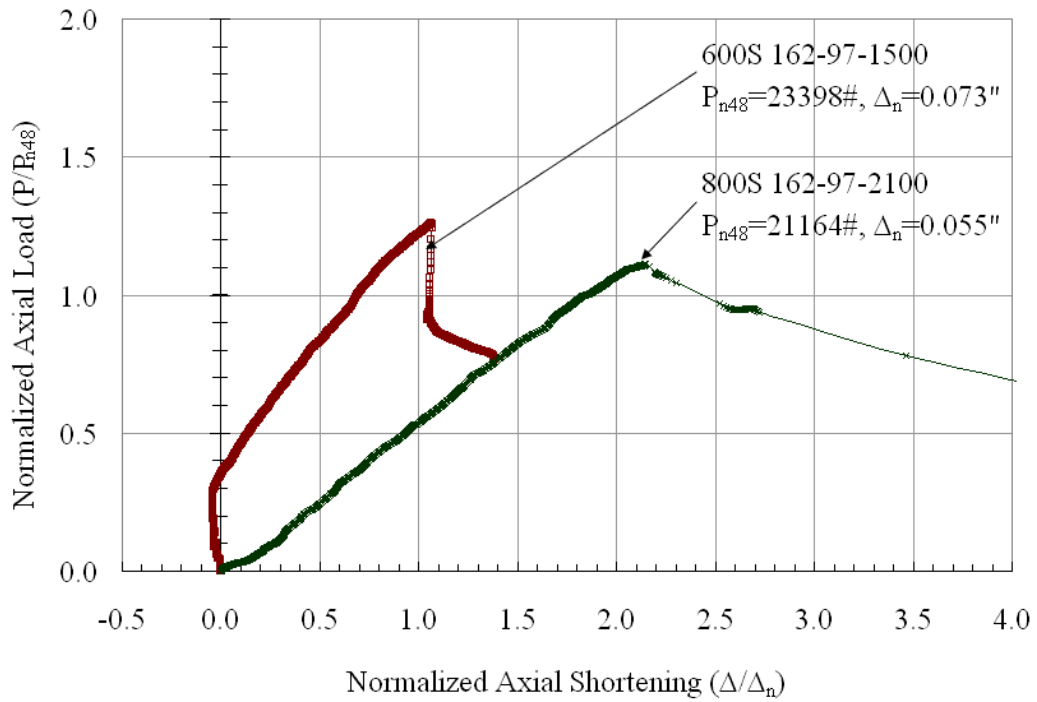


Figure 4.19 Comparison of Studs 600S162-97-1500 (2.7x) and 800S162-97-2100 (4.3x)

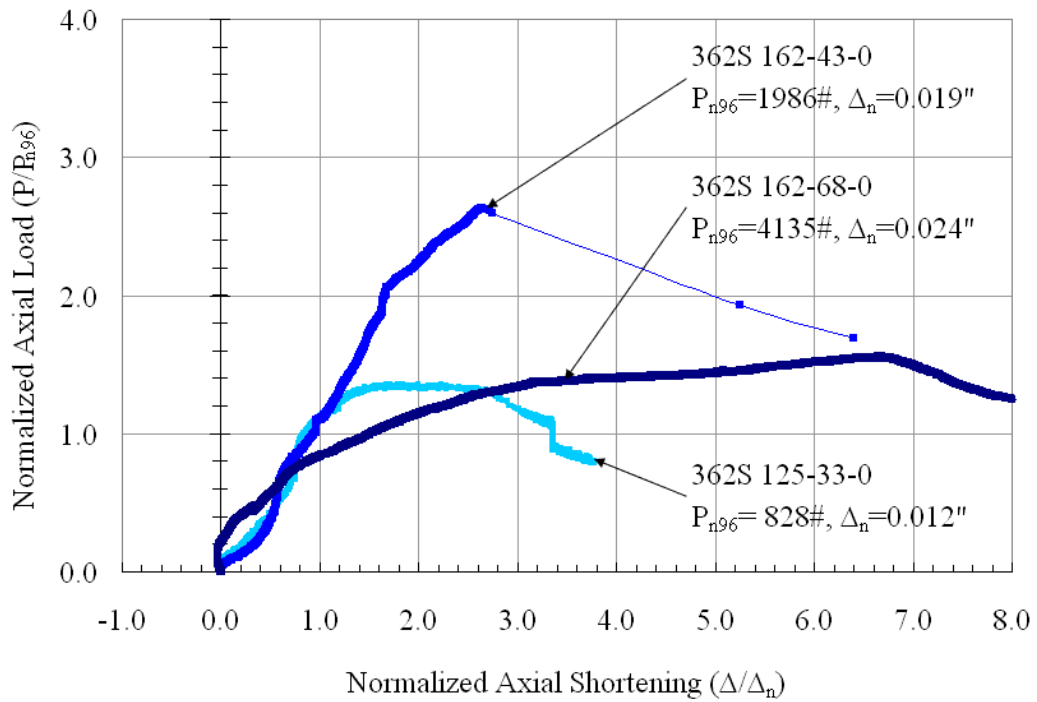


Figure 4.20 Comparison of Studs 362S125-33-0, 362S162-43-0 and 362S162-68-0

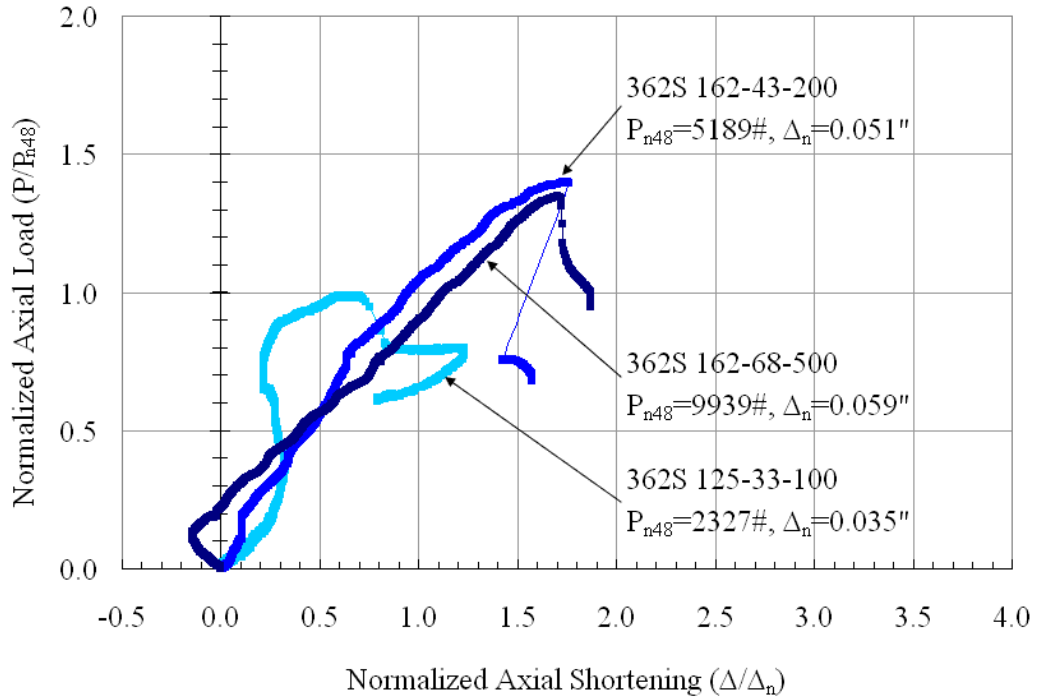


Figure 4.21 Comparison of Studs 362S125-33-100 (1.7x), 362S162-43-200 (1.2x) and 362S162-68-500 (1.8x)

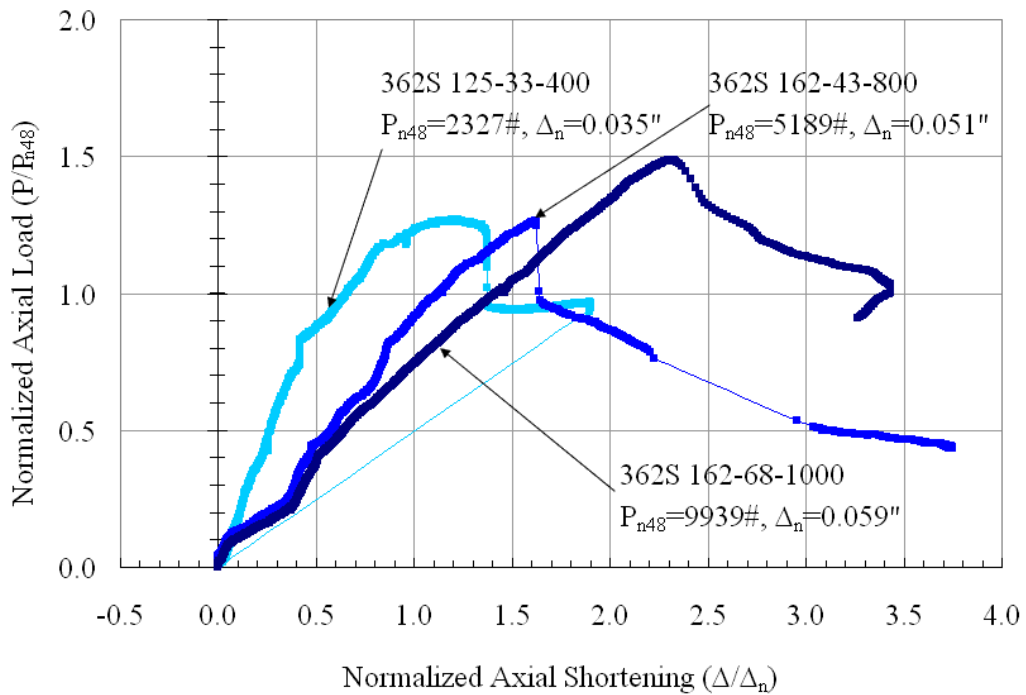


Figure 4.22 Comparison of Studs 362S125-33-400 (6.2x), 362S162-43-800 (5.4x) and 362S162-68-1000 (3.3x)

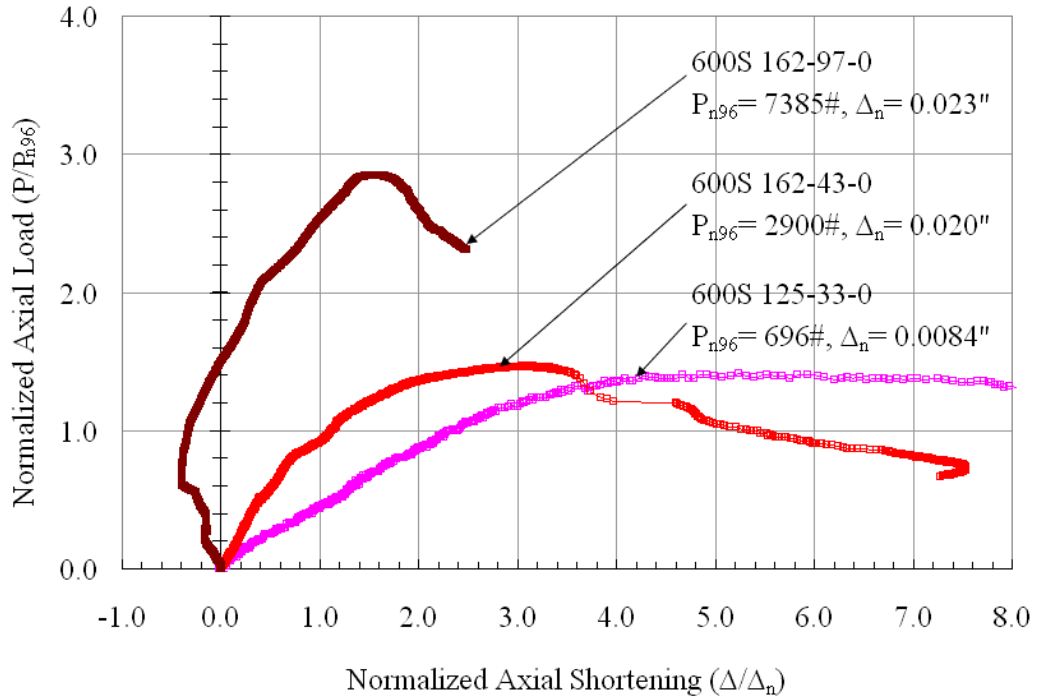


Figure 4.23 Comparison of Studs 600S125-33-0, 600S162-43-0 and 600S162-97-0

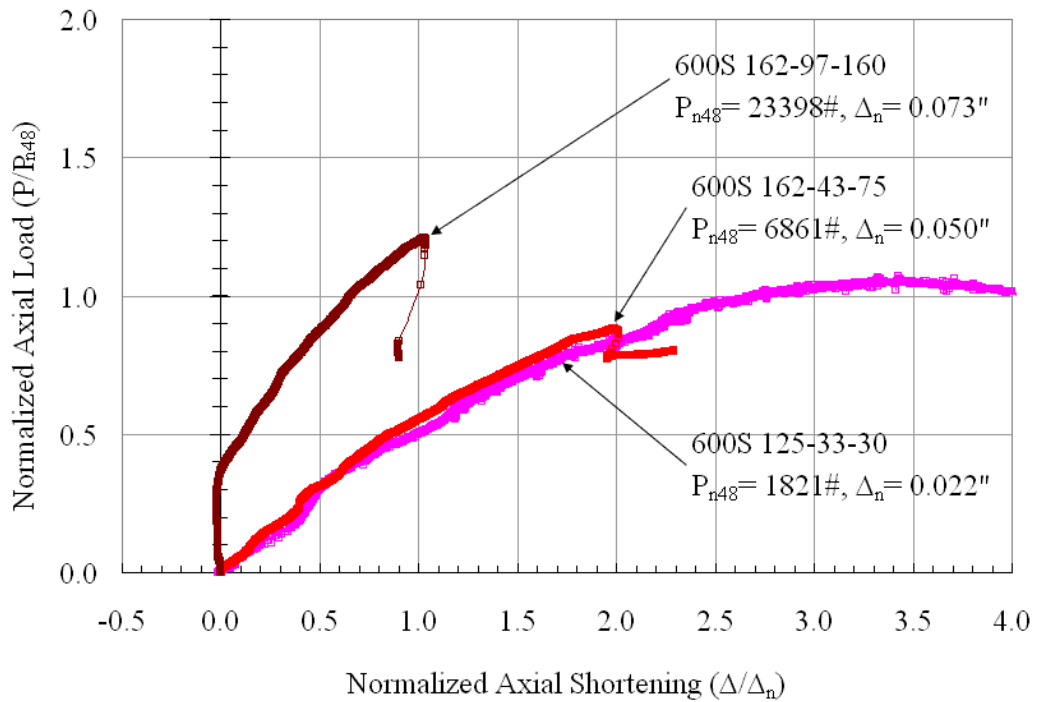


Figure 4.24 Comparison of Studs 600S125-33-30 (0.2x), 600S162-43-75 (0.6x) and 600S162-97-160 (0.3x)

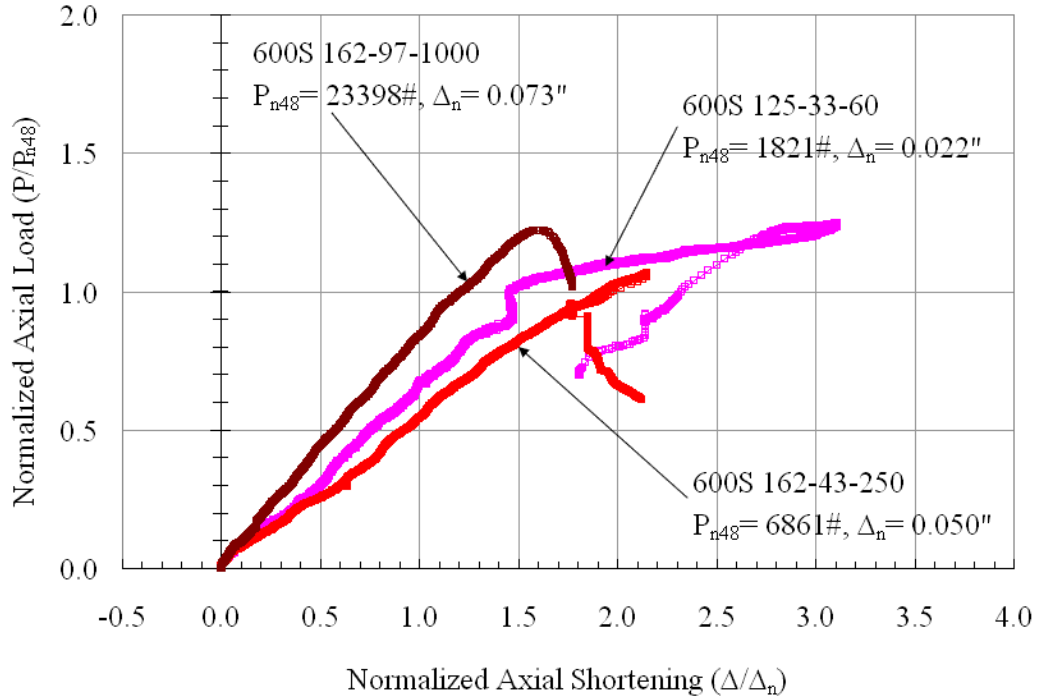


Figure 4.25 Comparison of Studs 600S125-33-60 (1.3x), 600S162-43-250 (1.6x) and 600S162-97-1000 (1.7x)

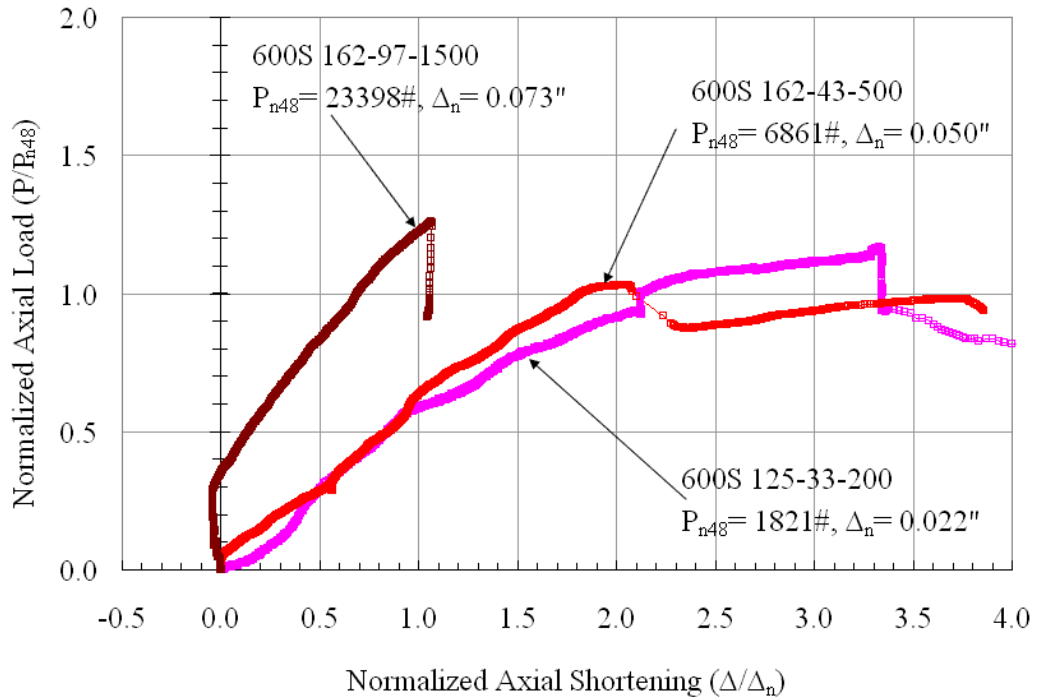


Figure 4.26 Comparison of Studs 600S125-33-200 (7.4x), 600S162-43-500 (3.4x) and 600S162-97-1500 (2.7x)

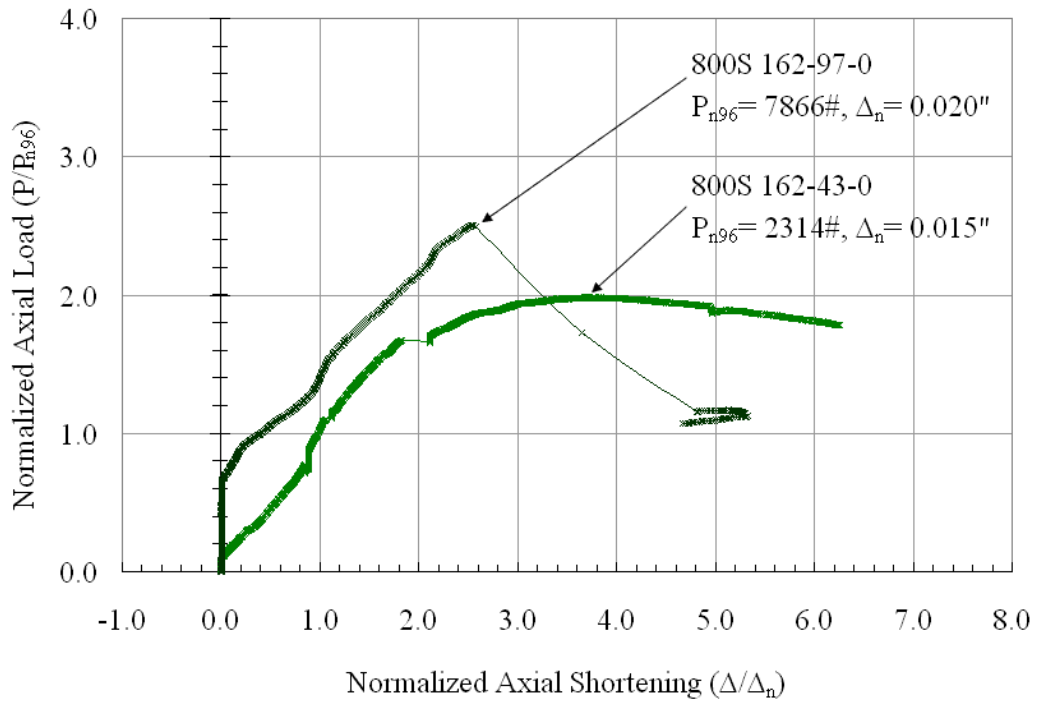


Figure 4.27 Comparison of Studs 800S162-43-0 and 800S162-97-0

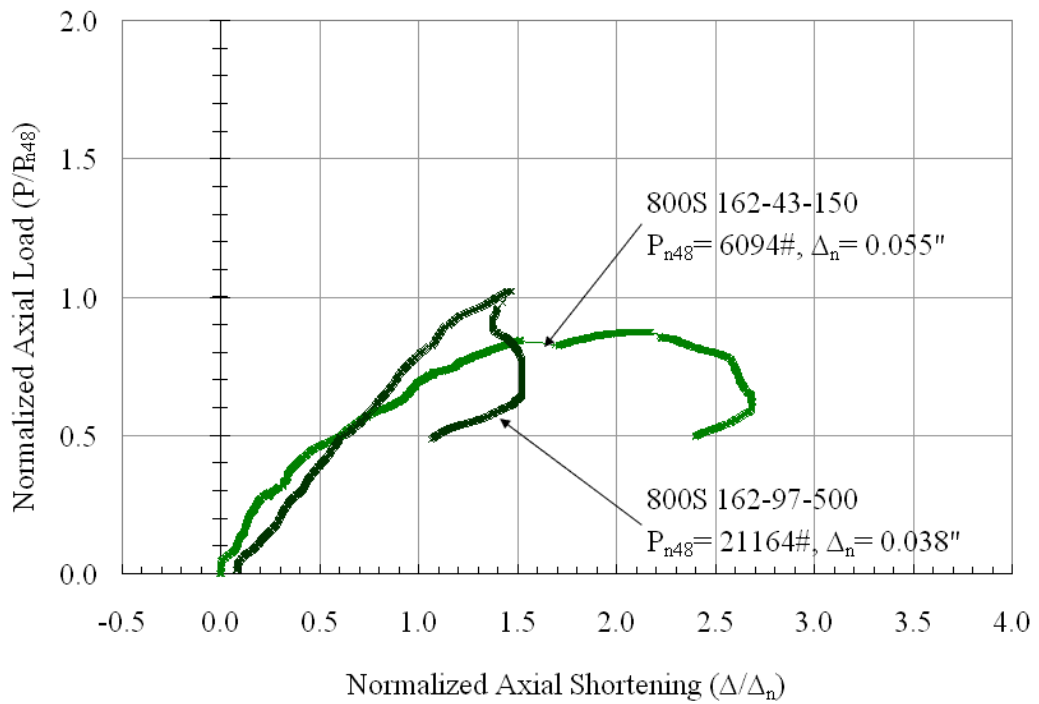


Figure 4.28 Comparison of Studs 800S162-43-150(1.3x) and 800S162-97-500 (1.2x)

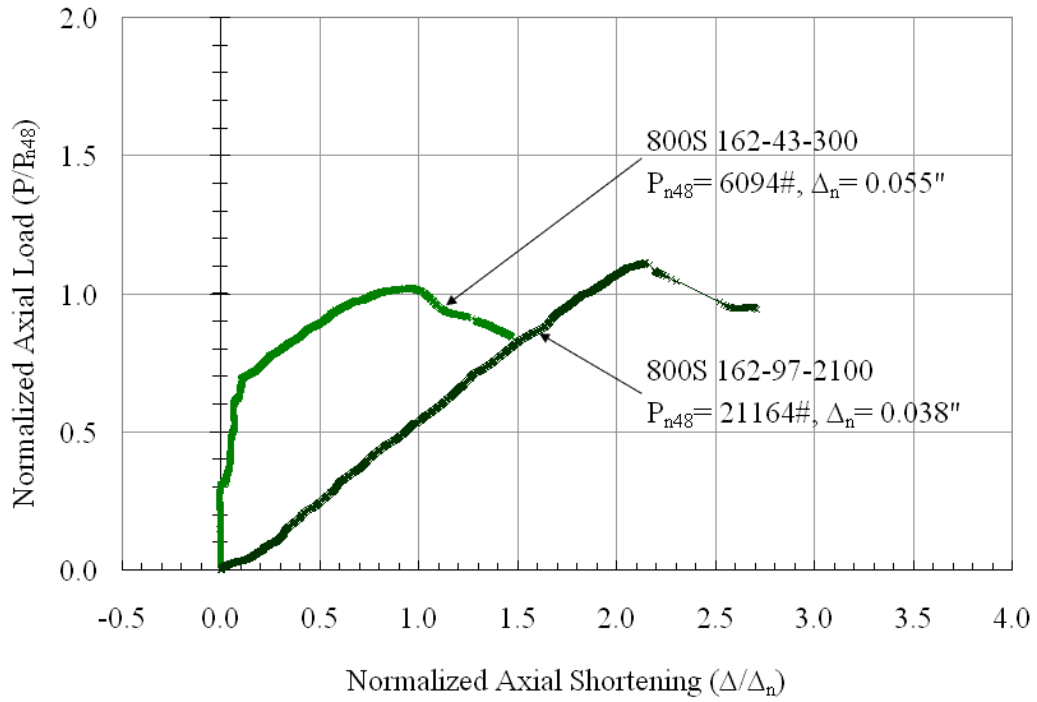


Figure 4.29 Comparison of Studs 800S162-43-300 (2.3x) and 800S162-97-2100 (4.3x)

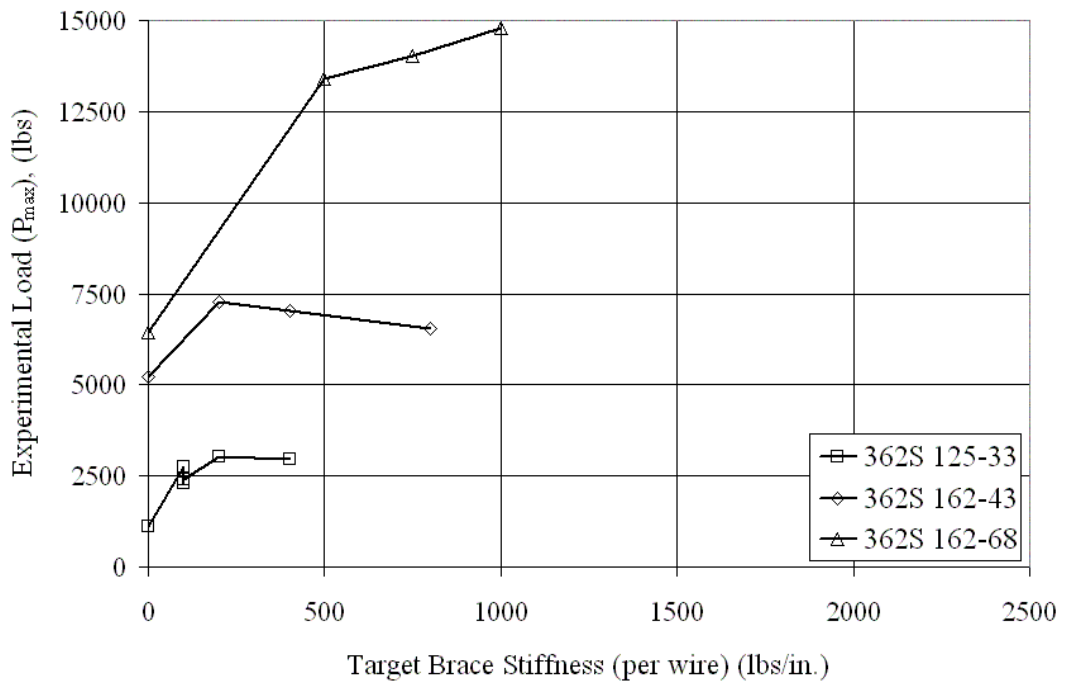


Figure 4.30 Experimental Load vs. Target Brace Stiffness for 362 Series of Lipped Cee Studs

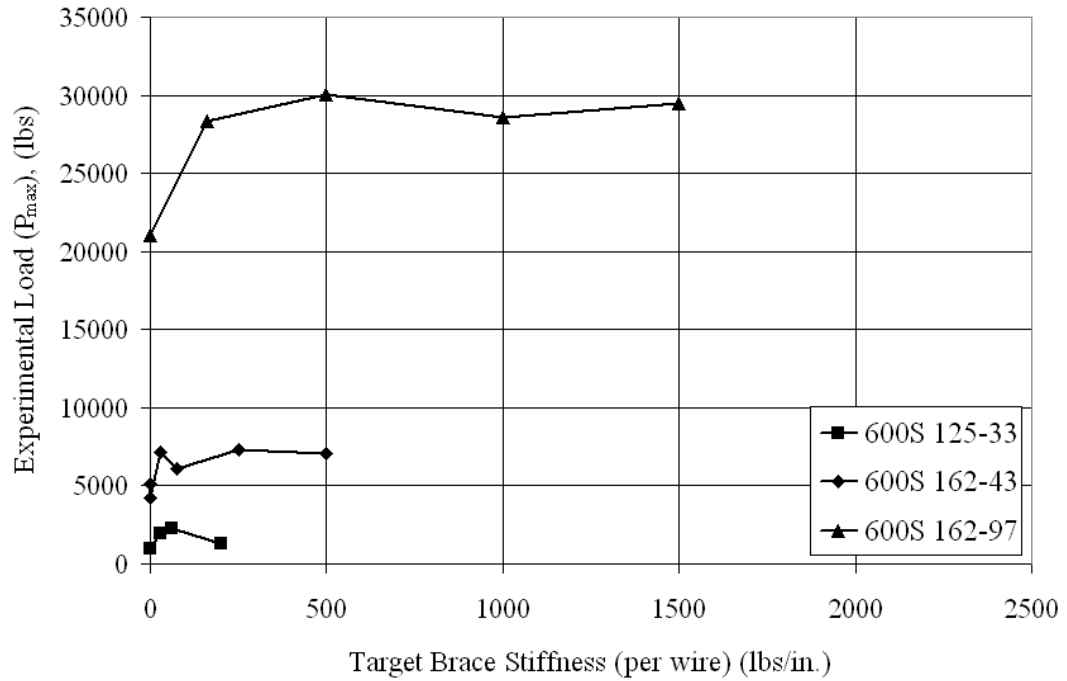


Figure 4.31 Experimental Load vs. Target Brace Stiffness for 600 Series of Lipped Cee Studs

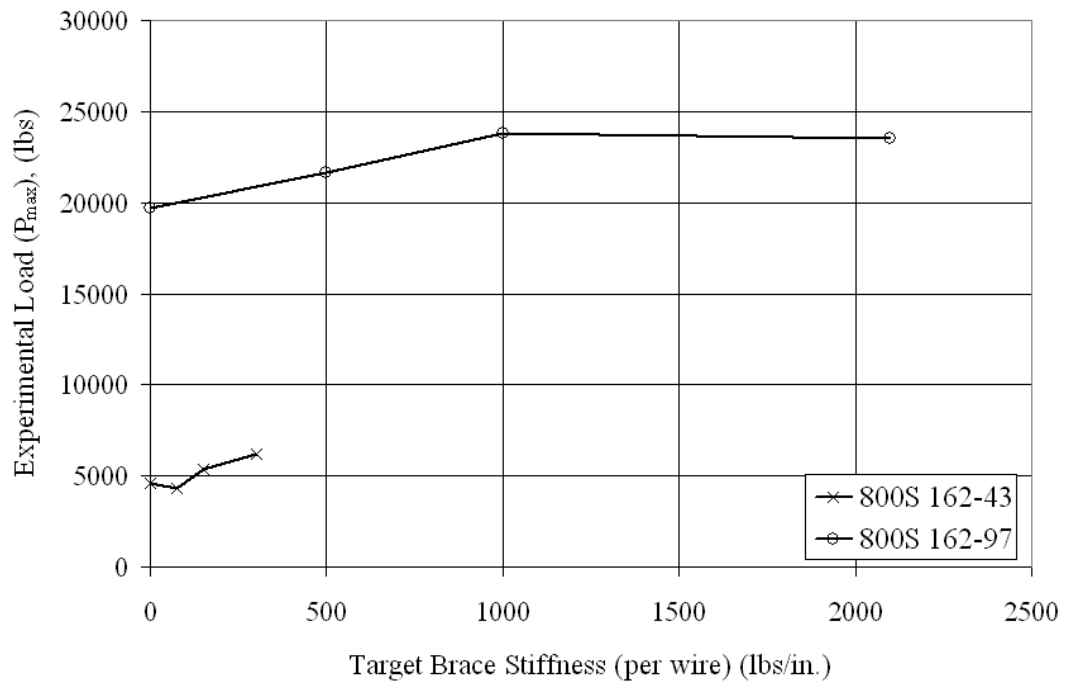


Figure 4.32 Experimental Load vs. Target Brace Stiffness for 800 Series of Lipped Cee Studs



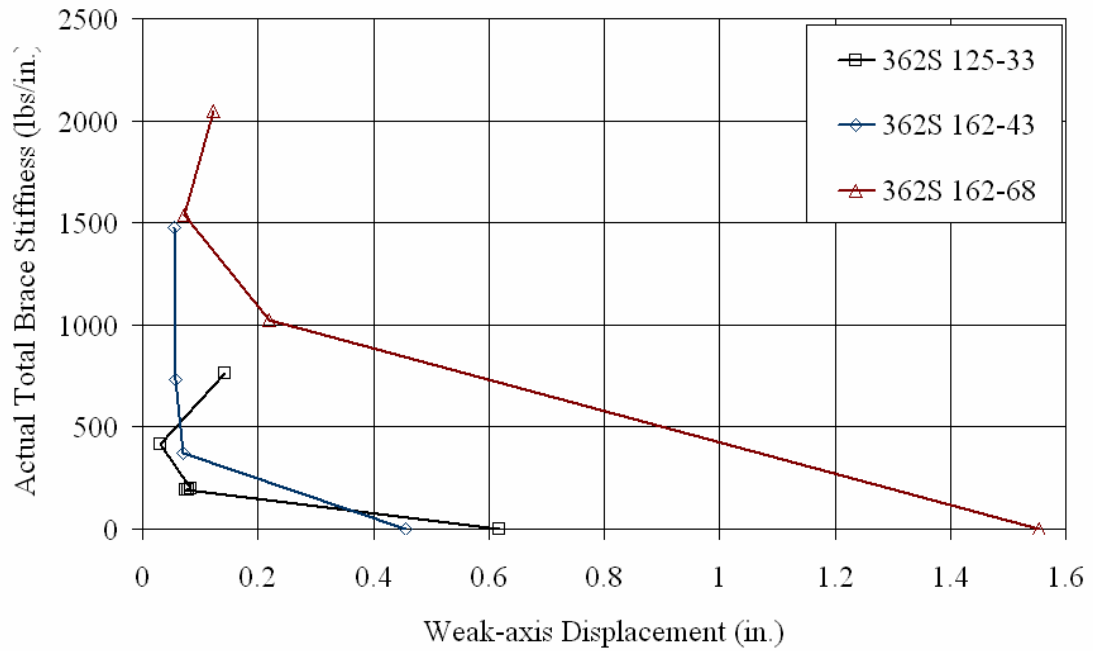


Figure 4.33 Total Brace Stiffness vs. Weak Axis Lateral Displacement for the 362 Series of Lipped Cee-Studs

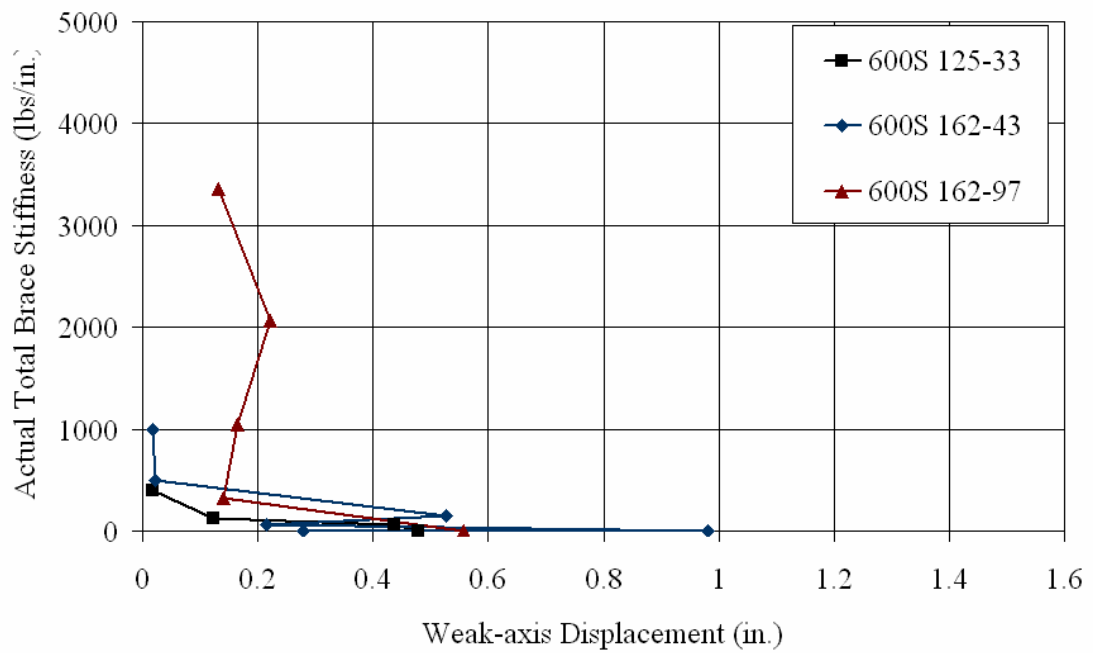


Figure 4.34 Total Brace Stiffness vs. Weak Axis Lateral Displacement for the 600 Series of Lipped Cee-Studs

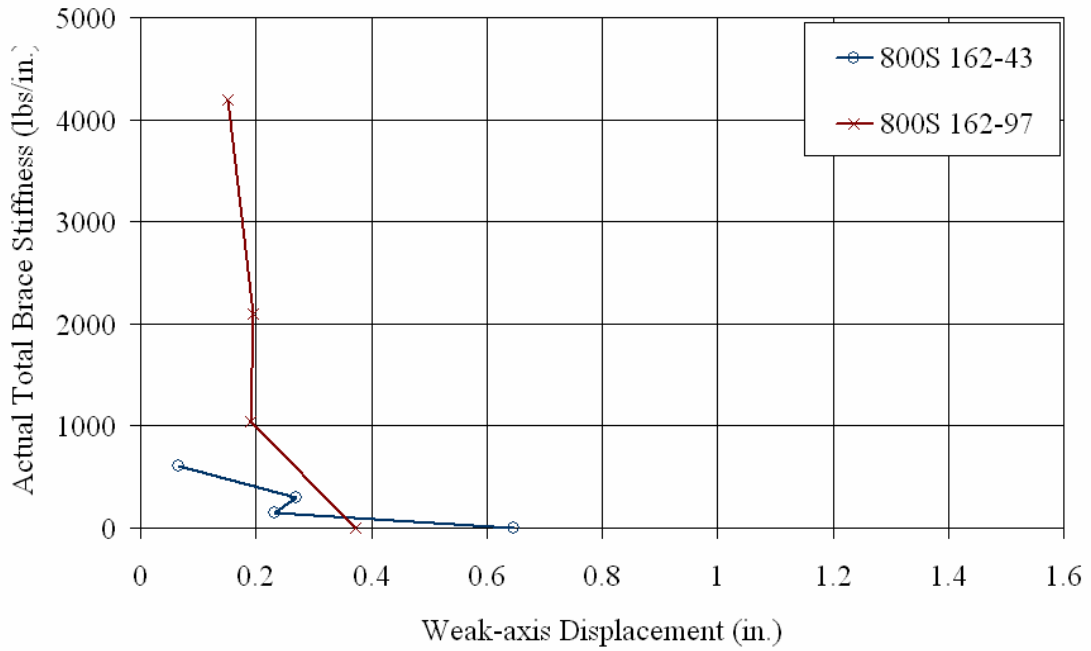


Figure 4.35 Total Brace Stiffness vs. Target Brace Stiffness for the 800 Series Lipped Cee Studs

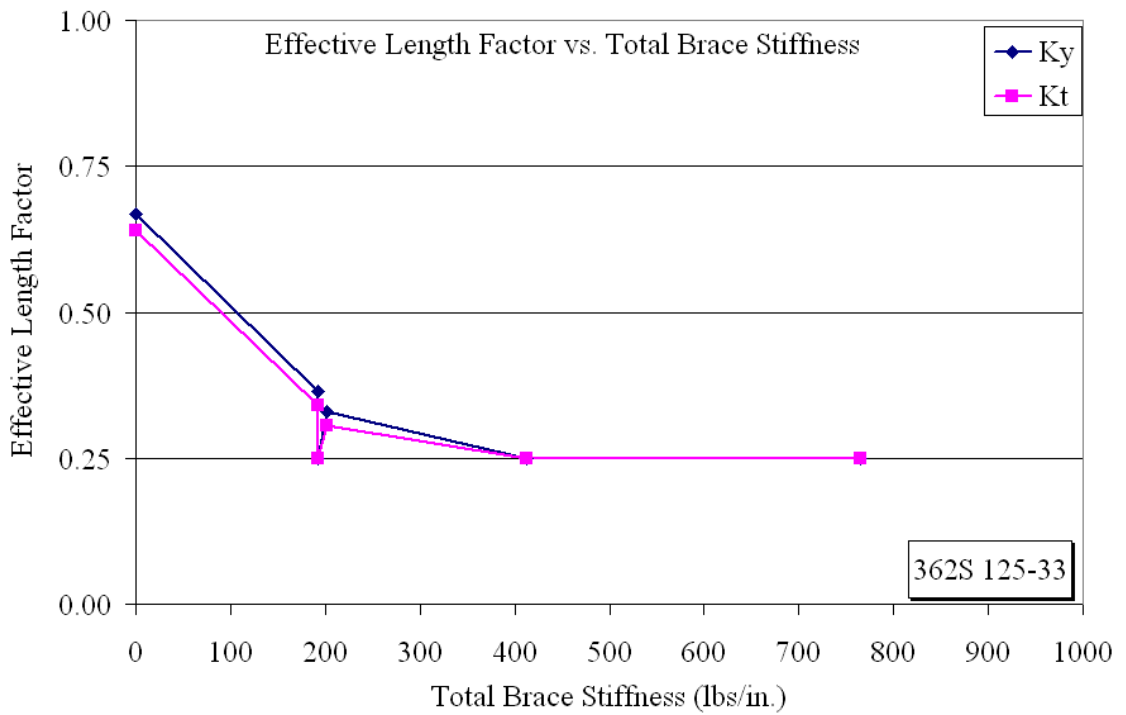


Figure 4.36 Effective Length Factor vs. Total Brace Stiffness for 362S-125-33 Series of Lipped Cee Studs

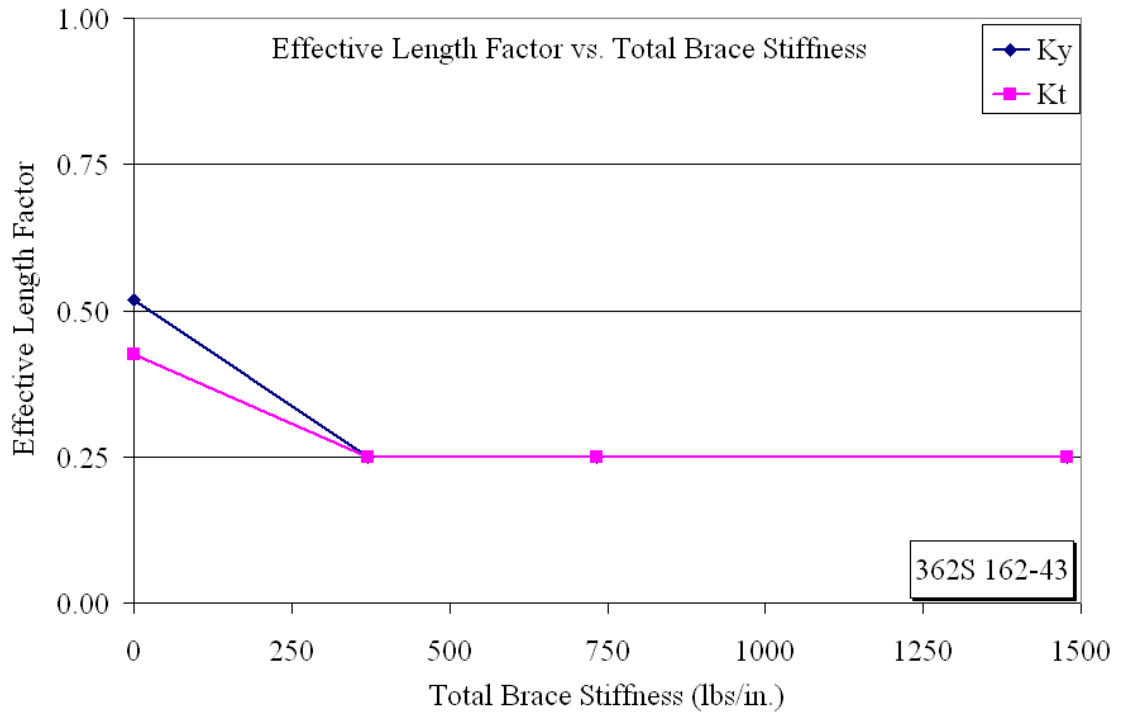


Figure 4.37 Effective Length Factor vs. Total Brace Stiffness for 362S-162-43 Series of Lipped Cee Studs

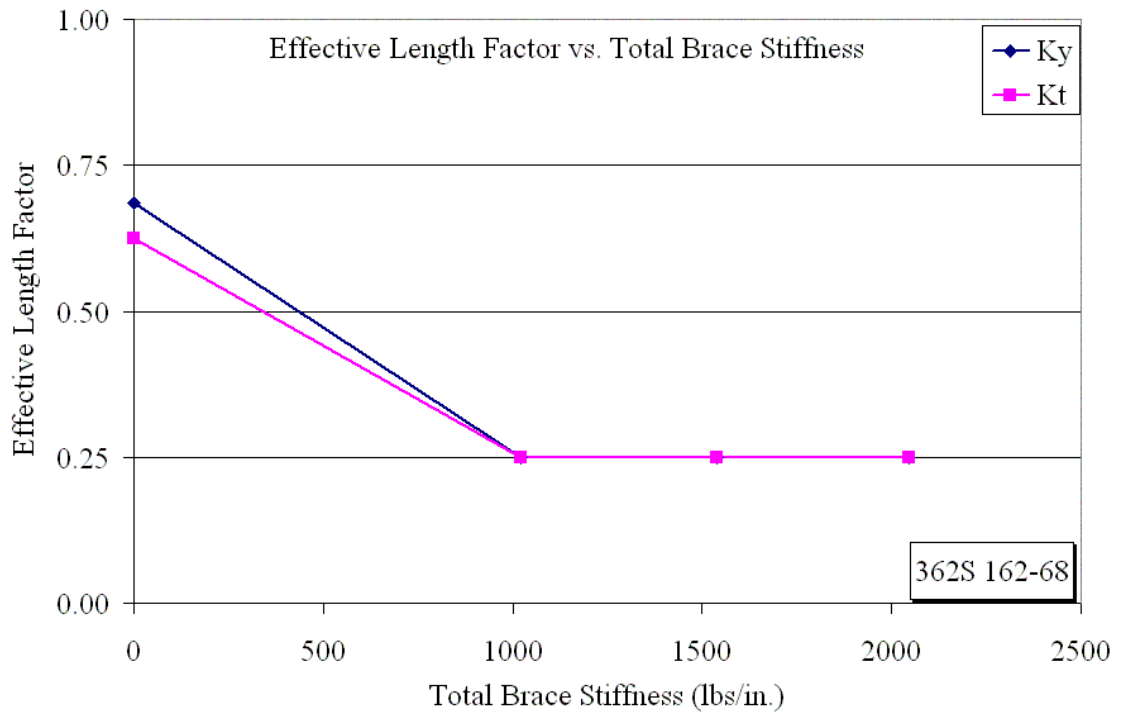


Figure 4.38 Effective Length Factor vs. Total Brace Stiffness for 362S-162-68 Series of Lipped Cee Studs

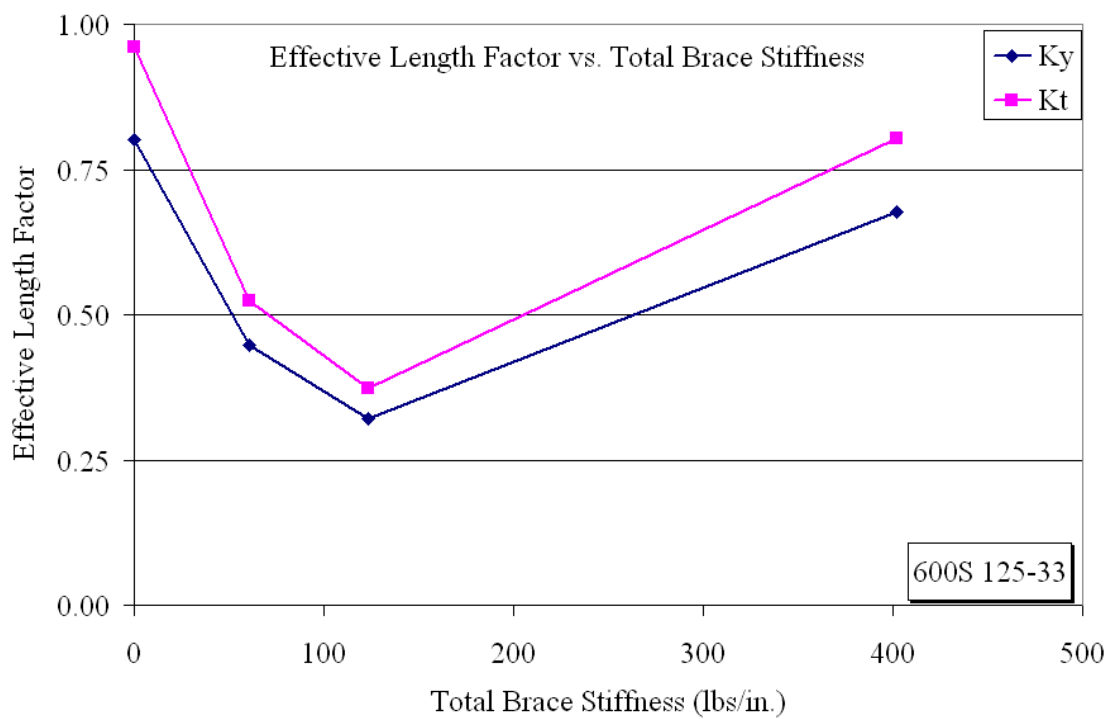


Figure 4.39 Effective Length Factor vs. Total Brace Stiffness for 600S-125-33 Series of Lipped Cee Studs

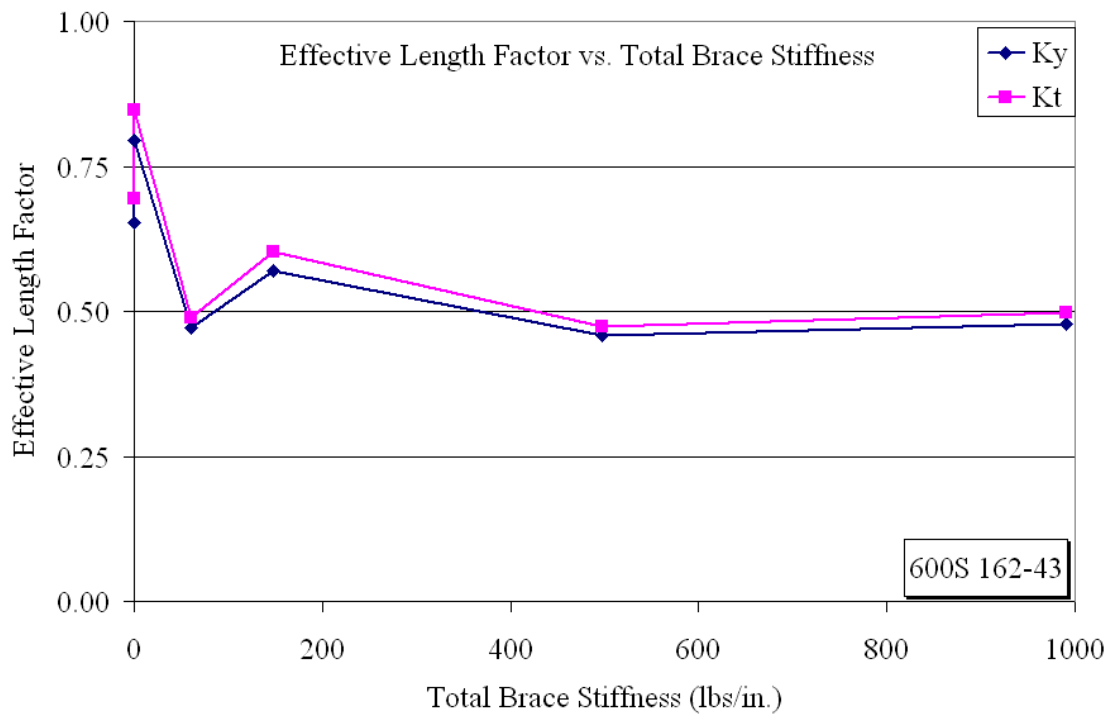


Figure 4.40 Effective Length Factor vs. Total Brace Stiffness for 600S-162-43 Series of Lipped Cee Studs

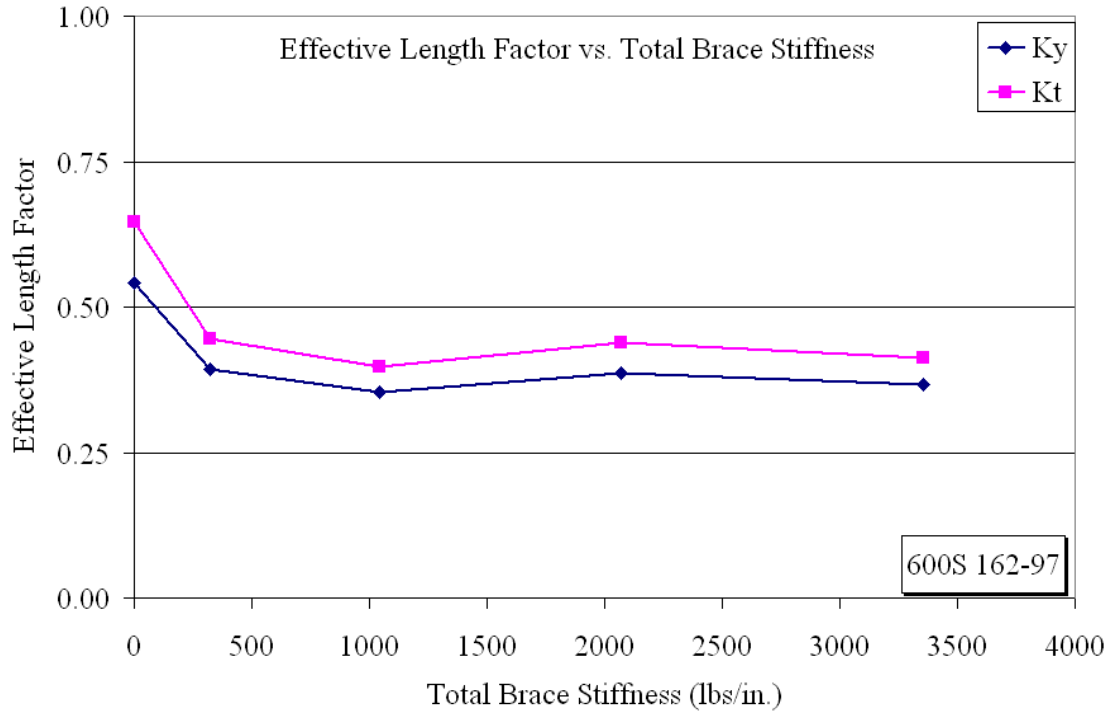


Figure 4.41 Effective Length Factor vs. Total Brace Stiffness for 600S-162-97 Series of Lipped Cee Studs

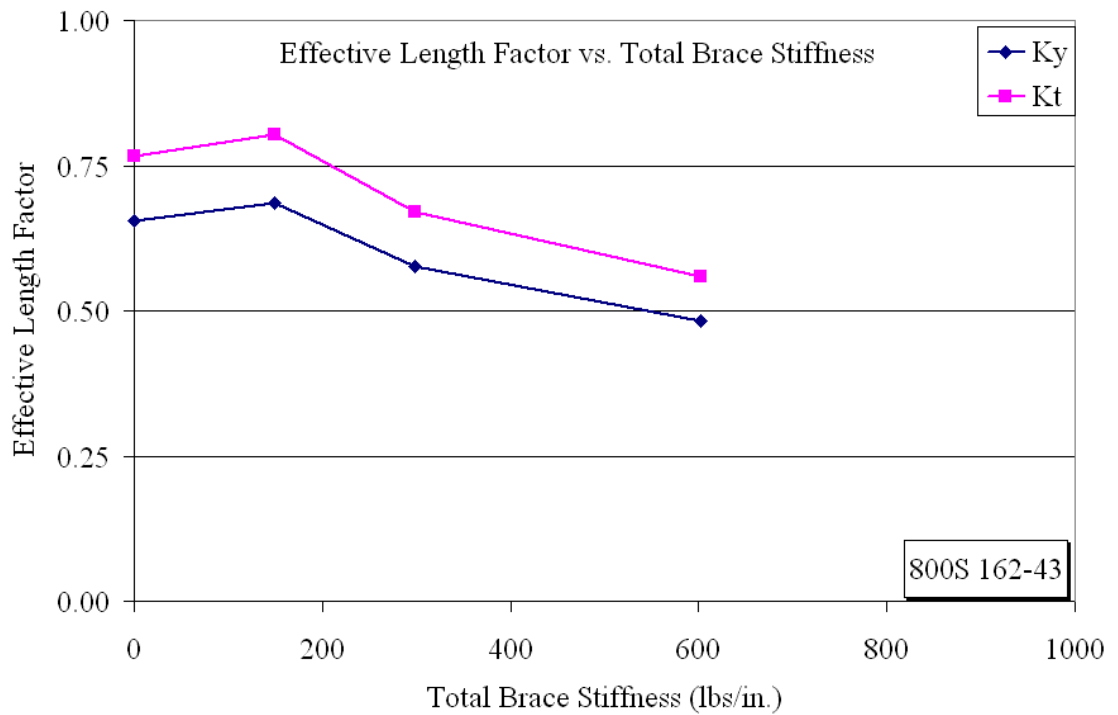


Figure 4.42 Effective Length Factor vs. Total Brace Stiffness for 800S-162-43 Series of Lipped Cee Studs

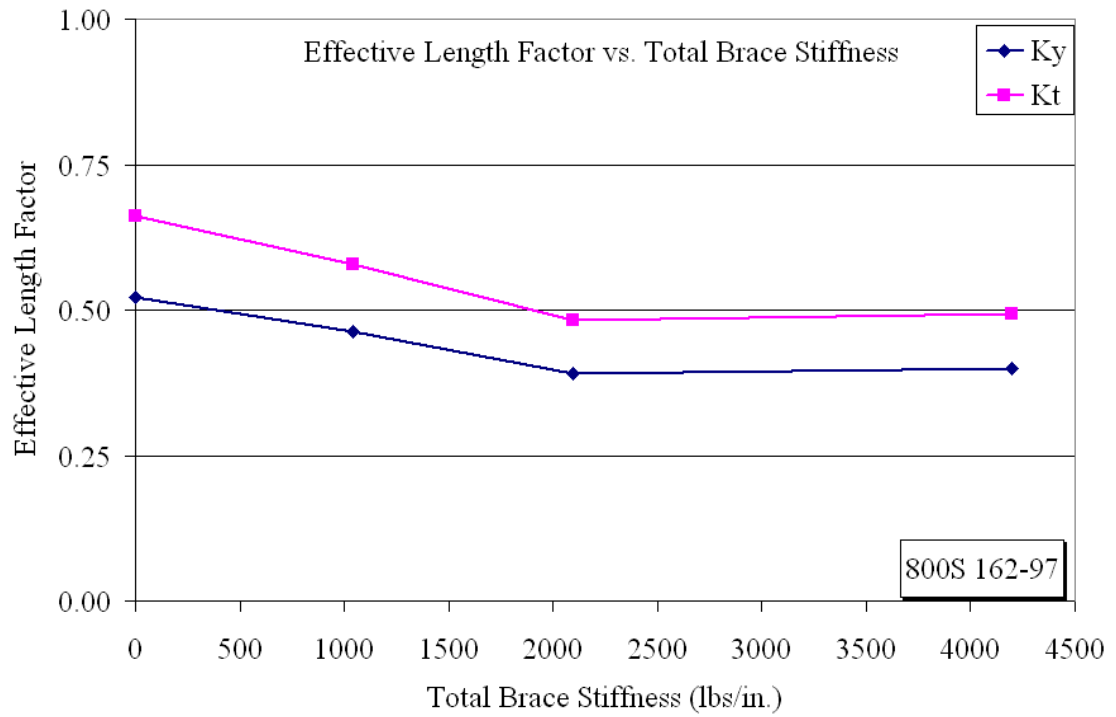


Figure 4.43 Effective Length Factor vs. Total Brace Stiffness for 800S-162-97 Series of Lipped Cee Studs

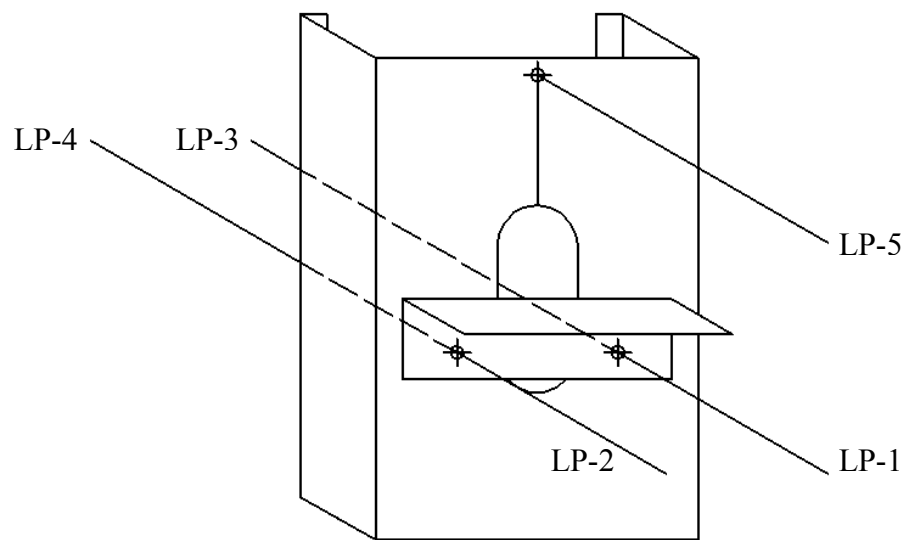


Figure 4.44 Location of Linear Potentiometers on the Bridging Connection

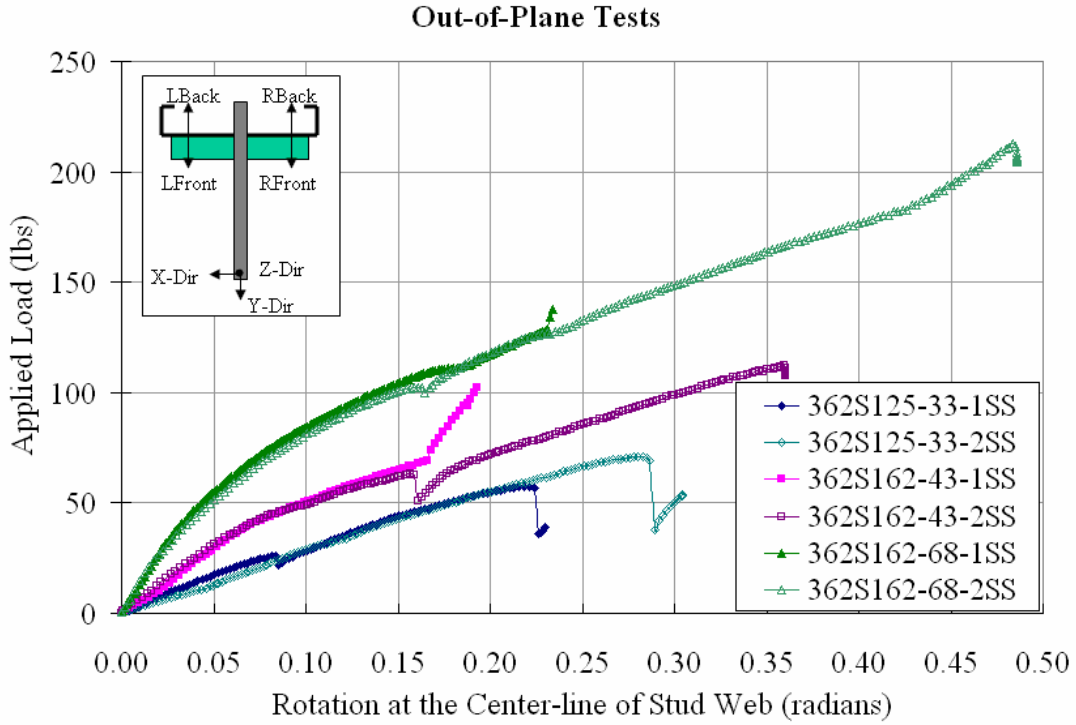


Figure 4.45 Plot of Applied Load vs. Calculated Rotation at the Center-line of the Web for the 362S Series of Studs with SS Connection.

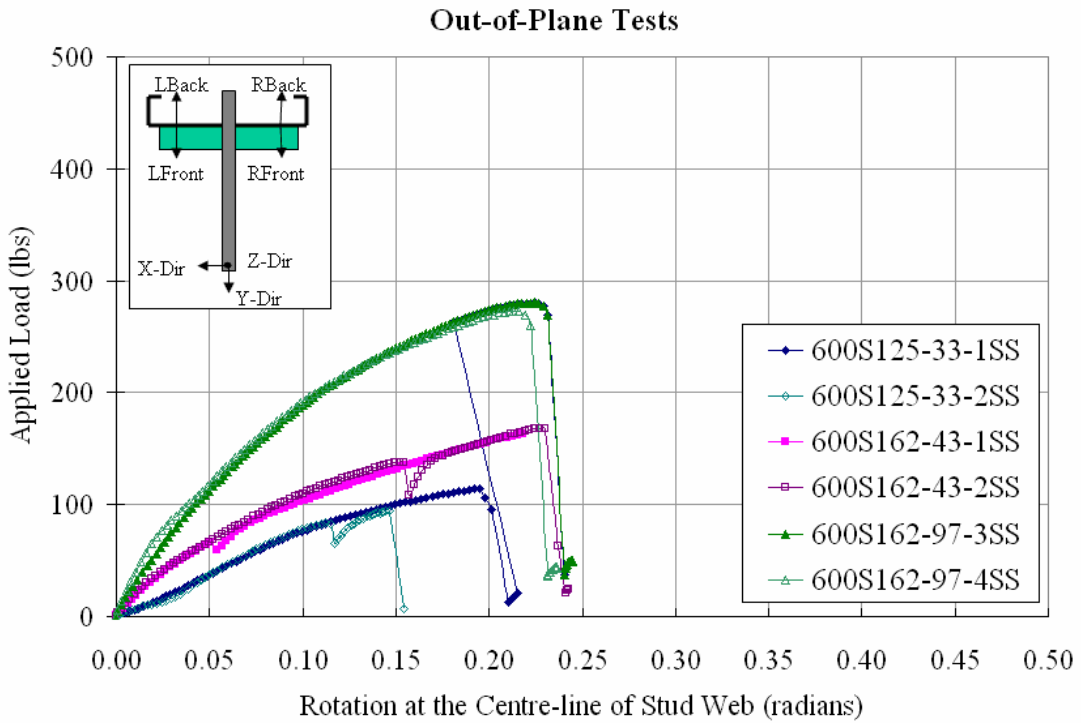


Figure 4.46 Plot of Applied Load vs. Calculated Rotation at the Center-line of the Web for the 600S Series of Studs with SS Connection.

Out-of-Plane Tests

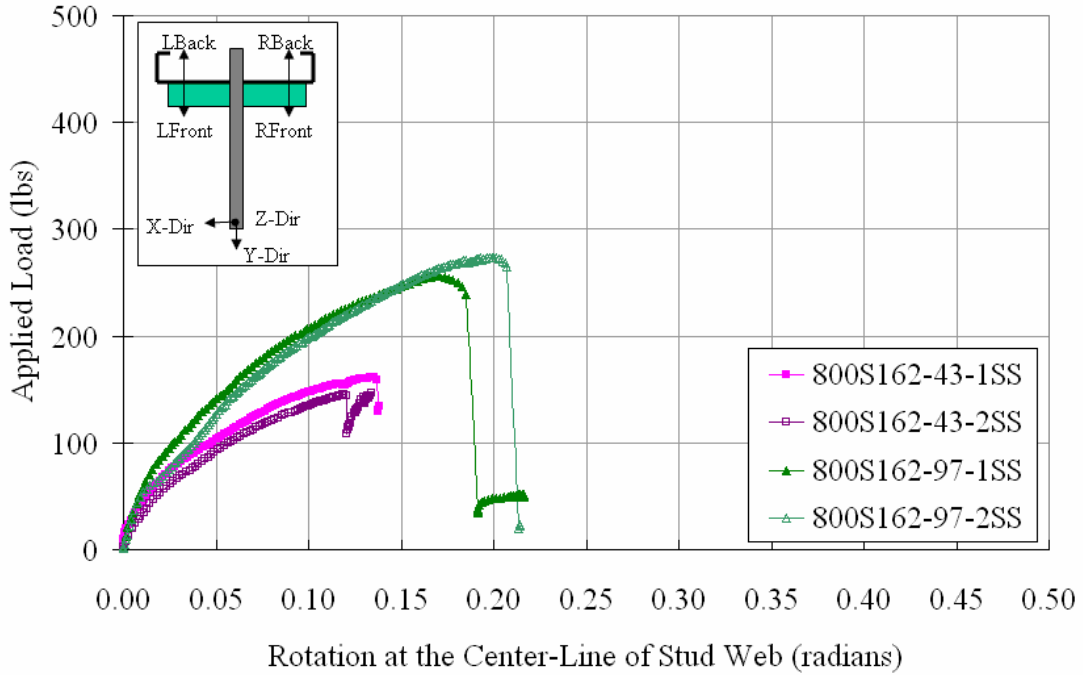


Figure 4.47 Plot of Applied Load vs. Calculated Rotation at the Center-line of the Web for the 800S Series of Studs with SS Connection.

Out-of-Plane Tests

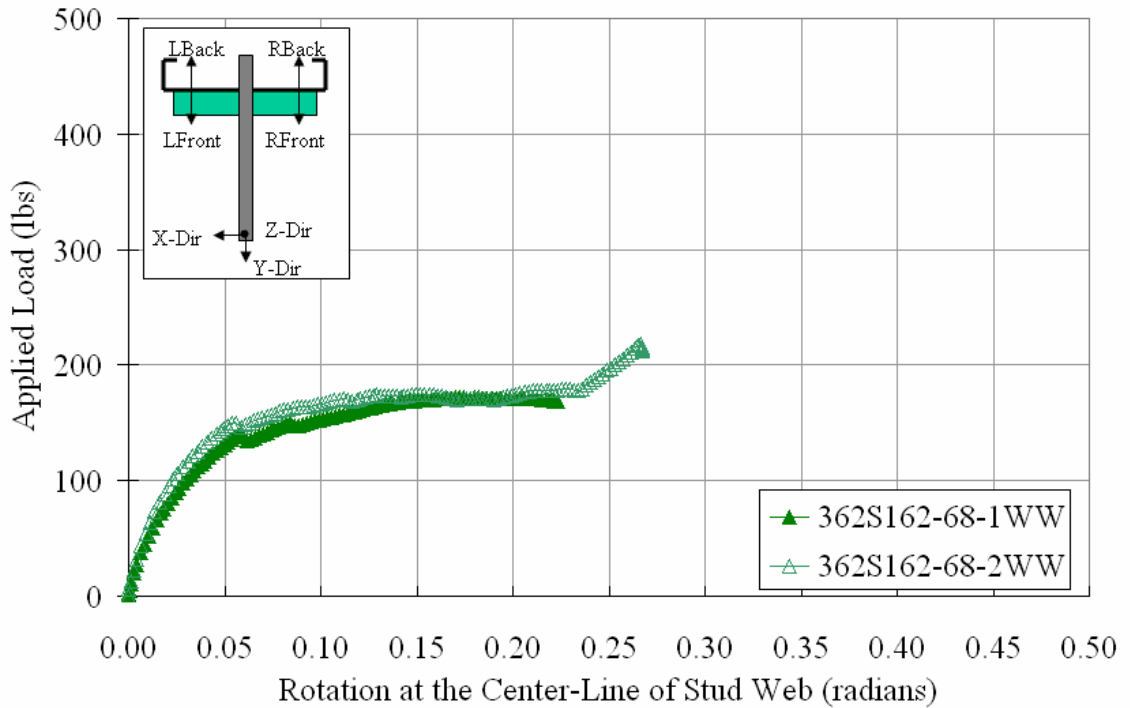


Figure 4.48 Plot of Applied Load vs. Calculated Rotation at the Center-line of the Web for the 362S Series of Studs with WW Connection



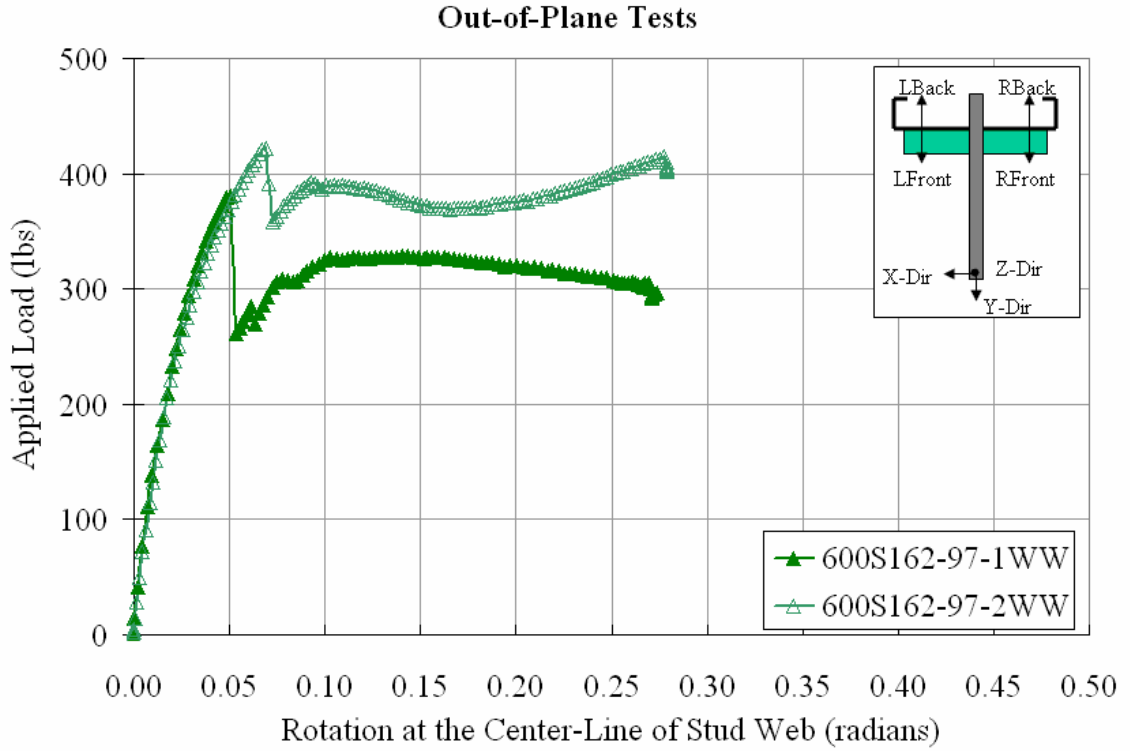


Figure 4.49 Plot of Applied Load vs. Calculated Rotation at the Center-line of the Web for the 600S Series of Studs with WW Connection

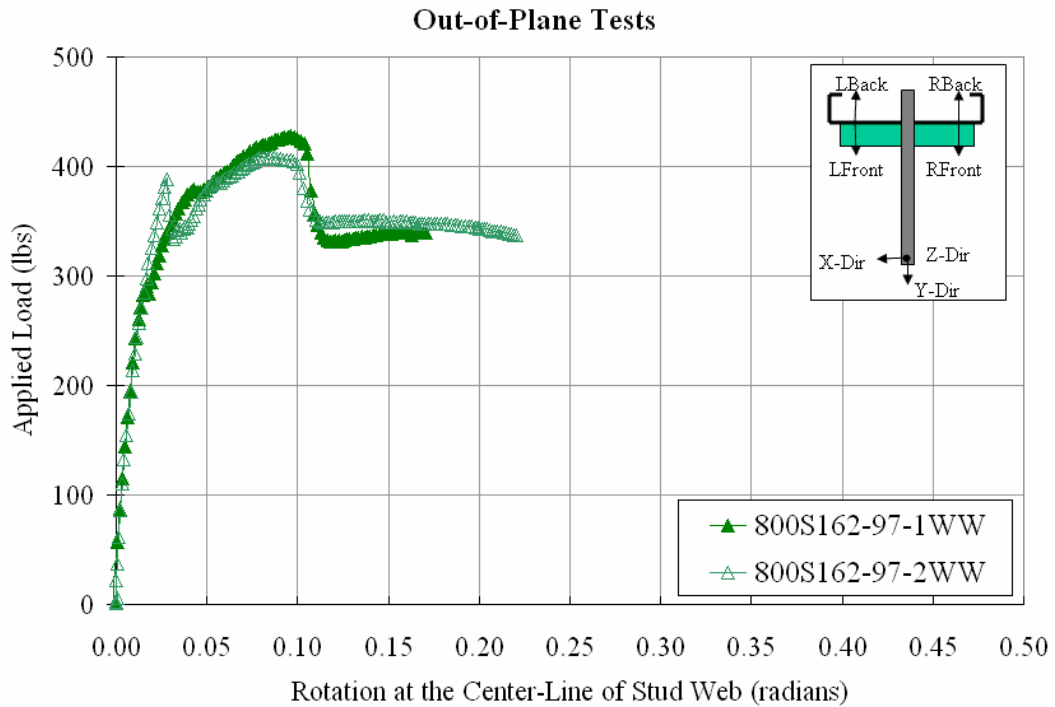


Figure 4.50 Plot of Applied Load vs. Calculated Rotation at the Center-line of the Web for the 800S Series of Studs with WW Connection

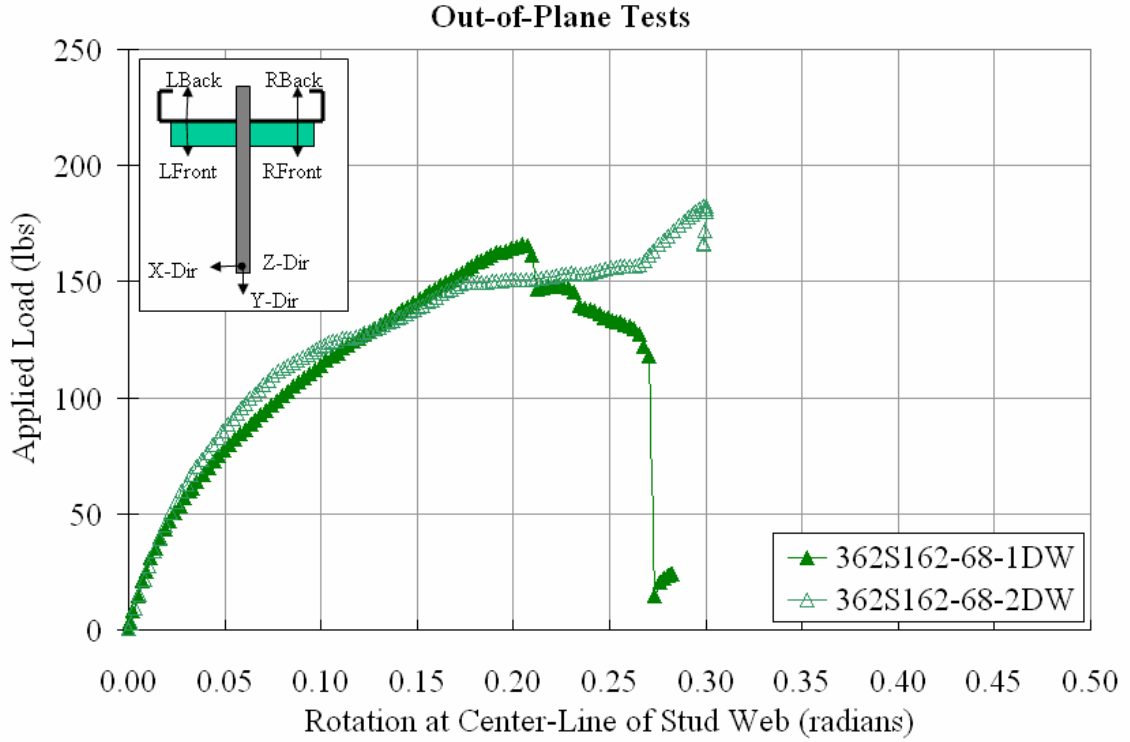


Figure 4.51 Plot of Applied Load vs. Calculated Rotation at the Center-line of the Web for the 362S Series of Studs with DW Connection

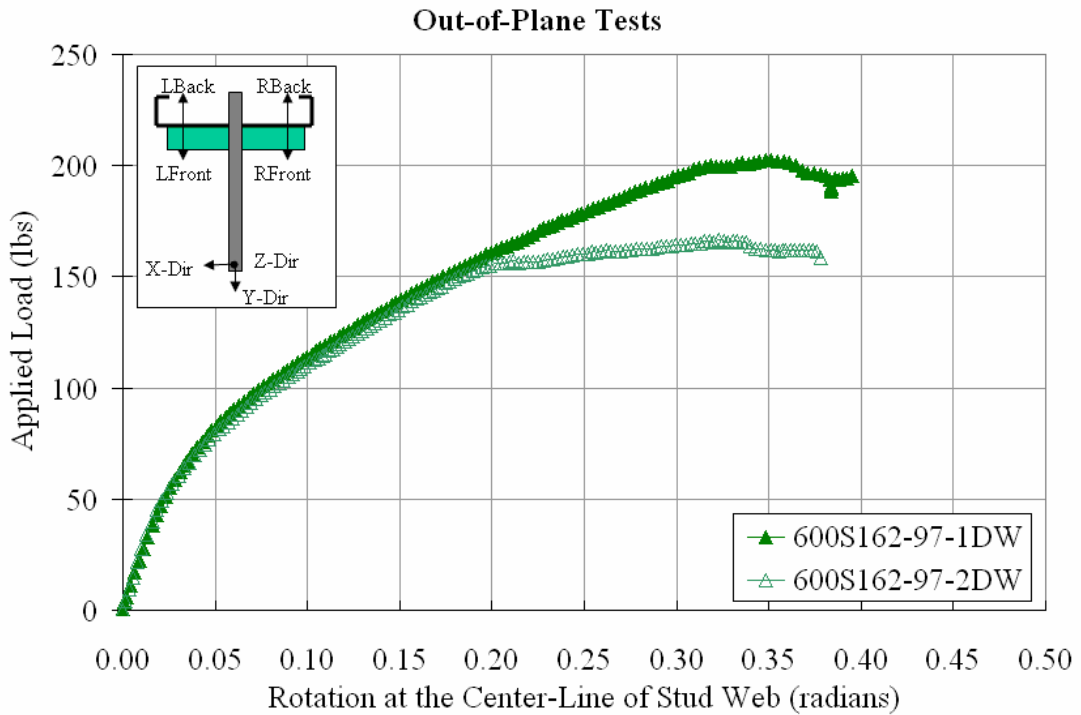


Figure 4.52 Plot of Applied Load vs. Calculated Rotation at the Center-line of the Web for the 600S Series of Studs with DW Connection

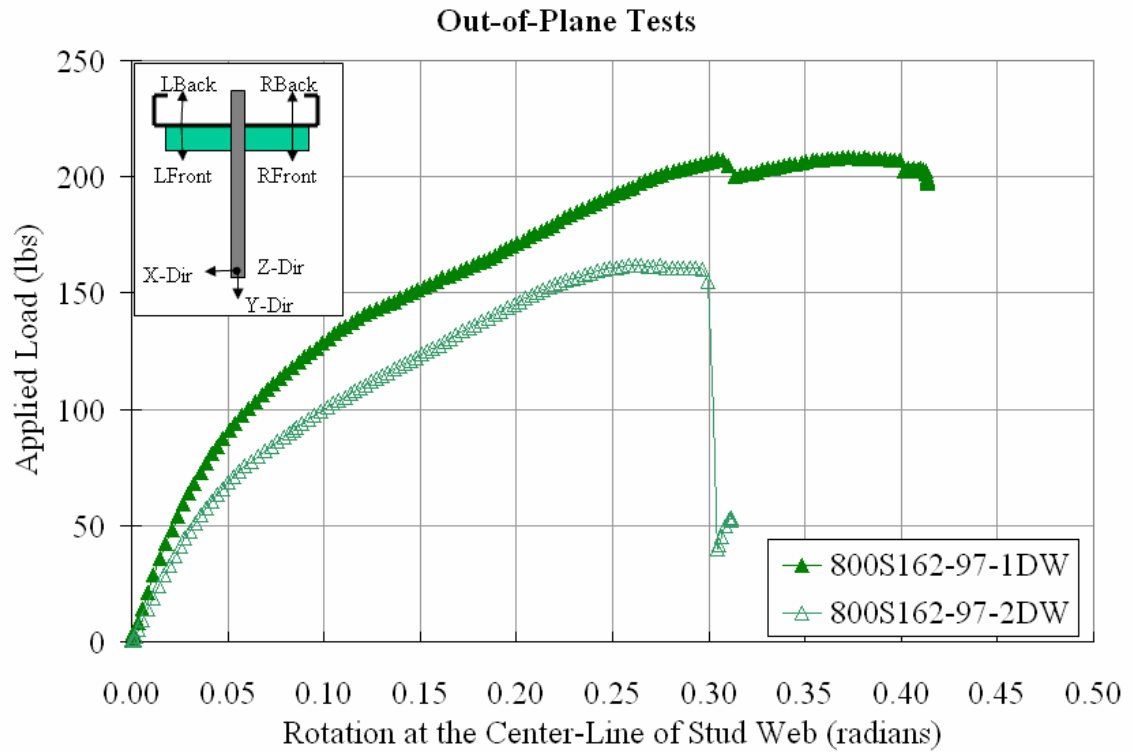


Figure 4.53 Plot of Applied Load vs. Calculated Rotation at the Center-line of the Web for the 800S Series of Studs with DW Connection

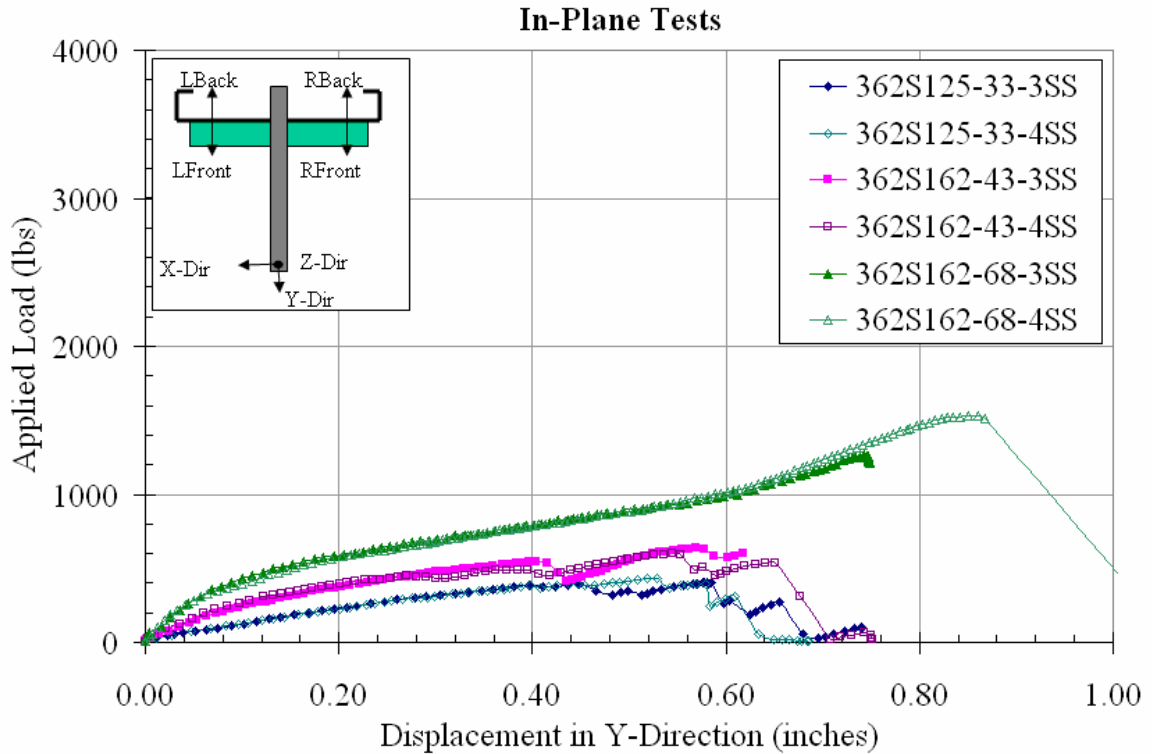


Figure 4.54 Plot of Applied Load vs. Displacement at the Center-line of the Web for the 362S Series of Studs

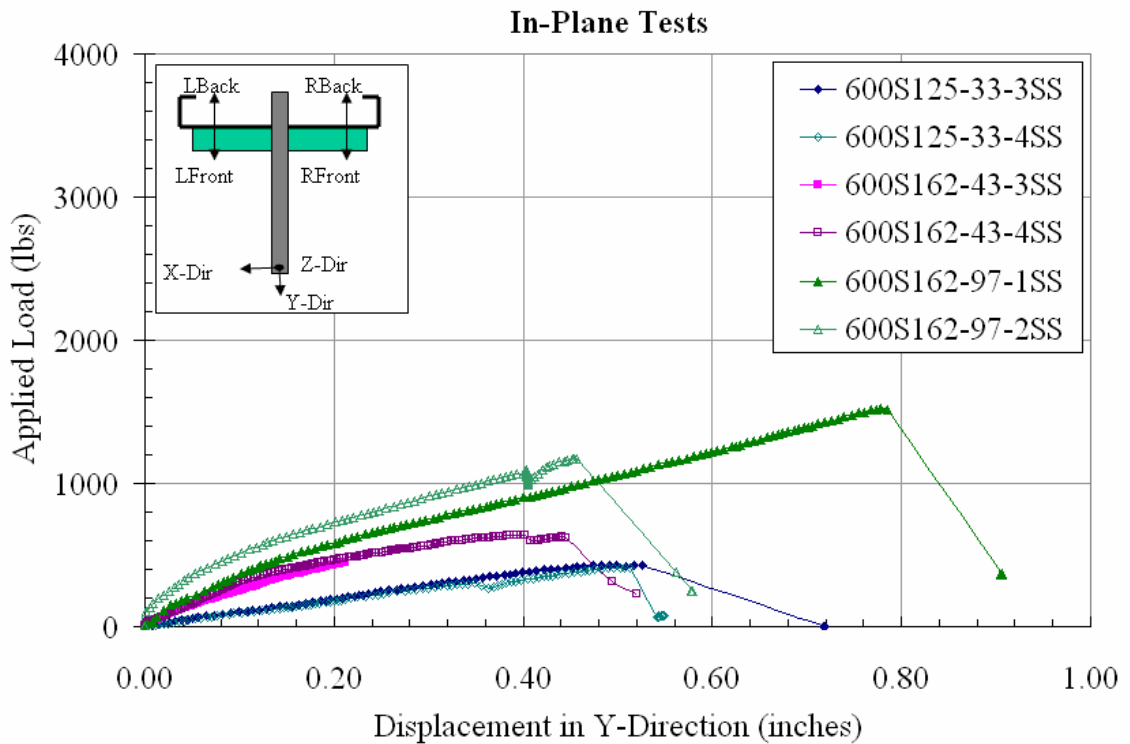


Figure 4.55 Plot of Applied Load vs. Displacement at the Center-line of the Web for the 600S Series of Studs

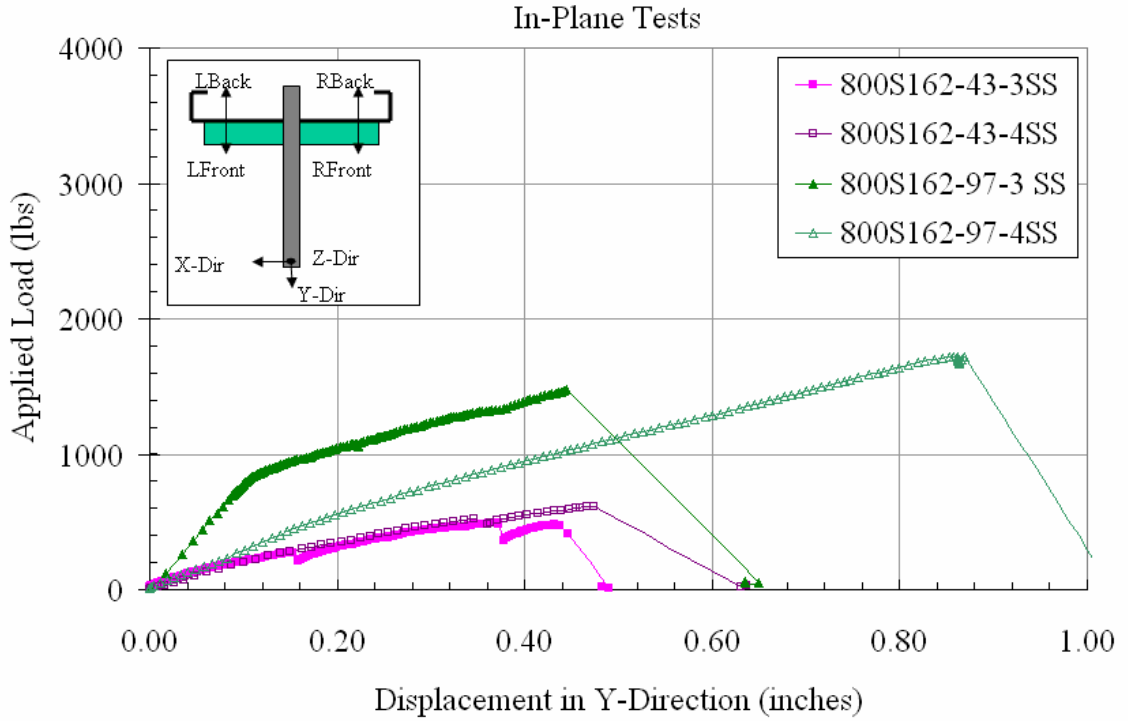


Figure 4.56 Plot of Applied Load vs. Displacement at the Center-line of the Web for the 800S Series of Studs

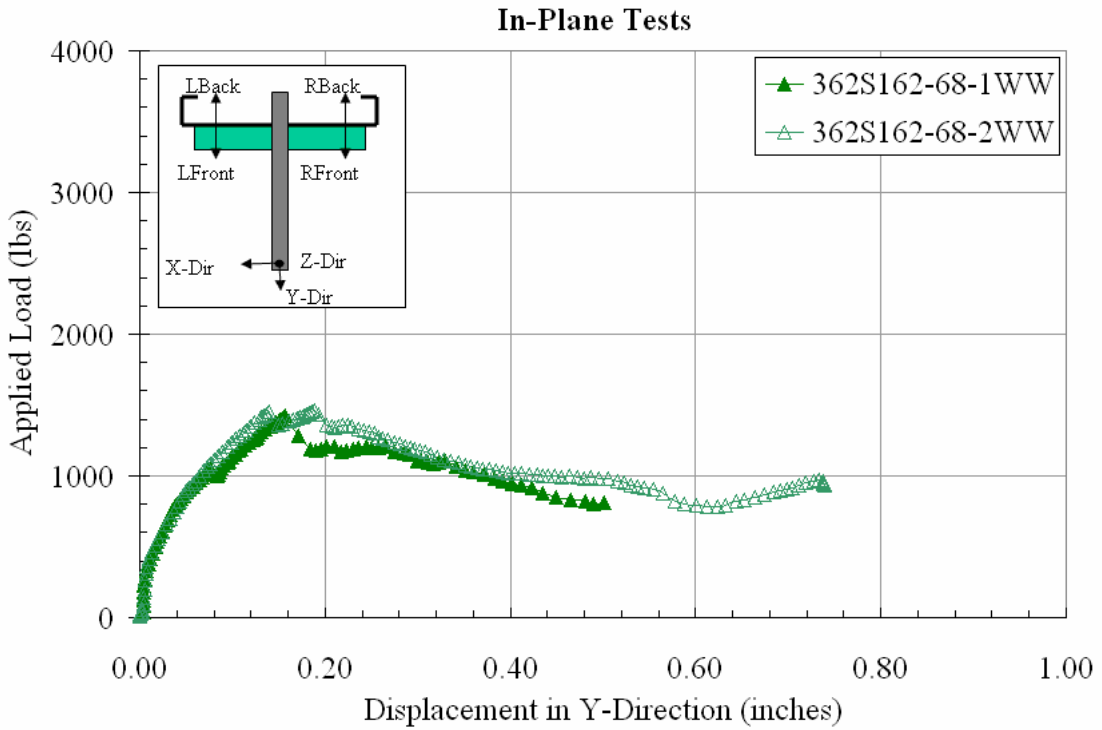


Figure 4.57 Plot of Applied Load vs. Displacement at the Center-line of the Web for the 362S Series of Studs

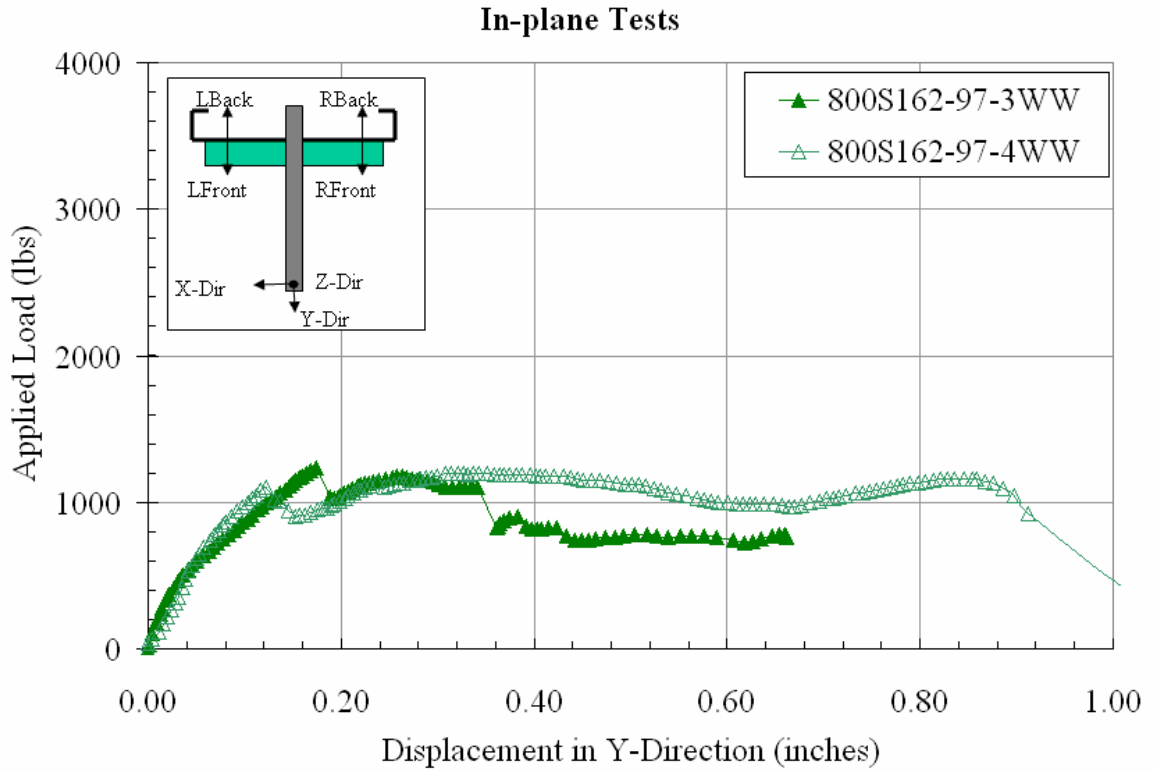


Figure 4.58 Plot of Applied Load vs. Displacement at the Center-line of the Web for the 600S Series of Studs

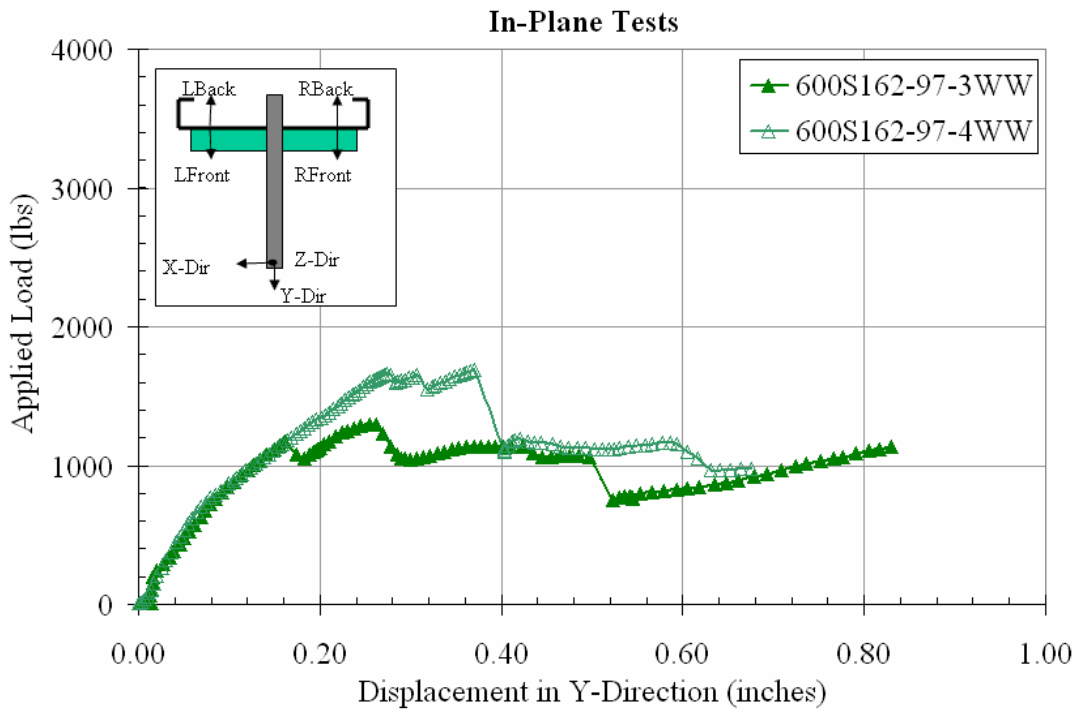


Figure 4.59 Plot of Applied Load vs. Displacement at the Center-line of the Web for the 800S Series of Studs

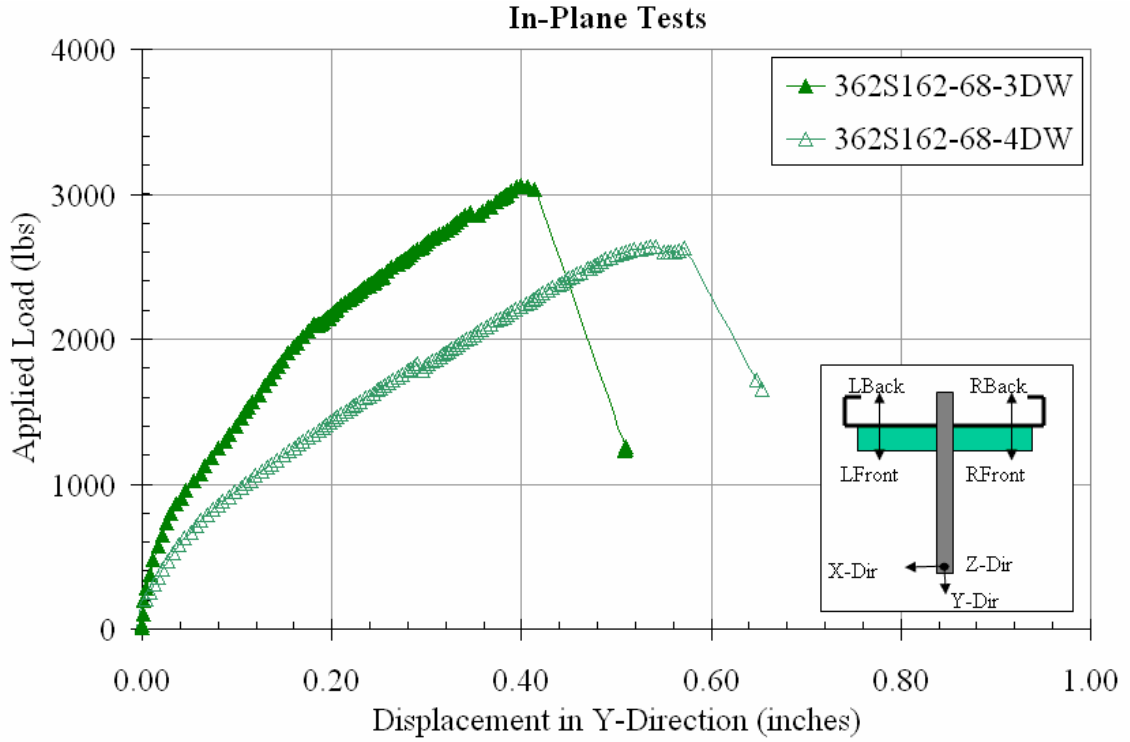


Figure 4.60 Plot of Applied Load vs. Displacement at the Center-line of the Web for the 362S Series of Studs

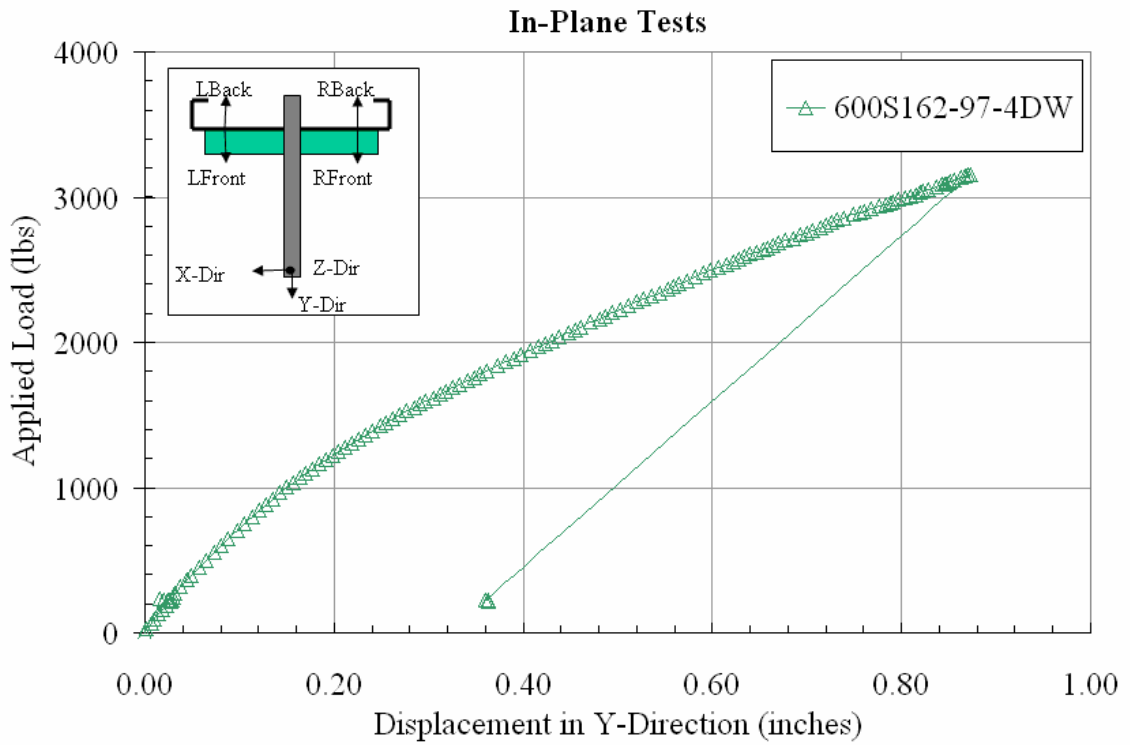


Figure 4.61 Plot of Applied Load vs. Displacement at the Center-line of the Web for the 600S Series of Studs

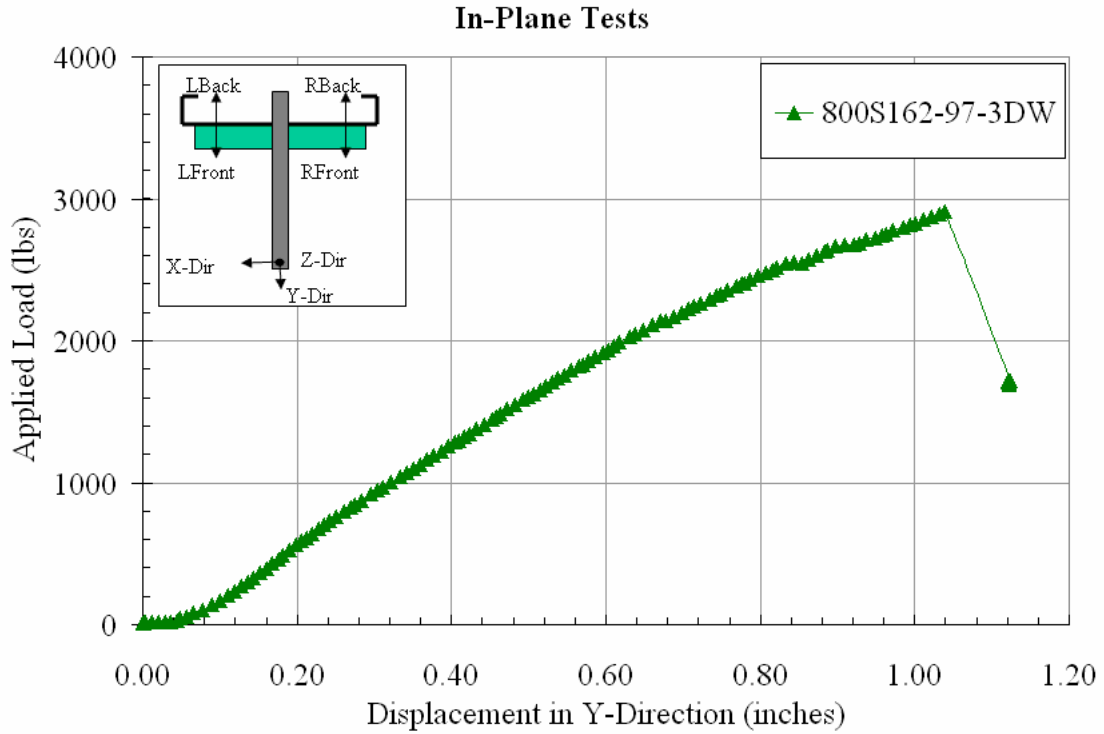


Figure 4.62 Plot of Applied Load vs. Displacement at the Center-line of the Web for the 800S Series of Studs

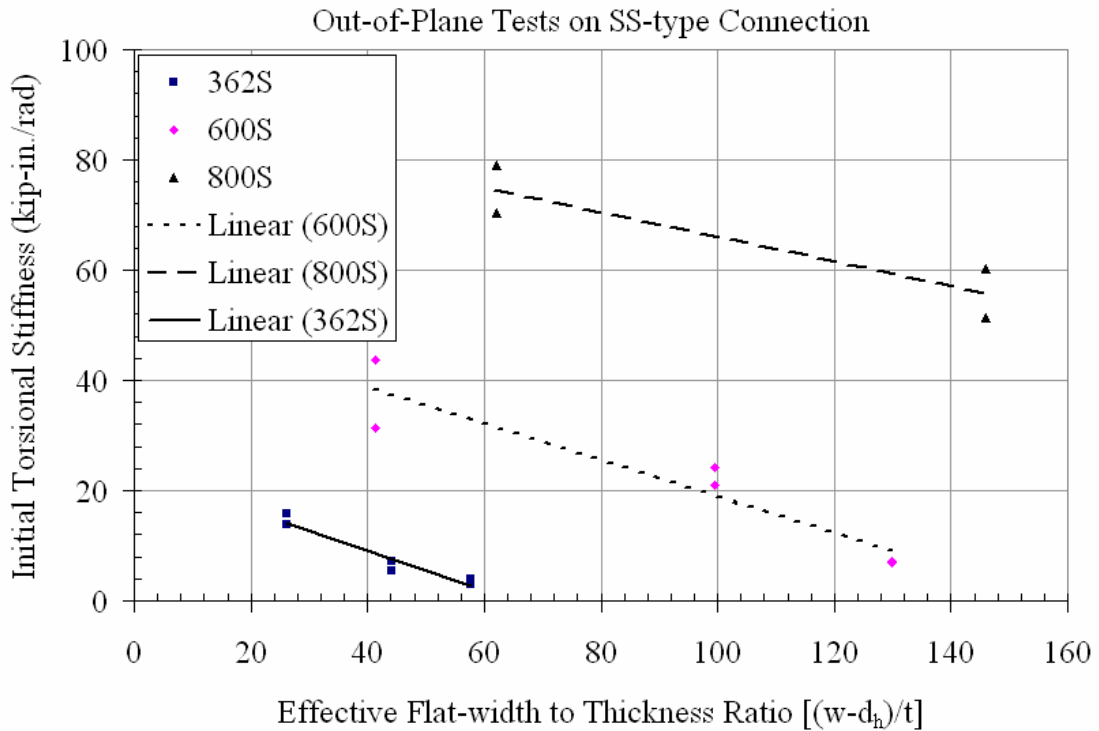


Figure 4.63 Plot of Initial Torsional Stiffness vs. Effective Flat-width to Thickness Ratio for the Out-of-Plane loading Tests on SS-type Connection



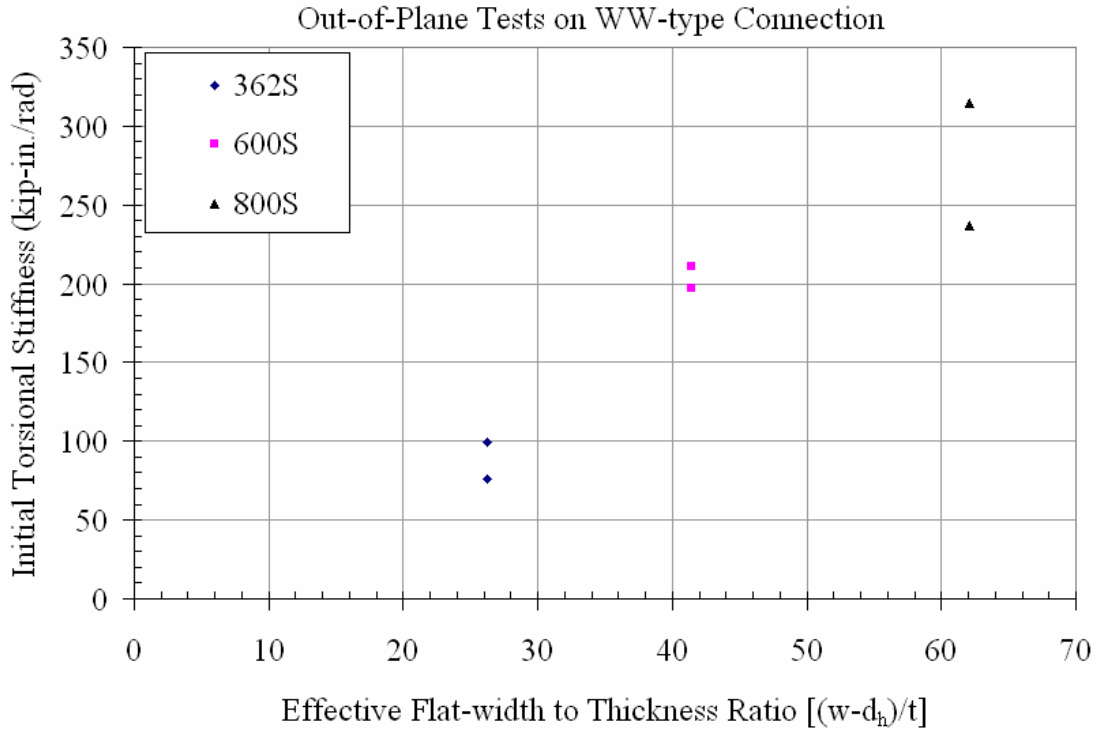


Figure 4.64 Plot of Initial Torsional Stiffness vs. Effective Flat-width to Thickness Ratio for the Out-of-Plane loading Tests on WW-type Connection

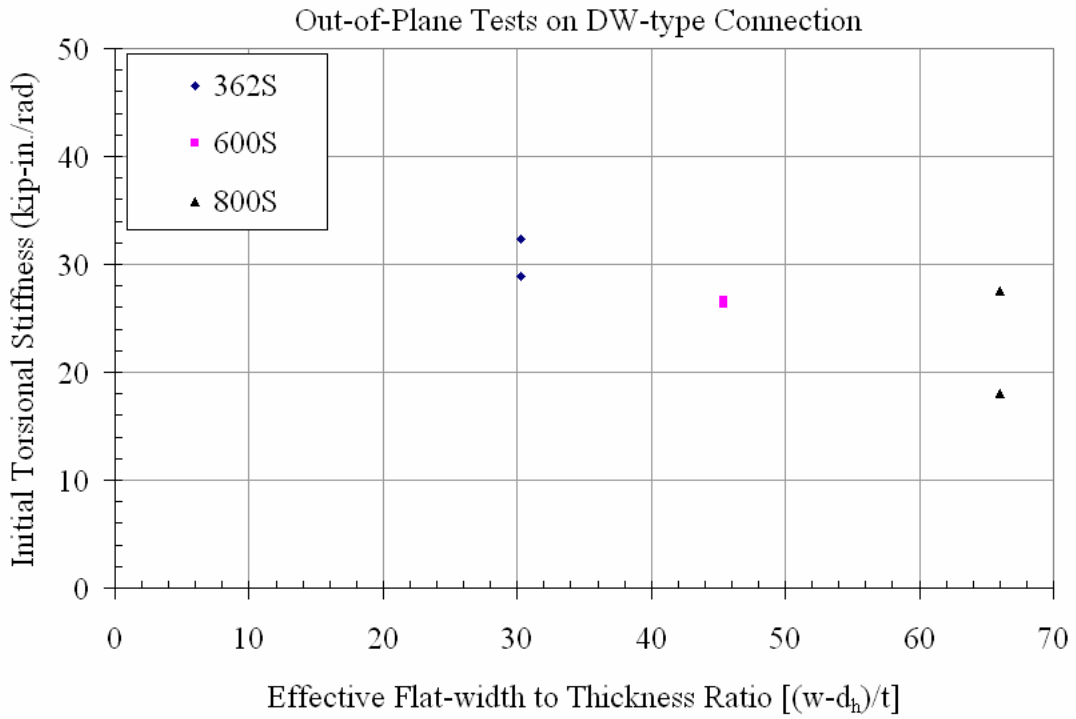


Figure 4.65 Plot of Initial Torsional Stiffness vs. Effective Flat-width to Thickness Ratio for the Out-of-Plane loading Tests on DW-type Connection

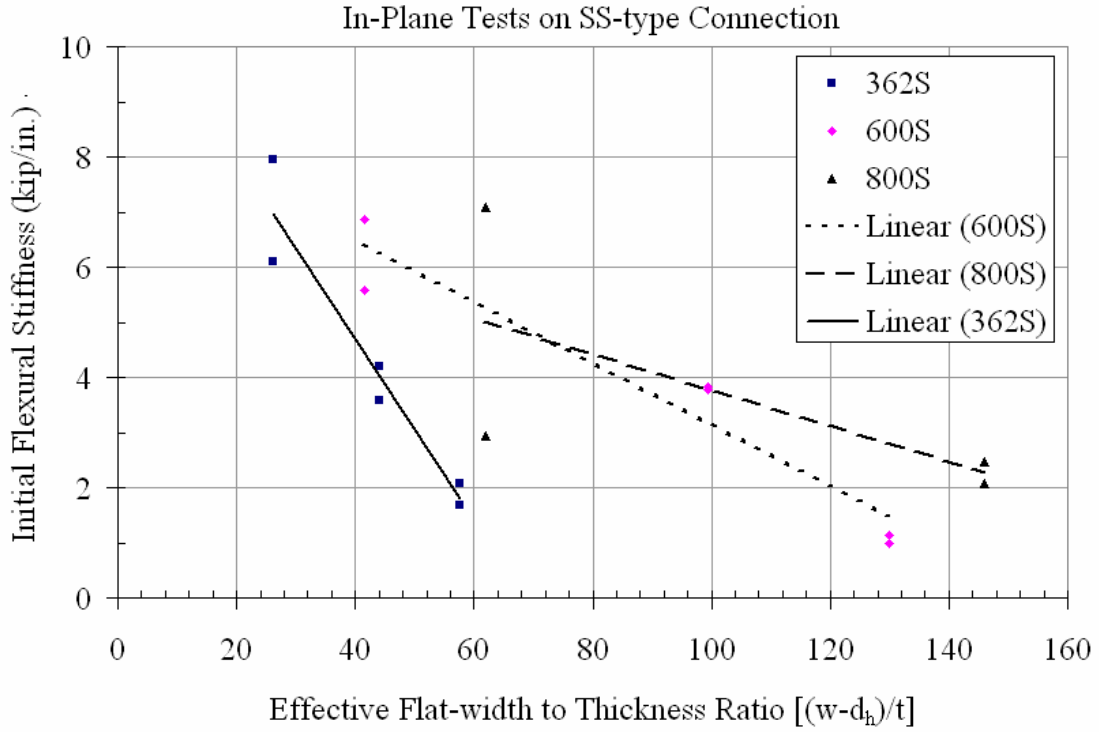


Figure 4.66 Plot of Initial Flexural Stiffness vs. Effective Flat-width to Thickness Ratio for the In-Plane loading Tests on SS-type Connection

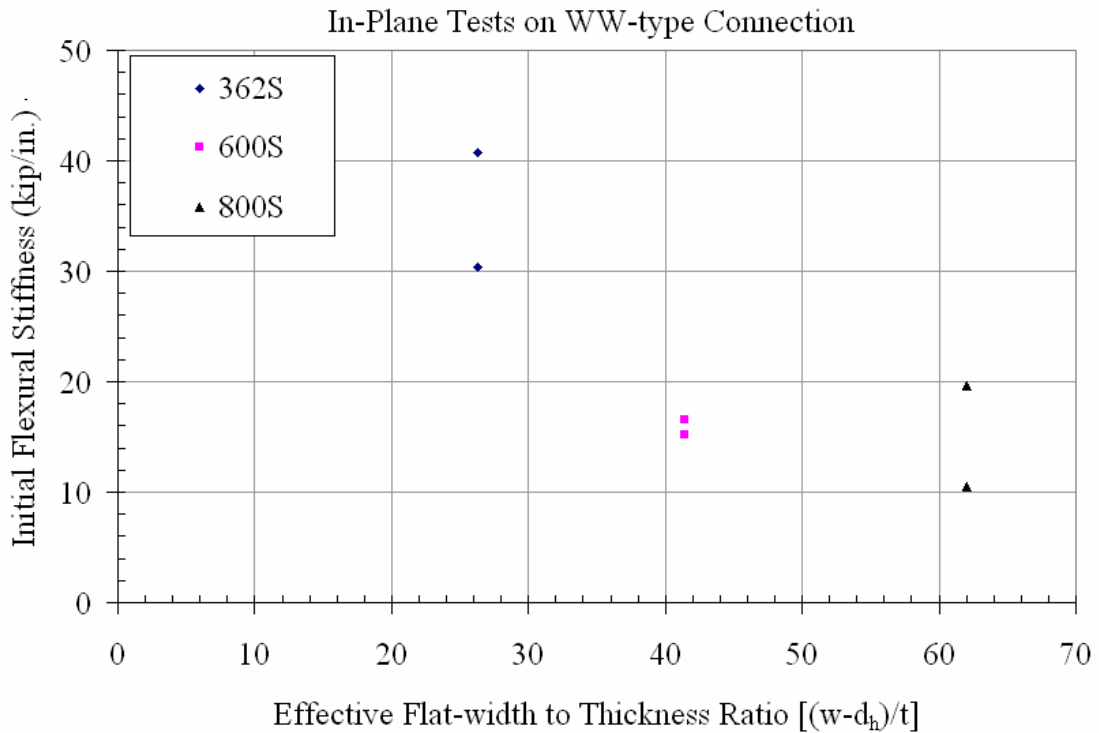


Figure 4.67 Plot of Initial Flexural Stiffness vs. Effective Flat-width to Thickness Ratio for the In-Plane loading Tests on WW-type Connection

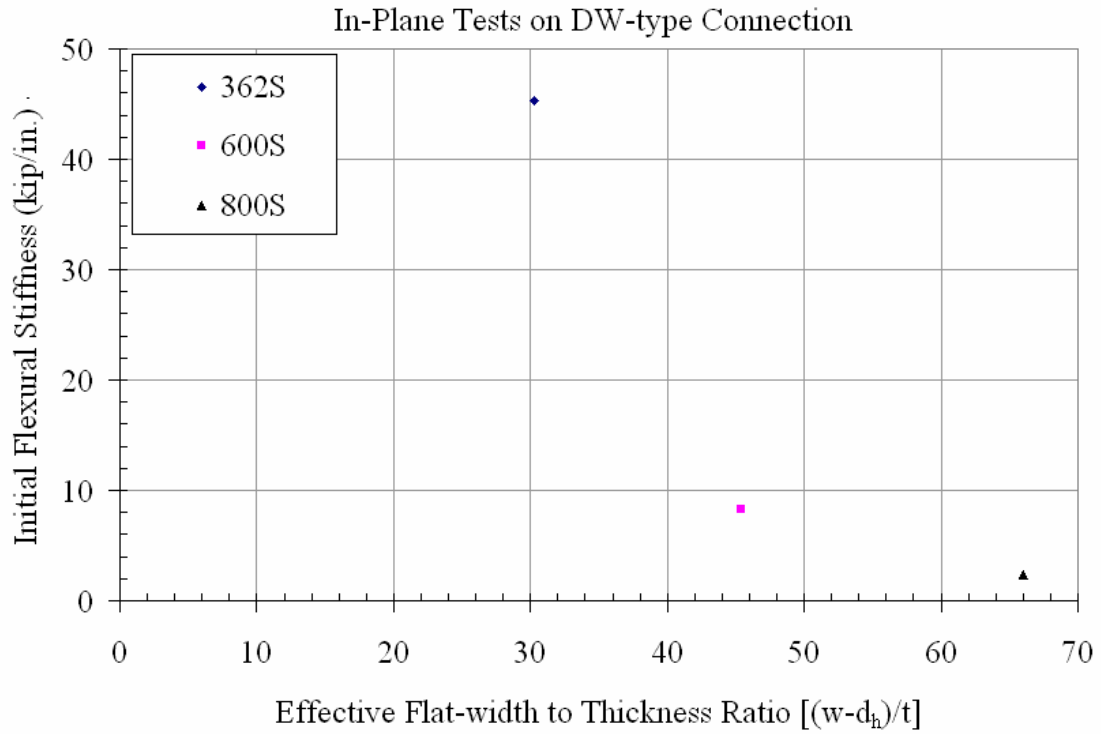


Figure 4.68 Plot of Initial Flexural Stiffness vs. Effective Flat-width to Thickness Ratio for the In-Plane loading Tests on DW-type Connection

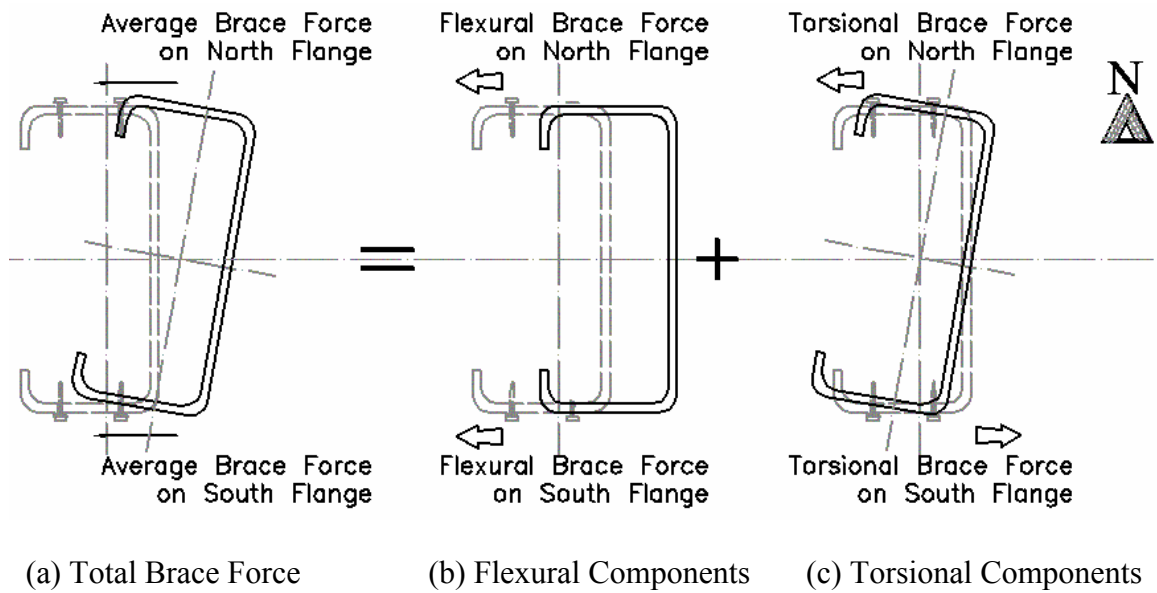


Figure 4.69 Brace Forces as a Resultant of Flexural and Torsional Components

## CHAPTER 5 ANALYTICAL EVALUATION

This chapter discusses the analytical methods used to determine the axial load capacity of the cee-stud, initial flexural stiffness and initial torsional stiffness of the bracing connections. The calculations of the total connection stiffness from the experimental results are also presented. The axial capacity was calculated for each stud cross-section using the experimentally determined mechanical properties of the eight groups of cee-studs. The flexural and torsional stiffness of the bracing connections were determined using basic structural mechanics and applying the elastic spring analogy to the connection components.

### **5.1 Analytical Load Capacity of Unbraced and Fully Braced Studs**

The axial load capacity of braced and unbraced studs was determined using MathCAD worksheets developed by Chen for AISI (1999). Table 5.1 gives the calculated axial load capacities based on two different effective length factors. The end conditions of the stud were considered pinned for weak axis flexural buckling, fixed for strong axis flexural buckling and fixed for torsional buckling about the shear center. The reasons for choosing these support conditions and the effects on stud behavior have been discussed in Chapter 4. The effective length factor for the case of an unbraced stud, for strong axis flexural buckling,  $K_x = 0.5$ , for weak axis flexural buckling,  $K_y = 1.0$  and for torsional buckling,  $K_t = 0.5$ . The effective length factor for the case of a braced stud, for strong axis flexural buckling,  $K_x = 0.5$ , for weak axis flexural buckling,  $K_y = 0.5$  and for torsional buckling,  $K_t = 0.25$ . The MathCAD worksheets accounts for the size of the

punchouts and their locations. The axial load capacity is affected by the size of the punchout, the effect of which is in reduction of the axial load capacity. The effective cross-sectional area is determined based on the effective width of the web across the punchout as per Section B2.2, AISI (1999). The critical buckling stress is computed as the minimum of the strong axis buckling stress, the weak axis buckling stress or the torsional buckling stress. The axial loads predicted by the AISIWIN (2000) program whose results are given in Tables 4.3 and 4.4 did not include the effect of punchouts and hence are greater than the values given in Table 5.1 for the same cross-section of the cee-stud. It may be observed that in both the analytical determinations of axial load capacities fall below the actual experimental maximum load. This is because of the support restraint that is present in the test specimens.

These MathCAD worksheets were used to compare the results obtained from AISIWIN (2000). It can be observed that AISIWIN gives a higher prediction of the axial load capacity than the MathCAD worksheets results. It must be noted here that, using both these analytical methods, the axial capacity was far conservative due to which the brace stiffness and demand happens to be less than the experimentally required value. This leads to a bracing requirement that is unconservative for all practical purposes. The reason being that the support conditions in the standard industry practice, using standard tracks, offers far more rigidity than the ideal cases of pinned ends. The two analytical methods used to determine the axial load capacities of the cee-studs though have the option of specifying the effective lengths, it is a judgment call by the practicing engineer to safely choose the effective lengths.

## **5.2 Analytical Bridging Connection Stiffness of a Flexible Bracing**

The experimental values of initial connection stiffness have been determined in Chapter 4. Referring back to Table 4.13, the initial torsional stiffness at 10% of the maximum load is calculated as the ratio of the applied load to the corresponding rotation of the web. It was observed that within this load range, the initial slopes of the plots were nearly linear. Similarly, Table 4.15 gives the initial flexural stiffness at 10% of the maximum load, calculated as the ratio of the applied load to the corresponding Y-displacement of Point A, the point of application of the load on the channel bridging, measured by a string potentiometer.

The total actual stiffness of the bridging system is calculated using Eq. 2.22, as described in Chapter 2. The total actual stiffness is the reciprocal of the sum of reciprocals of the connection stiffness and the brace stiffness, because the bridging connection is in series with the bracing system. The bridging connection is comprised of several connecting elements that are in series with one another and their equivalent connection stiffness determination is given in Urala (2004). The total connection stiffness was determined from both the experimental results of the bridging tests and the analytical models developed for each connection type. The comparisons of the calculated experimental stiffness with calculated analytical stiffness are presented in Tables 5.2 and 5.3 for the initial flexural stiffness and the initial torsional stiffness, respectively.

### **5.2.1 Initial Flexural Stiffness of the Bracing Connection**

The following assumptions were made in finding the analytical value of initial flexural stiffness:

- The bridging channel was considered to be under tension due to the applied load and the deformation was computed using the following equation:

$$\frac{\Delta}{P} = \frac{L}{A E} \quad (5.1)$$

- The clip angle acts as a beam supported at two points, subjected to two point loads. The moment of inertia of the angle was taken about its horizontal leg. For the SS type connection, the angle was considered to be simply-supported between the screws, and for the WW type connection, the angle was considered to be fixed at the welds. The MathCAD worksheet for this calculation is given in Urala (2004) and provides the calculations for this analytical determination.
- The web was considered as a rectangular plate with either simple or fixed edges at the boundaries. The plate was considered to be subjected to concentrated loads at the location of the screws or the welds. The plate buckling equation (Roark 1985) for a rectangular plate subjected to a concentrated load is given as:

$$\frac{\Delta}{P} = C(1 - \mu^2) \frac{a b}{E t^3} \quad (5.2)$$

where	C	=	Support fixity coefficient of the steel plate
	E	=	Elastic modulus of cold-formed steel
	P	=	Applied load
	a, b	=	Dimensions of the rectangular plate
	t	=	Thickness of the rectangular plate
	$\Delta$	=	Displacement due to applied load, P
	$\mu$	=	Poisson's ratio of steel, 0.3

The effective width of the web plate was calculated as per Section B2.2, AISI (1999) which is as follows:

when  $\lambda > 0.673$

$$b = \frac{w}{\lambda} \left[ 1 - \frac{0.22}{\lambda} - \frac{0.8 d_h}{w} \right] \quad (5.3a)$$

when  $\lambda \leq 0.673$  or

$$b = w - d_h \quad (5.3b)$$

where  $d_h$  = Diameter of the elongated circular punchout

The slenderness factor is calculated using the relation

$$\lambda = \frac{1.052}{\sqrt{k}} \frac{w}{t} \sqrt{\frac{f_y}{E}} \quad (5.4)$$

where  $k$  = Plate buckling coefficient

= 24.0 for simply-supported edges

= 40.8 for fixed-fixed edges

The effect of the length of the punchout was considered to be negligible since the web is assumed to be infinite in that direction while the predominant flexural displacement was along the shorter span direction between the flanges of the cee-stud cross-section. In all the cases, the stiffness and deformation of the screws or the welds was calculated and found that these components had little effect on the overall connection stiffness, and hence they were later neglected for simplicity.

The flexural stiffness values are plotted in Figures 5.1, 5.2 and 5.3 against the slenderness factor of the stud web, determined using Eq. 5.4 for the three connection types (SS, WW and DW), respectively. The plots contain four different data sets representing the following cases of initial flexural stiffness for the in-plane loading tests:

- Experimental lower bound values (LBV)
- Experimental upper bound values (UBV)
- Analytical value for a rectangular plate with four simply-supported edges
- Analytical value for a rectangular plate with four fixed edges

#### **5.2.1.1 SS type connection**

It can be observed that in Figure 5.1 and Table 5.2 for the SS Type connection the analytical calculation of the initial flexural stiffness increases exponentially with decrease



in the web slenderness factor ( $\lambda$ ). It can also be observed that the analytical flexural stiffness values for the rectangular plate with either fixed edges or simply-supported edges form the upper and lower bounds to the experimental values of the initial flexural stiffness for the SS Type connection. For the eight groups of studs in the experimental program, the slenderness factor varied from 0.43 to 1.43 and the experimental initial flexural stiffness varied from 7.94 to 1.00 kip/in., respectively. The analytical flexural stiffness for the lower slenderness factors show a greater difference for the type of support condition than the higher slenderness factors that show almost equal values for the different types of support conditions.

#### **5.2.1.2 WW type connection**

The analytical initial flexural stiffness values, shown in Figure 5.2 for the WW Type connection, decrease linearly with increasing web slenderness factor ( $\lambda$ ). It was clearly observed that the analytical flexural stiffness values for a rectangular plate with either fixed edges or simply-supported edges form the upper and lower bounds to the experimental values of the initial flexural stiffness for the WW Type connection. For the three groups of studs in the experimental program, the slenderness varied from 0.43 to 0.63 and the corresponding experimental initial flexural stiffness varied from 40.8 to 10.5 kip/in, respectively.

#### **5.2.1.3 DW type connection**

The analytical initial flexural stiffness values shown in Figure 5.3 for the DW Type connection, decrease linearly with increasing web slenderness factor ( $\lambda$ ). Except for one value of experimental stiffness, the analytical values form the upper and lower bound values to the experimental initial flexural stiffness values. For the three groups of studs in the experimental program, the slenderness varied from 0.43 to 0.63 and the

corresponding experimental initial flexural stiffness varied from 50.4 to 2.4 kip/in., respectively.

From the above three figures, it can be generalized that the analytical determination of initial flexural stiffness values is close enough to the values determined from the experimental results.

### **5.2.2 Initial Torsional Stiffness of the Bracing Connection**

The following assumptions were made in determining the initial torsional stiffness of the bracing connection:

- The bridging channel was considered to be rigid enough not to deform under the influence of the applied out-of-plane load. This assumption was verified and found to be true since all the torsional deformation was occurring at the stud web.
- The clip angles in case of the SS and WW Type connections were considered to be initially rigid compared to the stiffness of the web.
- The web was considered as a rectangular plate with fixed edges. The plate was considered to be subjected to two point loads. The first point load was a direct pull at the location of the screw or the weld. The second point load was the resultant of the bearing pressure of the clip angle on the web. For simplicity, the two point loads were considered to be of equal magnitude and equidistant from the vertical centerline of the web.

The initial torsional stiffness values determined using Eq. 5.4 are plotted in Figure 5.4 against the web slenderness factor for the SS Type connection. The plot contains four different data sets representing the following cases of initial torsional stiffness for the out-of-plane loading tests:

- Experimental lower bound values (LBV)
- Experimental upper bound values (UBV)
- Analytical value for a rectangular plate with four fixed edges

With calculations based on above assumptions the results obtained for the analytical initial torsional stiffness of the SS Type connection is not accurate or even in

the same range as that of the values determined from the experimental tests and can be observed in Figure 5.4 and Table 5.3. This requires a further study and more exact model of the connection has to be developed. There are several factors contributing to the torsional stiffness and the flexural stiffness of the clip angle and the bracing channel has to be converted to an equivalent torsional stiffness. The bearing of the clip angle is causes uniformly varying load on the web which has a resultant that is not at the same distance as the location of the connection point load. This causes an unsymmetrical load distribution about the vertical centerline of the web. This uniformly varying load is also affected by the presence of the web punchout causing a trapezoidal load on the loaded portion of the web. Based on some of the experimental observations during the test, the clip angle has been the controlling critically stiff element and hence its stiffness is important in calculating the initial torsional stiffness of the connection. Further analysis is required to assess the initial torsional stiffness analytically.

### 5.3 Total Stiffness of the Bridging Connection

The determination of the total stiffness of the bridging system has been discussed in detail in Chapter 4. The initial stiffness of the bridging connection is determined experimentally at an applied load of 10% of the maximum load attained during the bracing tests and is explained in Section 4.2 of this report.

#### 5.3.1 Initial Flexural Stiffness

The determination of the total flexural stiffness of the bridging connection has been discussed in Chapter 2 and is given by Eq. 2.2, which is given as:

$$\frac{1}{\beta_{\text{act}}} = \frac{1}{\beta_{\text{conn}}} + \frac{1}{\beta_{\text{brace}}} \quad (2.22)$$

For each cee-stud any of the three connection types can be used to secure the mid-height bracing. The stiffness of each connection type is given in Table 4.16 which is based on two test results per stud and connection type. Table 5.4 gives the total equivalent flexural stiffness of the bridging connection for each of the 37 axially loaded studs. It is assumed that the bridging connection remains elastic when the axially loaded cee-stud has reached its full capacity. This is evident by the fact that the connection stiffness is greater than the brace stiffness. However the total actual stiffness is slightly lower than the total brace stiffness. This is because the connection itself undergoes deformations under the applied load. The connection stiffness given in Table 5.4 is obtained as the average value from the two tests for each stud and connection type.

### 5.3.2 Initial Torsional Stiffness

The determination of the total torsional stiffness of the bridging connection has been discussed in Chapter 2 and is given by Eq. 2.2, as given above. For each cee-stud any of the three connection types can be used to secure the mid-height bracing. The torsional stiffness of the brace wire is determined assuming that the torsional buckling occurs about the centroid of the gross-section rather than the shear center. This is because the brace wires restrain the stud from strong axis displacement. If the force in the brace wire is  $P$ , the deformation of the brace is  $\Delta$ , then the stiffness of the brace wire is given by:

$$\frac{P}{\Delta} = \frac{A E}{L} \quad (5.5)$$

If the cross-section rotates by an angle  $\theta$ , then for small angular deformations,

$$\theta = \frac{\Delta}{D/2} \quad (5.6)$$

Substituting Eq. 5.5 in 5.6, we get the torsional stiffness of the bracing as:

$$\frac{PL}{\theta} = \frac{AED}{2} \quad (5.7)$$

- where A = Area of cross-section of brace wire  
 E = Elastic modulus of steel wire = 29,000,000 psi.  
 D = Distance between the brace wires = depth of the cee-stud  
 L = Length of brace wire  
 P = Force in the brace wire

Table 5.5 gives the calculated values of torsional stiffness of the brace wire. Table 5.6 gives the total equivalent torsional stiffness of the bridging connection for each of the 36 axially loaded studs. The values of the experimental initial torsional stiffness for two test specimens per stud cross section and connection type has been previously given in Table 4.17 and the average value of those two is given in Table 5.6

Table 5.1 Axial Load Capacities of Test Specimens Using AISI (1999) MathCAD Worksheets

Stud Designation				Tension Coupon Test Results		AISI (1999) MathCAD worksheets					Required Ideal Brace Stiffness
				Yield Stress	Ultimate Stress	As-Built Section Area	As-Built Ultimate Capacity (P <sub>u</sub> )		As-Built Unfactored Capacity (P <sub>n</sub> )		β <sub>ideal</sub>
				F <sub>y</sub>	F <sub>u</sub>		Unbraced	Mid-Point Brace	No Brace	Mid-Point Brace	
D	S	B	t	ksi	ksi	in. <sup>2</sup>	lbs	lbs	lbs	lbs	lbs/in.
362	S	125	33	48.53	55.48	0.2028	429	1587	505	1867	78
362	S	162	43	47.04	58.20	0.3089	2221	6968	2613	8197	342
362	S	162	68	52.01	67.80	0.5154	3713	11549	4369	13587	566
600	S	125	33	24.03	45.24	0.2537	587	1542	690	1814	76
600	S	162	43	46.24	54.88	0.4135	2156	5832	2536	6862	286
600	S	162	43a	50.30	59.38	0.4346	2461	6715	2895	7900	329
600	S	162	97	60.20	70.21	0.9807	6287	19904	7396	23417	976
800	S	162	43	40.23	54.90	0.4829	1967	5156	2314	6066	253
800	S	162	97	42.50	67.49	1.1841	6694	17468	7876	20550	856

As-Built sectional properties were based on the experimentally measured dimensions  
 Ideal Brace Stiffness was obtained using Yura's Bracing Equation 2.14 (Yura 1995)  
 Design factor used in calculating the Unfactored Capacity was 0.85

Table 5.2 Comparison of Initial Flexural Stiffness of the In-Plane Tests

Stud Designation					Slenderness Factor	Initial Stiffness		Analytical Stiffness	
D	S	B	t	C	$\lambda$	Lower	Upper	Simple	Fixed
						kip/in.	kip/in.	kip/in.	kip/in.
362	S	125	33	SS	0.8984	1.68	2.07	0.65	1.34
362	S	162	43	SS	0.6768	3.57	4.20	1.45	2.97
362	S	162	68	SS	0.4343	6.10	7.94	6.25	12.64
600	S	125	33	SS	1.0733	1.00	1.14	0.17	0.35
600	S	162	43	SS	1.1406	3.79	3.82	0.38	0.78
600	S	162	97	SS	0.5493	5.57	6.86	4.78	9.62
800	S	162	43	SS	1.4328	2.07	2.46	0.19	0.39
800	S	162	97	SS	0.6296	2.95	7.08	2.34	4.71
362	S	162	68	WW	0.4343	30.42	40.79	25.82	49.78
600	S	162	97	WW	0.5493	15.24	16.52	14.13	27.63
800	S	162	97	WW	0.6296	10.51	19.67	7.29	14.40
362	S	162	68	DW	0.4343	45.36	50.41	15.70	31.09
600	S	162	97	DW	0.5493	8.26	8.26	7.55	15.25
800	S	162	97	DW	0.6296	2.40	2.40	3.23	6.60

Table 5.3 Comparison of Initial Torsional Stiffness of the In-Plane Tests

Stud Designation					Slenderness Factor	Initial Stiffness		Analytical Stiffness	
D	S	B	t	C	$\lambda$	Lower	Upper	Simple	Fixed
						kip-in./rad	kip-in./rad	kip-in./rad	kip-in./rad
362	S	125	33	SS	0.8984	2.96	4.00	-	0.51
362	S	162	43	SS	0.6768	5.33	7.04	-	1.12
362	S	162	68	SS	0.4343	13.88	15.72	-	4.13
600	S	125	33	SS	1.0733	7.02	7.20	-	0.62
600	S	162	43	SS	1.1406	21.04	24.08	-	1.37
600	S	162	97	SS	0.5493	31.38	43.60	-	14.25
800	S	162	43	SS	1.4328	51.41	60.32	-	1.73
800	S	162	97	SS	0.6296	70.32	78.95	-	18.44
362	S	162	68	WW	0.4343	75.79	99.27	-	-
600	S	162	97	WW	0.5493	197.37	211.10	-	-
800	S	162	97	WW	0.6296	236.61	314.45	-	-
362	S	162	68	DW	0.4343	28.89	32.40	-	-
600	S	162	97	DW	0.5493	26.31	26.72	-	-
800	S	162	97	DW	0.6296	18.04	27.58	-	-



Table 5.4 Total Flexural Stiffness of the Bridging Connections

Stud Designation					Total Brace Stiffness	Experimental Initial Flexural Stiffness of the Bridging Connection			Total Flexural Stiffness of the Bridging Connection		
						$\beta_{provided}$	SS Type	WW Type	DW Type	SS Type	WW Type
D	S	B	t	ID	lbs/in.	lbs/in.	lbs/in.	lbs/in.	lbs/in.	lbs/in.	lbs/in.
362	S	125	33	5	0	0					
362	S	125	33	3	192	1875			174		
362	S	125	33	4	192	1875			174		
362	S	125	33	6	201	1875			182		
362	S	125	33	1	413	1875			338		
362	S	125	33	2	765	1875			543		
362	S	162	43	1	0	0					
362	S	162	43	2	371	3885			339		
362	S	162	43	4	734	3885			617		
362	S	162	43	3	1478	3885			1071		
362	S	162	68	5	0	0					
362	S	162	68	3	1023	7020	35605	47885	893	994	1001
362	S	162	68	4	1538	7020	35605	47885	1262	1475	1490
362	S	162	68	2	2046	7020	35605	47885	1584	1935	1962
600	S	125	33	2	0						
600	S	125	33	4	61	1070			57		
600	S	125	33	3	123	1070			110		
600	S	125	33	1	402	1070			292		

Table 5.4 (Continued) Total Flexural Stiffness of the Bridging Connections

Stud Designation					Total Brace Stiffness	Experimental Initial Flexural Stiffness of the Bridging Connection			Total Flexural Stiffness of the Bridging Connection		
						$\beta_{provided}$	SS Type	WW Type	DW Type	SS Type	WW Type
D	S	B	t	ID	lbs/in.	lbs/in.	lbs/in.	lbs/in.	lbs/in.	lbs/in.	lbs/in.
600	S	162	43	6	0						
600	S	162	43	6a	0						
600	S	162	43	5	61	3800			60		
600	S	162	43	2	148	3800			142		
600	S	162	43	1	497	3800			440		
600	S	162	43	4	990	3800			785		
600	S	162	97	5	0						
600	S	162	97	4	324	6215	15880	8260	308	317	312
600	S	162	97	3	1041	6215	15880	8260	892	977	924
600	S	162	97	1	2069	6215	15880	8260	1552	1831	1655
600	S	162	97	2	3357	6215	15880	8260	2180	2771	2387
800	S	162	43	4	0						
800	S	162	43	2	149	2265			140		
800	S	162	43	3	299	2265			264		
800	S	162	43	5	602	2265			476		
800	S	162	97	3	0						
800	S	162	97	2	1041	5015	15090	2400	862	974	726
800	S	162	97	1	2093	5015	15090	2400	1477	1838	1118
800	S	162	97	4	4195	5015	15090	2400	2284	3283	1527

Table 5.5 Calculated Brace Stiffness and Total Brace Stiffness of the Test Specimens

Stud Designation					Target Brace Stiffness	As-Built Depth of Stud	Wire				Torsional Stiffness of Wire
							Dia.	Area	L	Nos.	
D	S	B	t	ID	lbs/in.	in.	in.	in. <sup>2</sup>	in.		lbs-in./rad
362	S	125	33	5	0	3.613	-	-	-	-	0
362	S	125	33	3	100	3.613	0.016	0.000201	60.75	1	11
362	S	125	33	4	100	3.613	0.016	0.000201	60.75	1	11
362	S	125	33	6	100	3.613	0.016	0.000201	58	1	11
362	S	125	33	1	200	3.613	0.016	0.000201	56.5	2	21
362	S	125	33	2	400	3.613	0.016	0.000201	30.5	2	21
362	S	162	43	1	0	3.564	-	-	-	-	0
362	S	162	43	2	200	3.564	0.024	0.000452	70.75	1	23
362	S	162	43	4	400	3.564	0.024	0.000452	35.75	1	23
362	S	162	43	3	800	3.564	0.024	0.000452	35.5	2	47
362	S	162	68	5	0	3.638	-	-	-	-	0
362	S	162	68	3	500	3.638	0.033	0.000855	48.5	1	45
362	S	162	68	4	750	3.638	0.033	0.000855	32.25	1	45
362	S	162	68	2	1000	3.638	0.033	0.000855	24.25	1	45
600	S	125	33	2	0	6.020	-	-	-	-	0
600	S	125	33	4	30	6.020	0.01	0.000079	75	1	7
600	S	125	33	3	60	6.020	0.01	0.000079	37	1	7
600	S	125	33	1	200	6.020	0.016	0.000201	29	1	18

Table 5.5 (Continued) Calculated Brace Stiffness and Total Brace Stiffness of the Test Specimens

Stud Designation					Target Brace Stiffness	As-Built Depth of Stud	Wire				Torsional Stiffness of Wire
							Dia.	Area	L	Nos.	
D	S	B	t	ID	lbs/in.	in.	in.	in. <sup>2</sup>	in.		lbs-in./rad
600	S	162	43	6	0	6.021	-				0
600	S	162	43	6a	0	5.984	-				0
600	S	162	43	5	30	6.021	0.01	0.000079	75.25	1	7
600	S	162	43	2	75	6.021	0.016	0.000201	79	1	18
600	S	162	43	1	250	6.021	0.024	0.000452	52.75	1	39
600	S	162	43	4	500	6.021	0.024	0.000452	26.5	1	39
600	S	162	97	5	0	6.082	-				0
600	S	162	97	4	160	6.082	0.024	0.000452	81	1	40
600	S	162	97	3	500	6.082	0.0348	0.000951	53	1	84
600	S	162	97	1	1000	6.082	0.0625	0.003068	86	1	271
600	S	162	97	2	1500	6.082	0.0625	0.003068	53	1	271
800	S	162	43	4	0	7.921	-				0
800	S	162	43	2	75	7.921	0.016	0.000201	78.25	1	23
800	S	162	43	3	150	7.921	0.016	0.000201	39	1	23
800	S	162	43	5	300	7.921	0.016	0.000201	38.75	2	46
800	S	162	97	3	0	8.044	-				0
800	S	162	97	2	500	8.044	0.0348	0.000951	53	1	111
800	S	162	97	1	1000	8.044	0.0625	0.003068	85	1	358
800	S	162	97	4	2100	8.044	0.0475	0.001772	24.5	1	207

Table 5.6 Total Torsional Stiffness of the Bridging Connections

Stud Designation					Torsional Stiffness of the Brace	Experimental Initial Flexural Stiffness of the Bridging Connection			Total Flexural Stiffness of the Bridging Connection		
						SS Type	WW Type	DW Type	SS Type	WW Type	DW Type
D	S	B	t	ID	lbs-in./rad	lbs-in./rad	lbs-in./rad	lbs-in./rad	lbs-in./rad	lbs-in./rad	lbs-in./rad
362	S	125	33	5	0	0					
362	S	125	33	3	11	3475			11		
362	S	125	33	4	11	3475			11		
362	S	125	33	6	11	3475			11		
362	S	125	33	1	21	3475			21		
362	S	125	33	2	21	3475			21		
362	S	162	43	1	0	0					
362	S	162	43	2	23	6185			23		
362	S	162	43	4	23	6185			23		
362	S	162	43	3	47	6185			46		
362	S	162	68	5	0	0					
362	S	162	68	3	45	14800	87530	30645	45	45	45
362	S	162	68	4	45	14800	87530	30645	45	45	45
362	S	162	68	2	45	14800	87530	30645	45	45	45
600	S	125	33	2	0	0					
600	S	125	33	4	7	7110			7		
600	S	125	33	3	7	7110			7		
600	S	125	33	1	18	7110			18		

Table 5.6 (Continued) Total Torsional Stiffness of the Bridging Connections

Stud Designation					Torsional Stiffness of the Brace	Experimental Initial Flexural Stiffness of the Bridging Connection			Total Flexural Stiffness of the Bridging Connection		
						SS Type	WW Type	DW Type	SS Type	WW Type	DW Type
D	S	B	t	ID	lbs-in./rad	lbs-in./rad	lbs-in./rad	lbs-in./rad	lbs-in./rad	lbs-in./rad	lbs-in./rad
600	S	162	43	6	0	0					
600	S	162	43	6a	0	0					
600	S	162	43	5	7	22560			7		
600	S	162	43	2	18	22560			18		
600	S	162	43	1	39	22560			39		
600	S	162	43	4	39	22560			39		
600	S	162	97	5	0	0					
600	S	162	97	4	40	37490	204240	26515	40	40	40
600	S	162	97	3	84	37490	204240	26515	84	84	84
600	S	162	97	1	271	37490	204240	26515	269	270	268
600	S	162	97	2	271	37490	204240	26515	269	270	268
800	S	162	43	4	0	0					
800	S	162	43	2	23	55865			23		
800	S	162	43	3	23	55865			23		
800	S	162	43	5	46	55865			46		
800	S	162	97	3	0	0					
800	S	162	97	2	111	74635	275530	22810	111	111	110
800	S	162	97	1	358	74635	275530	22810	356	357	352
800	S	162	97	4	207	74635	275530	22810	206	207	205

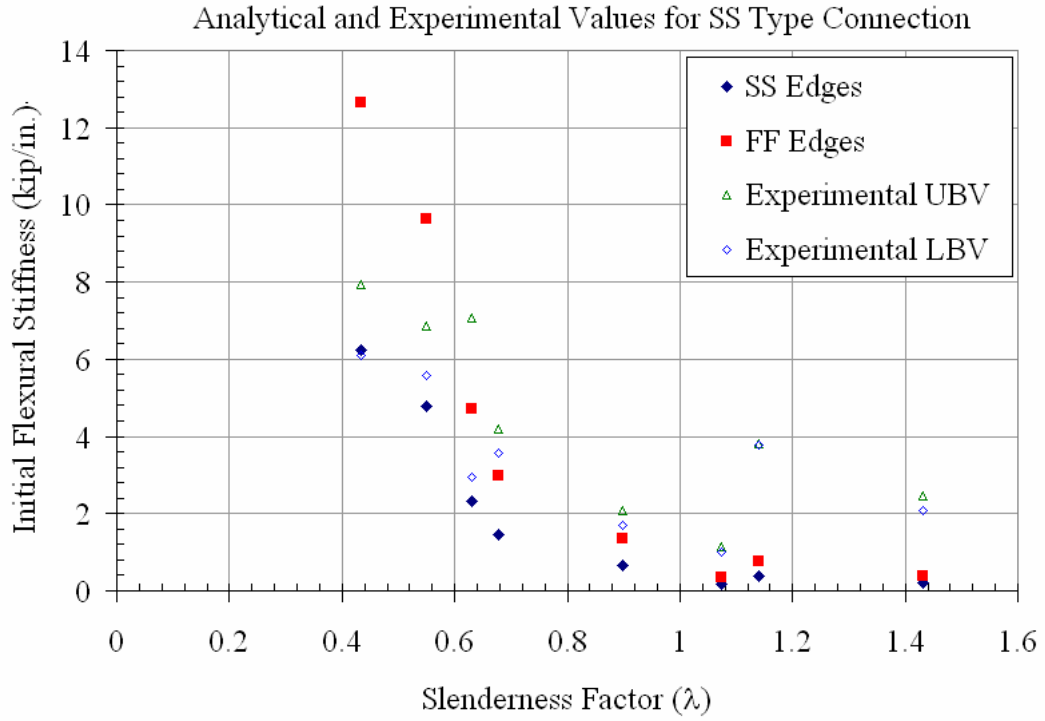


Figure 5.1 Flexural Stiffness of the SS Type Connection

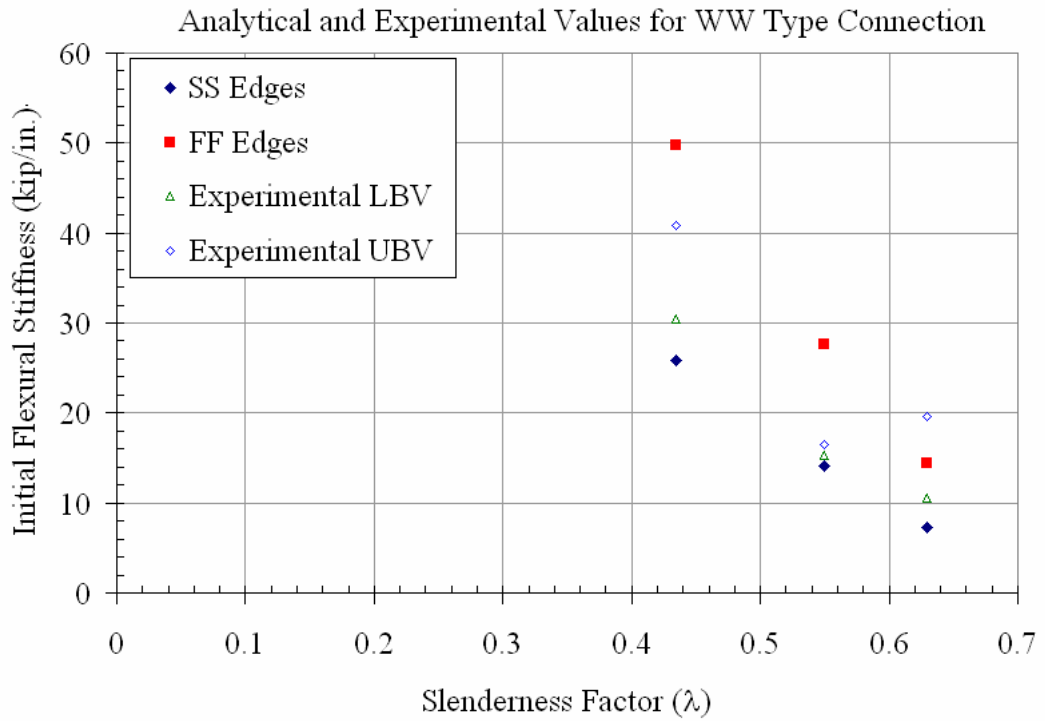


Figure 5.2 Flexural Stiffness of the WW Type Connection

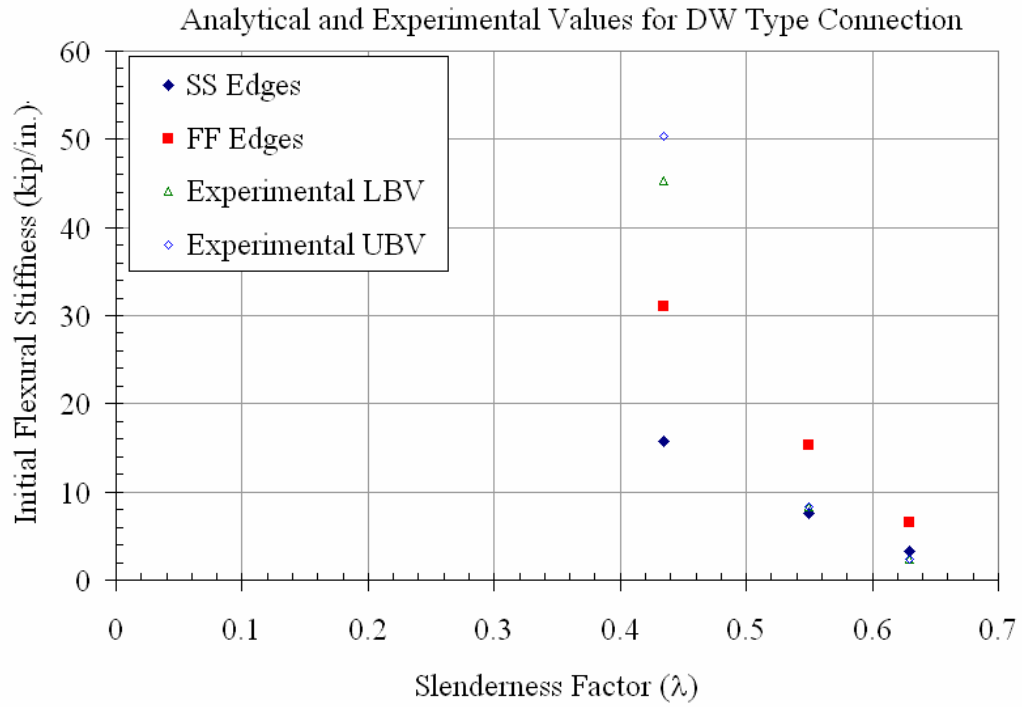


Figure 5.3 Flexural Stiffness of the DW Type Connection

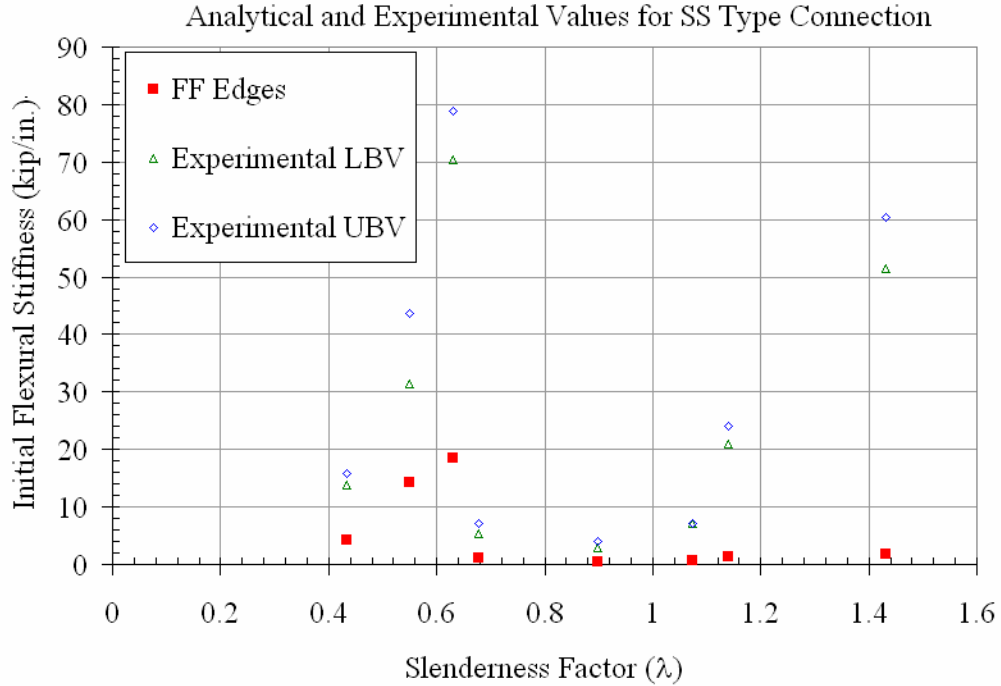


Figure 5.4 Torsional Stiffness of the SS Type Connection



## CHAPTER 6 CONCLUSIONS AND DESIGN RECOMMENDATIONS

The current provisions of the North American Cold-Formed Steel Specification do not specify the minimum requirements of the bracing strength and stiffness for structural wall stud assembly systems. These load bearing steel studs can also be used as stand-alone columns. The current provisions of the AISC-LRFD Specification (AISC 1999) have been discussed in Section 2.5 for hot-rolled steel members, but there are no equivalent provisions in the current North American Cold-Formed Steel Specification (2001). An experimental investigation was conducted at the Structures Laboratory, Department of Civil and Coastal Engineering, University of Florida, Gainesville, to ascertain the bracing strength and stiffness requirements for single column axially loaded cee-studs with mid-height lateral bracing about the weak axis. The experimental results and analytical evaluations of this investigation have been provided in Chapters 3, 4 and 5. This chapter describes the proposed minimum bracing requirements based on the experimental results and analytical calculation that were performed. In addition, a standard test procedure for determining the bracing connection strength and stiffness has been developed.

### **6.1 General Conclusions and Recommendations**

The following observations can be made based on the results of this research through its experimental investigation and analytical evaluation:

1. The compressive axial load capacity of a cold-formed cee-stud predicted by the current provisions of the AISI Specification (1999), under-predicts the axial capacity owing to ideal support conditions that are non-existent in general practice.

The bracing strength and stiffness is directly proportional to the axial load capacity leading to under-prediction of the actual ideal bracing requirement.

2. The mounting of the cee-stud in industry standard track offers partial base fixity and causes a reduction in the effective length of the compression member, leading to higher axial load capacity of the cee-stud. This, in turn, leads to higher demand on the mid-height lateral bracing for flexural and torsional buckling. The fixity factor varies for each stud cross-section and a separate study is recommended to ascertain these values.
3. The depth of the track and its connection type may affect the axial load capacity of the stud and hence a separate study is recommended to determine the effect of different track geometry on the support fixity.
4. The support fixities are different for different buckling modes that the mono-symmetric cee-stud section is subjected to and hence the same effective length factors cannot be used for all the different buckling modes.
5. Based on the type of mid-height bracing, the stud is either forced into flexural buckling or flexural-torsional buckling even if the unbraced stud predominantly would fail by torsional buckling. This adversely affects the performance of the stud in a wall-stud panel system. The critical buckling stresses for each of the buckling modes has to be evaluated and the axial capacity needs to be determined based on the application of the stud.
6. The critical buckling stress, using the provisions in the AISI Specification (1999), is a minimum of weak axis flexural buckling stress, strong axis buckling stress and torsional buckling stress. The bracing required to ideally brace the cee-stud must be meet the demands not only in flexural buckling but also in torsional buckling due to the any of the limiting critical buckling stress states.
7. The initial flexural stiffness of the three industry standard bracing connections has been predicted from basic structural mechanics. Based on the fixity of a rectangular web plate, two cases were developed that form the upper and lower bounds to the experimental results. A similar procedure to determine the initial torsional stiffness was also undertaken. Additional work is required to develop a provision for torsional stiffness.
8. The stiffness and strength of the mid-height lateral bracing was drastically affected by the higher axial capacities in the experiments. The tests showed more than a 50% increase in the axial capacity of the unbraced cee-stud due to non-ideal support conditions. This led to non conservative prediction of the ideal bracing requirement for the eight groups of cee-studs that were evaluated in the investigation. Thus, bracing strength and stiffness of a few studs, which were classified as over braced, were actually under braced in the experiments.

9. The braced studs reached axial capacities greater than the unbraced studs and exhibited higher stiffness. The brace factor hence must be increased by a certain multiplier to account for this increased demand.
10. With increasing the brace stiffness for a particular cee-stud cross-section, the mid-height lateral displacement decreased, however, the axial capacities remained nearly the same.
11. The braced studs that failed by distortional buckling did not attain their predicted axial capacity since the critical buckling stress due to distortional buckling mode is less than that for the global buckling modes. It is necessary to consider distortional buckling as one of the limiting critical buckling modes for certain ranges of effective web depth-to-thickness ratios.
12. The effect of the size, shape and location of the web punchouts is critical for an analytical axial load capacity prediction. In the experiments, it was observed that maximum deformation occurred in the vicinity of the punchouts at close to ultimate loads. This surely indicates that even a better prediction of the axial load considering the support fixity will be affected by the punchouts, and hence a separate study is required to determine these effects.
13. Three standard industry bracing connections were tested for their strength and initial stiffness. The SS Type and the WW Type performed equally well in both the out-of-plane load tests and in-plane load tests. The WW Type had definitely higher stiffness when compared to the SS Type connection. The DW Type connection performed extremely well in the in-plane tests. Based on the stud cross-section and its usage, a suitable connection type should be chosen for the purpose of mid-height lateral bracing of the cee-stud.
14. It was observed that in the WW Type and DW Type tests, the connections failed due to poor performance of the weld. However, this may not be a very critical requirement due to the reasons mentioned below.
15. In all the bracing connection tests the analytical evaluation of the connection stiffness showed that the bracing stiffness is controlled by the stiffness of the stud web and the effects of other components are negligible.
16. Comparison of the experimental values of brace stiffness to the connection stiffness shows that the brace stiffness values are much lesser than the connection stiffness. Since the two spring stiffnesses are in series, the contribution of the connection stiffness to the total system stiffness is negligible due to the magnitude of values. The total system stiffness is slightly less than the brace stiffness. A suitable stiffness reduction factor may be used based on the connection type to simplify the calculations.
17. Initial geometric imperfections in the studs affect their axial load capacity and hence the maximum allowable imperfections must be as per the ASTM C645-00

(2000) for non-structural steel studs and ASTM C955-01 (2001) for structural steel studs.

## 6.2 Design Recommendations

This section gives the minimum requirements of the mid-height lateral bracing for the cold-formed lipped cee-studs subjected to compressive axial loading. The equations given below are as per Yura's (1995) recommendations. It must be made note of here that the out-of-straightness of the stud was taken at  $\Delta_o = L / 384$ .

The ideal brace stiffness is given by:

$$\beta_{\text{brace, ideal}} = \frac{[4 - 2/n]P_n}{L_b} \quad (2.14)$$

The required brace stiffness is at least:

$$\beta_{\text{brace, required}} = 2\beta_{\text{brace, ideal}} \quad (6.1)$$

The ideal brace strength is given by:

$$P_{\text{brace, ideal}} = 0.004 P_n \quad (6.2)$$

The minimum required brace strength is at least:

$$P_{\text{brace, required}} = 0.01 P_n \quad (6.3)$$

where  $L_b$  = Unbraced length, or distance between the braces, inches.

$P_{\text{brace, ideal}}$  = Ideal bracing of the cee-stud, kips.

$P_{\text{brace, required}}$  = Minimum required brace strength, kips.

$P_n$  = Nominal axial capacity when the assumed brace stiffness is greater than or equal to  $\beta_{\text{ideal}}$ , kips.

$n$  = Number of equally spaced intermediate brace locations

$\beta_{\text{brace, ideal}}$  = Ideal brace stiffness

$\beta_{\text{brace, required}}$  = Minimum required brace stiffness

The flexibility or ability of a brace connection to slip should be considered in the evaluation of the actual bracing system stiffness,  $\beta_{act}$ , as follows:

$$\frac{1}{\beta_{act}} = \frac{1}{\beta_{conn}} + \frac{1}{\beta_{brace}} \quad (2.22)$$

where  $\beta_{conn}$  = Stiffness of the connection

$\beta_{brace}$  = Stiffness of the brace

The flexural stiffness and torsional stiffness have to be determined separately and then the connection system employed in bracing the cee-stud must be checked for the above minimum requirements. The unit for the initial flexural stiffness is (kip/in.) and that of the initial torsional stiffness is (kip-in./rad).

## LIST OF REFERENCES

- American Institute of Steel Construction (AISC), 1999, *Load and Resistance Factor Design Specification for Structural Steel Buildings*, Third Edition, American Institute of Steel Construction, Chicago, IL.
- American Iron and Steel Institute (AISI), 1996, Specification for the Design of Cold-Formed Steel Structural Members, American Iron and Steel Institute, Washington, D.C.
- American Iron and Steel Institute (AISI), 1999, Specification for the Design of Cold-Formed Steel Structural Members Supplement No.-1, American Iron and Steel Institute, Washington, D.C.
- American Iron and Steel Institute (AISI), 2001a, North American Specification for the Design of Cold-Formed Steel Structural Members – Code and Commentary, AISI, Washington, D.C.
- American Iron and Steel Institute (AISI), 2001b, Commentary on North American Specification for the Design of Cold-Formed Steel Structural Members – Code and Commentary, AISI, Washington, D.C.
- AISIWIN (Demo) V5.0, 2002, Devco Software, Inc. 245, NE Conifer, P.O. Box 1211, Corvallis, OR.
- American Society for Testing Materials (ASTM), 2000, Standard Specification for Nonstructural Steel Framing Members, ASTM C645-00, American Society for Testing and Materials, Philadelphia, PA.
- American Society for Testing Materials (ASTM), 2001 a, *Standard Test Methods for Tension Testing of Metallic Materials*, ASTM E8-01e2, American Society for Testing and Materials, Philadelphia, PA.
- American Society for Testing Materials (ASTM), 2001 b, Standard Specification for Load-Bearing (Transverse and Axial) Steel Studs, Runners (Tracks), and Bracing or Bridging for Screw Application of Gypsum Panel Products and Metal Plaster Bases, ASTM C955-01, American Society for Testing and Materials, Philadelphia, PA.
- Beshara, B., LaBoube, R.A., 2001, “Pilot Study: Lateral Braced C-Sections Under Bending”, *Thin Walled Structures*, Vol. 39, p 827-839.

- Bleich, F., 1952, *Buckling Strength of Metal Structures*, McGraw-Hill, New York, NY.
- Chajes, A., 1974, *Principles of Structural Stability*, Prentice-Hall, New Jersey, NJ.
- Galambos, T.V., 1998, *Guide to Stability Design Criteria for Metal Structures*, Fifth Edition, John Wiley & Sons, New York.
- Helwig, T.A., Yura, J.A., 1999, "Torsional Bracing of Columns", *Journal of Structural Engineering*, Vol. 125, No. 5, p 547-555.
- Kwon, Y.B., Hancock, G.J., 1991, "Strength Tests of Cold-Formed Channel Sections Undergoing Local and Distortional Buckling", Research Report No. R640, School of Civil and Mining Engineering, University of Sydney, Australia.
- Kavanagh, K.T., Ellifritt, D.S., 1993, "Bracing of Cold-Formed Channels Not Attached to Deck or Sheeting", *Bracing for Stability*, Structural Stability Research Council, Bethlehem, PA.
- Miller, T.H., 1990, "Behavior of Cold-Formed Steel Wall Stud Assemblies Subject to Eccentric Axial Loads", Ph.D. Thesis, Cornell University, Ithaca, N.Y.
- Miller, T.H., Pekoz, T., 1994, "Behavior of Gypsum-Sheathed Cold-Formed Steel Wall Studs", *Journal of Structural Engineering*, Vol. 120, No. 5, p 1644-1650.
- Plaut, R.H., 1993, "Requirements for Lateral Bracing of Columns with Two Spans", *Journal of Structural Engineering*, Vol. 119, No. 10, p 2913-2931.
- Shanley, F.R., 1947, "Inelastic Column Theory", *Journal of the Aeronautical Sciences*, Vol. 14, No. 5, p 261-268.
- Shanley, F.R., 1957, *Strength of Materials*, McGraw-Hill, New York.
- Schafer, B.W., 2000, "Distortional Buckling of Cold-Formed Steel Columns", *Final Report to the American Iron and Steel Institute*, Washington, D.C.
- Steel Studs Manufacturers Association (SSMA), 2001, *Product Technical Information*, Steel Studs Manufacturers Association, ICBO ER-4943P, Chicago, IL.
- Urala, V., 2004, "Bracing Requirements of Cold-Formed Steel Cee-Studs Subjected to Axial Compression", Masters Thesis, University of Florida, Gainesville, FL.
- Winter, G., 1959, "Cold-Formed, Light-Gage Steel Construction", *Journal of Structural Engineering*, Vol. 85, No. ST 9, p 151-171.
- Winter, G., 1960, "Lateral Bracing of Columns and Beams", *Transactions of the American Society of Civil Engineers*, Vol. 125, p 807-845.
- Young, B., Rasmussen, K.J.R., 1999, "Behavior of Cold-Formed Singly Symmetric Columns", *Thin Walled Structures*, Vol. 33, p 83-102.

- Young, B., Rasmussen, K.J.R., 2000, "Inelastic Bifurcation of Cold-Formed Singly Symmetric Columns", *Thin Walled Structures*, Vol. 36, p 213-230.
- Yu, W-W., 1991, *Cold-Formed Steel Design*, Third Edition, John Wiley and Sons, New York.
- Yura, J.A., 1996, "Winter's Bracing Model Revisited", *Engineering Structures Journal*, Elsevier, Vol. 18, No. 10, pp 821-825.
- Yura, J.A., 1995, "Bracing for Stability – State of the Art", *Bracing for Stability*, Structural Stability Research Council, Bethlehem, Pa.
- Zuk, W., (1956), "Lateral Bracing Forces on Beams and Columns", *Journal of Engineering Mechanics*, Vol. 82, EM3, p 1032-1 – 1032-16.





**American Iron and Steel Institute**

1140 Connecticut Avenue, NW  
Suite 705  
Washington, DC 20036

[www.steel.org](http://www.steel.org)

